FUNCTIONAL ANALYSIS OF mRNA METHYLATION IN PLANTS

MI ZHANG, BSc, MSc.

Thesis submitted to the University of Nottingham

for the degree of Doctor of Philosophy

May 2018

ABSTRACT

RNA modifications, which collectively constitute the epitranscriptome, have been found to play a crucial role in regulating gene expression. N^6-methyladenosine (m^6A) is a ubiquitous base modification in mRNAs of most eukaryotes and is implicated in multiple biological processes. The formation of m^6A is catalysed by the methyltransferase (MTase) complex (m^6A writer complex), composing of MTA, MTB, FIP37, Virilizer and Hakai (an E3 ubiquitin ligase). As a novel member of the MTase complex, the role of Hakai in mRNA methylation both in plants and in mammals is not yet understood. In addition, the biological functions of m^6A in plants is far from well characterised. The aim of this study is to elucidate the function of Hakai, interactions between different components of the MTase complex and the regulatory role of m^6A in root development. Based on characterising mutants and transgenic lines generated via CRISPR-Cas9, crossing and floral dip transformation in combination with m^6A measurements, confocal microscopy, transcriptional and protein level analysis, proteomic assay, etc., the following results and conclusions are reached. The knockout of *Hakai* led to approximately 40% decrease of m^6A level and this could be restored by complementation with a wild-type *Hakai* transgene. MTA, FIP37 and Virilizer among known m^6A writer proteins were interacting partners of Hakai. *mta hakai* double mutants demonstrated more severe developmental defects while *hakai fip37* and *hakai virilizer* appear to be lethal. Therefore, Hakai is an important m^6A writer protein, acting synergistically with other m^6A writer proteins to properly perform m^6A modification and regulate plant growth and development. In addition, novel

proteins interacting with both MTA and Hakai were identified, including two zinc-finger proteins (AT1G32360 and AT5G53440) and Hakai is required for the interaction between MTA and AT1G32360. All low m^6A mutants demonstrated strong auxin-insensitive phenotypes: dramatically shorter primary roots and reduced lateral roots relative to WT, indicating m^6A might have a regulatory role in mediating the auxin signalling network. Strikingly, auxin response factor 7 (ARF7) protein level increased upon the knockout of *FIP37* or *Virilizer* while its mRNA level and ARF8 protein level were unchanged. Given that ARF7 contains upstream open reading frames (uORFs) but this is not the case for ARF8, we propose that m^6A might be responsible for translational regulation of some uORF-containing transcripts. Collectively, the data in this study shed new light on interactions between m^6A writer proteins and regulatory mechanisms of m^6A modification, which will aid our understanding of the function of eukaryotic mRNA methylation.

ACKNOWLEDGEMENTS

Firstly, I would like to thank my supervisor, Prof. Rupert G. Fray for giving me the opportunity to work on "mRNA methylation". I am so honoured to work with a so nice, patient, knowledgeable and helpful supervisor. No matter what kind of problems I have got, he is always there to help. I would like to thank him for supervising me, teaching me, helping me and sharing so many good ideas with me. I would also like to thank Dr. Zsuzsanna Bodi, who has taught me so many experimental techniques and helped me a lot since I joined Rupert's group.

I would also like to thank my co-supervisor, Prof. Graham Seymour and my assessor, Dr. Ranjan Swarup, for giving me many good suggestions and supervising my work progress. I would like to thank all the PhD students in Rupert's group, especially Nathan Archer, Fatima Alzahrani and Doha Albalawi, for helping me while I was working in the lab. It was a very pleasant experience to work with them. I would like to thank Prof. Gordon. G. Simpson and his group in the University of Dundee for taking care of me, teaching me and helping me during my visit to their lab. I would like to thank all the colleagues in Plant Sciences who have helped me in the past three years.

Besides, I would like to thank China Scholarship Council and the University of Nottingham for sponsoring me in the past three years. Finally, I would like to thank all my family members, especially my husband for understanding me, supporting me and loving me all the time.

TABLE OF CONTENTS

LIST OF ABBREVIATIONS

Abbreviations	Full names
2,4-D	2,4-dichlorophenoxyacetic acid
2'-OMe	2'-*O*-methylation
ABI3A6	homozygous *mta* mutant complemented by *MTA* cDNA under the embryo-specific *ABI3* promoter
Am	2'-*O*-dimethyladenosine
Amp	ampicillin
APA	alternative polyadenylation
ARFs	auxin response factors
Aux/IAA	auxin/indole acetic acid
AuxREs	auxin response elements
circRNAs	circular RNAs
CLIP	crosslinking and immunoprecipitation
CMC	1-Cyclohexyl-3-(2-morpholinoethyl)-carbodiimide metho-p-toluenesulfonate
CPSF30	cleavage and polyadenylation specificity factor 30
CRISPR-Cas9	clustered regularly interspaced short palindromic repeat-CRISPR associated 9
DII	Domain II of Aux/IAA proteins
DSBs	double-strand breaks
DTT	dithiothreitol
eIF3	eukaryotic initiation factor 3
eIF3h	subunit h of eukaryotic initiation factor 3
ESCs	embryonic stem cells
FDR	false discovery rate
FIP37	FKBP12 INTERACTING PROTEIN 37
Fl(2)d	Female lethal 2
FTO	fat mass and obesity-associated protein
hm^5C	5-hydroxymethylcytidine
HR	homologous recombination

Abbreviations	Full names
Hsp70	heat shock protein 70
IAA	indole-3-acetic acid
Ime4	inducer of meiosis 4
IP	immunoprecipitation
Kan	kanamycin
LB (primer)	left border primer on the T-DNA in genotyping PCR
lncRNAs	long non-coding RNAs
LP	left primer on the genomic DNA in genotyping PCR
LR (root)	lateral root
m^1A	N^1-methyladenosine
m^5C	5-methylcytidine
m^6A	N^6-methyladenosine
m^6A-LAIC-seq	m^6A-level and isoform-characterisation sequencing
m^6Am	N^6,2'-*O*-dimethyladenosine
MeRIP-seq	methylated RNA immunoprecipitation sequencing
METTL14	methyltransferase like 14
METTL3	methyltransferase like 3
miCLIP	m^6A individual-nucleotide-resolution cross-linking and immunoprecipitation
miRNA	microRNA
mORF	main open reading frame
MRB1	yeast methylated RNA-binding protein 1
mRNAs	messenger RNAs
MTase	methyltransferase
Mum2	muddled meiosis 2
NAA	1-naphthalene acetic acid
NHEJ	non-homologous end joining
NPA	*N*-1-naphthylphthalamic acid
nt	nucleotide
PAM	Protospacer-adjacent motif
PA-m^6A-seq	photo-crosslinking-assisted m^6A-sequencing

Abbreviations	Full names
PAR-CLIP	photoactivatable ribonucleoside-enhanced crosslinking and immunoprecipitation
PCR	polymerase chain reaction
PMSF	phenylmethanesulfonyl fluoride
RBM15	RNA binding motif protein 15
RNase	ribonuclease
RP	right primer on the genomic DNA in genotyping PCR
rRNAs	ribosomal RNAs
RT	reverse transcription
SAM	*S*-adenosylmethionine
SCARLET	site-specific cleavage and radioactive-labelling followed by ligation-assisted extraction and thin-layer chromatography
SDS	sodium dodecyl sulfate
sgRNA	single guide RNA
Sxl	*Sex-lethal*
TAP	tandem affinity purification
TIR1/AFBs	TRANSPORT INHIBITOR RESPONSE 1/AUXIN SIGNALING F-BOX PROTEINS
TLC	thin layer chromatography
tRNAs	transfer RNAs
uORFs	upstream open reading frames
UTR	untranslated region
UV	ultraviolet
WT	wild type
WTAP	Wilms' tumour 1-associating protein
XIST	X-inactive specific transcript
Y2H	yeast two hybrid
YTH	YT521-B homology
YTHDF	YTH domain family protein
Ψ	pseudouridine

LIST OF FIGURES

LIST OF TABLES

CHAPTER 1 GENERAL INTRODUCTION

1.1 RNA MODIFICATIONS

Like DNA and protein modifications, RNA modifications, which collectively constitute the epitranscriptome, are now also recognised as facilitating important regulatory mechanisms for gene expression and functions (Saletore et al., 2012). There are more than 140 chemical modifications found in RNAs and those in transfer RNAs (tRNAs) and ribosomal RNAs (rRNAs) are the most abundant and extensively-studied (Limbach et al., 1994; Machnicka et al., 2013; Burgess et al., 2016; Roundtree et al., 2017). In messenger RNAs (mRNAs), as well as the canonical 5' 7-methylguanosine (m^7G) cap and 3' poly(A) tail, which are essential for mRNA stability, pre-mRNA splicing, translation initiation, etc., internal mRNA modifications have also been found and these have gained more attention in recent years (Roundtree et al., 2017).

1.1.1 Diverse mRNA Modifications and Their Chemical Properties

Recent advances in detection technology for RNA modifications, especially high-throughput sequencing in combination with old detection methods enable the identification and characterisation of chemical modifications in relatively low abundance mRNAs. Major chemical modifications in eukaryotic internal mRNAs include N^6-methyladenosine (m^6A), N^1-methyladenosine (m^1A), pseudouridine (Ψ), 5-methylcytidine (m^5C) and 5-hydroxymethylcytidine (hm^5C) (Figure 1.1). Though most of these RNA modifications were discovered

decades ago, their importance in regulating mRNA metabolism has been largely ignored until recent years when the development of transcriptome-wide sequencing technology has made detailed studies possible (Fray and Simpson, 2015; Li X et al., 2017; Roundtree et al., 2017).

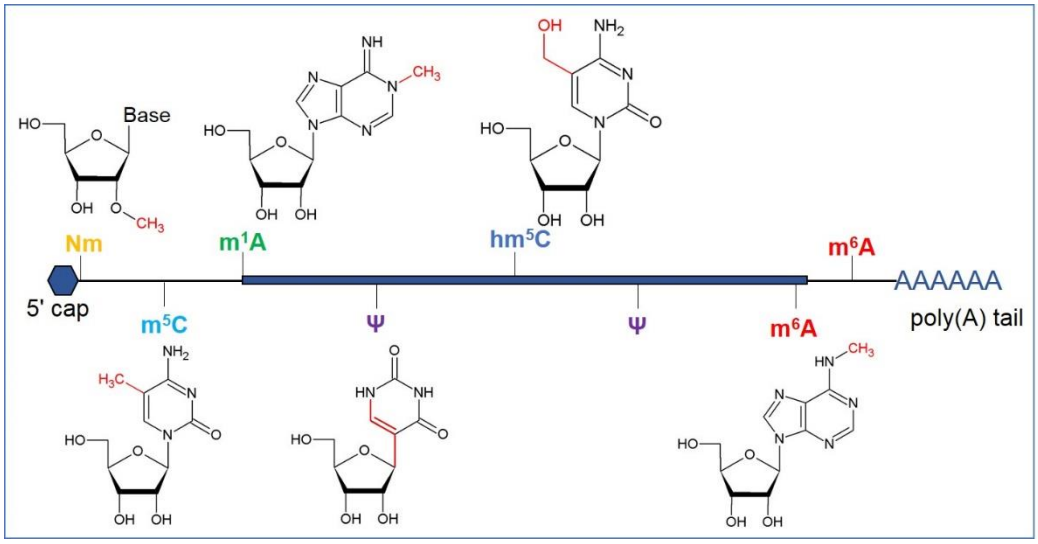

Figure 1.1 Chemical modifications in eukaryotic mRNAs (Adapted from Roundtree et al., 2017). Nm: 2'-*O*-methylation; m^5C: 5-methylcytidine; m^1A: N^1-methyladenosine; Ψ: pseudouridine; hm^5C: 5-hydroxymethylcytidine; m^6A: N^6-methyladenosine. The blue rectangle represents the coding sequence and the black line segment flanking the blue rectangle refers to untranslated regions (UTRs).

Among the above mRNA modifications, m^6A and m^1A represent methylation at the N^6 and N^1 positions of adenosine, respectively. However, their chemical properties and depositions on mRNAs are distinct. m^6A is the most abundant internal modification in eukaryotic mRNAs, but is among the hardest to be detected (Zhong et al., 2008; Golovina et al., 2013). This is because m^6A modification does not affect Watson-Crick base pairing therefore it cannot be revealed in cDNA libraries by altering base pairing or impeding reverse transcription (RT) with or without preliminary chemical treatments (e.g., m^1A

and Ψ) (Dai et al., 2007; Golovina et al., 2013; Harcourt et al., 2017). Unlike m^6A, m^1A has the methyl group at the Watson-Crick interface and introduces a positive charge, which can stall RT or lead to misincorporation at m^1A sites in the readthrough cDNAs (Agris et al., 1986; Helm et al., 1999; Helm, 2006; Hauenschild et al., 2015). Though m^1A is not as abundant as m^6A, the positive charge caused by m^1A may dramatically affect RNA structures and RNA-protein interactions (Roundtree et al., 2017). m^1A is prevalent in tRNAs and rRNAs and proved to be involved in stabilising tRNA tertiary structure and regulating ribosome biogenesis (Saikia et al., 2010; Peifer et al., 2013). Recent transcriptome-wide sequencing based on specific m^1A antibody reveals m^1A is also present in human and mouse mRNAs (Dominissini et al., 2016; Li et al., 2016). m^1A locates uniquely near the transcription start site while m^6A is enriched near stop codons and in 3' untranslated regions (3' UTRs) (Bodi et al., 2012; Dominissini et al., 2012, 2016; Meyer et al., 2012).

Other RNA modifications mentioned earlier (Ψ and m^5C) are relatively easier to be detected because of their special chemical properties. Ψ is a carbon-carbon glycoside isomer of uridine (U) and is regarded as the fifth nucleotide of RNA due to its abundance in RNAs (Cohn 1960; Bakin and Ofengand, 1993; Song et al., 2017). Ψ as well as U and guanosine (G) can be labelled by 1-Cyclohexyl-3-(2-morpholinoethyl)-carbodiimide metho-p-toluenesulfonate (CMC), but after subsequent alkaline hydrolysis (pH = 10.4, not high enough to degrade RNAs), only the CMC-Ψ adduct at N^3 position of Ψ remains (Naylor 1965; Ho and Gilham, 1967, 1971; Bakin and Ofengand, 1993). As the N^3 site of U or Ψ is at the Watson-Crick face, CMC-Ψ adducts terminate RT following CMC treatment.

Thus, the comparison of CMC-treated and untreated transcripts enables the detection of Ψ modification by looking for truncated RT products (Harcourt et al., 2017). Recently, four independent transcriptome-wide mappings assisted by CMC pretreatment uncovered the prevalence, distribution and some functions of mRNA pseudouridylation (Carlile et al., 2014; Lovejoy et al., 2014; Schwartz et al., 2014a; Li et al., 2015). These high-throughput sequencing methods demonstrated Ψ sites not only in known or unknown non-coding RNAs, including tRNAs, rRNAs, small non-coding RNAs and long non-coding RNAs (lncRNAs), but also in mRNAs in yeast (*Saccharomyces cerevisiae*), human and mouse. Three of them show that Ψ is distributed all along mRNA transcripts (Carlile et al., 2014; Schwartz et al., 2014a; Li et al., 2015). However, Ψ sites are found underrepresented in 3' UTRs of yeast mRNAs while the distribution of Ψ in human and mouse mRNAs demonstrates underrepresentation in 5' UTRs (Carlile et al., 2014; Li et al., 2015). Nevertheless, the consistent conclusion regarding the function of Ψ is that Ψ is indicated to be involved in stress response, such as heat shock (Carlile et al., 2014; Schwartz et al., 2014a; Li et al., 2015).

m^5C modification on genomic DNA can be detected by using the sodium bisulfite treatment. After this treatment, cytosine is converted to uracil whereas m^5C remains unchanged (Frommer et al., 1992). Modified bisulfite treatment, in which conditions are modified so as to protect RNAs from degradation, can be used to detect m^5C modifications in RNAs (Gu et al., 2005; Schaefer et al., 2009). Comparing sequences of bisulfite-treated and untreated RNA transcripts can reveal m^5C-modified sites (Li X et al., 2017). Coupling bisulfite conversion with next-generation sequencing reveals that m^5C modifications are not randomly

distributed across the human transcriptome, but enriched in UTRs and near Argonaute binding regions (Squires et al., 2012). In DNAs, m^5C can be oxidised to hm^5C by ten-eleven translocation (Tet) family proteins and this appears to be also the case in RNAs (Fu L et al., 2014). In *Drosophila melanogaster*, hm^5C is primarily located in the coding sequences, which is different from that of m^5C (Delatte et al., 2016).

Additional chemical modifications, such as 2'-*O*-methylation (2'-OMe or Nm), N^6,2'-*O*-dimethyladenosine (m^6Am) and adenosine to inosine editing (A-to-I editing), are also present in mRNAs of most eukaryotes. 2'-OMe, methylation of the ribose 2' hydroxyl, takes place on the first and second nucleoside adjacent to the 5' cap (Perry et al., 1975; Wei et al., 1976). Further methylation of 2'-*O*-methyladenosine (Am) at the N^6 position of the adenosine gives rise to m^6Am (Wei et al., 1976; Kruse et al., 2011). A-to-I editing is a special category of RNA modifications, termed RNA editing, which is catalysed post-transcriptionally by adenosine deaminase acting on RNA (ADAR) enzymes (Nishikura, 2010). However, these chemical modifications (Am, m^6Am and A-to-I editing) are absent in plants (Nishikura, 2010; Fray and Simpson, 2015).

The different deposition patterns of the RNA modifications discussed above suggests they have diverse functions. However, further studies are needed to decipher the biological functions of these chemical modifications (especially m^5C, hm^5C and Ψ) in mRNAs.

1.1.2 Detection Methods for m^{6}A Modification

1.1.2.1 Methods based on radioisotope labelling and chromatography

m^{6}A was fortuitously discovered in 1974 by several groups studying 5' terminal methylation (Desrosiers et al., 1974; Perry and Kelley, 1974). Early studies combined labelling by ^{3}H-methyl methionine, alkaline hydrolysis/enzymatic digestion and chromatography based on the ability to obtain pure poly(A) RNAs (Desrosiers et al., 1974; Perry and Kelley, 1974; Perry et al., 1975; Dubin and Taylor, 1975; Wei et al., 1976; Wei and Moss, 1977). ^{3}H-methyl methionine can be applied to cells as the methyl source, which is then metabolically incorporated into *S*-adenosylmethionine (SAM), a methyl donor in many methylation reactions in cells (Meyer and Jaffrey, 2014). DEAE-Sephadex chromatography can be used to analyse methylated nucleoside constituents of RNAs. Early studies showed that there are both base and ribose methylation in mRNAs and approximately 80% of the base methylation is from m^{6}A (Desrosiers et al., 1974; Perry and Kelley, 1974; Dubin and Taylor, 1975). Later, Wei et al. (1976) for the first time discovered that m^{6}A sites show sequence specificity, exclusively as Gm^{6}AC and Am^{6}AC. They also showed that 70% of m^{6}A is in Gm^{6}AC and 30% is in Am^{6}AC (Wei and Moss, 1977).

Another method of measuring overall m^{6}A levels relying on radioisotope is two-dimensional thin layer chromatography (TLC) (Keith, 1995; Zhong et al., 2008). The TLC assay is based on digesting poly(A) RNAs by ribonuclease T1 (RNase T1) to cut after every G residue, followed by labelling with [γ-^{32}P]ATP at 5' ends

of digested fragments. Labelled polynucleotides are further digested by nuclease P1 to form mononucleotides and then separated on two-dimensional cellulose TLC plates developed in different solvents (Zhong et al., 2008). Modified m^6A can be determined by comparing its mobility with known molecules (Figure 1.2) (Keith, 1995; Zhong et al., 2008). The drawback of this method is that it does not cover all A sites but only those after G, which account for 70% of m^6A modification (Zhong et al., 2008; Wang and Zhao, 2016).

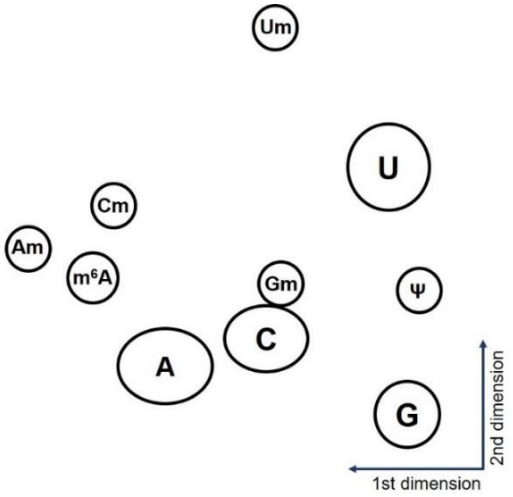

Figure 1.2 Relative positions of major and modified 5' nucleotides on two-dimensional thin layer chromatography (Adapted from Keith, 1995 and Zhong et al., 2008). A: adenosine; C: cytosine; U: uridine; G: guanosine; Am: 2'-*O*-methyladenosine; Cm: 2'-*O*-methylcytosine; Um: 2'-*O*-methyluridine; Gm: 2'-*O*-methylguanosine; m^6A: N^6-methyladenosine.

In contrast, liquid chromatography coupled with classic mass spectrometry (LC-MS) or tandem mass spectrometry (LC-MS/MS) can also be used to determine the global abundance of m^6A (Wang and Zhao, 2016; Helm and Motorin, 2017). In most cases, RNA is digested into single nucleosides using nuclease P1 and alkaline phosphatase and subsequently analysed by high-performance liquid chromatography (HPLC), HPLC-MS or LC-MS/MS (Clancy et al., 2002; Jia et

al., 2011; Zheng et al., 2013; Liu et al., 2014; Schwartz et al., 2014b; Shen et al., 2016). Though this method covers all A sites with very high sensitivity, it is not easy to be used mainly because special equipment and expertise are required and a large amount of RNA sample is needed and RNA is more difficult to be dealt with in mass spectrometry assay compared with protein samples (Wang and Zhao, 2016; Helm and Motorin, 2017).

1.1.2.2 Methods based on high-throughput sequencing

Transcriptome-wide localisation of m^6A was not available until 2012 when two groups developed similar m^6A detection methods based on combining RNA immunoprecipitation using m^6A-specific antibodies with next generation sequencing, termed m^6A-seq and methylated RNA immunoprecipitation sequencing (MeRIP-seq), respectively (Dominissini et al., 2012; Meyer et al., 2012). In both methods, poly(A) RNAs or RiboMinus-treated RNAs of mammalian cells are fragmented into around 100-nucleotide (nt)-long oligonucleotides prior to immunoprecipitation using an anti-m^6A antibody. Afterwards, libraries are constructed from immunoprecipitated fragments and also those without immunoprecipitation (input control), followed by high-throughput sequencing (Dominissini et al., 2012; Meyer et al., 2012). The main difference of these two methods lies in their downstream computational methods for aligning reads and m^6A peak calling (Saletore et al., 2012).

However, the above two transcriptome-wide m^6A detection methods demonstrate relatively low resolution since m^6A sites can be mapped within a

100-200 nt transcript region but precise positions cannot be confirmed (Chen K et al., 2015; Ke et al., 2015; Linder et al., 2015; Wang and Zhao, 2016). In 2013, Schwartz et al. (2013) generated maps of m^6A sites in meiotic yeast transcripts with increased resolution by optimising previously published m^6A-seq. In their method, fragment size of RNAs was decreased and a ligation-based strand-specific library preparation protocol capturing both ends of the fragmented RNA was employed to ensure that the methylated position is within the sequenced fragment (Schwartz et al., 2013). In addition, methylation-deficient control strains were used to eliminate many false-positive m^6A peaks (Schwartz et al., 2013). Later, m^6A sequencing strategies with higher resolution or single-nucleotide resolution were reported (Chen K et al., 2015; Ke et al., 2015; Linder et al., 2015). One of them is photo-crosslinking-assisted m^6A-sequencing (PA-m^6A-seq), which couples photoactivatable ribonucleoside-enhanced crosslinking and immunoprecipitation (PAR-CLIP) with previous m^6A sequencing (Chen K et al., 2015). In this method, 4-thiouridine (4SU) is incorporated into RNAs of living human cells. In the following immunoprecipitation step, full-length mRNAs rather than fragmented ones are used. After ultraviolet (UV) crosslinking, crosslinked RNAs are digested to around 30 nt using RNase T1 and then subjected to library preparation and sequencing. Because 4SU incorporation and UV crosslinking induce T-to-C transition nearby m^6A modified sites, this method improves the resolution of m^6A sequencing to ~ 23 nt. However, this method is only applicable to living cells and m^6A sites that do not harbour a nearby site for 4SU incorporation may be missed (Wang and Zhao, 2016; Li X et al., 2017). Additionally, another two approaches adapted from UV crosslinking and immunoprecipitation (CLIP),

denominated as m^{6}A-CLIP and m^{6}A individual-nucleotide-resolution cross-linking and immunoprecipitation (miCLIP), enable the identification of m^{6}A at a single-nucleotide resolution (Ke et al., 2015; Linder et al., 2015). This is based on the fact that RT of RNA cross-linked to a specific m^{6}A antibody results in mutations or truncations in cDNA libraries (Ke et al., 2015; Linder et al., 2015). Another recently developed m^{6}A detection method, termed m^{6}A-level and isoform-characterisation sequencing (m^{6}A-LAIC-seq), for the first time claims to quantitatively compare methylated versus nonmethylated transcripts by employing excess anti-m^{6}A antibody, full-length transcripts and spike-in controls on a genome-wide scale (Molinie et al., 2016). However, m^{6}A sites cannot be defined in this method due to the usage of full-length mRNAs.

1.1.2.3 Methods of detecting m^{6}A at specific sites

One limitation of the above transcriptome-wide sequencing technologies for detecting m^{6}A is that they all rely on specific anti-m^{6}A antibodies. Unfortunately, all existing m^{6}A antibody-based immunoprecipitation procedures are often associated with false positives (Wang and Zhao, 2016). To address this problem, Liu et al. (2013) developed a method to validate specific m^{6}A sites, termed site-specific cleavage and radioactive-labelling followed by ligation-assisted extraction and thin-layer chromatography (SCARLET). The procedure is as follows (Figure 1.3). Firstly, a candidate site of interest is chosen and poly(A) RNAs are digested by RNase H in the presence of a complementary 2'-OMe/2'-H chimeric oligonucleotide to achieve site-specific cleavage 5' to the candidate site. Afterwards, the free 5' end is labelled with ^{32}P and splint-ligated to a 116

nt-long single-stranded DNA oligonucleotide to protect the ^{32}P-labelled nucleotide residue from the following digestion. The ligated product is then digested by RNase T1 and RNase A to cut off all the RNA nucleotides except for the ^{32}P-labelled candidate site. The labelled product is purified by gel excision and further digested by nuclease P1 to form mononucleotides. The mixture is finally separated on TLC to analyse the proportion of m^{6}A at the candidate site (Liu et al., 2013). This method has been used by Ke et al. (2015) and Linder et al. (2015) to confirm and precisely localise the m^{6}A sites identified by their m^{6}A-CLIP or miCLIP.

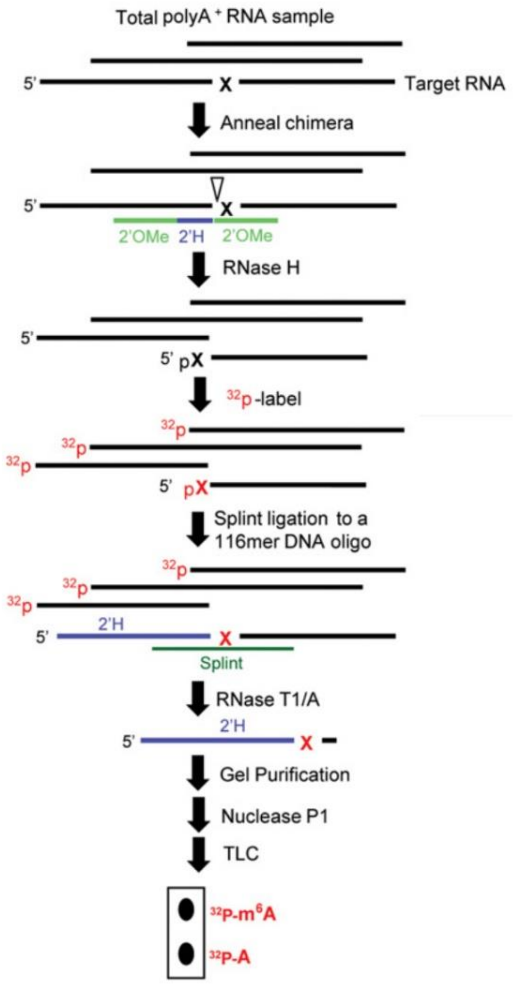

Figure 1.3 Schematic diagram of site-specific cleavage and radioactive-labelling followed by ligation-assisted extraction and thin-layer chromatography (SCARLET) (Liu et al., 2013).

Other reported approaches to the detection of m^6A at specific sites include m^6A-sensitive ligation assay (Dai et al., 2007) and m^6A-sensitive RT assays (Harcourt et al., 2013; Vilfan et al., 2013). All these methods are based on the different chemical properties of m^6A and normal A residues. For example, in the ligation assay, two DNA oligonucleotides are ligated via T4 DNA ligase using a RNA with or without m^6A as a template. The oligonucleotide substrate containing G at 3' end can form a non-Watson-Crick G-A base pair with A or m^6A in the RNA template. However, the ligation reaction is significantly slower when it is m^6A instead of A (Dai et al., 2007; Meyer and Jaffrey, 2014). In terms of methods based on RT, incorporation efficiency of thymidine opposite unmodified A is much higher relative to that opposite m^6A when using a polymerase from *Thermus thermophilus* (*Tth*) in RT (Harcourt et al., 2013). Similarly, in another method termed single-molecule, real-time (SMRT) RT assay, the frequency of fluorescence pulses at m^6A site on the RNA template is significantly decreased compared to the same RNA template containing the normal A site, indicating phospholinked nucleotide binding is affected by m^6A in the RNA template (Vilfan et al., 2013). Though these methods can successfully analyse m^6A at specific sites to some extent, they all have their own defects. The ligation assay itself is not robust enough and cannot give sufficiently clear and quantitative data. The RT assay using *Tth* DNA polymerase is restricted to high-abundance cellular RNAs and SMRT requires special equipment for the assay (Wang and Zhao, 2016).

1.2 CHARACTERISTICS OF m^6A MODIFICATION

Since the first discovery of m^6A in mRNAs in the 1970s, m^6A has been proved to be conserved among different eukaryotes, including mammals (Desrosiers et al., 1974; Perry and Kelley, 1974; Dubin and Taylor, 1975), plants (Kennedy and Lane, 1979; Nichols, 1979; Haugland and Cline, 1980; Zhong et al., 2008), *Drosophila* (Haussmann et al., 2016; Lence et al., 2016) and yeast (Clancy et al., 2002). In plants, early studies showed that m^6A is present in mRNAs of maize (*Zea mays*) (Nichols, 1979), wheat (*Triticum aestivum*) (Kennedy and Lane, 1979) and oat (*Avena sativa*) (Haugland and Cline, 1980). There are approximately two m^6A residues per 1,600 nucleotide residues in maize poly(A)-containing RNAs and m^6A accounts for 75-80% of the total methylation activity in poly(A)-rich RNAs from imbibing wheat embryos, similar to the ratios of m^6A in mammalian mRNAs (Nichols, 1979; Kennedy and Lane, 1979; Perry and Kelley, 1974; Dubin and Taylor, 1975). Early studies in both mammals and plants revealed that m^6A modification demonstrates sequence specificity, with m^6A occurring at Gm^6AC and Am^6AC (Wei et al., 1976; Nichols and Welder, 1981). Later, the consensus sequence for m^6A sites was extended to RRACH (where A is the methylation site, R = purine and H = A, C, or U) (Wei and Moss, 1977; Harper et al., 1990). Recent high-throughput sequencing confirms this consensus sequence in a transcriptome-wide level and it is conserved in mammals, yeast, plants and *Drosophila* (Dominissini et al., 2012; Meyer et al., 2012; Schwartz et al., 2013; Luo et al., 2014; Lence et al., 2016).

The location of m^6A across the transcript is asymmetric. In 1975, Perry et al. (1975) for the first time discovered that m^6A residues are absent from poly(A) tails and they are located internal to the poly(A) near the 3' end of mouse mRNAs. Consistently, Bodi et al. (2012) showed that m^6A is predominantly positioned towards the 3' end of transcripts in a region 100-150 bp before the poly(A) tail using methods based on chemical fragmentation and TLC analysis. Thereafter, transcriptome-wide sequencing methods further verified the earlier results (Dominissini et al., 2012; Meyer et al., 2012, Schwartz et al., 2013; Chen K et al., 2015; Ke et al., 2015). Original MeRIP-seq and m^6A-seq show that mammalian methylations are highly enriched in 3' UTRs and near stop codons, though the enrichment of m^6A around stop codons is not found in m^6A-CLIP with single-nucleotide resolution (Dominissini et al., 2012; Meyer et al., 2012; Ke et al., 2015). In yeast, m^6A sites are 3' biased and tightly correlated with the stop codon (Schwartz et al., 2013). In *Arabidopsis*, Luo et al. (2014) found that m^6A deposition is not only around stop codons and within 3' UTRs but also abundant around the start codon. However, our previous fragmentation analysis (Bodi et al., 2012) and our unpublished extensive MeRIP-seq data did not show this 5'-end enrichment of m^6A modifications in *Arabidopsis*. Collectively, m^6A methylomes demonstrate very high conservation in terms of general distribution within transcripts and sequence context across eukaryotes.

Though m^6A occurs primarily within the RRACH consensus sequence, only a portion of the RRACH sites contain the actual observed m^6A modification. In addition to the consensus sequence, early studies using an *in vitro* methylation system showed that other structural features or the overall context in which m^6A

occurs also affect the formation of m^6A (Narayan et al., 1994; Rottman et al., 1994). Therefore, it is necessary to uncover the molecular mechanism underlying the selectivity, regulation and function of m^6A modification in living cells (Zhong et al., 2008; Dominissini et al., 2012; Ping et al., 2014; Fray and Simpson, 2015).

1.3 THE METHYLTRANSFERASE COMPLEX (m^6A WRITERS)

1.3.1 METTL3 and Its Orthologues

Identification of enzymes that catalyse the formation of m^6A is a priority to elucidate the mechanism of m^6A modification. Early studies in the 1990s showed that m^6A formation in mRNAs is catalysed by a multi-subunit complex (now also known as m^6A writers) (Bokar et al., 1994, 1997). The first characterisation of mRNA m^6A methyltransferase (MTase) in human HeLa cells discovered three components, MT-A1, MT-A2 and MT-B, with molecular masses of 30, 200 and 875 kDa, respectively (Bokar et al., 1994). The MTase activity requires at least MT-A2 and MT-B. MT-A2 contains a 70-kDa SAM binding subunit, which was designated MT-A70 and is now known as methyltransferase like 3 (METTL3) (Bokar et al., 1994, 1997; Ping et al., 2014). A phylogenetic analysis reveals four subfamily lineages of MT-A70 related proteins (Lineage A-D). Lineage A-C are unique to eukaryotes while Lineage D contains a small cluster of bacterial DNA m^6A MTases and is the most distantly related (Bujnicki et al., 2002).

After identification and purification of METTL3 in mammals, its orthologues in other eukaryotes have also been identified, including MTA in *Arabidopsis* (AT4G10760) (Zhong et al., 2008), Inducer of meiosis 4 (Ime4) in yeast (Clancy et al., 2002; Bodi et al., 2010) and *Dm* Ime4 in *Drosophila* (Hongay and Orr-Weaver, 2011). METTL3 is ubiquitously expressed in human tissues and is observed to be localised in speckles, where it is enriched with pre-mRNA splicing factors (Bokar et al., 1997). Knockdown of METTL3 in both HeLa and 293FT cells decreases the m^6A level in mRNAs (Liu et al., 2014). Complete knockout of MTA in *Arabidopsis* leads to an arrest at the globular stage during seed development. The m^6A modification is undetectable in the arrested seeds while the m^6A level recovers in the complementation line containing a full-length *MTA* cDNA under the control of the constitutive cauliflower mosaic virus (CaMV) 35S promoter (Zhong et al., 2008). In yeast, m^6A is only found during sporulation and this change requires Ime4 expression (Clancy et al., 2002; Bodi et al., 2010). Knockdown of *Dm* Ime4 in *Drosophila* reduces the m^6A level by approximately 70% (Lence et al., 2016).

1.3.2 METTL14 and Its Orthologues

As a homologue of METTL3, methyltransferase like 14 (METTL14) belongs to Lineage B of METTL3 related proteins and shares 43% identity with METTL3 (Bujnicki et al., 2002; Ping et al., 2014; Yue et al., 2015). Moreover, METTL14 possesses similar domains essential for the catalytic activity as METTL3 (Ping et al., 2014). Like METTL3, METTL14 is also localised in nuclear speckles (Ping et al., 2014). Knockdown of cellular METTL14 demonstrates stronger

decrease in the m^6A level compared with that in METTL3 knockdown cells and METTL14 shows much higher MTase activity *in vitro* (Liu et al., 2014; Wang Y et al., 2014). These results suggest that METTL14 may play a more important role than METTL3 in m^6A modification. Combination of METTL3 and METTL14 exhibits even higher MTase activity, indicating they function synergistically (Liu et al., 2014; Wang Y et al., 2014). Gel filtration analysis shows that METTL3 and METTL14 form a stable heterodimer core complex (Liu et al., 2014). METTL3 depletion affects the nuclear speckle localisation of METTL14 and vice versa, which confirms that METTL3 and METTL14 work as a heterodimer (Ping et al., 2014). Structural analysis in three recent reports demonstrate the crystal structure of METTL3-METTL14 heterodimer but suggest that METTL3 primarily functions as the catalytic core while METTL14 serves as an RNA-binding platform (Wang X et al., 2016; Wang P et al., 2016; Śledź and Jinek, 2016). It is very interesting that there are two catalytic components in the MTase complex, indicating that these two catalytic components may target different sets of RNAs. Given that there are conflicting conclusions about the active catalytic component in the MTase complex based on biochemical and structural studies, more functional analyses should be performed in living cells to answer this question.

Orthologues of METTL14 exist in other species (Bujnicki et al., 2002), but have not yet been well characterised. Depletion of *Drosophila* METTL14 decreases m^6A level by about 70% (Lence et al., 2016). Homozygous *Drosophila ime4 mettl14* double mutant demonstrates similar phenotypes as *ime4* single knockout mutant, though more severe, suggesting that *Drosophila* Ime4 and METTL14

control similar biological pathways in *vivo* (Lence et al., 2016). In plants, the orthologue of METTL14 is termed MTB (AT4G09980), which has been identified to be associated with the m^6A writer complex by tandem affinity purification (TAP) but its role in mRNA methylation has yet to be determined (Růžička et al., 2017). In addition, comparison of MTA and MTB in terms of MTase activity, target transcripts and biological functions should be carried out based on characterising MTB in plants.

1.3.3 WTAP and Its Orthologues

The initial discovery of Wilms' tumour 1-associating protein (WTAP) as a component of the MTase complex is from the study of MTA in *Arabidopsis* (Zhong et al., 2008). In this study, MTA was found to interact with the orthologue of WTAP in *Arabidopsis*, FKBP12 INTERACTING PROTEIN 37 (FIP37, AT3G54170) both *in vitro* and *in vivo*. In addition, FIP37 and MTA co-localised in nuclear speckles (Zhong et al., 2008). Two recent papers confirmed that FIP37 is a core component of *Arabidopsis* MTase complex (Shen et al., 2016; Růžička et al., 2017).

Wilms' tumour 1-associating protein (WTAP) was originally identified as a protein that specifically interacts with Wilms' tumour suppressor gene 1 (WT1), which is essential for normal development of the genitourinary system (Little et al., 2000). Previous studies showed that WTAP is required for cell cycle progression, mammalian early embryo development and alternative splicing of WTAP pre-mRNA (Horiuchi et al., 2013). Recent studies proved that WTAP is

another crucial component of the MTase complex in mammals (Liu et al., 2014; Ping et al., 2014; Schwartz et al., 2014b). WTAP does not harbour any obvious catalytic domains and demonstrates no catalytic activity itself or effect on the activity of METTL3-METTL14 complex *in vitro* (Liu et al., 2014; Ping et al., 2014). However, knockdown of WTAP in human HeLa and 293FT cells leads to greater m^6A reduction compared with the effects of knocking down METTL3 or METTL14 (Liu et al., 2014). WTAP is a nuclear protein and WTAP depletion decreases the accumulation of both METTL3 and METTL14 in nuclear speckles (Ping et al., 2014). Moreover, the knockout of WTAP causes a significantly reduced amount of RNA associated with METTL3 (Ping et al., 2014). Therefore, a WMM (WTAP-METTL3-METTL14) complex is suggested in mammals, in which WTAP binds to the m^6A consensus RRACH motif of mRNA and recruits catalytic subunits – METTL3 and METTL14, and then the METTL3-METTL14 complex carries out m^6A MTase activity in the m^6A motif (Ping et al., 2014). In addition, m^6A sites are divided into two distinct classes: WTAP-dependent and WTAP-independent. WTAP-dependent sites are located internally on transcripts while WTAP-independent sites reside in the first transcribed base as a part of cap structure (Schwartz et al., 2014b).

In addition to *Arabidopsis* FIP37, other orthologues of WTAP include *Drosophila* Fl(2)d (Female lethal 2) and yeast Mum2 (Muddled meiosis 2) (Zhong et al., 2008; Penn et al., 2008; Schwartz et al., 2013). *Drosophila* Fl(2)d regulates *Sex-lethal* (*Sxl*)-dependent alternative splicing (Penn et al., 2008), which is consistent with a partial function of WTAP. Deletion of Fl(2)d causes significant reduction of m^6A level and decreases the interaction between

Drosophila Ime4 and METTL14, suggesting *Drosophila* Fl(2)d is required for full m^6A methylation and may work as a stabiliser in the complex (Lence et al., 2016). Yeast Ime4, Mum2 and another crucial component – Slz1 (not conserved in mammals and plants) form yeast MTase complex (referred to as the MIS complex) (Agarwala et al., 2012). Depletion of Mum2 leads to the loss of m^6A enrichment in m^6A-seq (Schwartz et al., 2013). The expression of *SLZ1* is activated by *IME1* (a master regulator of yeast meiosis) and Slz1 facilitates Ime4 and Mum2 entering the nucleus from the cytoplasm upon the induction of meiosis (Agarwala et al., 2012; Schwartz et al., 2013; Yue et al., 2015).

1.3.4 Other Components Involved in the MTase Complex

1.3.4.1 Virilizer

In addition to the above components of the MTase complex, recently other proteins that have interactions with the known components (METTL3, METTL14 and WTAP in mammals; MTA, MTB and FIP37 in *Arabidopsis*) have also been discovered. Using shotgun proteomics, Horiuchi et al. (2013) found that WTAP forms a protein complex including Virilizer (KIAA1429), Hakai, RBM15 and other proteins to regulate alternative splicing and cell cycle. Virilizer and Hakai also localise to nuclear speckles and the nucleoplasm (Horiuchi et al., 2013). *Drosophila* Virilizer is biochemically shown to interact with Fl(2)d in the context of sex-specific splicing (Ortega et al., 2003). This discovery led Schwartz et al. (2014b) to focus on mammalian Virilizer among candidates associating with MTase components in their proteomics screen.

Around 94% depletion of Virilizer and subsequent m^6A-seq in human A549 cells reveal that m^6A peak scores decrease by approximately four fold, substantially and significantly more prominent than that observed upon knockdown of METTL3 or METTL14, indicating that Virilizer is required for full methylation programme in mammals (Schwartz et al., 2014b). Similar to Fl(2)d, *Drosophila* Virilizer is required for sex determination and full m^6A methylation (Niessen et al., 2001; Lence et al., 2016). In plants, Virilizer (AT3G05680) is also identified as a component of the MTase complex but like its animal counterparts its role in mRNA methylation is not fully understood (Růžička et al., 2017).

1.3.4.2 Hakai

Mammalian Hakai is an E3 ubiqintin ligase containing a RING domain, a SH2 domain (Src homology 2, a short phosphotyrosine recognition sequence) and a proline-rich domain (Fujita et al., 2002; Mukherjee et al., 2012). In epithelial cells, Hakai interacts with E-cadherin in a tyrosine phosphorylation-dependent manner, inducing ubiquitination of the E-cadherin complex. This process promotes the endocytosis and disrupts cell to cell adhesions, which is a hallmark of tumour progression (Fujita et al., 2002; Pece and Gutkind, 2002; Figueroa et al., 2009a). In addition, Hakai can also promote tumorigenesis by enhancing the RNA-binding ability of PTB-associated splicing factor (PSF) to mRNAs that encode cancer-related proteins (Figueroa et al., 2009a,b). Though Hakai is found to interact with WTAP to regulate alternative splicing and cell cycle in mammals, its involvement in the MTase complex has not been reported in mammals (Horiuchi et al., 2013). In *Arabidopsis*, Hakai (AT5G01160) is co-purified with

MTB, FIP37 and Virilizer using GS-tagged Virilizer as a bait (Růžička et al., 2017), but its specific role in m^{6}A modification is still unknown. Additionally, general functions of Hakai in plants are also not clear. In contrast to minimal extracellular matrix and strong cell-cell adhesion in mammalian epithelial cells, all plant tissues possess their special extracellular matrix, termed cell walls (Seymour et al., 2004). Moreover, no cadherin-related proteins have been discovered in plants (Hulpiau and Van Roy, 2009). Thus, plant Hakai may exhibit some distinct functions relative to its counterpart in mammals.

1.3.4.3 RBM15 and its orthologues

Recently, another protein and its paralogue from Split End (SPEN) family in mammals – RNA binding motif protein 15 (RBM15) and RBM15B were shown to be involved in mediating the m^{6}A methylation on the lncRNA X-inactive specific transcript (*XIST*), which regulates the silencing of gene transcription on the X chromosome during female mammalian development (Patil et al., 2016). Knockdown of RBM15 and/or RBM15B results in significantly reduced levels of methylated *XIST*. In human HEK293T cells, METTL3 is co-precipitated with RBM15 or RBM15B and knockdown of WTAP reduces their interaction. Following formaldehyde crosslinking and immunoprecipitation, METTL3 immunoprecipitates contain significantly more *XIST* than control ones at RBM15/15B binding sites. Moreover, knockdown of WTAP, RBM15 and/or RBM15B leads to significantly less METTL3-bound *XIST*, suggesting RBM15/15B is the component of the MTase complex that accounts for m^{6}A modification in *XIST* (Patil et al., 2016). Additionally, knockdown of RBM15

and RBM15B also reduces m^6A levels in cellular mRNA, indicating that RBM15 and RBM15B also participate in m^6A modification in mRNAs (Patil et al., 2016).

Likewise, the orthologue of RBM15 in *Drosophila*, Spenito, was recently reported as a novel component of *Drosophila* m^6A MTase complex (Lence et al., 2016; Kan et al., 2017). Spenito was shown to interact with both Ime4 and Fl(2)d independently of the presence of RNA (Lence et al., 2016). Knockdown of Spenito leads to a severe m^6A decrease and loss of it results in similar splicing defects as observed upon depletion of members in the MTase complex (Lence et al., 2016). Co-immunoprecipitation assay of m^6A writers in *Drosophila* by Kan et al. (2017) demonstrated that Spenito can specifically co-immunoprecipitate wih Fl(2)d and METTL14 and modestly with Ime4, which also suggests that Spenito is a bona fide member of *Drosophila* MTase complex. The orthologue of human RBM15 in *Arabidopsis* is FPA, which harbours conserved domains as those in RBM15, including three repeated RNA recognition motifs in the N-terminal region and a SPEN-Paralog-Ortholog-Conserved (SPOC) domain in the C-terminal region (Hornyik et al., 2010; Su et al., 2015). FPA is a component of the autonomous pathway and controls flowering time by regulating the expression of alternatively polyadenylated antisense RNAs at the locus encoding the floral repressor FLOWERING LOCUS C (FLC) (Hornyik et al., 2010). However, whether it is involved in mediating m^6A modification in *Arabidopsis* remains unknown.

In summary, the components of the m^6A MTase complex are quite conserved across different organisms in eukaryotes. To better understand how the MTase

complex works in catalysing m^6A formation, we need to know how the components of this complex interact with each other. The interactions between different components have been elucidated to some extent in mammals, but the interactions of plant counterparts remain a mystery.

1.4 DEMETHYLASE (m^6A ERASERS)

The discovery of human fat mass and obesity-associated protein (FTO) as the first m^6A demethylase (also known as m^6A erasers) in 2011 was a key advance that reignited researchers' interest in investigating m^6A biology (Jia et al., 2011). This discovery also revealed m^6A as a reversible and dynamic mRNA modification, which is similar to DNA and histone modifications (Fu Y et al., 2014).

The original function of FTO is associated with human body mass index and energy homeostasis (Dina et al., 2007; Frayling et al., 2007). Overexpression of *FTO* leads to increased food intake and obesity whereas inactivation of *FTO* protects human bodies against obesity (Fischer et al., 2009; Church et al., 2010). FTO is a member of non-heme Fe(II)- and α-ketoglutarate (KG)-dependent dioxygenase AlkB superfamily proteins (Jia et al., 2011). Previous studies show that FTO is able to catalyse oxidative demethylation of 3-methylthymine (3-meT) in single-stranded DNAs and 3-methyluracil (3-meU) in single-stranded RNAs (Gerken et al., 2007; Jia et al., 2008). Moreover, slightly higher demethylation efficiency in single-stranded RNA suggests that methylated RNAs are preferred substrates for FTO (Jia et al., 2008). Therefore, Jia et al. (2011) proposed that

m^{6}A might also be a substrate of FTO. In agreement with their hypothesis, FTO can catalyse oxidative demethylation of m^{6}A in an Fe(II)- and α-KG-dependent manner *in vitro* (Jia et al., 2011). FTO knockdown by siRNA leads to increased amounts of m^{6}A in mRNA whereas overexpression of *FTO* results in decreased m^{6}A level in human cells (Jia et al., 2011). Indirect immunofluorescence analysis of endogenous FTO shows that FTO partially co-localises with nuclear speckles, supporting that m^{6}A in nuclear RNA is a substrate of FTO (Jia et al., 2011). While investigating FTO-dependent demethylation, two intermediates were discovered – *N*^{6}-hydroxymethyladenosine (hm^{6}A) and *N*^{6}-formyladenosine (f^{6}A), which form in a stepwise manner, but the functional implications of these two intermediates are still unknown (Fu et al., 2013).

In 2013, Hess et al. (2013) confirmed that FTO can act as an m^{6}A demethylase *in vivo*. However, their MeRIP-seq data demonstrate that over 5,000 new m^{6}A peaks appear in the mRNAs of over 1,500 genes from *FTO*-deficient mice, indicating FTO does not globally target all m^{6}A-modified mRNAs but instead demethylates specific mRNA subsets (Hess et al., 2013, Hess and Brüning, 2014). A recent study showed that m^{6}Am is also demethylated by FTO and FTO preferentially demethylates m^{6}Am rather than m^{6}A, reducing the stability of m^{6}Am mRNAs (Mauer et al., 2017).

ALKBH5 is another reported mammalian demethylase, which is primarily co-localised with nuclear speckles and affects mRNA export and RNA metabolism (Zheng et al., 2013). *Alkbh5* deficiency causes increased m^{6}A level and impaired spermatogenesis in mice (Zheng et al., 2013). Unlike FTO, ALKBH5 directly

reverses m^6A to adenosine with no detected intermediates (Fu Y et al., 2014; Yue et al., 2015). Given that FTO and ALKBH5 have diverse intracellular localisation and tissue distribution (FTO is also found in the cytosol and it is highly abundant in the brain and adipose tissue whereas *ALKBH5* is predominantly expressed in testes), they may act on different sets of transcripts (Maity and Das, 2016). To date, no FTO orthologues have been characterised in plants (Robbens et al., 2008; Jia et al., 2013). Phylogenetic analysis has predicted 13 ALKBH family proteins in *Arabidopsis*, which demonstrate diverse subcellular localisations (Mielecki et al., 2012). Recently, two *Arabidopsis* ALKBH proteins – ALKBH9B and ALKBH10B, have been characterised as plant m^6A demethylases. ALKBH9B catalyses the demethylation of m^6A present in viral genomes and affects virus infection while the demethylation activity of ALKBH10 stabilises key flowering-related genes, thereby promoting *Arabidopsis* floral transition (Duan et al., 2017; Martínez-Pérez et al., 2017). In addition, distinct m^6A demethylases may exist in plants.

1.5 m^6A RECOGNITION PROTEINS (m^6A READERS)

While m^6A methylases and demethylases dynamically regulate m^6A formation, RNA binding proteins that recognise m^6A (termed m^6A readers) are thought to decide the fate of m^6A methylated mRNAs (Yue et al., 2015; Burgess et al., 2016).

1.5.1 YTH Domain Proteins

In 2012, an RNA affinity chromatography approach using a methylated RNA bait and a control one followed by mass spectrometry identified two YTH (YT521-B homology) domain family proteins, YTHDF2 and YTHDF3, as novel m^6A binding proteins (Dominissini et al., 2012). The YTH domain was initially found by searching homologues of human splicing factor YT521-B (Stoilov et al., 2002). It contains 100-150 amino acid residues and is typical for eukaryotes and particularly abundant in plants (Stoilov et al., 2002). Structural analysis demonstrates that the YTH domain is predicted to comprise four α helices and six β strands with the conservation of aromatic residues within the β stands, which is reminiscent of structures of RNA recognition motif (RRM) and other RNA binding motifs (Zhang Z et al., 2010). Thus, the YTH domain is regarded as a novel RNA binding domain. To date, five YTH domain proteins – cytoplasmic YTHDF1-3 and nuclear YTHDC1 and YTHDC2 have been identified as mammalian m^6A readers (Xu et al., 2014).

Functions of these five human YTH domain proteins have been characterised in recent years. YTHDF2 recognises m^6A core consensus motif Gm^6AC and regulates mRNA degradation by transferring bound mRNA from the translatable pool to mRNA decay sites (Wang X et al., 2014). In contrast, YTHDF1 also binds to m^6A-modified mRNAs, but it promotes mRNA translation by interacting with translation initiation factors (Wang et al., 2015). YTHDC1 localises in a novel subnuclear domain, termed YT bodies (Nayler et al., 2000). It also selectively binds to m^6A-containing RNAs and the top binding motif of

YTHDC1 is GG(m^6A)C (Xu et al., 2014). YTHDC1 plays a primary role in mediating splicing (Xiao et al., 2016). Recently, functions of another two human YTH domain proteins (YTHDF3 and YTHDC2) have been elucidated. On the one hand, YTHDF3 acts in concert with YTHDF1 to promote translation, but on the other hand, it affects mRNA decay mediated through YTHDF2 (Shi et al., 2017). Similarly, YTHDC2 selectively binds m^6A at its consensus motif. It enhances the translation efficiency of its targets and also decreases their mRNA abundance, with critical functions in spermatogenesis (Hsu et al., 2017). Diverse and overlapping functions of the five human YTH domain proteins indicate that they work cooperatively to mediate mRNA metabolism and simultaneously they have their specific roles due to distinct sequence characteristics (Hsu et al., 2017; Shi et al., 2017).

Yeast methylated RNA-binding protein 1 (MRB1, also known as Ydr374c, Pho92), the homologue of human YTHDF2, is the only protein possessing the YTH domain and reported as an m^6A recognition protein in yeast (Schwartz et al., 2013; Kang et al., 2014). *MRB1* is expressed in a meiosis-specific manner, which is consistent with the meiosis-restricted methylation, and deletion of MRB1 leads to defects in meiotic progression (Schwartz et al., 2013). A structural and biochemical study using *Zygosaccharomyces rouxii* elucidates how m^6A modification is being recognised by MRB1. MRB1 forms a complex with a heptaribonucleotide and the m^6A modification is recognized and sandwiched by an aromatic cage. Mutations of YTH domain residues in the RNA binding site can abolish the formation of the complex (Luo and Tong, 2014). *Drosophila* YTH domain protein, YT521-B, is confirmed to bind m^6A and is

involved in m^{6}A-depedent splicing in sex determination (Lence et al., 2016; Kan et al., 2017).

While there are five proteins containing the YTH domain in human cells, there are 13 predicted proteins possessing the YTH domain in *Arabidopsis* and 12 predicted YTH domain proteins in rice (Li et al., 2014). One *Arabidopsis* YTH domain protein has been tested and it can bind to single-stranded RNAs *in vitro* (Li et al., 2014). Both *Arabidopsis* and rice YTH domain proteins demonstrate diverse tissue- and development-specific expression patterns, opening the possibility for complex post-transcriptional gene regulatory mechanisms (Li et al., 2014; Fray and Simpson, 2015). One relatively well characterised YTH domain protein in *Arabidopsis* is the orthologue of the 30-kD subunit of the mammalian Cleavage and Polyadenylation Specificity Factor 30 (CPSF30, AT1G30460) (Fray and Simpson, 2015). It is an RNA binding protein and is required for polyadenylation and 3' end formation (Delaney et al., 2006; Thomas et al., 2012). Interestingly, the YTH domain of *Arabidopsis* CPSF30 only presents in its full-length transcript owing to two different alternative polyadenylation patterns of *CPSF30* pre-mRNAs (Delaney et al., 2006; Zhang et al., 2008). However, the capacity of binding m^{6}A through plant YTH domain proteins, including known CPSF30, is completely unknown so far.

1.5.2 Other Candidate m^{6}A Readers

In addition to the YTH domain proteins, another RNA-binding protein, human antigen R, HuR (also known as ELAVL1), has also been identified as a potential

m^{6}A recognition protein in a pull-down assay using an m^{6}A-containing bait (Dominissini et al., 2012). Further analysis of HuR binding sites and m^{6}A deposition sites reveals that the majority of HuR binding sites are about 100-nt away from the m^{6}A site, suggesting HuR may indirectly (through other proteins or mRNA structure changes) interact with m^{6}A if it associates with m^{6}A (Chen K et al., 2015).

Most recently, three members of the heterogeneous nuclear ribonucleoprotein (HNRNP) family were shown to be another set of m^{6}A readers, including HNRNPA2B1 involved in mediating primary microRNA (pri-miRNAs) processing, HNRNPC and HNRNPG in recognising RNAs with altered structures by the m^{6}A mark (Alarcón et al., 2015a; Liu et al., 2015; 2017). In addition, m^{6}A located in the 5' UTR can directly bind eukaryotic initiation factor 3 (eIF3) to promote cap-independent translation (Meyer et al., 2015). Functions of m^{6}A involving these proteins are discussed in detail below in 1.6.1.

Overall, m^{6}A metabolism is dynamically regulated by its writers (the MTase components), erasers (m^{6}A demethylases) and readers (m^{6}A recognition proteins) (Table 1.1). m^{6}A modification exerts its functions by affecting RNA structure, protein-RNA interactions or being directly recognised by m^{6}A recognition proteins to induce subsequent reactions to modulate the fate of a target mRNA (Fu Y et al., 2014; Cao et al., 2016; Wang and Zhao, 2016). Discovery of more m^{6}A recognition proteins will shed new light on the understanding of dynamic regulation and various functions of m^{6}A modification via its recognition proteins.

Table 1.1 Proteins involved in m^6A mRNA methylation

Categories	Organism	Protein name	Known interacting m^6A components	References
m^6A writers	Mammals	METTL3	METTL14, WTAP	Bokar et al., 1994, 1997; Liu et al., 2014; Ping et al., 2014
		METTL14	METTL3, WTAP	Bujnicki et al., 2002; Liu et al., 2014; Ping et al., 2014; Wang Y et al., 2014
		WTAP	METTL3, METTL14, Virilizer, RBM15, Hakai	Horiuchi et al., 2013; Liu et al., 2014; Ping et al., 2014
		Virilizer	–	Schwartz et al., 2014b
		RBM15/ 15B	METTL3	Patil et al., 2016
	Arabidopsis	MTA	FIP37	Zhong et al., 2008
		MTB	–	Bujnicki et al., 2002; Růžička et al., 2017
		FIP37	MTA	Zhong et al., 2008
		Virilizer	MTB, FIP37, Hakai	Růžička et al., 2017
		Hakai	–	Růžička et al., 2017
	Drosophila	Ime4	METTL14, Fl(2)d	Hongay and Orr-Weaver, 2011; Kan et al., 2017
		METTL14	Ime4, Fl(2)d	Lence et al., 2016; Kan et al., 2017
		Fl(2)d	Ime4, METTL14	Lence et al., 2016; Kan et al., 2017
		Virilizer	Fl(2)d	Ortega et al., 2003; Lence et al., 2016
		Spenito	Ime4, METTL14, Fl(2)d	Lence et al., 2016; Kan et al., 2017
	Yeast	Ime4	Mum2, Slz1	Agarwala et al., 2012
		Mum2	Ime4	Agarwala et al., 2012; Schwartz et al., 2013
		Slz1	Ime4, Ime1	Agarwala et al., 2012; Schwartz et al., 2013
m^6A erasers	Mammals	FTO	–	Jia et al., 2011
		ALKBH5	–	Zheng et al., 2013
	Arabidopsis	ALKBH9B	–	Martínez-Pérez et al., 2017
		ALKBH10B	–	Duan et al., 2017
m^6A readers	Mammals	YTHDF1	–	Wang et al., 2015
		YTHDF2	–	Wang X et al., 2014
		YTHDF3	–	Shi et al., 2017
		YTHDC1	–	Xu et al., 2014
		YTHDC2	–	Hsu et al., 2017
		ELAVL1	–	Dominissini et al., 2012; Chen K et al., 2015
		HNRNPA2B1	–	Alarcón et al., 2015a
		HNRNPC	–	Liu et al., 2015
		HNRNPG	–	Liu et al., 2017
	Yeast	MRB1	–	Schwartz et al., 2013

Note: – represents unknown interactions.

1.6 FUNCTIONS OF m^6A MODIFICATION

Early in the 1990s, some studies implicated m^6A being involved in regulating mRNA metabolism (Bokar et al., 1997). To date, many studies of proteins involved in dynamic mRNA m^6A formation and regulation have revealed the regulatory roles of m^6A in RNA metabolism (including mRNA stability, pre-mRNA processing, nuclear export, translation, RNA structures and other types of RNAs, etc.). Consequently, affected molecular processes influence multiple biological processes in different eukaryotic organisms.

1.6.1 Molecular Effects of m^6A Modification

1.6.1.1 m^6A affects mRNA stability and gene expression

Transcriptome-wide sequencing data indicate an overall negative impact of m^6A modification on mRNA stability and gene expression in mammals (Schwartz et al., 2014b; Geula et al., 2015; Molinie et al., 2016). Consistently, knockdown of METTL3, METTTL14 or WTAP in human cells leads to noticeably increased expression of their m^6A target transcripts compared with that of all transcripts. Additionally, the reduced global m^6A methylation increases the lifetime of nascent RNAs (Liu et al., 2014). Knockdown of METTL3 or METTL14 in mouse embryonic stem cells (mESCs) results in downregulation of most pluripotency factors and upregulation of some developmental factors. Moreover, METTL3 or METTL14 targets demonstrate increased RNA stability in METTL3 or METTL14 knockdown cells (Wang Y, et al., 2014). Further

analysis shows that loss of m^6A methylation enhances the RNA binding ability of HuR (a RNA stabiliser) to increase RNA stability, suggesting the presence of m^6A methylation on some transcripts in mESCs, particularly those encoding developmental regulators, blocks HuR binding and destabilises them to maintain the mESCs at their ground state (Wang Y, et al., 2014). A very recent study also demonstrates that in both human Hela cells and mESCs, mRNAs containing m^6A modifications have shorter half-lives but many of these mRNAs have increased half-lives in *mettl3* knockout cells (Ke et al., 2017).

As mentioned in 1.5.1, YTHDF2 is involved in destabilising m^6A-containing mRNAs. YTHDF2 binds to m^6A through the carboxy-terminal YTH domain and localises the recognised mRNA to cellular RNA decay sites (e.g., processing bodies) through its amino-terminal domain (Wang X et al., 2014). Du et al. (2016) discovered that the degradation following the recognition of m^6A-containing mRNAs by YTHDF2 is due to YTHDF2 recruiting the CCR4-NOT deadenylase complex through a direct interaction between the YTHDF2 N-terminal region and the SH domain of the CNOT1 subunit, leading to the deadenylation of m^6A-containing mRNAs by two deadenylase subunits CAF1 and CCR4. Thus, both of the above two studies reveal how YTHDF2 is involved in mRNA degradation, albeit using two different underlying pathways.

Collectively, m^6A modifications in mammals are generally inversely correlated with mRNA stability and gene expression but this may not be the case for some specific transcripts. Distinct from mammalian high-throughput sequencing data, m^6A-seq in *Arabidopsis* demonstrates a positive correlation between m^6A

modification and mRNA abundance (Luo et al., 2014). However, another study investigating the function of *Arabidopsis* FIP37 in shoot stem cell development shows that m^{6}A modifications on key shoot meristem genes inversely correlate with mRNA stability to prevent shoot meristem over-proliferation (Shen et al., 2016). Therefore, the contrary findings about the influence of m^{6}A on mRNA stability and gene expression may reflect genome-wide versus gene-specific effects both in mammals and plants (Wang and Zhao, 2016).

1.6.1.2 m^{6}A affects alternative splicing

The localisation of m^{6}A-related proteins, including METTL3, METTL14, WTAP, Virilizer, FTO and ALKBH5, in nuclear speckles, suggests a possible role of m^{6}A in regulating splicing/alternative splicing (Bokar et al., 1997; Jia et al., 2011; Horiuchi et al., 2013; Zheng et al., 2013; Ping et al., 2014). Among the m^{6}A-related proteins mentioned above, METTL14 is reported to co-localise well with the pre-mRNA splicing factor SC35 (serine/arginine-rich splicing factor 2) in nuclear speckles (Ping et al., 2014); FTO partially co-localises with not only SC35, but also other splicing or splicing-related speckle factors – SART1 (U4/U6.U5 tri-snRNP-associated protein 1) and RNA polymerase II phosphorylated at Ser2 (Pol II-S2P) (Jia et al., 2011); ALKBH5 co-localises with splicing factors SC35, SM (Smith antigen) and ASF/SF2 (alternative splicing factor/splicing factor 2) in nuclear speckles (Zheng et al., 2013).

Transcriptome-wide characterisation of m^{6}A modification shows that m^{6}A-containing transcripts tend to have more isoforms and differentially spliced

exons and introns possess significantly more m^{6}A modifications (Dominisinni et al., 2012). In agreement with this, the majority of mRNAs bound by METTL3 or WTAP are derived from multi-isoform genes (Ping et al., 2014). m^{6}A demethylase FTO also demonstrates a regulatory role in alternative splicing (Zhao et al., 2014; Bartosovic et al., 2017). FTO depletion in mouse pre-adipocyte cells enhances the RNA binding ability of pre-mRNA splicing factor serine/arginine-rich (SR) protein SRSF2, which may lead to increased inclusion of target exons (Zhao et al., 2014). However, a parallel study in human cells shows prevalent exon skipping events upon FTO knockdown (Bartosovic et al., 2017). Authors of the latter study regard this opposite trend as a result of FTO target sites bound by different splicing factors depending on the cellular and mRNA context (Bartosovic et al., 2017). Human cells depleted of a novel m^{6}A reader, HNRNPA2B1, exhibit similar alternative splicing patterns as that in METTL3 knockdown cells (Alarcón et al., 2015a). As an alternative splicing-related factor, YTHDC1 is shown to regulate splicing by promoting exon inclusion of targeted mRNAs through facilitating SRSF3 while blocking SRSF10 mRNA binding and this regulation is in an m^{6}A-dependent manner (Zhang B et al., 2010; Xiao et al., 2016).

In *Drosophila*, three recent studies all point out that *Sxl* is a major intronic m^{6}A target and m^{6}A is required for female-specific *Sxl* splicing (Haussmann et al., 2016; Lence et al., 2016; Kan et al., 2017). *Drosophila* female-specific *Sxl* splicing is affected in multiple m^{6}A pathway mutants. In contrast, overexpression of YT521-B, a *Drosophila* m^{6}A reader which plays an important

role in regulating m^{6}A-dependent *Sxl* splicing, can induce female-specific *Sxl* splicing (Kan et al., 2017).

In *Arabidopsis*, though the orthologue of *Drosophila* sex-specific splicing factor Fl(2)d, FIP37, has been proved to be a member of *Arabidopsis* MTase complex, there are no pronounced differences in all alternative splicing events between the wild type (WT) and homozygous *fip37* mutant – *fip37-4* complemented with *LEC1*:*FIP37* transgene (*FIP37* coding sequence driven by embryo-specific *LEC1* promoter) (Shen et al., 2016). However, the same *fip37* mutant we are using as that described in Shen et al. (2016) is not lethal when homozygous. Therefore, the possible role of FIP37 and plant m^{6}A in alternative splicing warrants further investigation.

1.6.1.3 m^{6}A affects alternative polyadenylation

Across the plant and animal kindoms, m^{6}A is predominantly enriched in 3' UTRs, implicating its possible role in regulating 3' end formation of transcripts. A correlation between m^{6}A modification and alternative polyadenylation (APA) comes from studies involving two recently developed m^{6}A sequencing methods – m^{6}A-CLIP and m^{6}A-LAIC-seq (Ke et al., 2015; Molinie et al., 2016). The former sequencing data demonstrate that in human brain and liver cells, transcripts with APA usage preferentially use distal poly(A) sites and the simultaneous knockdown of METTL3, METTL14 and WTAP results in that approximately two thirds of transcripts with altered APA usage switch to proximal poly(A) sites, suggesting some of the m^{6}As in 3' UTRs inhibit the usage

of proximal APA sites (Ke et al., 2015). In contrast, the latter study reveals that m^6A methylated transcripts tend to be coupled with proximal APA site usage whereas nonmethylated transcripts tend to use distal APA sites (Molinie et al., 2016). A very recent study about the function of FTO supports the former study (Bartosovic et al., 2017). FTO knockdown cells show pronouncedly higher usage of distal APAs relative to the control cells, indicating FTO promotes the usage of proximal APAs in a subset of genes (Bartosovic et al., 2017). Since all of these studies give only the global tendency of APA patterns by comparing different sets of transcripts and the regulatory mechanisms remain undetermined, more work needs to be carried out to reach a conclusion about the role of m^6A modification in mediating APA.

In plants, though no reported studies have investigated the correlation between m^6A and APA, it is still possible that m^6A modification in plants may participate in regulating 3' end formation of transcripts (Fray and Simpson, 2015). This is because FPA, *Arabidopsis* homologue of a novel member of the MTase complex – human RBM15 and *Drosophila* Spenito, is associated with APA in flowering time control. In addition, one of the YTH domain proteins in *Arabidopsis*, CPSF30, plays a crucial role in cleavage and polyadenylation.

1.6.1.4 m^6A affects mRNA export

As a connection between pre-mRNA processing in the nucleus and translation in the cytoplasm, mRNA export from the nucleus is also crucial for modulating gene expression and protein functions (Zhao et al., 2017a). Knockdown of

METTL3 results in a delay in the exit of mature *Per2* and *Arntl* mRNAs (which function in regulating the circadian clock) from the nucleus to the cytoplasm (Fustin et al., 2013). Consistently, ALKBH5-deficient cells demonstrate accelerated nuclear mRNA export (Zheng et al., 2013). Due to accelerated nuclear RNA export, cytoplasmic mRNA level is significantly increased in ALKBH5-deficient cells and only overexpression of the WT *ALKBH5*, rather than demethylation-inactive mutant can rescue this accelerated mRNA export from the nucleus, suggesting ALKBH5 regulates mRNA export mainly through its demethylation activity (Zheng et al., 2013). Further investigation showed that ALKBH5 co-localises with splicing factor ASF/SF2, whose phosphorylation status facilitates nuclear mRNA export. The knockdown of ALKBH5 decreases the level of ASF/SF2 in a demethylation-dependent manner. Moreover, ALKBH5 deficiency causes SRPK1, one of the main kinases responsible for the phosphorylation of ASF/SF2, to re-localise from nucleic locations to cytoplasm and only WT *ALKBH5* can rescue its native nuclear localisation (Zheng et al., 2013). In summary, studies to date in mammals suggest that m^6A modification generally promotes mRNA export from the nucleus to the cytoplasm.

1.6.1.5 m^6A affects translation

Recent studies have shown that m^6A modification enhances translation through several mechanisms. Firstly, m^6A reader YTHDF1 promotes mRNA translation by interacting with translation initiation factors (e.g., eukaryotic initiation factor 3, eIF3) and this promotion effect is m^6A-dependent (Wang et al., 2015). In addition, YTHDF3 and YTHDC2 can also accelerate translation (Hsu et al.,

2017; Shi et al., 2017). Aside from translation promotion via YTH domain proteins, 5' UTR m^6A can facilitate cap-independent translation under stresses (Meyer et al., 2015; Zhou et al., 2015). 5' UTR m^6A can directly bind eIF3, which is sufficient to recruit the 43S complex to initiate translation independently of the cap binding protein eIF4E (Meyer et al., 2015). The underlying mechanism is that stress-induced nuclear relocalisation of YTHDF2 preserves 5' UTR methylation of stress-induced transcripts by minimising the m^6A demethylation by FTO and increased 5' UTR m^6A enables translation initiation independently of 5' cap (Zhou et al., 2015). Another report shows that METTL3 directly promotes translation of oncogenes by recruiting eIF3 to the translation initiation complex, independently of its methyltransferase activity or m^6A recognition proteins (Lin et al., 2016). Interestingly, a recent study reveals that METTL3/METTL14-mediated m^6A modification and NSUN2-mediated m^5C formation at the 3' UTR of *p21* cooperatively enhance *p21* mRNA translation (Li Q et al., 2017). p21 is a universal inhibitor of cyclin-dependent kinase and its increased expression contributes to the growth arrest under stresses (Xiong et al., 1993; Li Q et al., 2017). The enhanced translation of p21 mediated by m^6A and m^5C modifications consequently promote oxidative stress-induced cellular senescence (Li Q et al., 2017). Taken together, these above studies indicate that m^6A modification promotes mRNA translation in mammals, though it is not clear whether or how these mechanisms coexist in human cells (Wang and Zhao, 2016). In yeast, there is also a positive correlation between the presence of m^6A and mRNA translation efficiency (Bodi et al., 2015).

1.6.1.6 m^{6}A modulates RNA structures

Early in 2005, a hypothesis was put forward that RNA secondary structure may affect efficient m^{6}A formation and m^{6}A sites may lie within the loop of a stem-loop structure (Bokar, 2005). Secondary structure strength assay using m^{6}A-seq data in yeast reveals that methylated sites are significantly less structured (Schwartz et al., 2013). Two structural studies both *in vitro* and *in vivo* demonstrate that RNA structures containing m^{6}A modification tend to be single-stranded and m^{6}A sites in RNA duplexes may destabilise the local structure (Roost et al., 2015; Spitale et al., 2015). Furthermore, m^{6}A modification may trigger conformation changes because the methyl group of m^{6}A must rotate to the major groove of the paired helix to fit into the local conformation (Roost et al., 2015). Zou et al. (2016) showed that m^{6}A itself serves as a "conformational marker", which induces different conformational outcomes in RNAs depending on the sequence context. As a consequence, this allows m^{6}A recognition proteins, e.g., FTO and ALKBH5, to distinguish m^{6}A from other substrates with similar nucleotide sequences (Zou et al., 2016). A recent support for the role of m^{6}A in altering the RNA structure and further affecting RNA-protein interactions come from two studies about HNRNPs that are responsible for pre-mRNA processing (Liu et al., 2015, 2017). m^{6}A alters the RNA structure and increases the accessibility of RNA binding motifs nearby (termed the m^{6}A-switch), which facilitates the binding of HNRNPC and HNRNPG to m^{6}A-methylated RNA targets (Liu et al., 2015, 2017). Additionally, the RNA-protein interactions regulated through the m^{6}A-switch affect the expression and alternative splicing patterns of target mRNAs (Liu et al., 2015, 2017). Overall, m^{6}A can not only

remodel the RNA structure and conformation, but can also function as a switch to affect RNA-protein interactions.

1.6.1.7 m^{6}A in mRNAs influences other types of RNAs

As both m^{6}A and microRNA (miRNA) target sites are enriched in 3' UTRs, it is possible that m^{6}A influences the function of microRNA and vice versa (Meyer et al., 2012). The first MeRIP-seq data revealed that 67% of m^{6}A-containing 3' UTRs also contain at least one predicted miRNA-binding site, whilst most highly expressed miRNAs have a significantly greater percentage of target transcripts that contain m^{6}A (Meyer et al., 2012). Ke et al. (2015) also discovered an overlap of m^{6}A sites with Agonaute protein binding sites in 3' UTRs. Argonaute proteins are key players in gene-silencing pathways guided by small RNAs including miRNAs (Höck and Meister, 2008; Hutvagner and Simard, 2008). Consistent with these transcriptome-wide sequencing data, in METTL3 or METTL14 knockdown mESCs, a miRNA target, Igfbp, demonstrates a significantly decreased binding by argonaute 2 (Ago2), a key factor of the RNA-induced silencing complex (Wang Y et al., 2014). Alarcón et al. (2015a,b) discovered a machinery whereby m^{6}A influences the processing of pri-miRNAs. The processing of pri-miRNAs starts with the recognition of the junction between the stem and the flanking single-stranded RNA of the pri-miRNA hairpin by a RNA-binding protein DGCR8. METTL3-dependent m^{6}A modification on pri-miRNAs acts like a marker to allow for the effective recognition of pri-miRNAs by DGCR8 to promote the initiation of miRNA biogenesis (Alarcón et al., 2015b). Their further investigation shows that a nuclear RNA-binding protein

HNRNPA2B1 functions as an m^6A reader to recognise m^6A-marked pri-miRNAs and interacts with DGCR8 as well to facilitate this process (Alarcón et al., 2015a). Similarly, METTL14 is reported to enhance the processing of pri-miRNA 126 by facilitating the recognition and binding of DGCR8 to pri-miRNA 126 (Ma et al., 2017).

Consistent with the hypothesis by Meyer et al. (2012), Chen T et al. (2015) uncovered a role of miRNAs in regulating m^6A formation in mRNAs. They found that m^6A peaks are enriched at miRNA target sites and an endonuclease responsible for miRNA maturation, Dicer, participates in regulating the formation of m^6A. Though Dicer has no direct interaction with METTL3, it regulates the binding of METTL3 to mRNAs (Chen T et al., 2015).

Apart from miRNAs, m^6A has also been shown to regulate functions of other types of RNAs, including lncRNAs and tRNAs. In human cells, lncRNA *XIST* is highly methylated and knockdown of m^6A writer proteins METTL3 or RBM15/15B impairs the gene silencing mediated by *XIST* on the X chromosome. Moreover, YTHDC1 is required for the recognition of m^6A on *XIST* and the normal function of *XIST* (Patil et al., 2016). Though in mammals m^6A modification is implicated in promoting mRNA export and translation, in the case of *XIST*, it is likely that other chemical modifications and/or RNA binding proteins prevent its export from the nuclear. Using an *Escherichia coli* translation system, Choi et al. (2016) found that m^6A modification of mRNA acts as a barrier to tRNA accommodation and translation elongation by perturbing the interaction between a near-cognate codon and tRNA. Very

recently, m^{6}A has also been shown to exist in circular RNAs (circRNAs) (Zhou et al., 2017). m^{6}A modification in circRNAs and mRNAs share the same m^{6}A writers (METTL3 and METTL14) and m^{6}A readers (YTHDF1 and YTHDF2). In addition, m^{6}A-containing circRNAs may be associated with mRNA stability mediated by YTHDF2 due to the discovery that m^{6}A-containing mRNAs encoded by the parent genes of m^{6}A-containing circRNAs have shorter half-lives among all m^{6}A-modified mRNAs (Zhou et al., 2017).

1.6.2 Biological Consequences of m^{6}A Modification

1.6.2.1 Viability and reproductive development

Functional analysis of proteins relevant to m^{6}A formation and regulation reveals that m^{6}A is crucial for viability and reproductive development across diverse species in eukaryotes. Loss of METTL3 in human cells leads to apoptosis and complete knockout of METTL3 in mice is lethal (Bokar, 2005; Dominissini et al., 2012; Liu et al., 2014; Geula et al., 2015). Mutation of the catalytic residue of Ime4 leads to several sporulation defects in yeast (Clancy et al., 2002; Bodi et al., 2010). In *Arabidopsis*, *MTA* expression is strongly associated with dividing tissues, particularly reproductive organs, shoot meristems, and emerging lateral roots. Inactivation of *Arabidopsis* MTA results in failure of the developing embryo to progress past the globular stage (Zhong et al., 2008). In *Drosophila*, *Dm Ime4* is expressed in ovaries and testes and the lethality caused by loss of this gene can be fully rescued by a wild-type transgenic copy of *Dm Ime4* (Hongay and Orr-Weaver, 2011), though three recent papers report that

Drosophila lacking Ime4 can survive but demonstrates multiple developmental and behavioural defects, such as flightless and affected locomotion (Haussmann et al., 2016; Lence et al., 2016; Kan et al., 2017).

Likewise, deficiency of m^6A-related proteins except for METTL3 and its orthologues also results in viability or reproductive defects. Knockdown of METTL14 or WTAP also leads to cell death in human Hela cells (Liu et al., 2014). The loss-of-function of MTB, FIP37 and Virilizer in *Arabidopsis* are also embryonic lethal (Vespa et al., 2004; Bodi et al., 2012; Růžička et al., 2017). In *Drosophila*, although knockout of Ime4 is now found not to be lethal, the loss of other m^6A writer components related to splicing, including Fl(2)d, Virilizer and Spenito, is lethal (Kan et al., 2017). In addition, ALKBH5 is found to be associated with male fertility in mice. *ALKBH5* mRNA shows the highest expression in testes and mice deficient in ALKBH5 have noticeably smaller testes and demonstrate compromised spermatogenesis (Zheng et al., 2013). In zebrafish, m^6A modification is required for its maternal-to-zygotic transition wherein maternal mRNAs marked with m^6A modification are recognised by YTHDF2 and this facilitates the clearance of methylated maternal mRNAs and the activation of zygotic transcripts (Zhao et al., 2017b).

1.6.2.2 Embryonic stem cell development

Recent studies proposed that m^6A modification is also involved in ESC development and somatic cell reprogramming (Batista et al., 2014; Wang Y et al., 2014; Aguilo et al., 2015; Chen T et al., 2015; Geula et al., 2015). The ESCs

reside in a “naïve” pluripotent state while epiblast stem cells (EpiSCs), derived from the post-implantation epiblast, resemble an advanced developmental stage, which are “primed” for differentiation (Geula et al., 2015). The transition from naïve pluripotency to differentiation is precisely regulated by a number of pluripotency markers and developmental factors (Yue et al., 2015). Knockdown of METTL3 or METTL14 in mESCs leads to loss of self-renewal capability (Wang Y et al., 2014). Consistently, inhibition of m^6A formation by knocking down *METTL3* expression hinders the reprogramming of mouse embryonic fibroblasts (MEFs) while overexpression of *METTL3* promotes the reprogramming efficiency (Chen T et al., 2015). However, some other studies have reached contrary conclusions with regard to the regulatory role of m^6A in stem cell development. Batista et al. (2014) and Geula et al. (2015) showed that complete knockout of METTL3 in mESCs causes the disruption of priming and differentiation capability and leads to a “hyper”-naïve pluripotent state (Batista et al., 2014; Geula et al., 2015). Similarly, knockdown of METTL3 or METTL14 in human glioblastoma stem cell (GSC) promotes GSC growth and self-renewal (Cui et al., 2017). The mechanistic differences underlying the conflicting phenotypes are that Wang’s data show that developmental regulators are more highly enriched in m^6A methylation than the pluripotency factors and most pluripotency factors are downregulated whereas some developmental regulators are significantly upregulated upon METTL3 or METTL14 knockdown (Wang Y et al., 2014); however, the study by Geula et al. (2015) demonstrates the opposite tendency: 80% of naïve pluripotency-promoting genes are modified with m^6A and knockout of METTL3 results in increased transcript level of pluripotency-promoting genes.

Recent studies show that the chromatin-associated zinc finger protein 217 (ZFP217) and miRNAs regulate m^6A modification in the pluripotency of ESCs and somatic cell reprogramming (Aguilo et al., 2015; Chen T et al., 2015). ZFP217 positively regulates ESC transcriptome and prevents the methylation of the core pluripotency and reprogramming factors by sequestering METTL3 (Aguilo et al., 2015). miRNAs regulate the activity of METTL3 by modulating its binding to mRNAs and increased m^6A abundance promotes the reprogramming of MEFs to pluripotent stem cells (Chen T et al., 2015). Collectively, m^6A modification is required for well-tuned stem cell development in mammals.

As mentioned earlier, m^6A modification in plants is also essential for embryo development because homozygous knockout of MTA, MTB, FIP37 or Virilizer in *Arabidopsis* is embryonic lethal (Vespa et al., 2004; Zhong et al., 2008; Bodi et al., 2012; Růžička et al., 2017). Shen et al. (2016) further revealed that FIP37-dependent m^6A modification prevents the over-proliferation of shoot meristem by confining the expression of two key shoot apical meristem regulators, *WUSCHEL* (*WUS*) and *SHOOTMERISTEMLESS* (*STM*).

1.6.2.3 Other growth and development processes

In addition to biological processes mentioned above, m^6A modification is also required for other growth and development processes. In mammals, m^6A modification is shown to be involved in controlling the circadian period, which is crucial for regulating many biological processes (Fustin et al., 2013). Silencing

of human METTL3 causes circadian period elongation, mainly because of RNA processing delay (Fustin et al., 2013). In addition, m^6A modification is involved in the mediation of human health and diseases, particularly cancer cell development. As an obesity-related protein, FTO-dependent m^6A demethylation is crucial for preadipocyte differentiation by controlling the splicing of adipogenic regulatory factor RUNX1T1 during adipogenesis (Zhao et al., 2014. Zhang et al., 2015). Moreover, FTO is also required for neurogenesis and its deficiency leads to impaired learning and memory (Li L et al., 2017).

Recently, increasingly more papers have reported the correlation of m^6A modification with cancer. For example, decreased m^6A modification by knocking down METTL3 or METTL14 promotes human glioblastoma stem cell (GSC) growth, self-renewal, and tumorigenesis while inhibition of FTO or ALKBH5 suppresses the proliferation of GSCs (Cui et al., 2017; Zhang et al., 2017); In hepatocellular carcinoma, the expression of METTL14 is down-regulated and m^6A modification is decreased in metastatic tumors compared with nonmetastatic tumors (Ma et al., 2017); In acute myeloid leukemia, FTO enhances leukemic oncogene-mediated cell transformation and leukemogenesis (Li Z et al., 2017); Knockdown of *ALKBH5* expression in human breast cancer cells significantly reduces their capacity for tumor initiation as a result of reduced numbers of breast cancer stem cells (Zhang et al., 2016). To summarise the findings in the above studies, the presence of m^6A suppresses the proliferation of cancer-related stem cells to reduce their capacity for tumorigenesis. Therefore, m^6A methylation machinery has been proposed to be a promising new therapeutic target for multiple kinds of cancers.

In *Drosophila*, the most important biological function of m^6A modification is that it is essential for sex determination via affecting female-specific *Sxl* splicing (Haussmann et al., 2016; Lence et al., 2016; Kan et al., 2017). In addition, m^6A and the expression of its writer components are enriched in the nervous system (Lence et al., 2016). Moreover, m^6A also participates in modulating adult behaviours due to the observations in *Drosophila* m^6A writer mutants: reduced lifespan, unable to fly, strongly compromised for negative geotaxis and mildly held-out wings (Lence et al., 2016; Kan et al., 2017).

In *Arabidopsis*, the lethality in homozygous *mta* mutant can be rescued by *MTA* cDNA under the embryo-specific *ABI3* promoter, which gives rise to surviving plants with reduced m^6A at the mature stage (termed ABI3A6 in this study) (Bodi et al., 2012). The ABI3A6 line demonstrates multiple developmental defects, including crinkled and bushy rosette leaves, shorter inflorescence internode lengths and abnormal flower architecture relative to the wild type (Bodi et al., 2012). In *Arabidopsis* roots, *MTA* promoter-activated *GUS* expression is primarily located in the lateral root initiation sites (Zhong et al., 2008), indicating that m^6A may be involved in regulating plant auxin response, because auxin is a key signal during lateral root initiation (Casimiro et al., 2003). However, the underlying mechanism of m^6A in affecting lateral root formation remains unknown.

1.6.2.4 Stress response

m^6A modification is also suggested to be involved in stress responses. Yeast meiosis and sporulation only occurs in the diploid under nutritional starvation and m^6A modification in yeast is confined to the meiosis process (Yamamoto et al., 1996; Bodi et al., 2010; Schwartz et al., 2013), indicating the positive correlation of m^6A with the response to nutrient deficiency in yeast. Bodi et al. (2015) revealed that mRNA methylation is enriched in transcripts occupying monosomal and polysomal fractions during meiosis induced by starvation. In *Arabidopsis*, RNA-seq of the low m^6A line ABI3A6 demonstrates that most of the up-regulated genes are involved in stress and stimulus responses, suggesting a role of m^6A in proper responses to stresses and stimuli (Bodi et al., 2012).

In mammals, the regulatory role of m^6A has been reported under several stress conditions. While investigating the transcriptome-wide deposition of m^6A in glioblastoma stem cells, Gene Ontology analysis shows that m^6A-methylated mRNAs are involved in DNA damage response and cellular stress response (Cui et al. 2017). A very recent study did show a positive role of m^6A in the UV-induced DNA damage response, involving immediate localisation of METTL3 to the damage sites and the recruitment of polymerase κ by METTL3 in the subsequent nucleotide excision repair (Xiang et al., 2017). In response to heat shock stress, m^6A in the 5' UTR promotes the translation of its target mRNAs, e.g., *Hsp70* (Meyer et al., 2015; Zhou et al., 2015). Similarly, m^6A and m^5C function in concert to accelerate p21 translation in oxidative stress-induced cellular senescence (Li Q et al., 2017). In hypoxic breast cancer stem cells,

ALKBH5-dependent m^6A demethylation enhances the expression of pluripotency-promoting gene *Nanog* and promotes the enrichment of breast cancer stem cells (Zhang et al., 2016). Aside from abiotic stresses, the m^6A level demonstrates a dramatic increase during HIV-1 infection in human cells, suggesting m^6A modification is required for HIV-1 replication (Lichinchi et al., 2016). In general, m^6A modification increases under multiple stresses, which is important for appropriate responses to stresses. However, it remains unclear whether m^6A plays a positive role in stress responses or it is a consequence of stress reactions.

1.7 PERSPECTIVES

In the past decade, emerging roles of m^6A mRNA modification participating in multiple molecular and biological processes have been proposed or verified, particularly in mammals. However, the underlying machineries remain poorly understood. In addition, it is not clear that phenotypes related to reduced m^6A modification directly result from a lack of methylation or are indirect consequences of other intermediary components (Maity and Das, 2016). In mammals, there are several conflicting and contradictory conclusions regarding functions of m^6A modification. These warrant further investigations to clarify the discrepancies. Nevertheless, the achievements in studies of mammalian m^6A modification provide some clues for studying the function of this RNA modification in plants: (1) Components of the MTase complex other than MTA, especially MTB, Virilizer and Hakai, should be well characterised. (2) The interactions between different members of the MTase complex need to be

assayed to better understand how this m^6A writer complex catalyse the formation of m^6A. (3) *Arabidopsis* possesses 13 proteins containing the YTH domain but their correlation with m^6A modification remains poorly understood. Moreover, more m^6A demethylases and new m^6A recognition proteins should be identified to further understand this dynamic RNA modification. (4) Specific roles of m^6A modification in plant differentiation should not be neglected, such as potential functions in regulating root development.

1.8 AIMS OF THE PROJECT

The aim of this project is to analyse the function of Hakai and interactions between different components involved in the MTase complex and to dissect the biological functions of m^6A in plants using low m^6A plants, focusing on the role of m^6A in root development.

1.9 REFERENCES

AGARWALA, S. D., BLITZBLAU, H. G., HOCHWAGEN, A. & FINK, G. R. 2012. RNA methylation by the MIS complex regulates a cell fate decision in yeast. PLoS Genetics, 8, e1002732.

AGRIS, P. F., SIERZPUTOWSKA-GRACZ, H. & SMITH, C. 1986. Transfer RNA contains sites of localized positive charge: carbon NMR studies of [^{13}C] methyl-enriched *Escherichia coli* and yeast tRNA^{Phe}. Biochemistry, 25, 5126-5131.

AGUILO, F., ZHANG, F., SANCHO, A., FIDALGO, M., DI CECILIA, S., VASHISHT, A., LEE, D.-F., CHEN, C.-H., RENGASAMY, M., ANDINO, B., et al. 2015. Coordination of m^{6}A mRNA methylation and gene transcription by ZFP217 regulates pluripotency and reprogramming. Cell Stem Cell, 17, 689-704.

ALARCÓN, C. R., GOODARZI, H., LEE, H., LIU, X., TAVAZOIE, S. & TAVAZOIE, S. F. 2015a. HNRNPA2B1 is a mediator of m^{6}A-dependent nuclear RNA processing events. Cell, 162, 1299-1308.

ALARCÓN, C. R., LEE, H., GOODARZI, H., HALBERG, N. & TAVAZOIE, S. F. 2015b. *N*^{6}-methyl-adenosine marks primary microRNAs for processing. Nature, 519, 482-485.

BAKIN, A. & OFENGAND, J. 1993. Four newly located pseudouridylate residues in *Escherichia coli* 23S ribosomal RNA are all at the peptidyltransferase center: analysis by the application of a new sequencing technique. Biochemistry, 32, 9754-9762.

BARTOSOVIC, M., MOLARES, H. C., GREGOROVA, P., HROSSOVA, D., KUDLA, G. & VANACOVA, S. 2017. N6-methyladenosine demethylase FTO

targets pre-mRNAs and regulates alternative splicing and 3'-end processing. Nucleic Acids Research.

BATISTA, P. J., MOLINIE, B., WANG, J., QU, K., ZHANG, J., LI, L., BOULEY, D. M., LUJAN, E., HADDAD, B., DANESHVAR, K., et al. 2014. m^6A RNA modification controls cell fate transition in mammalian embryonic stem cells. Cell Stem Cell, 15, 707-719.

BODI, Z., BOTTLEY, A., ARCHER, N., MAY, S. T. & FRAY, R. G. 2015. Yeast m^6A methylated mRNAs are enriched on translating ribosomes during meiosis, and under rapamycin treatment. PLoS One, 10, e0132090.

BODI, Z., BUTTON, J. D., GRIERSON, D. & FRAY, R. G. 2010. Yeast targets for mRNA methylation. Nucleic Acids Research, 38, 5327-5335.

BODI, Z., ZHONG, S., MEHRA, S., SONG, J., GRAHAM, N., LI, H., MAY, S. & FRAY, R. G. 2012. Adenosine methylation in *Arabidopsis* mRNA is associated with the 3′ end and reduced levels cause developmental defects. Frontiers in Plant Science, 3.

BOKAR, J. A. 2005. The biosynthesis and functional roles of methylated nucleosides in eukaryotic mRNA. In: GROSJEAN H. (Ed.) Fine-tuning of RNA functions by modification and editing, pp. 142-177. Springer.

BOKAR, J. A., RATH-SHAMBAUGH, M. E., LUDWICZAK, R., NARAYAN, P. & ROTTMAN, F. 1994. Characterization and partial purification of mRNA N^6-adenosine methyltransferase from HeLa cell nuclei. Internal mRNA methylation requires a multisubunit complex. Journal of Biological Chemistry, 269, 17697-17704.

BOKAR, J. A., SHAMBAUGH, M. E., POLAYES, D., MATERA, A. G. & ROTTMAN, F. M. 1997. Purification and cDNA cloning of the AdoMet-binding

subunit of the human mRNA (N^6-adenosine)-methyltransferase. RNA, 3, 1233-1247.

BUJNICKI, J. M., FEDER, M., RADLINSKA, M. & BLUMENTHAL, R. M. 2002. Structure prediction and phylogenetic analysis of a functionally diverse family of proteins homologous to the MT-A70 subunit of the human mRNA: m^6A methyltransferase. Journal of Molecular Evolution, 55, 431-444.

BURGESS, A., DAVID, R. & SEARLE, I. R. 2016. Deciphering the epitranscriptome: A green perspective. Journal of Integrative Plant Biology, 58, 822-835.

CAO, G., LI, H., YIN, Z. & FLAVELL, R. A. 2016. Recent advances in dynamic m^6A RNA modification. Open Biology, 6, 160003.

CARLILE, T. M., ROJAS-DURAN, M. F., ZINSHTEYN, B., SHIN, H., BARTOLI, K. M. & GILBERT, W. V. 2014. Pseudouridine profiling reveals regulated mRNA pseudouridylation in yeast and human cells. Nature, 515, 143-146.

CASIMIRO, I., BEECKMAN, T., GRAHAM, N., BHALERAO, R., ZHANG, H., CASERO, P., SANDBERG, G. & BENNETT, M. J. 2003. Dissecting *Arabidopsis* lateral root development. Trends in Plant Science, 8, 165-171.

CHEN, K., LU, Z., WANG, X., FU, Y., LUO, G. Z., LIU, N., HAN, D., DOMINISSINI, D., DAI, Q., PAN, T. & HE C. 2015. High-resolution N^6-methyladenosine (m^6A) map using photo-crosslinking-assisted m^6A sequencing. Angewandte Chemie International Edition, 54, 1587-1590.

CHEN, T., HAO, Y.-J., ZHANG, Y., LI, M.-M., WANG, M., HAN, W., WU, Y., LV, Y., HAO, J., WANG, L., et al. 2015. m^6A RNA methylation is regulated

by microRNAs and promotes reprogramming to pluripotency. Cell Stem Cell, 16, 289-301.

CHOI, J., IEONG, K.-W., DEMIRCI, H., CHEN, J., PETROV, A., PRABHAKAR, A., O'LEARY, S. E., DOMINISSINI, D., RECHAVI, G. & SOLTIS, S. M. 2016. N^6-methyladenosine in mRNA disrupts tRNA selection and translation elongation dynamics. Nature Structural & Molecular Biology, 23, 110-115.

CHURCH, C., MOIR, L., MCMURRAY, F., GIRARD, C., BANKS, G. T., TEBOUL, L., WELLS, S., BRÜNING, J. C., NOLAN, P. M., ASHCROFT, F. M. & COX R. G. 2010. Overexpression of *Fto* leads to increased food intake and results in obesity. Nature Genetics, 42, 1086-1092.

CLANCY, M. J., SHAMBAUGH, M. E., TIMPTE, C. S. & BOKAR, J. A. 2002. Induction of sporulation in *Saccharomyces cerevisiae* leads to the formation of N^6-methyladenosine in mRNA: a potential mechanism for the activity of the *IME4* gene. Nucleic Acids Research, 30, 4509-4518.

COHN, W. E. 1960. Pseudouridine, a carbon-carbon linked ribonucleoside in ribonucleic acids: isolation, structure, and chemical characteristics. Journal of Biological Chemistry, 235, 1488-1498.

CUI, Q., SHI, H., YE, P., LI, L., QU, Q., SUN, G., SUN, G., LU, Z., HUANG, Y., YANG, C., et al. 2017. m^6A RNA methylation regulates the self-renewal and tumorigenesis of glioblastoma stem cells. Cell Reports, 18, 2622-2634.

DAI, Q., FONG, R., SAIKIA, M., STEPHENSON, D., YU, Y.-T., PAN, T. & PICCIRILLI, J. A. 2007. Identification of recognition residues for ligation-based detection and quantitation of pseudouridine and N^6-methyladenosine. Nucleic Acids Research, 35, 6322-6329.

DELANEY, K. J., XU, R., ZHANG, J., LI, Q. Q., YUN, K.-Y., FALCONE, D. L. & HUNT, A. G. 2006. Calmodulin interacts with and regulates the RNA-binding activity of an Arabidopsis polyadenylation factor subunit. Plant Physiology, 140, 1507-1521.

DELATTE, B., WANG, F., NGOC, L. V., COLLIGNON, E., BONVIN, E., DEPLUS, R., CALONNE, E., HASSABI, B., PUTMANS, P., AWE, S. et al. 2016. Transcriptome-wide distribution and function of RNA hydroxymethylcytosine. Science, 351, 282-285.

DESROSIERS, R., FRIDERICI, K. & ROTTMAN, F. 1974. Identification of methylated nucleosides in messenger RNA from Novikoff hepatoma cells. Proceedings of the National Academy of Sciences, 71, 3971-3975.

DINA, C., MEYRE, D., GALLINA, S., DURAND, E., KÖRNER, A., JACOBSON, P., CARLSSON, L. M., KIESS, W., VATIN, V., LECOEUR, C., et al. 2007. Variation in *FTO* contributes to childhood obesity and severe adult obesity. Nature Genetics, 39, 724-726.

DOMINISSINI, D., MOSHITCH-MOSHKOVITZ, S., SCHWARTZ, S., SALMON-DIVON, M., UNGAR, L., OSENBERG, S., CESARKAS, K., JACOB-HIRSCH, J., AMARIGLIO, N., KUPIEC, M., et al. 2012. Topology of the human and mouse m^6A RNA methylomes revealed by m^6A-seq. Nature, 485, 201-206.

DOMINISSINI, D., NACHTERGAELE, S., MOSHITCH-MOSHKOVITZ, S., PEER, E., KOL, N., BEN-HAIM, M. S., DAI, Q., DI SEGNI, A., SALMON-DIVON, M., CLARK, W. C., et al. 2016. The dynamic N^1-methyladenosine methylome in eukaryotic messenger RNA. Nature, 530, 441-446.

DU, H., ZHAO, Y., HE, J., ZHANG, Y., XI, H., LIU, M., MA, J. & WU, L. 2016. YTHDF2 destabilizes m^{6}A-containing RNA through direct recruitment of the CCR4-NOT deadenylase complex. Nature Communications, 7.

DUAN, H.-C., WEI, L.-H., ZHANG, C., WANG, Y., CHEN, L., LU, Z., CHEN, P. R., HE, C. & JIA, G. 2017. ALKBH10B is an RNA *N*^{6}-methyladenosine demethylase affecting Arabidopsis floral transition. The Plant Cell, DOI: https://doi.org/10.1105/tpc.16.00912.

DUBIN, D. T. & TAYLOR, R. H. 1975. The methylation state of poly A-containing-messenger RNA from cultured hamster cells. Nucleic Acids Research, 2, 1653-1668.

FIGUEROA, A., FUJITA, Y. & GOROSPE, M. 2009a. Hacking RNA: Hakai promotes tumorigenesis by enhancing the RNA-binding function of PSF. Cell Cycle, 8, 3648-3651.

FIGUEROA, A., KOTANI, H., TODA, Y., MAZAN-MAMCZARZ, K., MUELLER, E.-C., OTTO, A., DISCH, L., NORMAN, M., RAMDASI, R. M., KESHTGAR, M., et al. 2009b. Novel roles of Hakai in cell proliferation and oncogenesis. Molecular Biology of the Cell, 20, 3533-3542.

FISCHER, J., KOCH, L., EMMERLING, C., VIERKOTTEN, J., PETERS, T., BRÜNING, J. C. & RÜTHER, U. 2009. Inactivation of the *Fto* gene protects from obesity. Nature, 458, 894-898.

FRAY, R. G. & SIMPSON, G. G. 2015. The Arabidopsis epitranscriptome. Current Opinion in Plant Biology, 27, 17-21.

FRAYLING, T. M., TIMPSON, N. J., WEEDON, M. N., ZEGGINI, E., FREATHY, R. M., LINDGREN, C. M., PERRY, J. R., ELLIOTT, K. S., LANGO, H., RAYNER, N. W., et al. 2007. A common variant in the *FTO* gene

is associated with body mass index and predisposes to childhood and adult obesity. Science, 316, 889-894.

FROMMER, M., MCDONALD, L. E., MILLAR, D. S., COLLIS, C. M., WATT, F., GRIGG, G. W., MOLLOY, P. L. & PAUL, C. L. 1992. A genomic sequencing protocol that yields a positive display of 5-methylcytosine residues in individual DNA strands. Proceedings of the National Academy of Sciences, 89, 1827-1831.

FU, L., GUERRERO, C. R., ZHONG, N., AMATO, N. J., LIU, Y., LIU, S., CAI, Q., JI, D., JIN, S.-G., NIEDERNHOFER, L. J., et al. 2014. Tet-mediated formation of 5-hydroxymethylcytosine in RNA. Journal of the American Chemistry Society, 136, 11582-11585.

FU, Y., DOMINISSINI, D., RECHAVI, G. & HE, C. 2014. Gene expression regulation mediated through reversible m^6A RNA methylation. Nature Reviews. Genetics, 15, 293-306.

FU, Y., JIA, G., PANG, X., WANG, R. N., WANG, X., LI, C. J., SMEMO, S., DAI, Q., BAILEY, K. A., NOBREGA, M. A., et al. 2013. FTO-mediated formation of N^6-hydroxymethyladenosine and N^6-formyladenosine in mammalian RNA. Nature Communications, 4, 1798.

FUJITA, Y., KRAUSE, G., SCHEFFNER, M., ZECHNER, D., LEDDY, H. E. M., BEHRENS, J., SOMMER, T. & BIRCHMEIER, W. 2002. Hakai, a c-Cbl-like protein, ubiquitinates and induces endocytosis of the E-cadherin complex. Nature Cell Biology, 4, 222-231.

FUSTIN, J.-M., DOI, M., YAMAGUCHI, Y., HIDA, H., NISHIMURA, S., YOSHIDA, M., ISAGAWA, T., MORIOKA, M. S., KAKEYA, H., MANABE,

I. & OKAMURA H. 2013. RNA-methylation-dependent RNA processing controls the speed of the circadian clock. Cell, 155, 793-806.

GERKEN, T., GIRARD, C. A., TUNG, Y.-C. L., WEBBY, C. J., SAUDEK, V., HEWITSON, K. S., YEO, G. S., MCDONOUGH, M. A., CUNLIFFE, S., MCNEILL, L. A., et al. 2007. The obesity-associated *FTO* gene encodes a 2-oxoglutarate-dependent nucleic acid demethylase. Science, 318, 1469-1472.

GEULA, S., MOSHITCH-MOSHKOVITZ, S., DOMINISSINI, D., MANSOUR, A. A., KOL, N., SALMON-DIVON, M., HERSHKOVITZ, V., PEER, E., MOR, N., MANOR, Y. S., et al. 2015. m^6A mRNA methylation facilitates resolution of naïve pluripotency toward differentiation. Science, 347, 1002-1006.

GOLOVINA, A. Y., DZAMA, M. M., PETRIUKOV, K. S., ZATSEPIN, T. S., SERGIEV, P. V., BOGDANOV, A. A. & DONTSOVA, O. A. 2013. Method for site-specific detection of m6A nucleoside presence in RNA based on high-resolution melting (HRM) analysis. Nucleic Acids Research, 42, e27.

GU, W., HURTO, R. L., HOPPER, A. K., GRAYHACK, E. J. & PHIZICKY, E. M. 2005. Depletion of *Saccharomyces cerevisiae* $tRNA^{His}$ guanylyltransferase Thg1p leads to uncharged $tRNA^{His}$ with additional m^5C. Molecular and Cellular Biology, 25, 8191-8201.

HARCOURT, E. M., EHRENSCHWENDER, T., BATISTA, P. J., CHANG, H. Y. & KOOL, E. T. 2013. Identification of a selective polymerase enables detection of N^6-methyladenosine in RNA. Journal of the American Chemical Society, 135, 19079-19082.

HARCOURT, E. M., KIETRYS, A. M. & KOOL, E. T. 2017. Chemical and structural effects of base modifications in messenger RNA. Nature, 541, 339-346.

HARPER, J. E., MICELI, S. M., ROBERTS, R. J. & MANLEY, J. L. 1990. Sequence specificity of the human mRNA N6-adenosine methylase *in vitro*. Nucleic Acids Research, 18, 5735-5741.

HAUENSCHILD, R., TSEROVSKI, L., SCHMID, K., THÜRING, K., WINZ, M.-L., SHARMA, S., ENTIAN, K.-D., WACHEUL, L., LAFONTAINE, D. L., ANDERSON, J., et al. 2015. The reverse transcription signature of *N*-1-methyladenosine in RNA-Seq is sequence dependent. Nucleic Acids Research, 43, 9950-9964.

HAUGLAND, R. A. & CLINE, M. G. 1980. Post-transcriptional modifications of oat coleoptile ribonucleic acids. 5'-terminal capping and methylation of internal nucleosides in poly (A) RNA, The FEBS Journal, 104, 271-277.

HAUSSMANN, I. U., BODI, Z., SANCHEZ-MORAN, E., MONGAN, N. P., ARCHER, N., FRAY, R. G. & SOLLER, M. 2016. m^6A potentiates Sxl alternative pre-mRNA splicing for robust *Drosophila* sex determination. Nature, 540, 301-304.

HELM, M. & MOTORIN, Y. 2017. Detecting RNA modifications in the epitranscriptome: predict and validate. Nature Reviews Genetics, 18, 275-291.

HELM, M. 2006. Post-transcriptional nucleotide modification and alternative folding of RNA. Nucleic Acids Research, 34, 721-733.

HELM, M., GIEGÉ, R. & FLORENTZ, C. 1999. A Watson-Crick base-pair-disrupting methyl group (m^1A9) is sufficient for cloverleaf folding of Human mitochondrial $tRNA^{Lys}$. Biochemistry, 38, 13338-13346.

HESS, M. E. & BRÜNING, J. C. 2014. The fat mass and obesity-associated (*FTO*) gene: obesity and beyond? Biochimica et Biophysica Acta, 1842, 2039-2047.

HESS, M. E., HESS, S., MEYER, K. D., VERHAGEN, L. A., KOCH, L., BRÖNNEKE, H. S., DIETRICH, M. O., JORDAN, S. D., SALETORE, Y., ELEMENTO, O., et al. 2013. The fat mass and obesity associated gene (*Fto*) regulates activity of the dopaminergic midbrain circuitry. Nature Neuroscience, 16, 1042-1048.

HO, N. W. & GILHAM, P. 1967. The reversible chemical modification of uracil, thymine, and guanine nucleotides and the modification of the action of ribonuclease on ribonucleic acid. Biochemistry, 6, 3632-3639.

HO, N. W. & GILHAM, P. 1971. Reaction of pseudouridine and inosine with *N*-cyclohexyl-*N*'-*β*-(4-methylmorpholinium) ethylcarbodiimide. Biochemistry, 10, 3651-3657.

HÖCK, J. & MEISTER, G. 2008. The Argonaute protein family. Genome Biology, 9, 210.

HONGAY, C. F. & ORR-WEAVER, T. L. 2011. *Drosophila* Inducer of MEiosis 4 (IME4) is required for Notch signaling during oogenesis. Proceedings of the National Academy of Sciences, 108, 14855-14860.

HORIUCHI, K., KAWAMURA, T., IWANARI, H., OHASHI, R., NAITO, M., KODAMA, T. & HAMAKUBO, T. 2013. Identification of Wilms' tumor 1-associating protein complex and its role in alternative splicing and the cell cycle. Journal of Biological Chemistry, 288, 33292-33302.

HORNYIK, C., TERZI, L. C. & SIMPSON, G. G. 2010. The spen family protein FPA controls alternative cleavage and polyadenylation of RNA. Developmental Cell, 18, 203-213.

HSU, P. J., ZHU, Y., MA, H., GUO, Y., SHI, X., LIU, Y., QI, M., LU, Z., SHI, H., WANG, J., et al. 2017. Ythdc2 is an N^6-methyladenosine binding protein that regulates mammalian spermatogenesis. Cell Research, 27, 1115-1127.

HULPIAU, P. & VAN ROY, F. 2009. Molecular evolution of the cadherin superfamily. The International Journal of Biochemistry & Cell biology, 41, 349-369.

HUTVAGNER, G. & SIMARD, M. J. 2008. Argonaute proteins: key players in RNA silencing. Nature Reviews. Molecular Cell Biology, 9, 22-32.

JIA, G., FU, Y. & HE C. 2013. Reversible RNA adenosine methylation in biological regulation. Trends in Genetics, 29.

JIA, G., FU, Y., ZHAO, X., DAI, Q., ZHENG, G., YANG, Y., YI, C., LINDAHL, T., PAN, T., YANG, Y. & HE C. 2011. *N*6-methyladenosine in nuclear RNA is a major substrate of the obesity-associated FTO. Nature Chemical Biology, 7, 885-887.

JIA, G., YANG, C., YANG, S., JIAN, X., YI, C., ZHOU, Z. & HE, C. 2008. Oxidative demethylation of 3-methylthymine and 3-methyluracil in single-stranded DNA and RNA by mouse and human FTO. FEBS Letters, 582, 3313-3319.

KAN, L., GROZHIK, A. V., VEDANAYAGAM, J., PATIL, D. P., PANG, N., LIM, K.-S., HUANG, Y.-C., JOSEPH, B., LIN, C.-J., DESPIC, V., et al. 2017. The m^6A pathway facilitates sex determination in *Drosophila*. Nature Communications, 8.

KANG, H.-J., JEONG, S.-J., KIM, K.-N., BAEK, I.-J., CHANG, M., KANG, C.-M., PARK, Y.-S. & YUN, C.-W. 2014. A novel protein, Pho92, has a conserved YTH domain and regulates phosphate metabolism by decreasing the mRNA stability of *PHO4* in *Saccharomyces cerevisiae*. Biochemical Journal, 457, 391-400.

KE, S., ALEMU, E. A., MERTENS, C., GANTMAN, E. C., FAK, J. J., MELE, A., HARIPAL, B., ZUCKER-SCHARFF, I., MOORE, M. J., PARK, C. Y., et al. 2015. A majority of m^6A residues are in the last exons, allowing the potential for 3' UTR regulation. Genes & Development, 29, 2037-2053.

KE, S., PANDYA-JONES, A., SAITO, Y., FAK, J. J., VÅGBØ, C. B., GEULA, S., HANNA, J. H., BLACK, D. L., DARNELL, J. E. & DARNELL, R. B. 2017. m^6A mRNA modifications are deposited in nascent pre-mRNA and are not required for splicing but do specify cytoplasmic turnover. Genes & Development, 31, 990-1006.

KEITH, G. 1995. Mobilities of modified ribonucleotides on two-dimensional cellulose thin-layer chromatography. Biochimie, 77, 142-144.

KENNEDY, T. & LANE, B. 1979. Wheat embryo ribonucleates. XIII. Methyl-substituted nucleoside constituents and 5′-terminal dinucleotide sequences in bulk poly(A)-rich RNA from imbibing wheat embryos. Canadian Journal of Biochemistry, 57, 927-931.

KRUSE, S., ZHONG, S., BODI, Z., BUTTON, J., ALCOCER, M. J., HAYES, C. J. & FRAY, R. 2011. A novel synthesis and detection method for cap-associated adenosine modifications in mouse mRNA. Scientific Reports, 1, 126.

LENCE, T., AKHTAR, J., BAYER, M., SCHMID, K., SPINDLER, L., HO, C. H., KREIM, N., ANDRADE-NAVARRO, M. A., POECK, B., HELM, M. &

Roignant J.-V. 2016. m^{6}A modulates neuronal functions and sex determination in *Drosophila*. Nature, 540, 242-247.

LI, D., ZHANG, H., HONG, Y., HUANG, L., LI, X., ZHANG, Y., OUYANG, Z. & SONG, F. 2014. Genome-wide identification, biochemical characterization, and expression analyses of the YTH domain-containing RNA-binding protein family in *Arabidopsis* and rice. Plant Molecular Biology Reporter, 32, 1169-1186.

LI, L., ZANG, L., ZHANG, F., CHEN, J., SHEN, H., SHU, L., LIANG, F., FENG, C., CHEN, D., TAO, H., et al. 2017. Fat mass and obesity-associated (FTO) protein regulates adult neurogenesis. Human Molecular Genetics, 26, 2398-2411.

LI, Q., LI, X., TANG, H., JIANG, B., DOU, Y., GOROSPE, M. & WANG, W. 2017. NSUN2-mediated m5C methylation and METTL3/METTL14-mediated m6A methylation cooperatively enhance p21 translation. Journal of Cellular Biochemistry, 9999.

LI, X., XIONG, X. & YI, C. 2017. Epitranscriptome sequencing technologies: decoding RNA modifications. Nature Methods, 14, 23-31.

LI, X., XIONG, X., WANG, K., WANG, L., SHU, X., MA, S. & YI, C. 2016. Transcriptome-wide mapping reveals reversible and dynamic N^1-methyladenosine methylome. Nature Chemical Biology, 12, 311-316.

LI, X., ZHU, P., MA, S., SONG, J., BAI, J., SUN, F. & YI, C. 2015. Chemical pulldown reveals dynamic pseudouridylation of the mammalian transcriptome. Nature Chemical Biology, 11, 592-597.

LI, Z., WENG, H., SU, R., WENG, X., ZUO, Z., LI, C., HUANG, H., NACHTERGAELE, S., DONG, L., HU, C., et al. 2017. FTO plays an oncogenic

role in acute myeloid leukemia as a *N*6-methyladenosine RNA demethylase. Cancer Cell, 31, 127-141.

LICHINCHI, G., GAO, S., SALETORE, Y., GONZALEZ, G. M., BANSAL, V., WANG, Y., MASON, C. E. & RANA, T. M. 2016. Dynamics of the human and viral m^6A RNA methylomes during HIV-1 infection of T cells. Nature Microbiology, 1, 16011.

LIMBACH, P. A., CRAIN, P. F. & MCCLOSKEY, J. A. 1994. Summary: the modified nucleosides of RNA. Nucleic Acids Research, 22, 2183-2196.

LIN, S., CHOE, J., DU, P., TRIBOULET, R. & GREGORY, R. I. 2016. The m^6A methyltransferase METTL3 promotes translation in human cancer cells. Molecular Cell, 62, 335-345.

LINDER, B., GROZHIK, A. V., OLARERIN-GEORGE, A. O., MEYDAN, C., MASON, C. E. & JAFFREY, S. R. 2015. Single-nucleotide-resolution mapping of m6A and m6Am throughout the transcriptome. Nature Methods, 12, 767-772.

LITTLE, N. A., HASTIE, N. D. & DAVIES, R. C. 2000. Identification of WTAP, a novel Wilms' tumour 1-associating protein. Human Molecular Genetics, 9, 2231-2239.

LIU, J., YUE, Y., HAN, D., WANG, X., FU, Y., ZHANG, L., JIA, G., YU, M., LU, Z., DENG, X., et al. 2014. A METTL3-METTL14 complex mediates mammalian nuclear RNA N^6-adenosine methylation. Nature Chemical Biology, 10, 93-95.

LIU, N., DAI, Q., ZHENG, G., HE, C., PARISIEN, M. & PAN, T. 2015. N^6-methyladenosine-dependent RNA structural switches regulate RNA-protein interactions. Nature, 518, 560-564.

LIU, N., PARISIEN, M., DAI, Q., ZHENG, G., HE, C. & PAN, T. 2013. Probing N^6-methyladenosine RNA modification status at single nucleotide resolution in mRNA and long noncoding RNA. RNA, 19, 1848-1856.

LIU, N., ZHOU, K. I., PARISIEN, M., DAI, Q., DIATCHENKO, L. & PAN, T. 2017. N^6-methyladenosine alters RNA structure to regulate binding of a low-complexity protein. Nucleic Acids Research, 45, 6051-6063.

LOVEJOY, A. F., RIORDAN, D. P. & BROWN, P. O. 2014. Transcriptome-wide mapping of pseudouridines: pseudouridine synthases modify specific mRNAs in *S. cerevisiae*. PLoS One, 9, e110799.

LUO, G.-Z., MACQUEEN, A., ZHENG, G., DUAN, H., DORE, L. C., LU, Z., LIU, J., CHEN, K., JIA, G., BERGELSON, J. & HE C. 2014. Unique features of the m^6A methylome in *Arabidopsis thaliana*. Nature Communications, 5, 5630.

LUO, S. & TONG, L. 2014. Molecular basis for the recognition of methylated adenines in RNA by the eukaryotic YTH domain. Proceedings of the National Academy of Sciences, 111, 13834-13839.

MA, J. Z., YANG, F., ZHOU, C. C., LIU, F., YUAN, J. H., WANG, F., WANG, T. T., XU, Q. G., ZHOU, W. P. & SUN, S. H. 2017. METTL14 suppresses the metastatic potential of hepatocellular carcinoma by modulating N^6-methyladenosine-dependent primary MicroRNA processing. Hepatology, 65, 529-543.

MACHNICKA, M. A., MILANOWSKA, K., OSMAN OGLOU, O., PURTA, E., KURKOWSKA, M., OLCHOWIK, A., JANUSZEWSKI, W., KALINOWSKI, S., DUNIN-HORKAWICZ, S., ROTHER, K. M., et al. 2013.

MODOMICS: a database of RNA modification pathways–2013 update. Nucleic Acids Research, 41, D262-D267.

MAITY, A. & DAS, B. 2016. *N*6-methyladenosine modification in mRNA: machinery, function and implications for health and diseases. The FEBS Journal, 283, 1607-1630.

MARTÍNEZ-PÉREZ, M., APARICIO, F., LÓPEZ-GRESA, M. P., BELLÉS, J. M., SÁNCHEZ-NAVARRO, J. A. & PALLÁS, V. 2017. *Arabidopsis* m^6A demethylase activity modulates viral infection of a plant virus and the m^6A abundance in its genomic RNAs. Proceedings of the National Academy of Sciences, 114, 10755-10760.

MAUER, J., LUO, X., BLANJOIE, A., JIAO, X., GROZHIK, A. V., PATIL, D. P., LINDER, B., PICKERING, B. F., VASSEUR, J.-J., CHEN, Q., et al. 2017. Reversible methylation of m^6A_m in the 5' cap controls mRNA stability. Nature, 541, 371-375.

MEYER, K. D. & JAFFREY, S. R. 2014. The dynamic epitranscriptome: N^6-methyladenosine and gene expression control. Nature Reviews. Molecular Cell Biology, 15, 313-326.

MEYER, K. D., PATIL, D. P., ZHOU, J., ZINOVIEV, A., SKABKIN, M. A., ELEMENTO, O., PESTOVA, T. V., QIAN, S.-B. & JAFFREY, S. R. 2015. 5' UTR m^6A promotes cap-independent translation. Cell, 163, 999-1010.

MEYER, K. D., SALETORE, Y., ZUMBO, P., ELEMENTO, O., MASON, C. E. & JAFFREY, S. R. 2012. Comprehensive analysis of mRNA methylation reveals enrichment in 3' UTRs and near stop codons. Cell, 149, 1635-1646.

MIELECKI, D., ZUGAJ, D. Ł., MUSZEWSKA, A., PIWOWARSKI, J., CHOJNACKA, A., MIELECKI, M., NIEMINUSZCZY, J., GRYNBERG, M. &

GRZESIUK, E. 2012. Novel AlkB dioxygenases–alternative models for *in silico* and *in vivo* studies. PLoS One, 7, e30588.

MOLINIE, B., WANG, J., LIM, K. S., HILLEBRAND, R., LU, Z.-X., VAN WITTENBERGHE, N., HOWARD, B. D., DANESHVAR, K., MULLEN, A. C., DEDON, P., et al. 2016. m^6A-LAIC-seq reveals the census and complexity of the m^6A epitranscriptome. Nature Methods, 13, 692-698.

MUKHERJEE, M., CHOW, S. Y., YUSOFF, P., SEETHARAMAN, J., NG, C., SINNIAH, S., KOH, X. W., ASGAR, N. F. M., LI, D., YIM, D., et al. 2012. Structure of a novel phosphotyrosine-binding domain in Hakai that targets E-cadherin. The EMBO Journal, 31, 1308-1319.

NARAYAN, P., LUDWICZAK, R. L., GOODWIN, E. C. & ROTTMAN, F. M. 1994. Context effects on N^6-adenosine methylation sites in prolactin mRNA. Nucleic Acids Research, 22, 419-426.

NAYLER, O., HARTMANN, A. M. & STAMM, S. 2000. The ER repeat protein YT521-B localizes to a novel subnuclear compartment. The Journal of Cell Biology, 150, 949-962.

NAYLOR, R., HO, N. W. & GILHAM, P. 1965. Selective chemical modifications of uridine and pseudouridine in polynucleotides and their effect on the specificities of ribonuclease and phosphodiesterases. Journal of the American Chemical Society, 87, 4209-4210.

NICHOLS, J. L. 1979. N^6-methyladenosine in maize poly(A)-containing RNA, Plant Science Letters, 15, 357-361.

NICHOLS, J. L., WELDER, L. 1981. Nucleotides adjacent to N^6-methyladenosine in maize poly(A)-containing RNA, Plant Science Letters, 21, 75-81.

NIESSEN, M., SCHNEITER, R. & NOTHIGER, R. 2001. Molecular identification of *virilizer*, a gene required for the expression of the sex-determining gene *Sex-lethal* in *Drosophila melanogaster*. Genetics, 157, 679-688.

NISHIKURA, K. 2010. Functions and regulation of RNA editing by ADAR deaminases. Annual Review of Biochemistry, 79, 321-349.

ORTEGA, A., NIKSIC, M., BACHI, A., WILM, M., SÁNCHEZ, L., HASTIE, N. & VALCÁRCEL, J. 2003. Biochemical function of female-lethal (2) D/Wilms' tumor suppressor-1-associated proteins in alternative pre-mRNA splicing. Journal of Biological Chemistry, 278, 3040-3047.

PATIL, D. P., CHEN, C.-K., PICKERING, B. F., CHOW, A., JACKSON, C., GUTTMAN, M. & JAFFREY, S. R. 2016. m^6A RNA methylation promotes *XIST*-mediated transcriptional repression. Nature, 537, 369-373.

PECE, S. & GUTKIND, J. S. 2002. E-cadherin and Hakai: signalling, remodeling or destruction? Nature Cell Biology, 4, E72-E74.

PEIFER, C., SHARMA, S., WATZINGER, P., LAMBERTH, S., KÖTTER, P. & ENTIAN, K.-D. 2013. Yeast Rrp8p, a novel methyltransferase responsible for m^1A 645 base modification of 25S rRNA. Nucleic Acids Research, 41, 1151-1163.

PENN, J. K., GRAHAM, P., DESHPANDE, G., CALHOUN, G., CHAOUKI, A. S., SALZ, H. K. & SCHEDL, P. 2008. Functioning of the Drosophila Wilms'-tumor-1-associated protein homolog, Fl(2)d, in Sex-lethal-dependent alternative splicing. Genetics, 178, 737-748.

PERRY, R. & KELLEY, D. 1974. Existence of methylated messenger RNA in mouse L cells. Cell, 1, 37-42.

PERRY, R. P., KELLEY, D. E., FRIDERICI, K. & ROTTMAN, F. 1975. The methylated constituents of L cell messenger RNA: evidence for an unusual cluster at the 5' terminus. Cell, 4, 387-394.

PING, X.-L., SUN, B.-F., WANG, L., XIAO, W., YANG, X., WANG, W.-J., ADHIKARI, S., SHI, Y., LV, Y., CHEN, Y.-S., et al. 2014. Mammalian WTAP is a regulatory subunit of the RNA N6-methyladenosine methyltransferase. Cell Research, 24, 177-189.

ROBBENS, S., ROUZÉ, P., COCK, J. M., SPRING, J., WORDEN, A. Z. & VAN DE PEER, Y. 2008. The *FTO* gene, implicated in human obesity, is found only in vertebrates and marine algae. Journal of Molecular Evolution, 66, 80-84.

ROOST, C., LYNCH, S. R., BATISTA, P. J., QU, K., CHANG, H. Y. & KOOL, E. T. 2015. Structure and thermodynamics of N^6-methyladenosine in RNA: a spring-loaded base modification. Journal of the American Chemical Society, 137, 2107-2115.

ROTTMAN, F., BOKAR, J., NARAYAN, P., SHAMBAUGH, M. & LUDWICZAK, R. 1994. N^6-adenosine methylation in mRNA: substrate specificity and enzyme complexity. Biochimie, 76, 1109-1114.

ROUNDTREE, I. A., EVANS, M. E., PAN, T. & HE, C. 2017. Dynamic RNA modifications in gene expression regulation. Cell, 169, 1187-1200.

RŮŽIČKA, K., ZHANG, M., CAMPILHO, A., BODI, Z., KASHIF, M., SALEH, M., EECKHOUT, D., EL-SHOWK, S., LI, H., ZHONG, S., et al. 2017. Identification of factors required for m^6A mRNA methylation in *Arabidopsis* reveals a role for the conserved E3 ubiquitin ligase HAKAI. New Phytologist, 215, 157-172.

SAIKIA, M., FU, Y., PAVON-ETERNOD, M., HE, C. & PAN, T. 2010. Genome-wide analysis of N^1-methyl-adenosine modification in human tRNAs. RNA, 16, 1317-1327.

SALETORE, Y., MEYER, K., KORLACH, J., VILFAN, I. D., JAFFREY, S. & MASON, C. E. 2012. The birth of the Epitranscriptome: deciphering the function of RNA modifications. Genome Biology, 13, 175.

SCHAEFER, M., POLLEX, T., HANNA, K. & LYKO, F. 2009. RNA cytosine methylation analysis by bisulfite sequencing. Nucleic Acids Research, 37, e12.

SCHWARTZ, S., AGARWALA, S. D., MUMBACH, M. R., JOVANOVIC, M., MERTINS, P., SHISHKIN, A., TABACH, Y., MIKKELSEN, T. S., SATIJA, R., RUVKUN, G., et al. 2013. High-resolution mapping reveals a conserved, widespread, dynamic mRNA methylation program in yeast meiosis. Cell, 155, 1409-1421.

SCHWARTZ, S., BERNSTEIN, D. A., MUMBACH, M. R., JOVANOVIC, M., HERBST, R. H., LEÓN-RICARDO, B. X., ENGREITZ, J. M., GUTTMAN, M., SATIJA, R., LANDER, E. S., et al. 2014a. Transcriptome-wide mapping reveals widespread dynamic-regulated pseudouridylation of ncRNA and mRNA. Cell, 159, 148-162.

SCHWARTZ, S., MUMBACH, M. R., JOVANOVIC, M., WANG, T., MACIAG, K., BUSHKIN, G. G., MERTINS, P., TER-OVANESYAN, D., HABIB, N., CACCHIARELLI, D., et al. 2014b. Perturbation of m6A writers reveals two distinct classes of mRNA methylation at internal and 5' sites. Cell Reports, 8, 284-296.

SEYMOUR, G. B., TUCKER, G. & LEACH, L. A. 2004. Cell adhesion molecules in plants and animals. Biotechnology and Genetic Engineering Reviews, 21, 123-132.

SHEN, L., LIANG, Z., GU, X., CHEN, Y., TEO, Z. W. N., HOU, X., CAI, W. M., DEDON, P. C., LIU, L. & YU, H. 2016. N^6-methyladenosine RNA modification regulates shoot stem cell fate in *Arabidopsis*. Developmental Cell, 38, 186-200.

SHI, H., WANG, X., LU, Z., ZHAO, B. S., MA, H., HSU, P. J., LIU, C. & HE, C. 2017. YTHDF3 facilitates translation and decay of N^6-methyladenosine-modified RNA. Cell Research, 27, 315-328.

ŚLEDŹ, P. & JINEK, M. 2016. Structural insights into the molecular mechanism of the m^6A writer complex. eLife, 5, e18434.

SONG, J. & YI, C. 2017. Chemical modifications to RNA: a new layer of gene expression regulation. ACS Chemical Biology, 12, 316-325.

SPITALE, R. C., FLYNN, R. A., ZHANG, Q. C., CRISALLI, P., LEE, B., JUNG, J.-W., KUCHELMEISTER, H. Y., BATISTA, P. J., TORRE, E. A., KOOL, E. T., et al. 2015. Structural imprints *in vivo* decode RNA regulatory mechanisms. Nature, 519, 486-490.

SQUIRES, J. E., PATEL, H. R., NOUSCH, M., SIBBRITT, T., HUMPHREYS, D. T., PARKER, B. J., SUTER, C. M. & PREISS, T. 2012. Widespread occurrence of 5-methylcytosine in human coding and non-coding RNA. Nucleic Acids Research, 40, 5023-5033.

STOILOV, P., RAFALSKA, I. & STAMM, S. 2002. YTH: a new domain in nuclear proteins. Trends in Biochemical Sciences, 27, 495-497.

SU, H., LIU, Y. & ZHAO, X. 2015. Split end family RNA binding proteins: Novel tumor suppressors coupling transcriptional regulation with RNA processing. Cancer Translational Medicine, 1, 21-25.

THOMAS, P. E., WU, X., LIU, M., GAFFNEY, B., JI, G., LI, Q. Q. & HUNT, A. G. 2012. Genome-wide control of polyadenylation site choice by CPSF30 in *Arabidopsis*. The Plant Cell, 24, 4376-4388.

VESPA, L., VACHON, G., BERGER, F., PERAZZA, D., FAURE, J.-D. & HERZOG, M. 2004. The immunophilin-interacting protein AtFIP37 from Arabidopsis is essential for plant development and is involved in trichome endoreduplication. Plant Physiology, 134, 1283-1292.

VILFAN, I. D., TSAI, Y.-C., CLARK, T. A., WEGENER, J., DAI, Q., YI, C., PAN, T., TURNER, S. W. & KORLACH, J. 2013. Analysis of RNA base modification and structural rearrangement by single-molecule real-time detection of reverse transcription. Journal of Nanobiotechnology, 11, 8.

WANG, P., DOXTADER, K. A. & NAM, Y. 2016. Structural basis for cooperative function of Mettl3 and Mettl14 methyltransferases. Molecular Cell, 63, 306-317.

WANG, X., FENG, J., XUE, Y., GUAN, Z., ZHANG, D., LIU, Z., GONG, Z., WANG, Q., HUANG, J. & TANG, C. 2016. Structural basis of N6-adenosine methylation by the METTL3-METTL14 complex. Nature, 534, 575-578.

WANG, X., LU, Z., GOMEZ, A., HON, G. C., YUE, Y., HAN, D., FU, Y., PARISIEN, M., DAI, Q., JIA, G., et al. 2014. N^6-methyladenosine-dependent regulation of messenger RNA stability. Nature, 505, 117-120.

WANG, X., ZHAO, B. S., ROUNDTREE, I. A., LU, Z., HAN, D., MA, H., WENG, X., CHEN, K., SHI, H. & HE, C. 2015. N^6-methyladenosine modulates messenger RNA translation efficiency. Cell, 161, 1388-1399.

WANG, Y. & ZHAO, J. C. 2016. Update: Mechanisms underlying N^6-methyladenosine modification of eukaryotic mRNA. Trends in Genetics, 32, 763-773.

WANG, Y., LI, Y., TOTH, J. I., PETROSKI, M. D., ZHANG, Z. & ZHAO, J. C. 2014. N^6-methyladenosine modification destabilizes developmental regulators in embryonic stem cells. Nature Cell Biology, 16, 191-198.

WEI, C. M., GERSHOWITZ, A. & MOSS, B. 1976. 5'-Terminal and internal methylated nucleotide sequences in HeLa cell mRNA. Biochemistry, 15, 397-401.

WEI, C.-M. & MOSS, B. 1977. Nucleotide sequences at the N^6-methyladenosine sites of HeLa cell messenger ribonucleic acid. Biochemistry, 16, 1672-1676.

XIANG, Y., LAURENT, B., HSU, C.-H., NACHTERGAELE, S., LU, Z., SHENG, W., XU, C., CHEN, H., OUYANG, J., WANG, S., et al. 2017. RNA m^6A methylation regulates the ultraviolet-induced DNA damage response. Nature, 543, 573-576.

XIAO, W., ADHIKARI, S., DAHAL, U., CHEN, Y.-S., HAO, Y.-J., SUN, B.-F., SUN, H.-Y., LI, A., PING, X.-L., LAI, W.-Y., et al. 2016. Nuclear m^6A reader YTHDC1 regulates mRNA splicing. Molecular Cell, 61, 507-519.

XIONG, Y., HANNON, G. J., ZHANG, H., CASSO, D., KOBAYASHI, R. & BEACH, D. 1993. p21 is a universal inhibitor of cyclin kinases. Nature, 366, 701-704.

XU, C., WANG, X., LIU, K., ROUNDTREE, I. A., TEMPEL, W., LI, Y., LU, Z., HE, C. & MIN, J. 2014. Structural basis for selective binding of m^{6}A RNA by the YTHDC1 YTH domain. Nature Chemical Biology, 10, 927-929.

YAMAMOTO, M. 1996. The molecular control mechanisms of meiosis in fission yeast. Trends in Biochemical Sciences, 21, 18-22.

YUE, Y., LIU, J. & HE, C. 2015. RNA N^6-methyladenosine methylation in post-transcriptional gene expression regulation. Genes & Development, 29, 1343-1355.

ZHANG, B., ZUR HAUSEN, A., ORLOWSKA-VOLK, M., JÄGER, M., BETTENDORF, H., STAMM, S., HIRSCHFELD, M., YIQIN, O., TONG, X., GITSCH, G., et al., 2010. Alternative splicing-related factor YT521: an independent prognostic factor in endometrial cancer. International Journal of Gynecological Cancer, 20, 492-499.

ZHANG, C., SAMANTA, D., LU, H., BULLEN, J. W., ZHANG, H., CHEN, I., HE, X. & SEMENZA, G. L. 2016. Hypoxia induces the breast cancer stem cell phenotype by HIF-dependent and ALKBH5-mediated m^{6}A-demethylation of NANOG mRNA. Proceedings of the National Academy of Sciences, 113, E2047-E2056.

ZHANG, J., ADDEPALLI, B., YUN, K.-Y., HUNT, A. G., XU, R., RAO, S., LI, Q. Q. & FALCONE, D. L. 2008. A polyadenylation factor subunit implicated in regulating oxidative signaling in *Arabidopsis thaliana*. PLoS One, 3, e2410.

ZHANG, M., ZHANG, Y., MA, J., GUO, F., CAO, Q., ZHANG, Y., ZHOU, B., CHAI, J., ZHAO, W. & ZHAO, R. 2015. The demethylase activity of FTO (fat mass and obesity associated protein) is required for preadipocyte differentiation. PLoS One, 10, e0133788.

ZHANG, S., ZHAO, B. S., ZHOU, A., LIN, K., ZHENG, S., LU, Z., CHEN, Y., SULMAN, E. P., XIE, K., BÖGLER, O., et al. 2017. m^6A demethylase ALKBH5 maintains tumorigenicity of glioblastoma stem-like cells by sustaining FOXM1 expression and cell proliferation program. Cancer Cell, 31, 591-606.

ZHANG, Z., THELER, D., KAMINSKA, K. H., HILLER, M., DE LA GRANGE, P., PUDIMAT, R., RAFALSKA, I., HEINRICH, B., BUJNICKI, J. M., ALLAIN, F. H.-T., et al. 2010. The YTH domain is a novel RNA binding domain. Journal of Biological Chemistry, 285, 14701-14710.

ZHAO, B. S., ROUNDTREE, I. A. & HE, C. 2017a. Post-transcriptional gene regulation by mRNA modifications. Nature Reviews. Molecular Cell Biology, 18, 31-42.

ZHAO, B. S., WANG, X., BEADELL, A. V., LU, Z., SHI, H., KUUSPALU, A., HO, R. K. & HE, C. 2017b. m^6A-dependent maternal mRNA clearance facilitates zebrafish maternal-to-zygotic transition. Nature, 542, 475-478.

ZHAO, X., YANG, Y., SUN, B.-F., SHI, Y., YANG, X., XIAO, W., HAO, Y.-J., PING, X.-L., CHEN, Y.-S., WANG, W.-J., et al. 2014. FTO-dependent demethylation of N6-methyladenosine regulates mRNA splicing and is required for adipogenesis. Cell Research, 24, 1403-1419.

ZHENG, G., DAHL, J. A., NIU, Y., FEDORCSAK, P., HUANG, C.-M., LI, C. J., VÅGBØ, C. B., SHI, Y., WANG, W.-L., SONG, S.-H., et al. 2013. ALKBH5 is a mammalian RNA demethylase that impacts RNA metabolism and mouse fertility. Molecular Cell, 49, 18-29.

ZHONG, S., LI, H., BODI, Z., BUTTON, J., VESPA, L., HERZOG, M. & FRAY, R. G. 2008. MTA is an *Arabidopsis* messenger RNA adenosine

methylase and interacts with a homolog of a sex-specific splicing factor. The Plant Cell, 20, 1278-1288.

ZHOU, C., MOLINIE, B., DANESHVAR, K., PONDICK, J. V., WANG, J., VAN WITTENBERGHE, N., XING, Y., GIALLOURAKIS, C. C. & MULLEN, A. C. 2017. Genome-wide maps of m6A circRNAs identify widespread and cell-type-specific methylation patterns that are distinct from mRNAs. Cell Reports, 20, 2262-2276.

ZHOU, J., WAN, J., GAO, X., ZHANG, X. & QIAN, S.-B. 2015. Dynamic m^6A mRNA methylation directs translational control of heat shock response. Nature, 526, 591-594.

ZOU, S., TOH, J. D., WONG, K. H., GAO, Y.-G., HONG, W. & WOON, E. C. 2016. N^6-methyladenosine: a conformational marker that regulates the substrate specificity of human demethylases FTO and ALKBH5. Scientific Reports, 6, 25677.

CHAPTER 2 GENERAL MATERIALS AND METHODS

2.1 PLANT MATERIALS AND GROWTH CONDITIONS

Plant materials used in this study were *Arabidopsis* (ecotype Colombia-0), including WT, T-DNA insertion mutants and other transgenic lines. Details of transgenic lines used in this study are listed in Table 2.1. *Arabidopsis* seeds were cultured on plates or on compost depending upon the intended subsequent use. *Arabidopsis* seeds planted on plates were sterilised by soaking in 5% (v/v) NaClO for 4 min and then washed with sterile water for 5 times before being planted on MS or 1/2 MS plates. Plates were put in the cold room (4°C, dark) for 2 days and then kept in the tissue culture room (16 h light/ 8 h dark, 22°C) until used. For seeds sown directly on compost, they were grown in the phytotron (16 h light/8 h dark, 22°C day/18°C night).

Table 2.1 Pre-existing transgenic and mutant *Arabidopsis* lines used in this study

Line name	Description	Source
SALK_109428	T-DNA inserted in the 5′ UTR of *Hakai* gemonic DNA	NASC
SALK_148797	T-DNA inserted in the 5′ UTR of *Hakai* gemonic DNA	NASC
GK-259E01	T-DNA inserted in the 5′ UTR of *Hakai* gemonic DNA	NASC
GK-217A12	T-DNA inserted in intron 1 of *Hakai* gemonic DNA	Kamil Růžička's group (Masaryk University) (Růžička et al., 2017)
ABI3A6	SALK_074069 with T-DNA inserted in exon 4 of *MTA* genomic DNA and complemented with *MTA* coding sequence driven by *ABI3* promoter (*ABI3*::*MTA*). Low m^6A line.	Rupert Fray's group (Bodi et al., 2012)
fip37	SALK_018636 with T-DNA inserted in intron 7 of *FIP37* genomic DNA. Hypomorphic mutant with very low m^6A level.	Kamil Růžička's group (Masaryk University) (Růžička et al., 2017)
virilizer	G to A mutation at the beginning of intron 5 of *Virilizer* genomic DNA, which disrupts its correct 5′ splicing. Hypomorphic mutant with very low m^6A level.	Kamil Růžička's group (Masaryk University) (Růžička et al., 2017)
MTA-GFP	SALK_114710 with T-DNA inserted in exon 6 of *MTA* genomic DNA and complemented with *MTA* coding sequence under its own promoter, with GFP tag downstream.	Rupert Fray's group
MTA-GFP/WT	*MTA* coding sequence under its own promoter in WT background, with GFP tag downstream.	Rupert Fray's group
MTB-GFP	*MTB* genomic DNA under its own promoter in *mtb* mutant background, with GFP tag downstream.	Rupert Fray's group
Virilizer-GFP	*virilizer* complemented with *Virilizer* genomic DNA under its own promoter, with GFP tag between them.	Kamil Růžička's group (Masaryk University) (Růžička et al., 2017)
cyclin B1 (*CycB1*)*;1*::*GUS*	*GUS* activated by *CycB1;1* promoter. A marker line for active cell division.	Ranjan Swarup's group (Casimiro et al., 2001)
ABI3A6× *CycB1;1*::*GUS*	ABI3A6 crossed with *CycB1;1*::*GUS*	Rupert G. Fray's group
AUX1-YFP	*aux1* complemented with *AUX1* genomic DNA under its own promoter and tagged with YFP	Ranjan Swarup's group (Swarup et al., 2004)
DR5::*VENUS*	*VENUS* reporter driven by *DR5* promoter, to mark transcriptional auxin response sites.	Malcolm J. Bennett's group (Band et al., 2012; Brunoud et al., 2012)
DII-VENUS	A fusion of the auxin-dependent degradation domain II of an Aux/IAA protein to VENUS fluorescent protein, to check the auxin accumulation.	Malcolm J. Bennett's group (Band et al., 2012; Brunoud et al., 2012)

2.2 GENOMIC DNA EXTRATION

DNA samples used for screening were extracted using Edwards buffer (200 mM Tris-HCl pH 7.5, 250 mM NaCl, 25 mM EDTA and 0.5% [w/v] sodium dodecyl sulfate [SDS]). The specific protocol is as follows. Plant tissues in a 2 ml Eppendorf tube were ground with the pellet pestle. 700 µl of Edwards buffer was added and mixed by vortexing for 1 min. Tubes were centrifuged at 14,000 rpm for 10 min and supernatants were transferred into new tubes. The same volume of isopropanol was added and mixed by inverting the tube 5 times. The mixture was precipitated at -20°C overnight. Next day, tubes were centrifuged at 14,000 rpm for 10 min and supernatants were discarded. The pellets were washed with 70% (v/v) ethanol. After discarding 70% (v/v) ethanol, the tubes were centrifuged again and the residual ethanol was removed by pipetting. After drying the pellets for 3 min using a vacuum pump, the pellets were resuspended in 30 µl of sterile water. After mixing by pipetting, the mixture was centrifuged and the liquid was transferred to a new tube. 1:30 dilution of this extract was used for PCR reaction. When needed, high-purity DNAs were extracted using GenElute Plant Genomic DNA Miniprep Kit (Sigma-Aldrich) according to the manufacturer's instructions.

2.3 GENERAL PCR REAGENTS AND PROGRAMMES

Generally, PCR reagents were prepared by mixing 1 ng - 1 µg template, 1 µM forward primer, 1 µM reverse primer, 0.2 mM dNTPs, 1× Q5 reaction buffer and 0.2 U Q5® High-Fidelity DNA Polymerase (New England BioLabs, NEB) in a

final volume of 20 µl. For a 50 µl reaction volume, 0.5 U Q5® High-Fidelity DNA Polymerase was used. PCR programme was set as follows. Initial denaturing: 94°C 5 min; denaturing: 94°C 30 s; annealing: 30 s, temperature depends on Tm values of primers; extension: 72°C, time depends on the size of PCR product; 35 cycles; final extension: 72°C 5 min.

2.4 GENOTYPING PCR

Original *Arabidopsis* mutant lines with T-DNA insertions and crossing progenies of these lines were screened by genotyping PCR. Three primers were used, with one on the T-DNA sequence (Left border primer on the inserted T-DNA, LB) and two flanking the inserted T-DNA on the genomic DNA sequence (Left primer, LP and right primer, RP) (Figure 2.1a). Because the inserted T-DNA sequence is too large (> 3,000 bp and sometimes more than one inserted copy) to be amplified under normal PCR conditions, thus, there should be no band using LP and RP and a correct band using LB and RP for a homozygous line when checking on the gel, whereas a heterozygous line shows bands for both PCR reactions and WT samples only show bands using LP and RP (Figure 2.1b). Details of all primers used in this study are listed in Appendix 1.

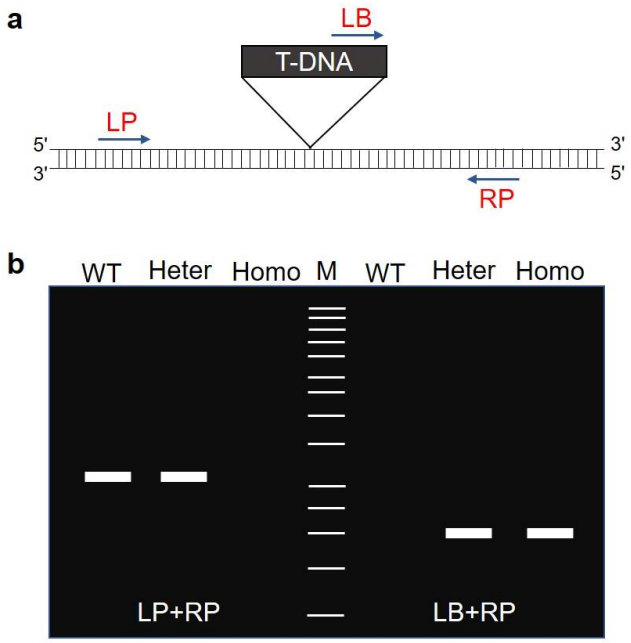

Figure 2.1 Schematic showing primer locations in genotyping PCR (**a**) and expected results for different lines on the agarose gel (**b**). (**a**) shows an example where the inserted T-DNA is in the same direction as that of the forward DNA strand. LP: left primer on genomic DNA; RP: right primer on genomic DNA; LB: left border primer on the inserted T-DNA; WT: the wild type; Heter: heterozygous line; Homo: homozygous line; M: HyperLadder 1kb (Bioline).

2.5 PCR PRODUCT PURIFICATION

For cloning and sequencing, PCR products were purified by gel excision. The excised gel band was put into a 0.5 ml Eppendorf tube, which was prepared in advance by making a hole at the bottom with a needle and placing a piece of soft filter paper to block the hole. After snap-freezing in the liquid nitrogen, the 0.5 ml tube was put into a 1.5 ml Eppendorf tube and centrifuged at 14,000 rpm for 15 min. The flow-through was transferred into a new 1.5 ml tube every 5 min. After centrifuging, 5 µl of Dextran (10 $mg \cdot ml^{-1}$) and 3 volumes of absolute ethanol were added and mixed by vortexing. After precipitation at -20°C

overnight, the mixture was centrifuged and the DNA pellet was washed with 70% (v/v) ethanol. After washing and drying, the DNA pellet was dissolved in 10 µl or less volume of sterile water and kept at -20°C until use.

2.6 CLONING OF PCR PRODUCT

Amplified PCR products were cloned to Gateway entry vectors to generate constructs needed. A detailed protocol can be found in 3.3.5.

2.7 TRANSFORMING COMPETENT *ESCHERICHIA COLI* CELLS

Cloning reactions were transformed to competent *E. coli* cells as follows. (1) 10 µl (or less, depending on the reaction volume) of the cloning reaction was added to a vial of chemically competent *E. coli* cells (DH5α or TOP10) and mixed gently. (2) The mixture was incubated on ice for 30 min and then heat-shocked for 90 seconds at 42°C. (3) The vial was immediately transferred onto ice and kept in ice for 3 min. (4) 700 µl of liquid LB medium was added into the vial and the mixture was transferred into a 1.5 ml Eppendorf tube. (5) The tube was incubated in a 37°C shaker (200 rpm) for 1 h and 30 min. (6) 100 µl or more (depending on the transformation efficiency) of *E. coli* culture was spread on a solid LB plate containing the appropriate antibiotic. (7) The plate was incubated upside down at 37°C overnight.

2.8 PLASMID DNA EXTRACTION

Plasmid DNA was prepared according to the manufacturer's instructions (GeneJET Plasmid Miniprep Kit, Thermo Scientific). (1) 10 ml of *E. coli* culture in liquid LB media was centrifuged at 14,000 rpm for 10 min. (2) The liquid was discarded and the pelleted cells were resuspended in 250 µl of the Resuspension Solution. (3) 250 µl of the Lysis Solution was added and mixed thoroughly by inverting the tube 4-6 times until the solution became slightly clear. (4) 350 µl of the Neutralization Solution was added and mixed immediately and thoroughly by inverting the tube 4-6 times. (5) The tube was centrifuged at 14,000 rpm for 10 min. (6) The supernatant was transferred to GeneJET spin column by pipetting. (7) The tube was centrifuged for 1 min and the flow-through was discarded. (8) The column was put back to the same collection tube and washed twice using 500 µl of the Wash Solution each time. (9) The flow-through was discarded and the column was centrifuged for 2 min to remove the residual Wash Solution. (10) The column was transferred into a fresh 1.5 ml Eppendorf tube and dried using a vacuum pump for 10 min. (11) 30 µl of sterile water was added to the centre of the column membrane without touching the membrane. (12) The column was incubated for 3 min at room temperature and centrifuged for 2 min to elute the plasmid DNA. (13) Plasmid DNA was stored at -20°C until use.

2.9 TRANSFORMING AGROBACTERIUM VIA ELECTROPORATION

Electroporation was used to transform the recombinant plasmid to *Agrobacterium tumefaciens*. To start with, electroporation cuvette was placed in

ice and frozen competent cells of *A. tumefaciens* strain C58 were left in ice to thaw. 2 µl of the recombinant plasmid DNA was mixed with 50 µl of electro-competent cells. The mixture was then transferred to the cold cuvette carefully to ensure that the mixture covered the bottom and no bubbles were present in the mixture. An electrical pulse was then given using the Micropulser™ electroporator (Bio-Rad) and 1 ml of liquid LB medium was added to the cuvette immediately, mixed gently and transferred to a 1.5 ml Eppendorf tube. The tube was incubated at 28°C for 3 h with vigorous shaking. The transformed culture was then spread on petri dishes containing solid LB medium supplemented with appropriate antibiotics. After incubating at 28°C for 2 days, single colonies were picked and cultured in liquid LB medium containing appropriate antibiotics. Correct colonies were confirmed by PCR.

2.10 FLORAL DIP TRANSFORMATION OF ARABIDOPSIS

Recombinant constructs were transformed to WT or mutant *Arabidopsis* plants by floral dip method (Clough and Bent, 1998). When *Arabidopsis* plants were almost ready to be used for transformation (with many open flowers), *Agrobacterium* cultures were prepared by culturing 200 ml of 1:100 dilution of smaller overnight cultures (200 ml of liquid LB medium + 2 ml of overnight cultures + appropriate antibiotics) at 28°C for 12 h to 24 h until OD_{600} reached 0.8-1.0. Cells were harvested by centrifugation for 10 min at 10,000 rpm. Cell pellets were resuspended in 5% (w/v) sucrose solution containing 0.02% (v/v) Silwet L-77 and 100 µM acetosyringone. The resuspension was kept at room temperature for more than 1 h to activate the Ti plasmid of the *Agrobacterium*.

During this period, already formed siliques on the *Arabidopsis* plants to be used for transformation were removed using scissors. For floral dip, the resuspension was added to a beaker and all above-ground tissues of plants were submerged in the resuspension for 40 seconds with gentle agitation. Afterwards, plants were kept in a tray and covered with a dark plastic bag to maintain humidity and avoid exposure to strong light. Next day, the black bag was removed and plants were cultured as usual. A week later, the floral dip was repeated to improve the transformation efficiency. Seeds were harvested approximately 3 weeks later when siliques became yellow and dry. These seeds are termed T_0 seeds and the subsequent generations are termed T_1, T_2, T_3, T_4…

2.11 TOTAL RNA EXTRACTION

Arabidopsis total RNA was prepared following the method of total RNA extraction from yeast with minor modifications (Schmitt et al., 1990). Plant samples were ground into powder using chilled mortar and pestle and liquid nitrogen. Ground samples were divided into several tubes. In each tube, 400 µl of AE buffer (50 mM sodium acetate pH 5.2, 10 mM EDTA), 40 µl of 10% (w/v) SDS and 400 µl of AE saturated phenol were added. Tubes were vortexed and incubated at 65°C for 4 min. Afterwards, to facilitate the separation of the aqueous and phenol phases, tubes were rapidly chilled in liquid nitrogen for 3 seconds and then taken out for 2 seconds. This was repeated 4-5 times until phenol crystals appeared. Tubes were then centrifuged at 14,000 rpm for 5 min and the supernatant was transferred to a new tube. An equal volume of phenol/chloroform was added to the new tube and mixed by vortexing. After

centrifuging for 5 min, the aqueous phase was again transferred to a new tube and precipitated by adding 1/10 volume of 3 M sodium acetate (pH 5.2) and 3 volumes of absolute ethanol. The mixture was vortexed and kept at -20°C overnight. Next day, tubes were centrifuged at 14,000 rpm for 10 min and then the RNA pellet was washed with 70% (v/v) ethanol. After drying, the RNA pellet was resuspended in sterile water (volume of water depends on the amount of the RNA pellet, normally 16 μl). The quality and quantity of total RNA were checked by NanoDrop™ 1000 spectrophotometer and run on 1.2% (w/v) TBE gel.

2.12 NORTHERN BLOTTING

2.12.1 Stock Solutions of Chemicals

10% (w/v) SDS: Dissolve 80 g SDS in 800 ml of sterile water. Cannot be autoclaved.

1 M sodium phosphate buffer (pH 6.5): Mix 137 ml of 1 M NaH_2PO_4 and 63 ml of 1 M Na_2HPO_4 stock solutions to a total volume of 200 ml. Dissolve 24 g NaH_2PO_4 (MW = 120 g·mol^{-1}) in 200 ml of deionised water to make 1 M NaH_2PO_4 stock solution. Dissolve 14.2 g Na_2HPO_4 (MW = 142 g·mol^{-1}) in 100 ml of deionised water to make 1 M Na_2HPO_4 stock solution. Autoclave and store at room temperature.

0.5 M EDTA (pH 8.0): Dissolve 18.61 g $Na_2EDTA{\cdot}2H_2O$ (MW = 372.24 g·mol^{-1}) in 100 ml of deionised water by adding 1.8-2 g of NaOH pellets to completely

dissolve $Na_2EDTA \cdot 2H_2O$ and adjust the pH to 8.0. Autoclave and store at room temperature.

Ethidium bromide buffer: 1,000 µl of deionised formamide, 550 µl of sterile water, 330 µl of formaldehyde (37%), 40 µl of EDTA (0.5 M, pH 8.0), 40 µl of 10 $mg \cdot ml^{-1}$ ethidium bromide and 40 µl of sodium phosphate buffer (1 M, pH 6.5).

5× Bromophenol blue loading dye: 0.25% (w/v) bromophenol blue, 0.25% (w/v) Xylenecynol FF and 40% (w/v) sucrose in H_2O.

20× SSC: Dissolve 140.26 g NaCl (MW = 58.44 $g \cdot mol^{-1}$) and 70.584 g sodium citrate dehydrate (MW = 294.1 $g \cdot mol^{-1}$) in 800 ml of deionised water. Autoclave and store at room temperature.

5 M NaCl: Dissolve 29.22 g NaCl in 100 ml of deionised water. Autoclave and store at room temperature.

2.12.2 Electrophoresis

Before making the gel, the gel tray, comb and electrophoresis tank were soaked using 1% (w/v) SDS for 30 min and then rinsed with sterile water. The agarose gel (1.2% [w/v]) was prepared by microwaving 1.2 g of agarose in the presence of 2 ml of sodium phosphate buffer (1 M, pH 6.5) and 90 ml of sterile water. When the gel cooled to about 60°C, 8 ml of formaldehyde (37%, pH 7.0) was added and mixed well before pouring the gel in the fume hood.

While waiting for the gel to set (it takes about 1 h), running buffer and RNA samples were prepared. The running buffer includes 13 ml of sodium phosphate

buffer (1 M, pH 6.5), 587 ml of sterile water and 50 ml of formaldehyde (37%, pH 7.0). 8 μg of total RNA was mixed with the same volume of Ethidium bromide buffer. The mixture was denatured at 65°C for 5 min and then immediately plunged into ice. Simultaneously, 8 μl of the ssRNA ladder (NEB) was prepared in the same way. 5× Bromophenol blue loading dye was added to the mixture with the final concentration as 1×. The gel was run at 90 V for 1 h and 30 min to 2 h. A circulator was used to keep the buffer even.

2.12.3 Blotting

To get ready for blotting, the nylon membrane (PerkinElmer) and two sheets of Whatman paper were cut to the same size of the gel to be blotted. 500 ml of 10× SSC (blotting buffer) and 200 ml of 2× SSC (for soaking the membrane and two sheets of Whatman paper) were also prepared. In addition, the tray for containing blotting buffer was cleaned by 1% (w/v) SDS and sterile water. After separating by electrophoresis, the gel was photographed via SYNGENE UV transilluminator in combination with the corresponding gel imaging system. The blotting was then assembled as shown in Figure 2.2 with the gel placed on the Whatman paper wick and the bottom side up. After blotting overnight, the membrane was rinsed with 2× SSC and then UV crosslinked.

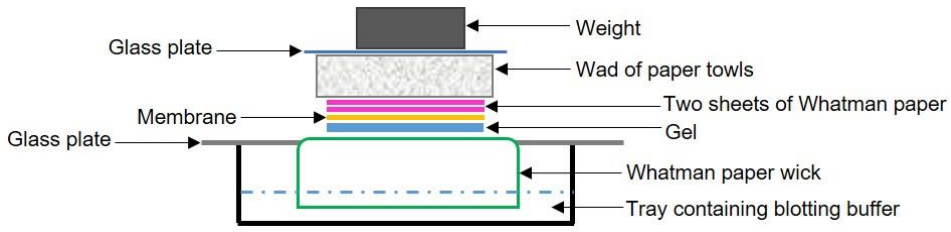

Figure 2.2 Blotting assembly in northern blotting.

2.12.4 Prehybridisation

After crosslinking, the membrane was placed RNA side towards the inside in a cylinder containing 20 ml of prehybridisation buffer (4 ml of 5 M NaCl, 3 ml of sterile water, 10 ml of formamide, 2 g of Dextran sulphate, 1 ml of heat-denatured salmon sperm DNA [10 $mg \cdot ml^{-1}$] and 2 ml of 10% [w/v] SDS). The cylinder was incubated at 55°C with rotation for at least 2 h.

2.12.5 Preparing RNA Probe

Firstly, DNA template for preparing RNA probe was amplified by PCR using primers containing T7 promoter sequence and *Arabidopsis* cDNA as the template. The transcription reagents were prepared as recommended in the protocol of Riboprobe® system-T7 kit (Promega). 1× Transcription optimised buffer, 10 mM dithiothreitol (DTT), 40 U Recombinant RNasin® Ribonuclease Inhibitor, 0.5 mM rATP, 0.5 mM rGTP, 0.5 mM rUTP, 12 µM rCTP, approximately 500 ng DNA template, 50 µCi [α-^{32}P]rCTP and 20 U T7 RNA Polymerase was mixed in a total volume of 20 µl in a 1.5 ml Eppendorf tube and incubated at 37°C for 1 h. Afterwards, 2 U RQ1 RNase-Free DNase was added and the mixture was incubated at 37°C for another 15 min. Prepared RNA probe was then purified via Bio-Spin® 30 column (Bio-Rad) as recommended by the manufacturer.

Subsequently, the RNA probe was fragmented using a carbonate/bicarbonate buffer system (Bodi et al., 2012). The volume of the RNA probe was brought to

80 µl using sterile water and then 10 µl of 400 mM $NaHCO_3$ and 10 µl of 600 mM Na_2CO_3 (both freshly prepared using sterile water) was added. The fragmentation was carried out at 60°C. The fragmentation time was calculated using the following formula: $t = (L_0-L_t)/(kL_0L_t)$, where L_0 = initial length of transcript (in kb), L_t = desired RNA fragment length (in kb, normally 0.05-0.06 kb), k = constant = 0.11 kb·min^{-1}, t = time (min).

2.12.6 Hybridisation

Fragmented RNA probe was added to the prehybridisation buffer directly and the hybridisation was carried out at 65°C while rotating for approximately 20 h.

2.12.7 Washing Membrane

The membrane was washed with SSC buffers of decreasing concentration containing 0.1% (w/v) SDS, starting with 2× SSC at room temperature for 5 min, followed by 2× SSC, 1× SSC, 0.2× SSC and 0.1× SSC at 65°C for 15 min each time. After washing, the membrane was sealed and put down under a phosphor screen (Fuji-Screen) for two days and scanned using Bio-Rad Molecular Imager FX system in combination with Quantity One software.

2.13 POLY(A) RNA PURIFICATION

Poly(A) RNA was purified from total RNA according to the protocol described in the Poly(A)Purist™ Kit (Ambion) in combination with home-made solutions.

Modified protocol is as follows. (1) Prepare the Oligo(dT) Cellulose: Prepare 25-30 mg Oligo(dT) Cellulose powder in a 2 ml tube and add 500 μl of 0.1 M NaOH. After a brief vortex, centrifuge the tube at 4,000× g and discard the supernatant. Wash the Oligo(dT) Cellulose with 1 ml of sterile water for 3 times. Afterwards, wash the Oligo(dT) Cellulose with 500 μl of 1× Binding buffer, which contains 6.3 μl of 3 M sodium acetate (pH 5.2), 243.7 μl of sterile water and 250 μl of 2× Binding buffer (4 M Tetramethyl ammonium chloride, 10 mM EDTA, 60 mM Trizma, 0.032% [v/v] Triton X-100). (2) Prepare the RNA sample: Start with 20 μg of total RNA and bring the sample volume to 250 μl using sterile water and 6.3 μl of 3 M sodium acetate (pH 5.2). (3) Bind to the Oligo(dT) Cellulose: Add 250 μl of 2× Binding buffer to the RNA sample and mix thoroughly. Afterwards, add each RNA sample to 1 tube of Oligo(dT) Cellulose. Heat the RNA/Oligo(dT) Cellulose mixture at 68^{o}C for 5 min and then rock the tube gently for 1 h at room temperature. Centrifuge the tube at 4,000× g for 3 min to pellet the Oligo(dT) Cellulose and keep the supernatant in the freezer until the recovery of poly(A) RNA has been confirmed. (4) Wash the Oligo(dT) Cellulose: Add 500 μl of Wash Solution 1 (1.3 M Tetramethyl ammonium chloride, 5 mM EDTA, 30 mM Trizma, 0.016% [v/v] Triton X-100) to the Oligo(dT) Cellulose pellet and vortex briefly to mix well. After centrifuging at 4,000× g for 3 min, discard the supernatant and wash the Oligo(dT) Cellulose pellet again using Wash Solution 1. Afterwards, wash the Oligo(dT) Cellulose twice with 500 μl of Wash Solution 2 (0.5 M Tetramethyl ammonium chloride, 5 mM EDTA, 30 mM Trizma, 0.016% [v/v] Triton X-100) each time. (5) Elute the poly(A) RNA and start the second round: Add 200 μl of preheated (68^{o}C) sterile water to the Oligo(dT) Cellulose pellet, mix briefly by

vortexing and then centrifuge immediately at 5,000× g for 3 min. Transfer the liquid to a fresh tube and keep the tube containing the Oligo(dT) Cellulose. Add 6.3 μl of 3 M sodium acetate (pH 5.2) and 43.7 μl of sterile water to the elution. Repeat from Step (3). (6) Recover the poly(A) RNA after a second round: After washes with Wash Solution 2 in the second round, elute the poly(A) RNA with 200 μl of preheated sterile water twice and keep two elutions separately. Centrifuge all elutions at 14,000 rpm and transfer the liquid to a fresh tube to get rid of the residual Oligo(dT) Cellulose. (7) Precipitate the poly(A) RNA: In each eluted poly(A) RNA sample, add 20 μl of 3 M sodium acetate (pH 5.2), 1 μl of glycogen and 600 μl of absolute ethanol. Mix by vortexing and leave the precipitation mixture at -20^{o}C overnight. (8) Next day, centrifuge the mixture to recover the poly(A) RNA pellet. Carefully wash and dry the pellet and resuspend the pellet in 6 μl of sterile water. Keep the poly(A) RNA sample at -80^{o}C until use.

2.14 m^{6}A MEASUREMENT

m^{6}A levels were measured by two-dimensional TLC analysis as described previously (Zhong et al., 2008). 50 ng of poly(A) RNA was digested by 1 μl of RNase T1 (1,000 U·ml^{-1}; Fermentas) in 1× polynucleotide kinase (PNK) buffer A at 37^{o}C for 1 h. 5′ ends of digested RNA fragments were labelled with 0.5 μl of [γ-^{32}P]ATP (6,000 Ci·mmol^{-1}; PerkinElmer) using 10 U of T4 PNK. After precipitation by 1/10 volume of 3 M sodium acetate (pH 5.2) and 3 volumes of absolute ethanol, the labelled RNA pellet was resuspended in nuclease P1 (Sigma-Aldrich) reaction mixture (1 μl of nuclease P1, 1 μl of nuclease P1 buffer,

8 µl of nuclease-free water). The reaction mixture was incubated at 37°C for at least 1 h to produce mononucleotides. After P1 digestion, 1 µl of the digested sample was loaded onto the cellulose TLC plate (20 × 20 cm; Merck) and developed in a solvent system, with isobutyric acid:0.5 M NH_4OH (5:3, v/v) as the first dimension buffer and isopropanol:HCl:water (70:15:15, v/v/v) as the second dimension buffer. The labelled nucleotides were identified and quantified by using a storage phosphor screen (Fuji-Screen) and Bio-Rad Molecular Imager FX system in combination with Quantity One software.

2.15 WESTERN BLOTTING

2.15.1 Protein Preparation

Two-week old seedlings harvested from plates containing 1/2 MS plus 1% (w/v) sucrose were ground into powder with liquid nitrogen. The powder was divided into 1.5 ml Eppendorf tubes (~ 100 mg in each one). In each tube, 400 µl of Lysis buffer (50 mM Tris-HCl pH 8.0, 10 mM EDTA pH 8.0, 1% [w/v] SDS, 1 mM phenylmethanesulfonyl fluoride [PMSF], 1% [v/v] Plant Protease Inhibitors [Sigma-Aldrich]) was added and mixed by vortexing. Tubes were kept on ice for 15 min and then centrifuged at 14,000 rpm for 5 min. Afterwards, supernatants were transferred into new tubes and used as protein samples. The protein content was measured according to instructions for "Bio-Rad Protein Assay". Five dilutions from concentrated bovine serum albumin (BSA, 1.36 $mg \cdot ml^{-1}$) was used to generate the standard curve for protein concentration assay. The absorbance of all prepared samples was measured at 595 nm using a

spectrophotometer and the protein concentration was calculated according to the standard curve by Excel.

2.15.2 Electrophoresis

Each protein sample (40 μg) was made up to 16 μl with sterile water and 4 μl of 5× Laemmi buffer (312.5 mM Tris-HCl pH 6.8; 50% [v/v] glycerol; 10% [w/v] SDS, 0.05% [w/v] bromophenol blue; 25% [v/v] β-mercaptoethanol) was added. The mixture was denatured at 95°C for 5 min and then loaded onto Bio-Rad Mini-PROTEAN® TGX™ Precast Gel. 7 μl of Bio-Rad protein marker (Precision Plus Protein™ Dual Color Standards) was also loaded. The gel was run in the electrophoresis buffer (25 mM Tris, 192 mM glycine, 0.1% [w/v] SDS) at 110 V for approximately 1 h and 30 min until the blue dye reached the bottom of the gel.

2.15.3 Transfer

Transferring was carried out following instructions for "Mini Trans-Blot® Electrophoretic Transfer Cell" (Bio-Rad). The gel was equilibrated using cold transfer buffer (25 mM Tris, 192 mM glycine and 20% [v/v] methanol, pH 8.3) for 30 min prior to transferring. Amersham™ Protran® western blotting membrane (nitrocellulose, pore size: 0.2 μm), filter paper and fibre pads were also soaked in cold transfer buffer before transferring. The transfer cassette was assembled according the manufacturer's instructions and the transfer was run at 120 V for 1 h.

2.15.4 Blocking and Incubation with Antibodies

The blocking and the following steps were carried out according to the protocol for "WesternBreeze® Chemiluminescent Western Blot Immunodetection" Kit. After blocking with 10 ml of Blocking Solution for 1 h, the membrane was rinsed twice with 20 ml of sterile water. Subsequently, the membrane was incubated with the primary antibody solution at room temperature for 1 h. The primary antibody was diluted according to the manufacturer's instructions. An anti-actin antibody, a rabbit polyclonal antibody targeting a set of actins in *Arabidopsis* (Agrisera) was used in this study as a control. After 4 washes with Antibody Wash Solution, the membrane was incubated with Secondary Antibody Solution for 30 min. Afterwards, the membrane was washed 4 times with Antibody Wash Solution and then washed twice with sterile water.

2.15.5 Incubation with Substrate

The Chemiluminescent Substrate was prepared following the manufacturer's instructions. The substrate was evenly applied onto the membrane and the reaction was developed at room temperature for 5 min. The extra substrate was removed by filter paper.

2.15.6 Detection

The membrane from the last step was placed between two pieces of transparency plastic and was then put into a cassette. In the dark room, a film was put on top

of the membrane and the exposure was kept for 1 min or longer (depending on the specificity of the primary antibody). Afterwards, the film was developed in Carestream® Kodak® autoradiography GBX developer/replenisher (Sigma-Aldrich) and then fixed by Carestream® Kodak® autoradiography GBX fixer/replenisher (Sigma-Aldrich). Finally, the film was scanned by GS-800™ Calibrated Imaging Densitometer (Bio-Rad) in combination with Quantity One software.

2.16 REFERENCES

BAND, L. R., WELLS, D. M., LARRIEU, A., SUN, J., MIDDLETON, A. M., FRENCH, A. P., BRUNOUD, G., SATO, E. M., WILSON, M. H., PÉRET, B., et al. 2012. Root gravitropism is regulated by a transient lateral auxin gradient controlled by a tipping-point mechanism. Proceedings of the National Academy of Sciences, 109, 4668-4673.

BODI, Z., ZHONG, S., MEHRA, S., SONG, J., GRAHAM, N., LI, H., MAY, S. & FRAY, R. G. 2012. Adenosine methylation in *Arabidopsis* mRNA is associated with the 3′ end and reduced levels cause developmental defects. Frontiers in Plant Science, 3.

BRUNOUD, G., WELLS, D. M., OLIVA, M., LARRIEU, A., MIRABET, V., BURROW, A. H., BEECKMAN, T., KEPINSKI, S., TRAAS, J., BENNETT, M. J. & VERNOUX T. 2012. A novel sensor to map auxin response and distribution at high spatio-temporal resolution. Nature, 482, 103-106.

CASIMIRO, I., MARCHANT, A., BHALERAO, R. P., BEECKMAN, T., DHOOGE, S., SWARUP, R., GRAHAM, N., INZÉ, D., SANDBERG, G.,

CASERO, P. J. & BENNETT M. 2001. Auxin transport promotes Arabidopsis lateral root initiation. The Plant Cell, 13, 843-852.

CLOUGH, S. J. & BENT, A. F. 1998. Floral dip: a simplified method for *Agrobacterium*-mediated transformation of *Arabidopsis thaliana*. The Plant Journal, 16, 735-743.

RŮŽIČKA, K., ZHANG, M., CAMPILHO, A., BODI, Z., KASHIF, M., SALEH, M., EECKHOUT, D., EL-SHOWK, S., LI, H., ZHONG, S., et al. 2017. Identification of factors required for m^6A mRNA methylation in *Arabidopsis* reveals a role for the conserved E3 ubiquitin ligase HAKAI. New Phytologist, 215, 157-172.

SCHMITT, M. E., BROWN, T. A. & TRUMPOWER, B. L. 1990. A rapid and simple method for preparation of RNA from *Saccharomyces cerevisiae*. Nucleic Acids Research, 18, 3091-3902.

SWARUP, R., KARGUL, J., MARCHANT, A., ZADIK, D., RAHMAN, A., MILLS, R., YEMM, A., MAY, S., WILLIAMS, L., MILLNER, P., et al. 2004. Structure-function analysis of the presumptive Arabidopsis auxin permease AUX1. The Plant Cell, 16, 3069-3083.

ZHONG, S., LI, H., BODI, Z., BUTTON, J., VESPA, L., HERZOG, M. & FRAY, R. G. 2008. MTA is an *Arabidopsis* messenger RNA adenosine methylase and interacts with a homolog of a sex-specific splicing factor. The Plant Cell, 20, 1278-1288.

CHAPTER 3 GENERATION AND CHARACTERISATION OF HAKAI KNOCKOUT MUTANTS AND HAKAI-GFP LINES

3.1 ABSTRACT

N^6-methyladenosine (m^{6}A) is the most abundant internal mRNA modification in most eukaryotes. Its formation is catalysed by the methyltransferase (MTase) complex (m^{6}A writer complex), which contains MTA as the major mRNA adenosine methylase in *Arabidposis*. MTA was initially shown to be closely associated with FIP37 and more recently additional components have been identified which expand the complex to include MTB, FIP37, Virilizer and Hakai (an E3 ubiquitin ligase). As a novel member of the MTase complex, the role of Hakai in mRNA methylation both in plants and in mammals is not yet understood. To study the function of Hakai, firstly *hakai* knockout mutants and the complementation line (Hakai-GFP/*hakai*) containing *Hakai* genomic DNA under its own promoter and with a GFP tag downstream were generated and characterised. Two homozygous *hakai* knockout mutants were obtained via CRISPR-Cas9 and a homozygous *Hakai* intron-located T-DNA insertion mutant was also characterised. The two *Hakai* CRISPR mutants showed complete knockout of *Hakai* transcripts and *Hakai* transcript in *Hakai* T-DNA insertion mutant was truncated and much reduced compared with that in WT. The m^{6}A level in *hakai* mutants was decreased by 33-44% and this could be recovered to the wild-type level in the Hakai-GFP/*hakai* line, suggesting Hakai is required for full m^{6}A methylation. *hakai* mutants demonstrated significantly increased lateral root formation on higher concentrations of sucrose (>3% [w/v]). In addition,

maximal Hakai-GFP expression was localised to root tips and lateral root initiation sites. Together, these results indicate that Hakai may interact with sugar signalling in regulating *Arabidopsis* lateral root development.

3.2 AIMS AND OBJECTIVES OF THIS CHAPTER

To study the function of Hakai, the work in this chapter is focused on generating and characterising *hakai* knockout mutants and transgenic lines expressing *GFP*-tagged *Hakai* under its own promoter (Hakai-GFP). Specifically, the transcriptional expression, m^6A levels, Hakai-GFP localisation and phenotypes are analysed utilising the *hakai* mutants and Hakai-GFP lines that are generated. These results provide initial data determining whether Hakai is part of the m^6A writer complex and to what extent it is required for m^6A formation.

3.3 METHODS

3.3.1 Genotyping *Hakai* T-DNA Insertion Mutants

To acquire *Hakai* knockout mutants, our first consideration was to screen pre-existing *Hakai* T-DNA insertion lines. Four putative *Hakai* T-DNA insertion lines were chosen. Among them, SALK_109428, GK-259E01 and SALK_148797 are located upstream of the start codon, possibly in the promoter region, and GK-217A12 is located in the first intron (Figure 3.1, Table 2.1). Genotyping methods are detailed in 2.4.

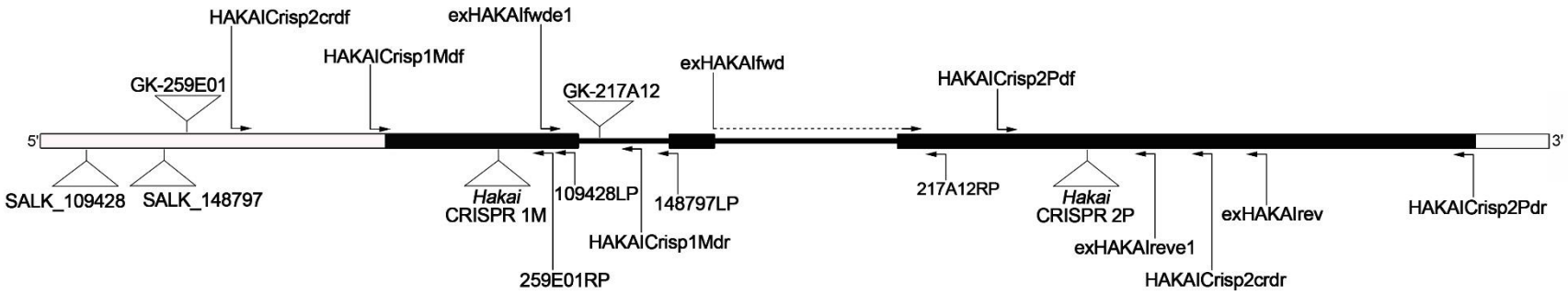

Figure 3.1 Schematic of *Hakai* genomic DNA sequence with T-DNA insertion sites, CRISPR target sites and primers used. White rectangle denotes UTR, black rectangle denotes exon and thick black line represents intron. Forward T-DNA insertions and primers are labelled above genomic DNA strands and those in the same direction as the complementary strand are labelled below genomic DNA strands. The two *Hakai* CRIPSR targets are towards the complementary DNA strand. *Hakai* CRISPR 1M denotes *Hakai* CRIPSR target site 1 overlapping *Mly*I recognition site and *Hakai* CRISPR 2P denotes *Hakai* CRIPSR target site 2 overlapping *Pvu*II recognition site. HAKAICrisp1Mdf, HAKAICrisp1Mdr, HAKAICrisp2Pdf, HAKAICrisp2Pdr, HAKAICrisp2crdf and HAKAICrisp2crdr were used for screening following *Hakai* CRISPR mutagenesis. LP and RP represent left primer and right primer on *Hakai* genomic DNA sequence. 259E01LP, 217A12LP, 109428RP and 148797RP are located upstream of the 5' UTR (not shown here). exHAKAIfwd and exHAKAIrev, exHAKAIfwde1 and exHAKAIreve1 are two pairs of primers for checking the expression level of *Hakai* by RT-PCR.

3.3.2 RT-PCR Analysis

To check the expression level of *Hakai* in candidate *Hakai* T-DNA insertion mutants by RT-PCR analysis, firstly, total RNAs were prepared following the protocol described in 2.11. To get rid of DNA contamination, prepared total RNAs were treated with DNase as follows. Sterile water was added to the RNA sample to bring the sample volume to 44 µl, and then 5 µl of 10× Turbo DNase buffer, 1 µl of Turbo DNase (Ambion) were added. The mixture was incubated at 37°C for 30 min. Afterwards, the volume of treated RNA sample was brought to 100 µl using sterile water, and then 100 µl of phenol/chloroform was added to the RNA sample and mixed by vortexing. After centrifuging at 14,000 rpm for 5 min, the supernatant was transferred to a new 1.5 ml Eppendorf tube and the same volume of chloroform was added and mixed by vortexing. After another centrifugation, the supernatant was again transferred to a new 1.5 ml tube and precipitated by adding 1/10 volume of 3 M sodium acetate (pH 5.2), 1 µl of glycogen and 3 volumes of absolute ethanol. The mixture was vortexed and precipitated at -20°C overnight. After washing and drying, the RNA pellet was dissolved in 10 µl of sterile water.

First-strand cDNAs were synthesised using Moloney Murine Leukemia Virus (M-MLV) reverse transcriptase (Promega) according to the manufacturer's instructions with some modifications. In each 0.2 ml PCR tube, 5 µl of total RNA, 3 µl of 100 µM Oligo(dT) and 7 µl of nuclease-free water were added and incubated at 70°C for 5 min and then chilled on ice immediately. Afterwards, 5 µl of M-MLV 5× Reaction Buffer, 2.5 µl of 10 mM dNTPs, 1.5 µl of nuclease-

free water and 1 μl of M-MLV reverse transcriptase (200 $U \cdot \mu l^{-1}$) were added. The mixture was incubated at 42°C for 90 min. The synthesised first-strand cDNAs were kept at -20°C until use. *AtActin2* (At3g18780) was used as a reference gene in RT-PCRs. PCR reagents and programmes were prepared and set following that in 2.3.

3.3.3 Generation of *Hakai* CRIPSR Mutants

Clustered regularly interspaced short palindromic repeat-CRISPR associated 9 (CRISPR-Cas9) was used to obtain additional *Hakai* knockout mutants. CRISPR-Cas9 used in genome engineering includes a DNA endonuclease Cas9 which cleaves the target DNA into double-strand breaks (DSBs) under the guidance of a single guide RNA (sgRNA) with 5' end composed of a 20-nt sequence complementary to the target DNA and 3' end as a double-stranded structure that binds to Cas9 (Figure 3.2a) (Jinek et al., 2012; Charpentier and Doudna, 2013; Doudna and Charpentier, 2014). The recognition of the target DNA sequence is based on the presence of a conserved protospacer-adjacent motif (PAM) downstream of the target DNA, which usually has the consensus sequence 5'-NGG-3' (Jinek et al., 2012). After cleavage, the DSBs are then repaired via two different cellular DNA repair mechanism – non-homologous end joining (NHEJ) and homologous recombination (HR) (Figure 3.2b). NHEJ-mediated repair utilises DNA ligase IV to re-join broken ends and produces random insertions or deletions (indels) (Kim and Kim, 2014; Belhaj et al., 2015). If a homologous DNA donor is provided as the template for DSB repair, this leads to precise gene corrections (a single-base-pair change) or insertions (Kim

and Kim, 2014; Bortesi and Fischer, 2015). In most cases, NHEJ repair mechanism predominates (Carroll, 2014; Belhaj et al., 2015; Bortesi and Fischer, 2015).

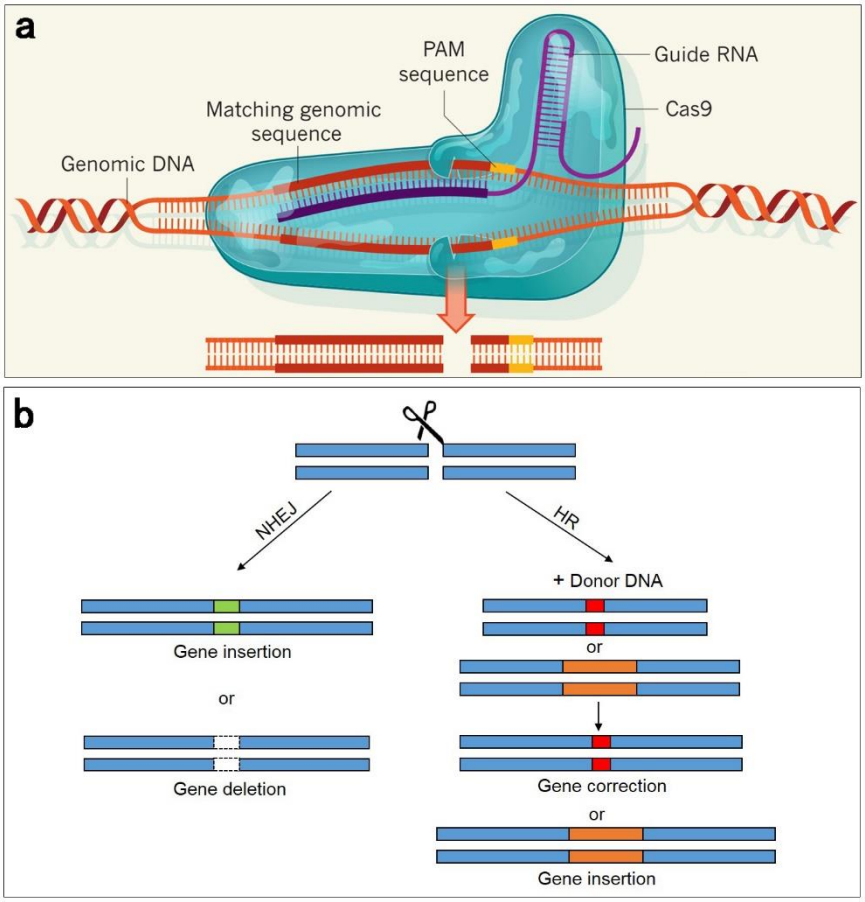

Figure 3.2 The mechanism of CRISPR-Cas9. (**a**) The DNA endonuclease Cas9 is guided to the target DNA via a single guide RNA (sgRNA) and its cleavage leads to double-strand breaks (DSBs). Protospacer-adjacent motif (PAM) sequence located downstream of the target DNA sequence is required for the recognition of target DNA (Charpentier and Doudna, 2013). (**b**) DSBs are repaired via either non-homologous end joining (NHEJ) or homologous recombination (HR) (adapted from Bortesi and Fischer, 2015).

CRISPR constructs were generated using the Golden Gate cloning method (Weber et al., 2011). In the present study, two sgRNA target sites were selected

and each of them overlaps a restriction enzyme site, *Mly*I and *Pvu*II, respectively (Figure 3.1), to facilitate the subsequent mutagenesis screening via the restriction enzyme site loss method (Voytas, 2013). sgRNAs were amplified from pICH86966::AtU6p::sgRNA_PDS construct (Addgene plasmid 46966) and assembled to Level 1 vector (pICH47751) as follows (Figure 3.3). In a 0.2 ml PCR tube, 100 ng Level 0 vector pICSL01009 (containing *Arabidopsis U6* promoter), 20 ng amplified sgRNA product, 100 ng Level 1 vector (pICH47751), 20 U *Bsa*I (NEB), 1× NEB CutSmart Buffer, 1 mM ATP, 1500 U T7 DNA Ligase (NEB) were mixed in a total volume of 10 μl and incubated in a thermocycler at 37°C for 5 min and then 20°C for 5 min, 20 cycles in total. Afterwards, the reaction was inactivated at 80°C for 20 min.

After transforming to competent *E. coli* cells (DH5α) and culturing on LB plus carbenicillin (100 $mg \cdot L^{-1}$), single colonies were checked by PCR and plasmid DNAs were prepared from correct colonies. Subsequently, plasmid containing sgRNA under *AtU6* promoter (AtU6p::sgRNA) was assembled to a Level 2 vector using the similar restriction-ligation system as above (Figure 3.4). The reagents include 100 ng Level 2 vector (pAGH4723), 100 ng pICH47732 plasmid (containing plant selectable marker NPTII), 100 ng pICH47742 plasmid (containing *Cas9* under CaMV 35S promoter), 100 ng AtU6p::sgRNA (pICH47751), 100 ng pICH41766 plasmid (containing a linker), 20 U *Bpi*I (NEB), 1× NEB CutSmart Buffer, 1 mM ATP and 1500 U T7 DNA Ligase (NEB) in a total volume of 10 μl. The PCR programme was the same as above. After transforming to DH5α competent cells and culturing on LB plus kanamycin (Kan)

(50 mg·L^{-1}), single colonies were checked by PCR and digestion of plasmid DNA. Correct ones were confirmed by sequencing.

For the CRISPR construct containing two sgRNA target sites, the linker was replaced by one of the AtU6p::sgRNAs. Specifically, one AtU6p::sgRNA sequence was amplified from generated AtU6p::sgRNA plasmid with primers containing the same overhangs upstream and downstream of the linker (Refer to Appendix 1 for detailed information about the primers). After restriction-ligation reaction and transformation, the final construct was confirmed by colony PCR and sequencing.

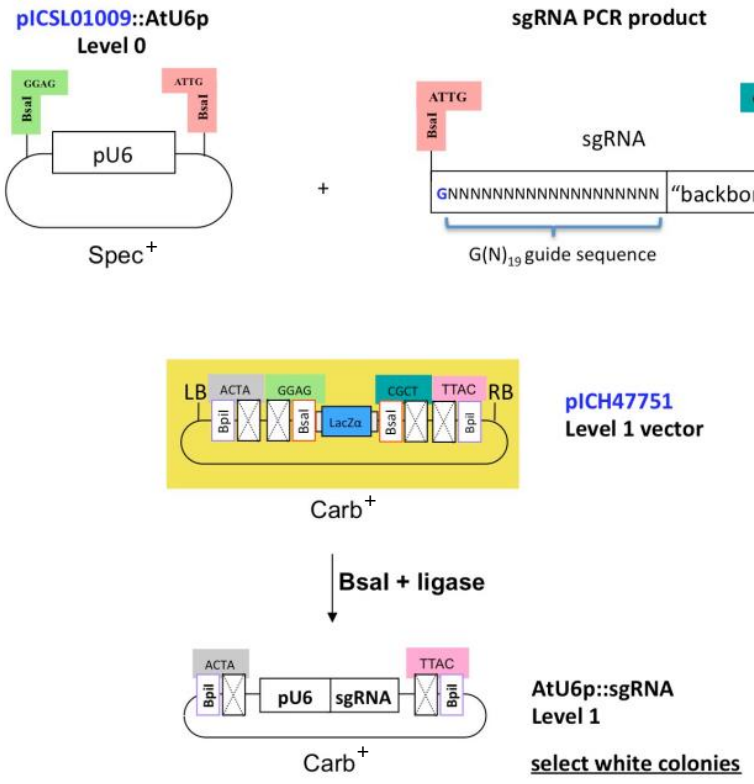

Figure 3.3 Assembly of sgRNA and its driven promoter *Arabidopsis U6* promoter to a Level 1 Golden Gate vector (Protocol from the Sainsbury laboratory). Spec^{+}: spectinomycin resistance; Carb^{+}: carbenicillin resistance.

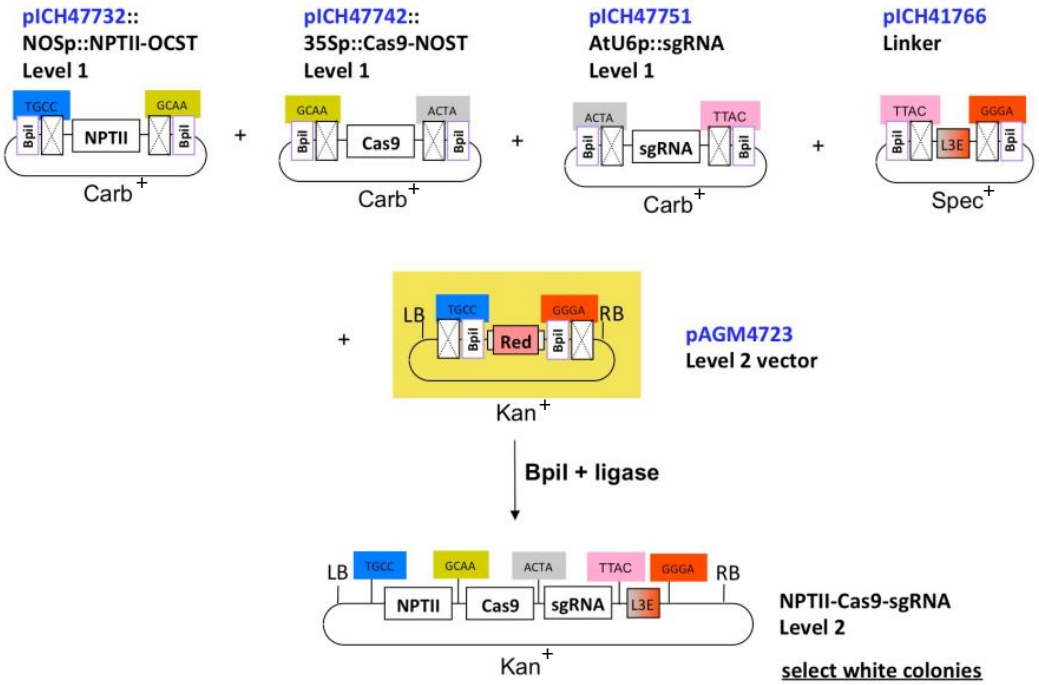

Figure 3.4 Level 1 Golden Gate vectors containing kanamycin selectable marker, Cas9 and sgRNA separately were assembled together to a Level 2 Goden Gate vector (Protocol from the Sainsbury laboratory). $Spec^+$: spectinomycin resistance; $Carb^+$: carbenicillin resistance; Kan^+: kanamycin resistance.

3.3.4 Screening of *Hakai* CRIPSR Mutants

After floral dip transformation to the wild-type *Arabidopsis*, T_0 seeds were planted on MS medium containing 50 $mg \cdot L^{-1}$ Kan to screen positive T_1 plants. Positive T_1 plants were transplanted to the compost. Genomic DNAs were extracted from leaves of these plants for the following screening by the restriction enzyme site loss method (Voytas, 2013). Firstly, genomic DNA was digested by the enzyme with recognition site overlapping the sgRNA target site (*Mly*I and *Pvu*II, respectively) to reduce unaltered wild-type DNA in the sample (Nekrasov et al., 2013). For the digestion by *Mly*I (NEB), ~ 500 μg genomic DNA was used in the presence of 1× CutSmart Buffer and 5 U *Mly*I in a total

volume of 10 µl. For the digestion by *Pvu*II (Thermo Scientific), 1× Buffer G and 5 U *Pvu*II were used. The digestion was carried out at 37°C for 1 h. Subsequently, PCR was performed using the digested DNA as the template and primers flanking the sgRNA target site (Figure 3.1, Appendix 1). PCR product was precipitated by 1/10 volume of 3 M sodium acetate (pH 5.2) and 3 volumes of absolute ethanol overnight. After washing and drying, the pelleted PCR product was dissolved in 4 µl of sterile water. A second digestion was followed using 2 µl of precipitated PCR product. Partially cut samples were sequenced using forward primers for PCR to confirm possible mutagenesis. To screen T_2 and the following generations, PCR was performed directly using diluted DNA sample as the template, followed by digestion and finally confirmed by sequencing. The presence of CRISPR construct in T_2 transgenic plants was checked by PCR using primers located on *Cas9* sequence (Appendix 1). In the subsequent generations, mutants absent of CRISPR-Cas9 constructs were selected.

3.3.5 Generation of Hakai-GFP Lines in Mutant and Wild-type Backgrounds

Gateway cloning was used to generate recombinant constructs containing *GFP*-tagged *Hakai* transgene. The procedures are illustrated in Figure 3.5. To start with, *Hakai* genomic DNA sequence including its own promoter was amplified by PCR. After gel excision and precipitation overnight, the DNA pellet was dissolved in 16.5 µl of sterile water. To clone the PCR product into Gateway entry vector using the pCR™8/GW/TOPO® TA Cloning® Kit (Invitrogen),

adenosine overhangs were added to the 3' ends by incubating the PCR product at 73°C for 30 min in the presence of 0.25 mM dNTPs, 1× Standard *Taq* Reaction Buffer and 5 U *Taq* DNA Polymerase in a final volume of 20 µl. The PCR product was then precipitated overnight by adding 2 µl of 3 M sodium acetate (pH 5.2) and 60 µl of absolute ethanol. Next day, the DNA pellet was dissolved in 10 µl of sterile water. The following TOPO cloning reaction was prepared by mixing 1 µl of PCR product (5-10 ng), 1 µl of salt solution, 3 µl of sterile water and 1 µl of TOPO vector. The reaction was incubated at room temperature for 30 min and then transformed to competent *E. coli* OneShot® TOP10 cells. After analysing the transformants by PCR, plasmids were prepared from correct single colonies and confirmed by sequencing. The plasmid containing correct and forward *Hakai* genomic DNA sequence was used for the following LR reaction using Gateway® LR Clonase™ II Enzyme Mix (Invitrogen).

To set up the LR reaction, 1 µl of the recombinant entry vector (50-100 ng), 1 µl of pGreen-based Gateway destination vector containing GFP tag (150 ng) and 6 µl of sterile water were mixed in a 0.2 ml PCR tube. After thawing the LR Clonase™ II Enzyme Mix on ice and a brief mix by vortexing, 2 µl of the LR Clonase™ II Enzyme Mix was added and the reaction was incubated at 25°C for 3 h. The reaction was terminated by adding 1 µl of the Protein K solution (2 $\mu g \cdot \mu l^{-1}$) and incubating the reaction at 37°C for 10 min. After transformation to competent *E. coli* OneShot® TOP10 cells and following the analysis as above, 1 µl of correct recombinant plasmid together with 1 µl of pSoup plasmid (100 $ng \cdot \mu l^{-1}$) (to support the replication of pGreen-based Gateway destination vector in *Agrobacterium*) was transformed to *Agrobacterium* strain C58 via

electroporation. The recombinant plasmid in *Agrobacterium* was then transformed to the wild-type *Arabidopsis* or *hakai* mutant lines (denominated as Hakai-GFP lines) via floral dip method as detailed in 2.10.

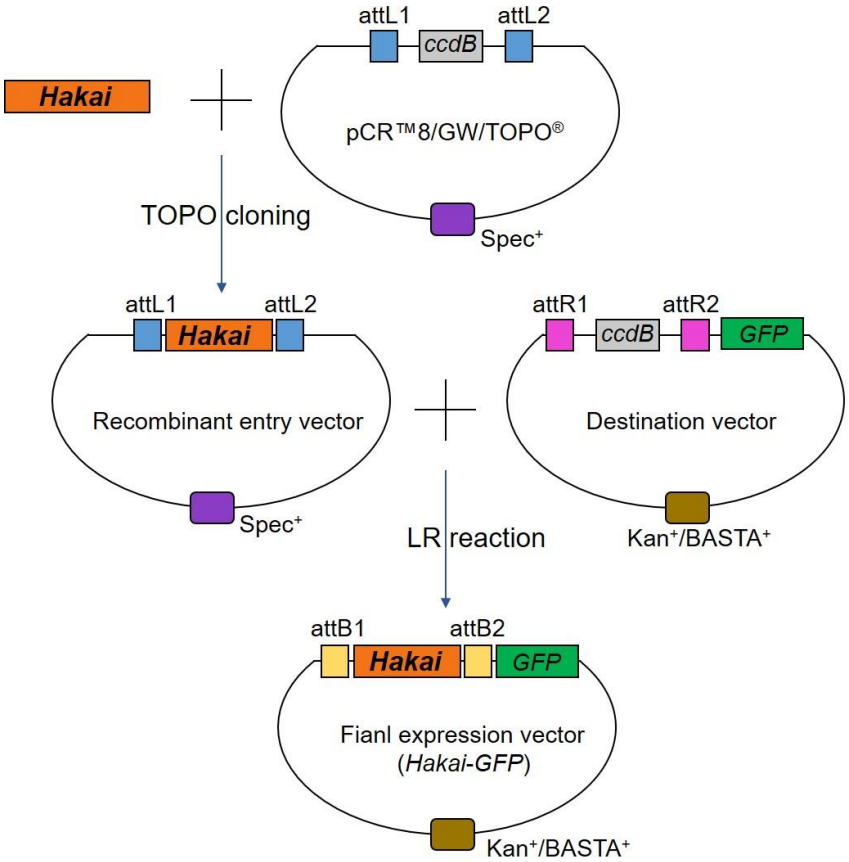

Figure 3.5 A schematic illustrating the generation of *Hakai-GFP* recombinant construct via Gateway cloning. $Spec^+$: spectinomycin resistance; Kan^+: kanamycin resistance; $BASTA^+$: BASTA resistance; att: attachment site; *ccdB* gene in Gateway vectors inhibits the propagation of *ccdB*-containing plasmids in standard *E. coli* strains.

3.3.6 Screening of Hakai-GFP Lines

Seeds harvested from floral-dipped *Arabidopsis* plants (T_0) were screened by planting seeds on medium with the appropriate antibiotic to screen positive T_1 plants. Subsequently, positive T_1 plants were further screened by PCR using the forward primer on *Hakai* sequence and the reverse one on *GFP* to confirm the

presence of the construct. In the following generations, homozygous Hakai-GFP lines were screened by planting 40-50 seeds on 1/2 MS medium plus the appropriate antibiotic or by checking the GFP signal under the Stereo Fluorescence Microscope (Leica). Afterwards, the localisation of GFP signal was checked under the confocal microscope (Leica TCS SP5) using the homozygous lines.

3.3.7 Checking Transcriptional Levels of *Hakai* by Northern Blotting

Transcriptional levels of *Hakai* in *hakai* mutants and Hakai-GFP lines were further analysed by northern blotting as described in 2.12. Primers used for amplifying the DNA template for RNA probe are listed in Appendix 1.

3.3.8 m^6A Measurement

The m^6A levels in *hakai* mutants and Hakai-GFP lines were analysed by two-dimensional TLC analysis according to that detailed in 2.14.

3.3.9 Analysis of Root Phenotypes

Seeds were prepared as described in 2.1 and cultured on vertical plates containing 1/2 MS basal medium plus different concentrations of sucrose or sorbitol. Seedlings were photographed on the 8th or 9th day of culturing in the tissue culture room. The number of lateral roots (LRs) was recorded and root

lengths were measured using Image J software. Statistical analysis was carried out via IBM SPSS Statistics 22.

3.4 RESULTS

3.4.1 Homozygous *Hakai* T-DNA Insertion Mutants and Their Transcriptional Levels of *Hakai*

Among four putative *Hakai* T-DNA insertion mutants – SALK_109428, GK-259E01, SALK_148797 and GK-217A12, SALK_148797 and GK-217A12 demonstrated correct bands in genotyping PCR using the forward primer on the inserted T-DNA (LB) and the reverse one (RP) on *Hakai* genomic DNA whereas there were no bands using both primers located on *Hakai* genomic DNA, thus these two lines were homozygous (Figure 3.6a-c). RT-PCR with the forward primer located upstream of GK-217A12 insertion site and the reverse one downstream of GK-217A12 insertion site (exHAKAIfwde1 and exHAKAIreve1, Figure 3.1, Appendix 1) showed that transcript levels of *Hakai* was knocked out in GK-217A12, but not in SALK_148797 (Figure 3.6d,e). However, RT-PCR using another pair of primers downstream of GK-217A12 insertion site (exHAKAIfwd and exHAKAIrev, Figure 3.1, Appendix 1) revealed that the *Hakai* transcript present in GK-217A12 might be truncated (Figure 3.6f). Therefore, GK-217A12 (henceforth termed 217A12) could be used as a *hakai* knockout mutant, despite not being ideal.

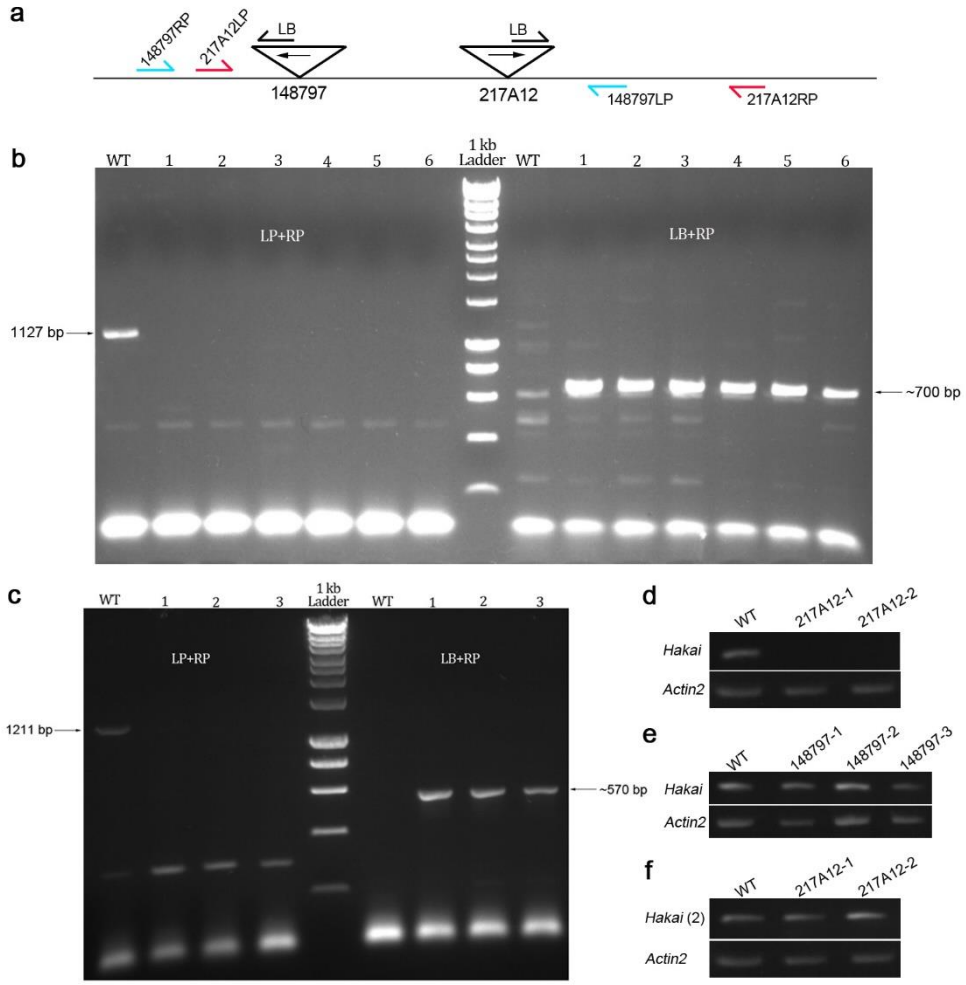

Figure 3.6 Screening *Hakai* T-DNA insertion mutants. (**a**) Schematic showing locations of SALK_148797 and GK-217A12 T-DNA insertion sites and primers used in genotyping PCRs. LP and RP represent left primer and right primer on *Hakai* genomic DNA sequence whilst LB refers to left border primer on the inserted T-DNA. (**b**) Genotyping PCR of SALK_148797. Sample 1 to 6 represent six individual DNA samples from line SALK_148797. (**c**) Genotyping PCR of GK-217A12. Sample 1 to 3 represent three individual DNA samples from line GK-217A12. (**d**) RT-PCR analysis of the expression of *Hakai* in GK-217A12 using primer pairs flanking GK-217A12 T-DNA insertion site. (**e**) RT-PCR analysis of the expression of *Hakai* in SALK_148797 using primer pairs flanking GK-217A12 T-DNA insertion site. (**f**) RT-PCR analysis of the expression of *Hakai* in GK-217A12 using primer pairs downstream of GK-217A12 T-DNA insertion site.

3.4.2 Homozygous *Hakai* CRISPR Mutants

Given that *Hakai* T-DNA insertion line 217A12 may be not ideal for generating a true null phenotype, CRISPR-Cas9-mediated mutagenesis was applied. Three CRISPR constructs aiming at knocking out *Hakai* were generated, including two constructs with a single sgRNA and one with two sgRNA genes, denominated as *Hakai*-CRISPR1M (overlapping *Mly*I recognition site), *Hakai*-CRISPR2P (overlapping *Pvu*II recognition site) and *Hakai*-CRISPR2cr (containing both of the above sgRNA genes), respectively. The sequencing results of completed constructs are shown in Supplementary figure 3.1.

After floral dip transformation, the total number of screened transgenic T_1 lines (termed *hakai*-1M, *hakai*-2P and *hakai*-2cr in accordance with the CRISPR constructs used for transformation) and plants showing mutations is summarised in Table 3.1. PCR products that were partially cut by the specific restriction enzyme (Figure 3.7) were confirmed by sequencing. No mutant plants were found in *hakai*-2P line whereas 8 out of 29 plants showed mutagenesis in *hakai*-1M line. In addition, the sequencing data showed that the mutagenesis in *hakai*-2cr lines occurred only in CRISPR target site overlapping *Mly*I recognition site (Figure 3.8b,c). Thus, the mutation at the sgRNA target site overlapping *Mly*I recognition site was more efficient than that at the sgRNA target site overlapping *Pvu*II recognition site. Multiple peaks in all sequenced mutants indicate that all mutant T_1 lines are heterozygous (Figure 3.8b).

Table 3.1 Summary of screening T_1 lines of *Hakai* CRISPR mutants

Line name	No. of positive plants selected by kanamycin	No. of plants screened by digestion and PCR	No. of plants showing mutagenesis	Presence of Cas9 in mutant lines
hakai-1M	29	29	8	Yes
hakai-2P	41	41	0	Yes
hakai-2cr	27	27	4	Yes

Note: 1M represents sgRNA target site overlapping *Mly*I recognition site; 2P represents overlapping *Pvu*II recognition site; 2cr refers to containing both of the above sgRNA genes on one CRISPR construct.

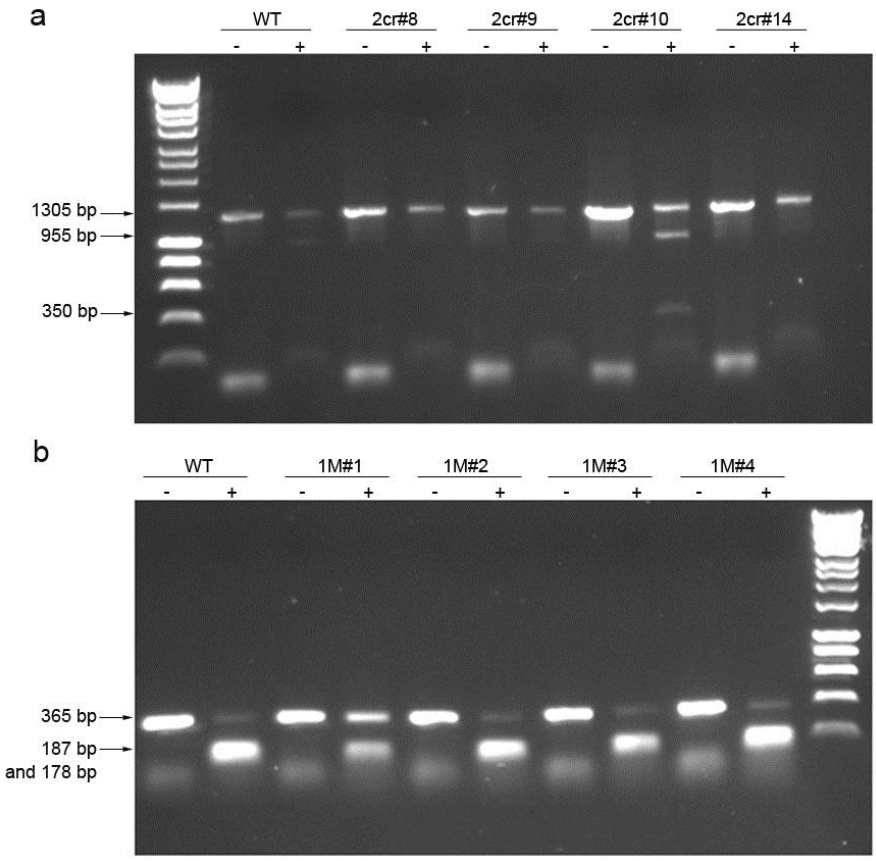

Figure 3.7 Screening for *Hakai* CRISPR mutants in the T_1 generation. (a) Digestion of *hakai*-2cr lines by *Mly*I. (b) Digestion of *hakai*-1M lines by *Mly*I. -, Undigested PCR product amplified by using primers flanking the sgRNA target site; +, Digested PCR product amplified by using primers flanking the sgRNA target site. 2cr represents containing two sgRNAs on one CRISPR construct and 1M represents sgRNA target site overlapping *Mly*I recognition site. Sample *hakai*-2cr#8, *hakai*-2cr#9, *hakai*-2cr#14 and *hakai*-1M#1 were clearly partially cut.

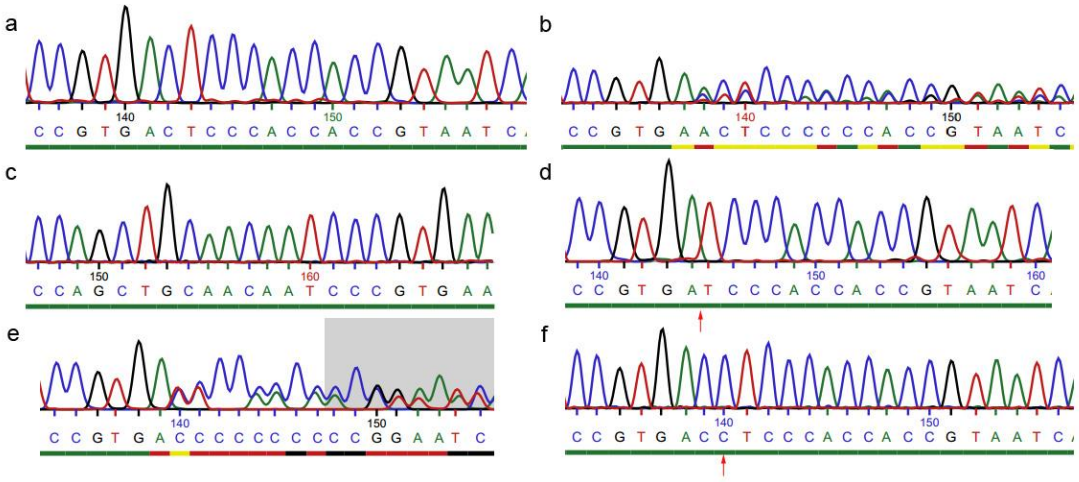

Figure 3.8 Sequencing profiles of *hakai* mutants compared with WT at sgRNA target sites. (**a**) The forward wild-type sequence at the sgRNA target site overlapping *Mly*I recognition site. (**b**) The forward sequence of T_1 generation at the sgRNA target site overlapping *Mly*I recognition site showed multiple peaks. (**c**) The forward sequence of T_1 generation at the sgRNA target site overlapping *Pvu*II recognition site showed no changes. (**d**) The forward sequence of *hakai*-2cr#14-37 at the sgRNA target site overlapping *Mly*I recognition site showed one nucleotide deletion of C. (**e**) The forward sequence of heterozygous *hakai*-2cr#14 at the sgRNA target site overlapping *Mly*I recognition site showed multiple peaks. (**f**) The forward sequence of *hakai*-2cr#21-17-6 at the sgRNA target site overlapping *Mly*I recognition site showed one nucleotide addition of C. Mutation sites are labelled with red arrows.

The screening of T_2 lines from mutant T_1 lines (*hakai*-1M#1, *hakai*-2cr#8, *hakai*-2cr#9, *hakai*-2cr#14, *hakai*-2cr#21) is summarised in Table 3.2. Though the mutagenesis efficiency was very low, seven plants in screened *hakai*-2cr#14 line showed mutation and two of them (*hakai*-2cr#14-37 and *hakai*-2cr#14-53) were homozygous, with one nucleotide deletion of C (Figure 3.8d,e). In addition, another heterozygous mutant (*hakai*-2cr#21-17) was discovered in *hakai*-2cr#21 line.

Table 3.2 Summary of screening T_2 lines of *Hakai* CRISPR mutants

Line name	No. of screened plants	No. of mutants	No. of homozygous mutants
hakai-1M#1	60	0	0
hakai-2cr#8	24	0	0
hakai-2cr#9	24	0	0
hakai-2cr#14	180	7	2
hakai-2cr#21	56	1	0

Note: 1M represents sgRNA target site overlapping *Mly*I recognition site; 2P represents overlapping *Pvu*II recognition site; 2cr refers to containing both of the above sgRNA genes on one CRISPR construct.

In the following T_3 line, homozygous *hakai*-2cr#14-37 and *hakai*-2cr#14-53 were confirmed by sequencing. Screening of homozygous mutants from heterozygous *hakai*-2cr#21-17 was continued. Furthermore, the absence of the CRISPR construct was confirmed by checking *Cas9* sequence by PCR (Figure 3.9). Finally, four T_4 plants in *hakai*-2cr#21-17-6 line demonstrated homozygous mutagenesis, all with one nucleotide addition of C (Figure 3.8f). In summary, two homozygous *Hakai* CRISPR mutant lines from which the T-DNA carrying the CRISPR sequences had been crossed out were obtained. Homozygous *hakai*-2cr#14-37 and *hakai*-2cr#21-17-6 (termed *hakai* 37 and *hakai* 21, respectively) were used in the following experiments.

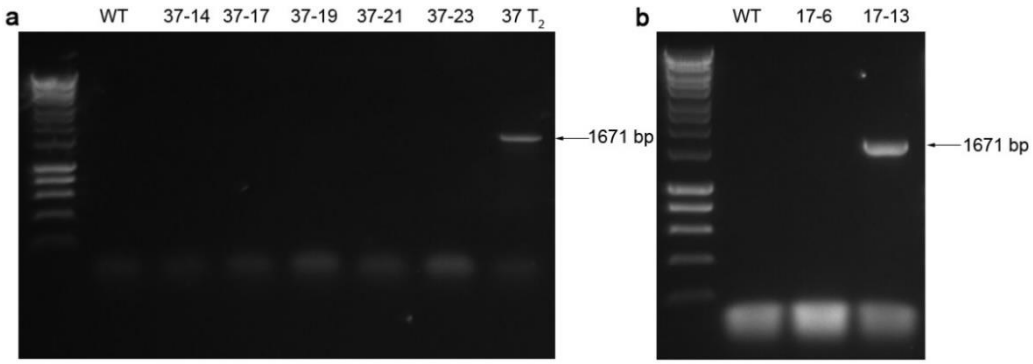

Figure 3.9 Identification of Cas9-free T_3 generation of *Hakai* CRISPR mutants by PCR using primers on *Cas9* sequence. (**a**) The presence of *Cas9* in T_3 progenies of *hakai*-2cr#14-37 (37-14, 37-17, 37-19, 37-21, 37-23) compared with that in T_2 parental line (labelled 37 T_2) and WT. (**b**) The presence of *Cas9* in two T_3 progenies of *hakai*-2cr#21-17.

To confirm the true mutagenesis via CRISPR-Cas9, *hakai* 37 and *hakai* 21 were backcrossed with the wild-type *Arabidopsis*, the same mutagenesis form was discovered in F_2 generations of both *hakai* 37 and *hakai* 21 crossed with WT, which verifies that the mutations caused in *hakai* 37 and *hakai* 21 were mediated via CRISPR-Cas9 (Figure 3.10).

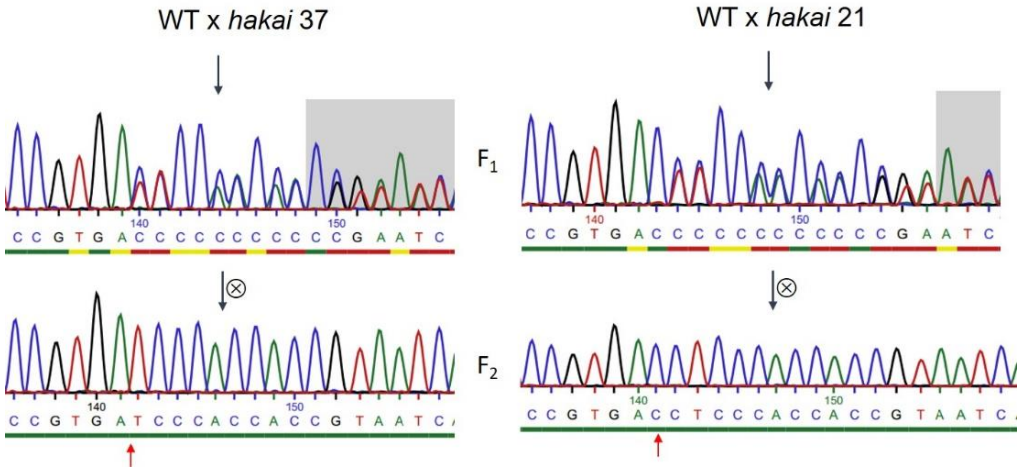

Figure 3.10 Sequencing profiles of the progeny of *hakai* mutants backcrossed with WT. Mutation sites are labelled with red arrows.

3.4.3 Homozygous Hakai-GFP Lines and Their GFP Localisation

Hakai genomic DNA with its own promoter (without stop codon and 3' UTR) was amplified (2,062 bp, Figure 3.11a) and cloned to Gateway destination vectors pGKGWG (no promoter, with GFP tag and Kan resistance for plants) or pGBGWG (no promoter, with GFP tag and BASTA resistance for plants) (Zhong et al., 2008a) by Gateway cloning. Two destination vectors with different plant selectable markers were chosen for the ease of screening when crossed with other lines. Single colonies were checked by PCR (Figure 3.11b) and the schematic of the final recombinant construct is shown in Figure 3.11c. Following *Agrobacterium* electroporation and floral dip transformation to the wild-type *Arabidopsis* and *hakai* 37, positive T_1 plants (denominated as Hakai-GFP) were screened by Kan or BASTA and confirmed by PCR using the forward primer on *Hakai* genomic sequence and the reverse one on *GFP* (Figure 3.12, Appendix 1).

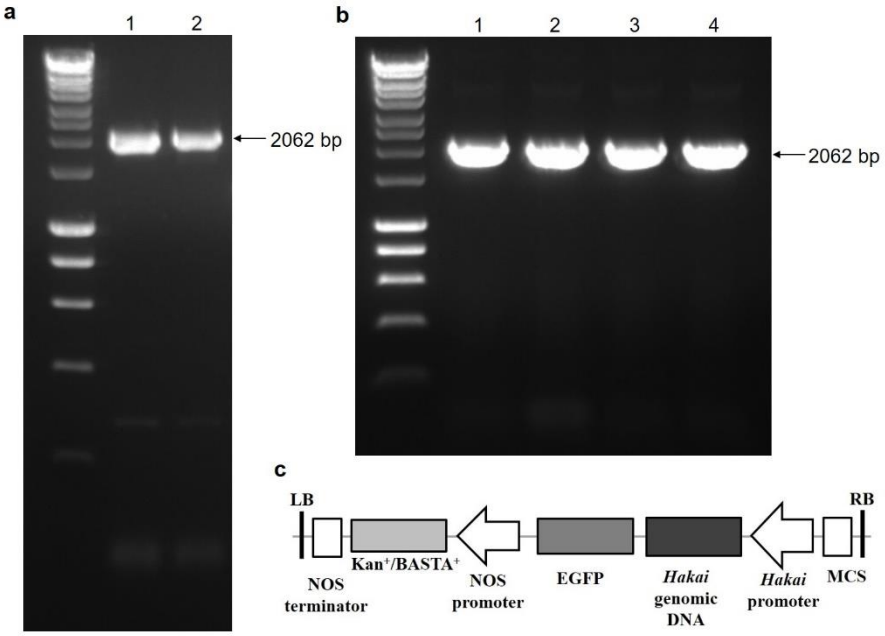

Figure 3.11 Generating *Hakai-GFP* constructs. (**a**) Amplifing *Hakai* genomic DNA with its own promoter. Sample 1 and 2 were two individual PCR products. (**b**) PCR to check *E. coli* single colonies after cloning *Hakai* genomic DNA sequence under its own promoter into Gateway destination vector pGKGWG. Sample 1 to 4 were PCR products from four individual single colonies. (**c**) The schematic of recombinant *Hakai-GFP* constructs; Kan^+: kanamycin resistance for plants; $BASTA^+$: BASTA resistance for plants.

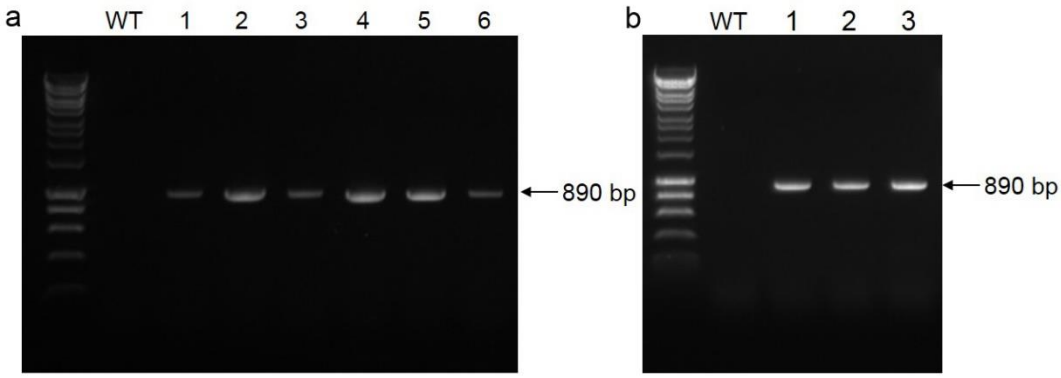

Figure 3.12 Checking positive Hakai-GFP T_1 plants by PCR. (**a**) Hakai-GFP in *hakai* 37 mutant background. Sample 1 to 6 represent six individual T_1 plants. (**b**) Hakai-GFP in WT background. Sample 1 to 3 represent three individual T_1 plants.

T_2 generation of Hakai-GFP lines with Kan resistance were planted on 1/2 MS medium plus 50 mg·L^{-1} Kan to screen homozygous lines and those with BASTA resistance were planted on vertical plates containing 1/2 MS medium to screen for the homozygous lines by viewing GFP signals in all seedlings. Two homozygous Hakai-GFP lines were discovered in both *hakai* 37 mutant background and WT background (Figure 3.13). These lines were termed Hakai-GFP/*hakai*#2, Hakai-GFP/*hakai*#5, Hakai-GFP/WT#1 and Hakai-GFP/WT#2. Among them, Hakai-GFP/WT#1 harbours BASTA resistance while others are resistant to Kan. Analysis of GFP signal by confocal microscopy showed that Hakai-GFP was primarily localised in the nuclei of root tips and LR initiation sites (Figure 3.14).

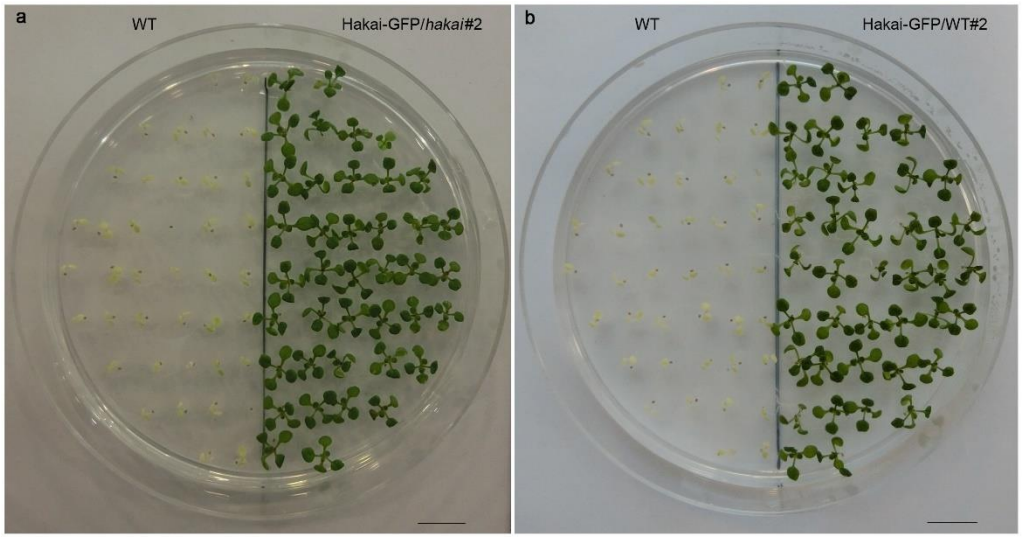

Figure 3.13 10-d old homozygous Hakai-GFP lines planted on 1/2 MS medium plus Kan. (**a**) Hakai-GFP/*hakai*#2. (**b**) Hakai-GFP/WT#2. Scale bar = 1 cm.

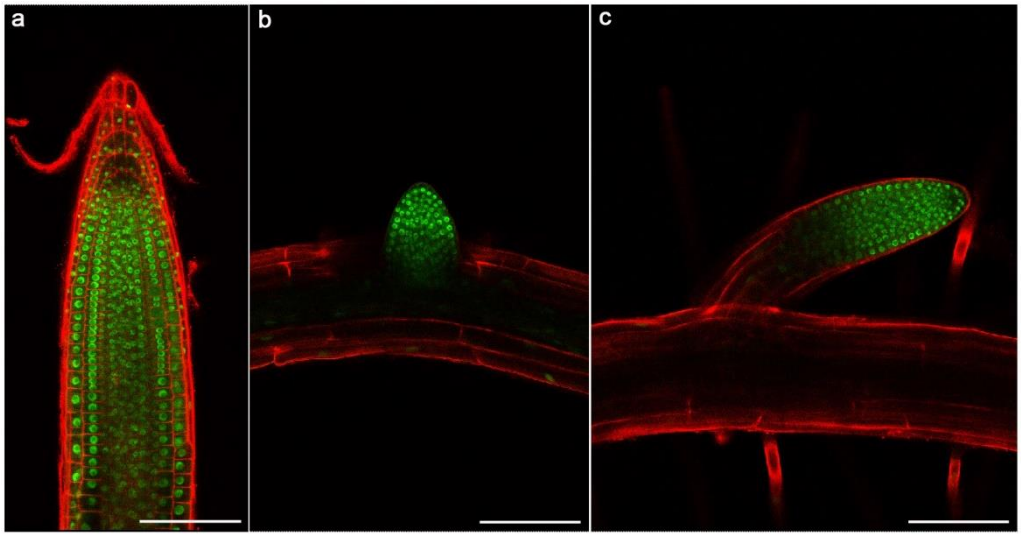

Figure 3.14 The localisation of Hakai-GFP in roots of Hakai-GFP/*hakai*. (**a**) Root tip of a primary root. (**b**) A lateral root initiation site. (**c**) A formed lateral root. Scale bar = 100 μm.

3.4.4 Transcriptional Levels of *Hakai* in *hakai* Mutants and Hakai-GFP Lines

Northern blotting demonstrated that the transcripts of *Hakai* in *Hakai* CRISPR mutants (*hakai* 37 and *hakai* 21) were completely knocked out while that in *Hakai* T-DNA insertion mutant 217A12 was much reduced and truncated relative to that in the wild-type *Arabidopsis* (Figure 3.15). In contrast, the complementation line Hakai-GFP/*hakai*#2 only showed very strong *Hakai-GFP* transgene transcript while Hakai-GFP line in WT background (Hakai-GFP/WT#1) showed both transcripts (Figure 3.15).

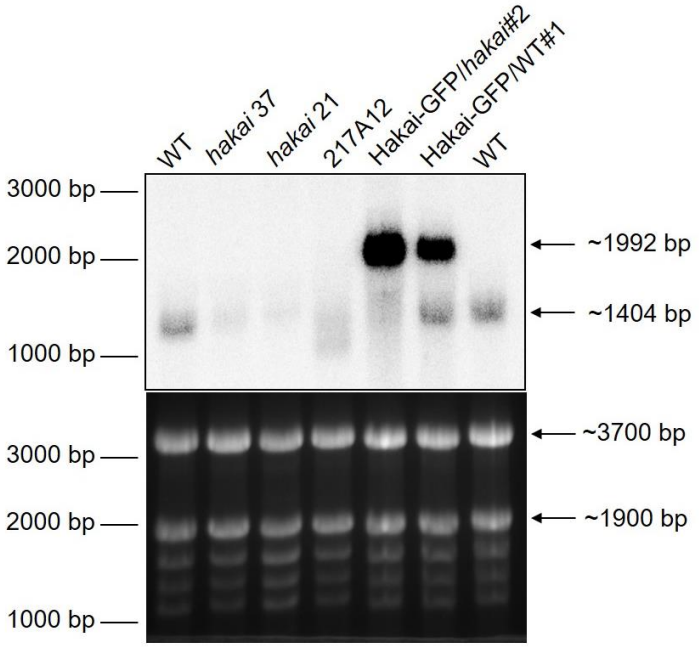

Figure 3.15 Transcriptional level of *Hakai* checked by northern blotting. Top: northern blotting membrane; Bottom: total RNAs loaded on the gel, 8 μg per sample.

3.4.5 m^{6}A Levels in *hakai* Mutants and the Complementation Line

m^{6}A measurement by two-dimensional TLC analysis (Figure 3.16) showed that the m^{6}A level in *hakai* mutants, especially *Hakai* CRISPR mutants, was significantly less than that in the wild-type *Arabidopsis*, with a 33-44% reduction (Figure 3.17). In contrast, the m^{6}A level in the complementation line Hakai-GFP/*hakai*#2 recovered to the wild-type level (Figure 3.17).

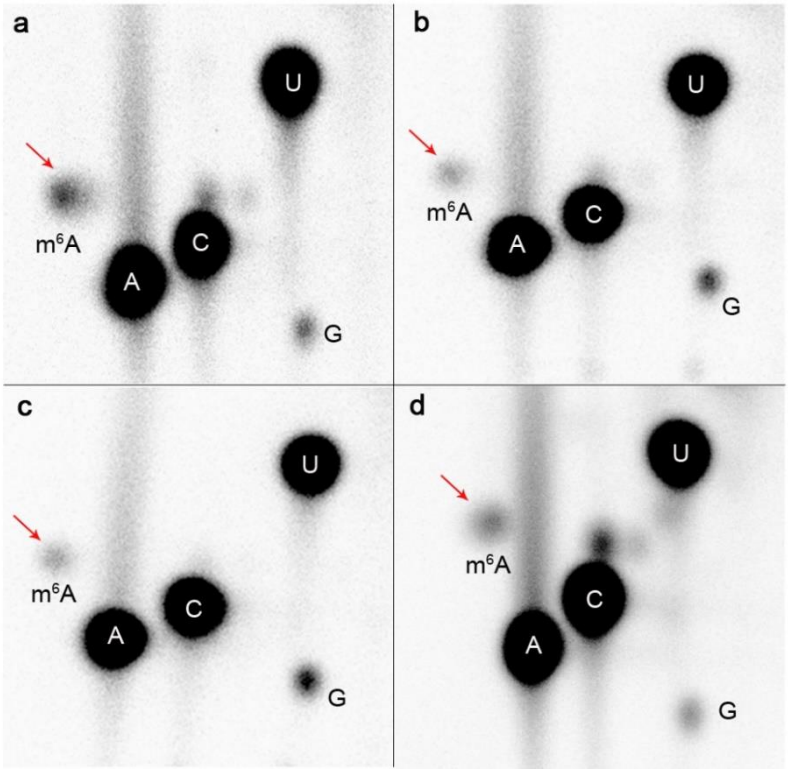

Figure 3.16 Two-dimensional TLC analysis of m^{6}A levels. (**a**) WT. (**b**) *hakai* 37. (**c**) 217A12. (**d**) Hakai-GFP/*hakai*#2. Spots representing m^{6}A are pointed with red arrows.

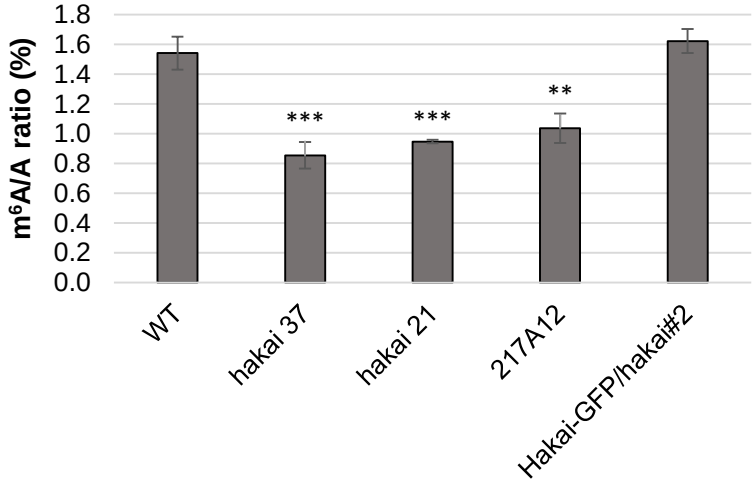

Figure 3.17 Summary of m^{6}A levels checked by two-dimensional TLC analysis. Data represent mean ± SEM from three biological replicates and statistically significant differences relative to WT were analysed by One-Way ANOVA and marked with asterisks (**, $p<0.01$; ***, $p<0.001$).

3.4.6 Root Phenotypes of *hakai* Mutants and the Complementation Line

Though above-ground phenotypes of *hakai* mutants resemble WT, our culturing of seedlings on petri dishes implied that more LRs formed in *hakai* mutants. Thus, we compared root development in WT and *hakai* mutants vertically cultured on 1/2 MS plus different concentrations of sucrose. Generally, *hakai* 37 and 217A12 showed significantly shorter primary roots on lower concentrations of sucrose (0% [w/v, the same for the following ones], 1% and 2%) relative to WT but this was not the case for *hakai* 21 (Figure 3.18a). However, this trend was no longer obvious on higher concentrations of sucrose (3%, 4% and 5%) (Figure 3.14b). In terms of LR development, though *hakai* 37 demonstrated fewer LRs compared with WT on 1% sucrose, all three *hakai* mutants showed dramatically increased LRs on higher concentrations of sucrose, particularly on 4% sucrose (Figure 3.18c,d). Because leaves of some seedlings on higher concentrations of sucrose became purple, an implication of being stressed, and osmotic stress may be the primary stress under our culturing conditions, we cultured WT and *hakai* seeds on 1/2 MS plus different concentrations of sorbitol (0 mM, 29 mM, 58 mM, 87 mM, 116 mM and 145 mM of sorbitol, equals 0%, 1%, 2%, 3%, 4% and 5% of sucrose, respectively). The statistical data showed that numbers of LRs on different concentrations of sorbitol demonstrated the same trend: except for *hakai* 37, which showed more LRs upon all tested concentrations of sorbitol, the difference of the number of LRs between WT and the other two *hakai* mutants were indistinguishable (Supplementary figure 3.2). Taken together, it suggests that increased LRs in *hakai* mutants on higher concentration of sucrose might not be a consequence of being stressed.

The root development in the complementation line of *hakai* 37, Hakai-GFP/*hakai*#2, was also compared with WT and *hakai* 37 cultured on 1% sucrose and 3% sucrose. On 1% sucrose, Hakai-GFP/*hakai*#2 behaved similarly to WT, complementing shorter primary roots and fewer LRs of *hakai* 37 (Figure 3.19). Very strangely, Hakai-GFP/*hakai*#2 also demonstrated significantly increased number of LRs as that in *hakai* 37 on 3% sucrose rather than complementing the phenotype of *hakai* 37 (Supplementary figure 3.3).

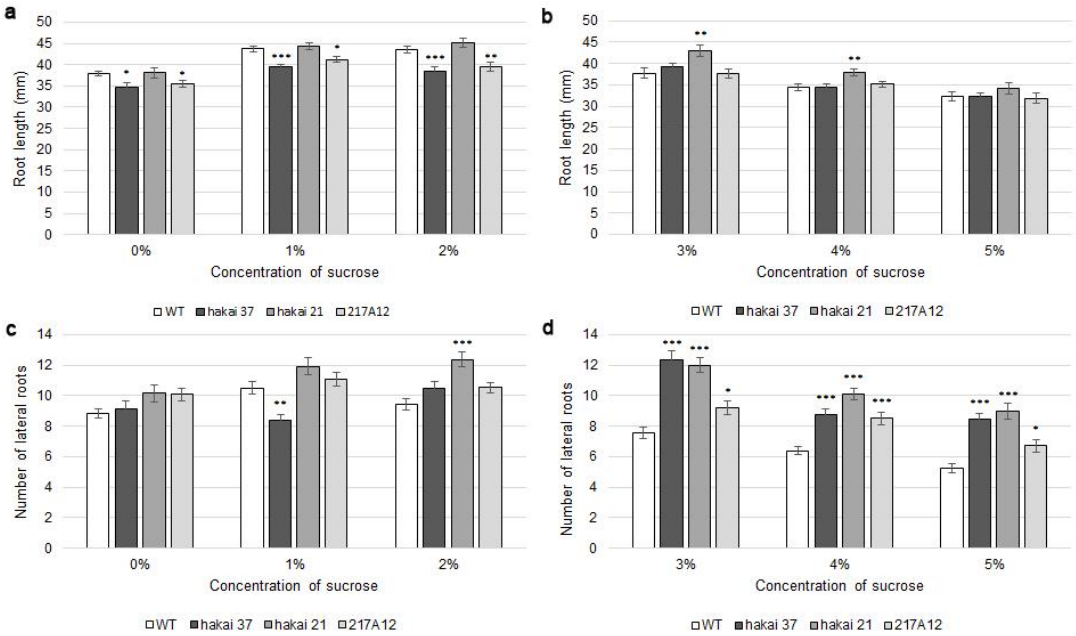

Figure 3.18 Root phenotypes of *hakai* mutants compared with WT vertically cultured on 1/2 MS plus different concentrations of sucrose. (**a**) Root lengths of 8-d old seedlings. (**b**) Root lengths of 9-d old seedlings. (**c**) The number of lateral roots of 8-d old seedlings. (**d**) The number of lateral roots of 9-d old seedlings. Data represent mean ± SEM and statistically significant differences compared with WT via One-Way ANOVA are marked with asterisks (*, $p<0.05$; **, $p<0.01$; ***, $p<0.001$).

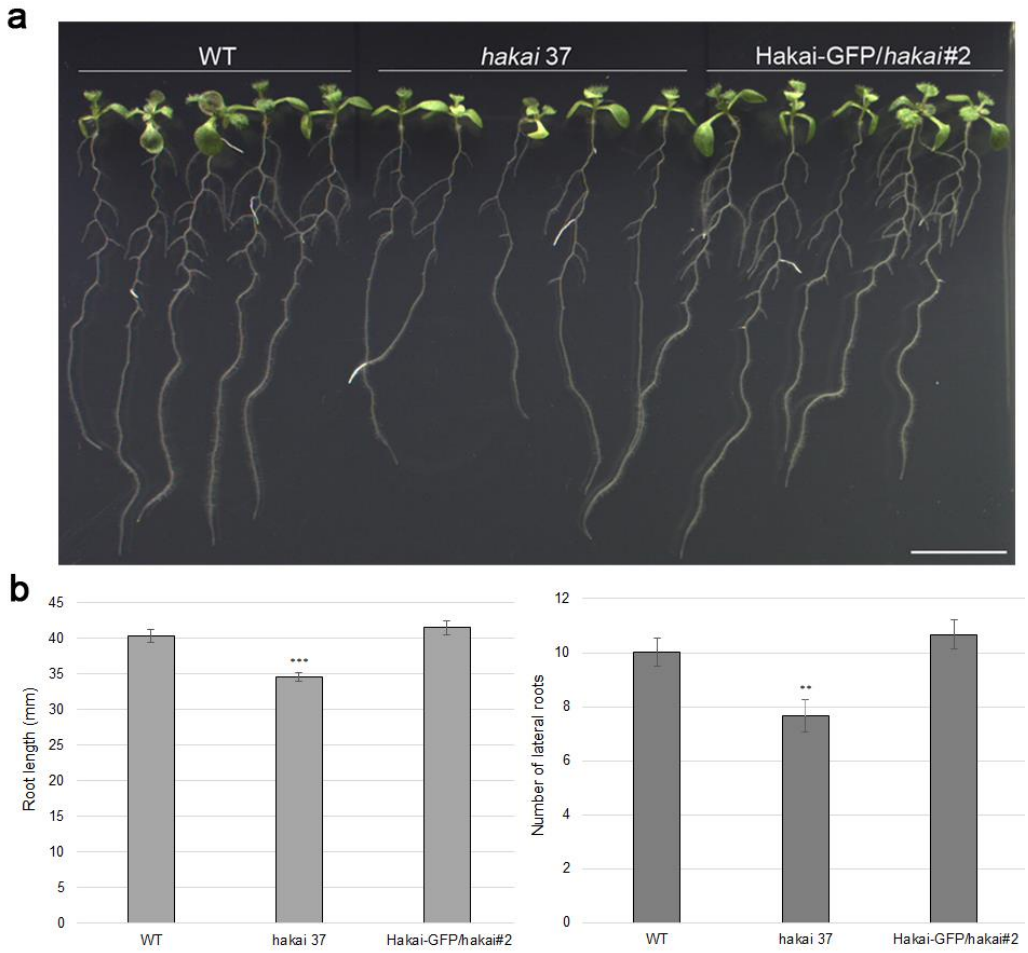

Figure 3.19 Root phenotype of 8-d old *hakai* 37 and its complementation line vertically cultured on 1/2 MS plus 1% sucrose. (**a**) The image of cultured seedlings. Scale bar = 1 cm. (**b**) Statistical data showing primary root lengths and the number of lateral roots. Data represent mean ± SEM and statistically significant differences compared with WT via One-Way ANOVA are marked with asterisks (**, $p<0.01$; ***, $p<0.001$).

3.5 DISCUSSION

3.5.1 The Efficiency of CRISPR-Cas9-mediated Mutagenesis

Previous studies have shown that the CRISPR-Cas9 system could be successfully used in editing plant genomes (Feng et al., 2013, 2014; Li et al., 2013; Nekrasov et al., 2013; Shan et al., 2013; Upadhyay et al., 2013; Brooks et

al., 2014; Jiang et al., 2013, 2014; Liang et al., 2014; Zhang et al., 2014; Butler et al., 2015; Lawrenson et al., 2015; Ma et al., 2015; Kishi-Kaboshi et al., 2017). These studies also illustrate that the mutagenesis efficiency of this system varies among different plant species, normally higher in tobacco and tomato than in *Arabidopsis* (Li et al., 2013; Nekrasov et al., 2013; Brooks et al., 2014). In *Arabidopsis*, CRISPR-Cas9 induced mutagenesis is predominantly single-nucleotide changes or short deletions while that in tobacco and tomato can be considerable DNA deletions or substitutions (Li et al., 2013; Brooks et al., 2014; Feng et al., 2014). Feng et al. (2014) found that gene modifications via CRISPR-Cas9 detected in *Arabidopsis* T_1 plants occurred mostly in somatic cells, and consequently there are no T_1 plants that are homozygous for a gene modification event. Homozygous gene modifications caused by CRISPR-Cas9 occur from the T_2 generation and are heritable in the following generations (Feng et al., 2014). However, Ma et al. (2015) did find homozygous mutagenesis in *Arabidopsis* T_1 plants but with very low frequency (1.7%). In contrast, the homozygous mutagenesis accounts for 24.7% in the first generation of rice transformants (Ma et al., 2015). Likewise, homozygous mutagenesis via CRISPR-Cas9 can be found in the first generation of transformed tomato plants (Brooks et al., 2014). The high mutagenesis efficiency of CRIPSR-Cas9 depends on the occurance of CRIPSR-Cas9-mediated mutagenesis in germ cells and only mutagenesis happens in germ cells can be inherited into the next generation. Therefore, *Cas9* driven by CaMV 35S promoter might not be efficiently expressed in germ cells of *Arabidopsis*. Consequently, the CRIPSR-Cas9-mediated mutagenesis could not take place efficiently in germ cells of *Arabidopsis*.

The process of screening CRISPR-Cas9-mediated mutagenesis targeting *Hakai* in this study confirms conclusions in previous studies. Screening a large number of plants to discover the homozygous *hakai* mutants indicates the low efficiency of CRISPR-Cas9 system in *Arabidopsis*. As to the mutation type, only one nucleotide deletion or addition was found in this study, but the mutation was stably inheritable because the backcrossed lines and plants in the subsequent generations of the homozygous mutant lines showed the same mutation. The different mutagenesis efficiency of two chosen sgRNA targets in the current study verifies that the efficiency of mutagenesis via CRISPR-Cas9 is partially dependent on the selected target sequence itself. Surprisingly, our northern blotting demonstrated that the transcript of *Hakai* in *Hakai* CRISPR mutants was efficiently knocked out, which may be regulated by some decay pathways, such as nonsense-mediated mRNA decay (NMD) pathway. NMD is a quality-control mechanism that eliminates aberrant transcripts that contain premature termination codons, thereby preventing the accumulation of truncated, potentially deleterious proteins (Shaul, 2015). The mechanism controlling the extremely efficient reduction of *Hakai* transcript upon CRISPR-Cas9-mediated mutagenesis is an interesting question to answer.

3.5.2 Hakai Is Required for Full m^6A Methylation

Though mammalian Hakai has been shown as an interacting partner of WTAP in cell cycle regulation, it has not been suggested as a member of mammalian m^6A writer complex (Horiuchi et al., 2013). Our previous co-immunoprecipitation assay demonstrates that Hakai is involved in the plant

MTase complex (Růžička et al., 2017). Thus, the current study was focused on elucidating the role of Hakai in m^6A modification. The m^6A level in *hakai* mutants reduced by 33-44% whereas that in the complementation line recovered to the wild-type level, which proves that the existence of Hakai contributes to the full m^6A abundance in *Arabidopsis* and suggests that Hakai is a bona fide member of the MTase complex. In contrast, m^6A level in *fip37* or *virilizer* knockdown mutants is more reduced, which is comparable to the decrease in ABI3A6 (Bodi et al., 2012; Růžička et al., 2017). In addition, full knockout of MTA, MTB, FIP37 or Virilizer is embryo lethal (Vespa et al., 2004; Zhong et al., 2008b; Bodi et al., 2012; Růžička et al., 2017) whereas *hakai* knockout mutant resembles WT. Therefore, the function of Hakai in the MTase complex may not be as important as other members or there may be some special roles of Hakai acting as a member of the complex. E3 ubiquitin ligases usually target proteins for decay by ubiquitination. Therefore, we had thought that Hakai could be a negative regulator and m^6A might go up in the *hakai* knockout mutant but in fact this was not the case. It is still possible that Hakai may be a negative regulator but also is physically required as a component of the m^6A writer complex. Perhaps the complex integrity is compromised when it is mutated thus there is less m^6A, even if it acts to negatively regulate protein(s) in the complex under specific developmental/environmental conditions.

3.5.3 A Possible Regulatory Role of Sugar Signal on *hakai* Phenotypes

It is well-known that auxin is a key signal during LR development (Casimiro et al., 2003). The process of *Arabidopsis* LR development and auxin signalling

pathway are detailed in Chapter 5. Aside from auxin, multiple environmental factors and nutritional cues also influence LR formation (Bellini et al., 2014). Soluble sugars, such as sucrose and glucose, affect *Arabidopsis* LR development in a complicated manner due to several reasons (Gibson, 2005). Firstly, plants have multiple sugar-response pathways and sugars can be sensed directly or act as signalling molecules. Secondly, alterations in sugar flux or in carbon/nitrogen ratios rather than sugar or sugar-metabolite levels may be actually involved in the sugar response (Gibson, 2005). One example is that *Arabidopsis* seedlings grown on nutrient media with a high sucrose to nitrogen ratio show dramatically repressed LR initiation (Malamy and Ryan, 2001). Thirdly, sugar signalling also "cross-talks" with numerous other factors, for example, light (Gibson, 2005). In addition, sugars can also affect osmotic potentials apart from as signalling molecules, complicating the understanding of sugar response (Gibson, 2005).

In the current study, significantly increased LR formation in *hakai* mutants on higher concentrations of sucrose (>3%) which could not be mimicked by seedlings cultured on the same concentrations of sorbitol indicates the interaction between sugar signalling and Hakai in regulating LR formation, though this phenotype could not be changed by the complementation with the wild-type *Hakai* transgene on 3% sucrose and one *hakai* mutant – *hakai* 37 demonstrated significantly fewer LRs on 1% sucrose. In addition, Hakai-GFP was primarily localised to root tips and LR initiation site, consistent with the localisation of MTA (Zhong et al., 2008b) and other members of the MTase complex (not shown). This suggests a general role of m^6A modification in mediating root development. As to the reason why Hakai-GFP/*hakai* could not

complement the root phenotypes of *hakai* 37 on 3% sucrose, it may be due to the fact that the generated *Hakai-GFP* construct is not identical to the natural endogenous *Hakai* gene (without 3' UTR and maybe not including the intact 5' UTR) or 3% sucrose (possibly represents an "extreme condition") may trigger a different set of gene expression changes compared with the influence of 1% sucrose.

The participation of E3 ubiquitin ligases involved in other pathways in regulating LR development has been reported (Xie et al., 2002; Sibout et al., 2006). One example is SINAT5, an *Arabidopsis* homologue of the RING-finger *Drosophila* protein SINA. It can ubiquitinate NAC1, which functions downstream of auxin signalling module and transduces the auxin signal for LR development. The ubiquitination of NAC1 by SINAT5 reduces the LR formation (Xie et al., 2000, 2002). Another E3 ubiquitin ligase, CONSTITUTIVE MORPHOGENIC 1 (COP1) directly interacts with the basic leucine zipper transcription factor HY5, a positive regulator of photomorphogenesis, and promotes its proteasome-mediated degradation (Holm et al., 2002). HY5 has also been implicated in negatively regulating auxin signalling pathway as the *hy5* mutant shows accelerated LR formation (Sibout et al., 2006). This indirectly suggests a role of COP1 in regulating LR development. As an E3 ubiquitin ligase, it is possible that Hakai plays a regulatory role in LR development with or without the involvement of sugar signalling.

3.6 CONCLUSIONS

In conclusion, two homozygous *hakai* knockout mutants were generated via CRISPR-Cas9 and a homozygous *Hakai* intron-located T-DNA insertion mutant was also used for characterisation. The complementation line (termed Hakai-GFP/*hakai*) was generated by transforming one *hakai* knockout mutant with a construct containing *Hakai* genomic DNA under its own promoter and with a GFP tag downstream. The transcript of *Hakai* was undetectable in *Hakai* CRISPR mutants and was much reduced and truncated in *Hakai* T-DNA insertion mutant relative to that in WT. The m^6A level in *hakai* mutants was 33-44% reduced compared with that in WT and the normal m^6A level could be restored in Hakai-GFP/*hakai*. *hakai* mutants demonstrated variable root phenotypes under different conditions but generally showed increased LRs on higher concentrations of sucrose (>3%). In addition, Hakai-GFP was primarily localised to root tips and LR initiation sites. Taken together, Hakai is required for full m^6A methylation and may interact with sugar signalling in regulating *Arabidopsis* LR development.

3.7 REFERENCES

BELHAJ, K., CHAPARRO-GARCIA, A., KAMOUN, S., PATRON, N. J. & NEKRASOV, V. 2015. Editing plant genomes with CRISPR/Cas9. Current Opinion in Biotechnology, 32, 76-84.

BELLINI, C., PACURAR, D. I. & PERRONE, I. 2014. Adventitious roots and lateral roots: similarities and differences. Annual Review of Plant Biology, 65, 639-666.

BODI, Z., ZHONG, S., MEHRA, S., SONG, J., GRAHAM, N., LI, H., MAY, S. & FRAY, R. G. 2012. Adenosine methylation in *Arabidopsis* mRNA is associated with the 3′ end and reduced levels cause developmental defects. Frontiers in Plant Science, 3.

BORTESI, L. & FISCHER, R. 2015. The CRISPR/Cas9 system for plant genome editing and beyond. Biotechnology Advances, 33, 41-52.

BROOKS, C., NEKRASOV, V., LIPPMAN, Z. B. & VAN ECK, J. 2014. Efficient gene editing in tomato in the first generation using the clustered regularly interspaced short palindromic repeats/CRISPR-associated9 system. Plant Physiology, 166, 1292-1297.

BUTLER, N. M., ATKINS, P. A., VOYTAS, D. F. & DOUCHES, D. S. 2015. Generation and inheritance of targeted mutations in potato (*Solanum tuberosum* L.) using the CRISPR/Cas system. PLoS One, 10, e0144591.

CARROLL, D. 2014. Genome engineering with targetable nucleases. Annual Review of Biochemistry, 83, 409-439.

CASIMIRO, I., BEECKMAN, T., GRAHAM, N., BHALERAO, R., ZHANG, H., CASERO, P., SANDBERG, G. & BENNETT, M. J. 2003. Dissecting *Arabidopsis* lateral root development. Trends in Plant Science, 8, 165-171.

CHARPENTIER, E. & DOUDNA, J. A. 2013. Rewriting a genome. Nature, 495, 50-51.

DOUDNA, J. A. & CHARPENTIER, E. 2014. The new frontier of genome engineering with CRISPR-Cas9. Science, 346, 1258096.

FENG, Z., MAO, Y., XU, N., ZHANG, B., WEI, P., YANG, D.-L., WANG, Z., ZHANG, Z., ZHENG, R., YANG, L., et al. 2014. Multigeneration analysis reveals the inheritance, specificity, and patterns of CRISPR/Cas-induced gene modifications in Arabidopsis. Proceedings of the National Academy of Sciences, 111: 4632-4637.

FENG, Z., ZHANG, B., DING, W., LIU, X., YANG, D.-L., WEI, P., CAO, F., ZHU, S., ZHANG, F., MAO, Y. & ZHU J.-K. 2013. Efficient genome editing in plants using a CRISPR/Cas system. Cell Research, 23, 1229-1232.

GIBSON, S. I. 2005. Control of plant development and gene expression by sugar signaling. Current Opinion in Plant Biology, 8, 93-102.

HOLM, M., MA, L.-G., QU, L.-J. & DENG, X.-W. 2002. Two interacting bZIP proteins are direct targets of COP1-mediated control of light-dependent gene expression in *Arabidopsis*. Genes & Development, 16, 1247-1259.

HORIUCHI, K., KAWAMURA, T., IWANARI, H., OHASHI, R., NAITO, M., KODAMA, T. & HAMAKUBO, T. 2013. Identification of Wilms' tumor 1-associating protein complex and its role in alternative splicing and the cell cycle. Journal of Biological Chemistry, 288, 33292-33302.

JIANG, W., YANG, B. & WEEKS, D. P. 2014. Efficient CRISPR/Cas9-mediated gene editing in *Arabidopsis thaliana* and inheritance of modified genes in the T2 and T3 generations. PLoS One, 9, e99225.

JIANG, W., ZHOU, H., BI, H., FROMM, M., YANG, B. & WEEKS, D. P. 2013. Demonstration of CRISPR/Cas9/sgRNA-mediated targeted gene modification in Arabidopsis, tobacco, sorghum and rice. Nucleic Acids Research, 41, e188.

JINEK, M., CHYLINSKI, K., FONFARA, I., HAUER, M., DOUDNA, J. A. & CHARPENTIER, E. 2012. A programmable dual-RNA-guided DNA endonuclease in adaptive bacterial immunity. Science, 337, 816-821.

KIM, H. & KIM, J.-S. 2014. A guide to genome engineering with programmable nucleases. Nature Reviews Genetics, 15, 321-334.

KISHI-KABOSHI, M., AIDA, R. & SASAKI, K. 2017. Generation of gene-edited *Chrysanthemum morifolium* using multicopy transgenes as targets and markers. Plant and Cell Physiology, 58, 216-226.

LAWRENSON, T., SHORINOLA, O., STACEY, N., LI, C., ØSTERGAARD, L., PATRON, N., UAUY, C. & HARWOOD, W. 2015. Induction of targeted, heritable mutations in barley and *Brassica oleracea* using RNA-guided Cas9 nuclease. Genome Biology, 16, 258.

LI, J.-F., NORVILLE, J. E., AACH, J., MCCORMACK, M., ZHANG, D., BUSH, J., CHURCH, G. M. & SHEEN, J. 2013. Multiplex and homologous recombination-mediated genome editing in *Arabidopsis* and *Nicotiana benthamiana* using guide RNA and Cas9. Nature Biotechnology, 31, 688-691.

LIANG, Z., ZHANG, K., CHEN, K. & GAO, C. 2014. Targeted mutagenesis in *Zea mays* using TALENs and the CRISPR/Cas system. Journal of Genetics and Genomics, 41, 63-68.

MA, X., ZHANG, Q., ZHU, Q., LIU, W., CHEN, Y., QIU, R., WANG, B., YANG, Z., LI, H., LIN, Y., et al. 2015. A robust CRISPR/Cas9 system for convenient, high-efficiency multiplex genome editing in monocot and dicot plants. Molecular Plant, 8, 1274-1284.

MALAMY, J. E. & RYAN, K. S. 2001. Environmental regulation of lateral root initiation in Arabidopsis. Plant Physiology, 127, 899-909.

NEKRASOV, V., STASKAWICZ, B., WEIGEL, D., JONES, J. D. & KAMOUN, S. 2013. Targeted mutagenesis in the model plant *Nicotiana benthamiana* using Cas9 RNA-guided endonuclease. Nature Biotechnology, 31, 691-693.

RŮŽIČKA, K., ZHANG, M., CAMPILHO, A., BODI, Z., KASHIF, M., SALEH, M., EECKHOUT, D., EL-SHOWK, S., LI, H., ZHONG, S., et al. 2017. Identification of factors required for m^6A mRNA methylation in *Arabidopsis* reveals a role for the conserved E3 ubiquitin ligase HAKAI. New Phytologist, 215, 157-172.

SHAN, Q., WANG, Y., LI, J., ZHANG, Y., CHEN, K., LIANG, Z., ZHANG, K., LIU, J., XI, J. J., QIU, J.-L. & GAO C. 2013. Targeted genome modification of crop plants using a CRISPR-Cas system. Nature Biotechnology, 31, 686-688.

SHAUL, O. 2015. Unique aspects of plant nonsense-mediated mRNA decay. Trends in Plant Science, 20, 767-779.

SIBOUT, R., SUKUMAR, P., HETTIARACHCHI, C., HOLM, M., MUDAY, G. K. & HARDTKE, C. S. 2006. Opposite root growth phenotypes of *hy5* versus *hy5 hyh* mutants correlate with increased constitutive auxin signaling. PLoS Genetics, 2, e202.

UPADHYAY, S. K., KUMAR, J., ALOK, A. & TULI, R. 2013. RNA-guided genome editing for target gene mutations in wheat. G3: Genes, Genomes, Genetics, 3, 2233-2238.

VESPA, L., VACHON, G., BERGER, F., PERAZZA, D., FAURE, J.-D. & HERZOG, M. 2004. The immunophilin-interacting protein AtFIP37 from Arabidopsis is essential for plant development and is involved in trichome endoreduplication. Plant Physiology, 134, 1283-1292.

VOYTAS, D. F. 2013. Plant genome engineering with sequence-specific nucleases. The Annual Reviews of Plant Biology, 64, 327-350.

WEBER, E., ENGLER, C., GRUETZNER, R., WERNER, S. & MARILLONNET, S. 2011. A modular cloning system for standardized assembly of multigene constructs. PLoS One, 6, e16765.

XIE, Q., FRUGIS, G., COLGAN, D. & CHUA, N.-H. 2000. *Arabidopsis* NAC1 transduces auxin signal downstream of TIR1 to promote lateral root development. Genes & Development, 14, 3024-3036.

XIE, Q., GUO, H.-S., DALLMAN, G., FANG, S., WEISSMAN, A. M. & CHUA, N.-H. 2002. SINAT5 promotes ubiquitin-related degradation of NAC1 to attenuate auxin signals. Nature, 419, 167-171.

ZHANG, H., ZHANG, J., WEI, P., ZHANG, B., GOU, F., FENG, Z., MAO, Y., YANG, L., ZHANG, H., XU, N., ZHU J.-K. 2014. The CRISPR/Cas9 system produces specific and homozygous targeted gene editing in rice in one generation. Plant Biotechnology Journal, 12, 797-807.

ZHONG, S., LI, H., BODI, Z., BUTTON, J., VESPA, L., HERZOG, M. & FRAY, R. G. 2008b. MTA is an *Arabidopsis* messenger RNA adenosine methylase and interacts with a homolog of a sex-specific splicing factor. The Plant Cell, 20, 1278-1288.

ZHONG, S., LIN, Z., FRAY, R. G. & GRIERSON, D. 2008a. Improved plant transformation vectors for fluorescent protein tagging. Transgenic Research, 17, 985-989.

3.8 SUPPLEMENTARY FIGURES

a

CTTGTTTACCTCTGACCAACTTGGGCGCGCCTGCAGCCTTCAAGTACTTCGACACCACCATAG
ACAGAAAGCGGTACACCTCTACAAAGGAGGTCCTGGACGCCACACTGATTCATCAGTCAATT
ACGGGGCTCTATGAAACAAGAATCGACCTCTCTCAGCTCGGTGGAGACAGCAGGGCTGACCC
CAAGAAGAAGAGGAAGGTGTGAGCTTGTCAAGCAGATCGTTCAAACATTTGGCAATAAAGTT
TCTTAAGATTGAATCCTGTTGCCGGTCTTGCGATGATTATCATATAATTTCTGTTGAATTACGT
TAAGCATGTAATAATTAACATGTAATGCATGACGTTATTTATGAGATGGGTTTTTATGATTAG
AGTCCCGCAATTATACATTTAATACGCGATAGAAAACAAAATATAGCGCGCAAACTAGGATA
AATTATCGCGCGCGGTGTCATCTATGTTACTAGATCGACGCTACTAGAATTCGAGCTCGGAGT
GATCAAAAGTCCCACATCGATCAGGTGATATATAGCAGCTTAGTTTATATAATGATAGAGTCG
ACATAGCGATTGATTACGGTGGTGGGAGTCAGTTTTAGAGCTAGAAATAGCAAGTTAAAATA
AGGCTAGTCCGTTATCAACTTGAAAAAGTGGCACCGAGTCGGTGCTTTTTTTCTAGACCCAGC
TTTCTTGTACAAAGTTGGCATTACGCTTTACGAGGATGCACATGTGACCGAGGGACACGAAGT
GATCCGTTTAAACTATCAGTGTTTGACAGGATATATTGGCGGGTAAACCTAAGAGAAAAGAG
CGTTTATTAGAATAATCGGATATTTAAAAGGGCGTGAAAAGGTTTATCCGTTCGTCCATTTGT
ATGTGCCAGCCGTGCGGCTGCATGAAATCCTGGCCGGTTTGTCTGATGCCAAGCTGGCGGCCT
GGCCGGCCAGCTTGGCCGCTGAAGAAACCGAGCGC

b

CTTGTTTACTCTGACCAACTTGGGCGCGCCTGCAGCCTTCAAGTACTTCGACACCACCATAGA
CAGAAAGCGGTACACCTCTACAAAGGAGGTCCTGGACGCCACACTGATTCATCAGTCAATTA
CGGGGCTCTATGAAACAAGAATCGACCTCTCTCAGCTCGGTGGAGACAGCAGGGCTGACCCC
AAGAAGAAGAGGAAGGTGTGAGCTTGTCAAGCAGATCGTTCAAACATTTGGCAATAAAGTTT
CTTAAGATTGAATCCTGTTGCCGGTCTTGCGATGATTATCATATAATTTCTGTTGAATTACGTT
AAGCATGTAATAATTAACATGTAATGCATGACGTTATTTATGAGATGGGTTTTTATGATTAGA
GTCCCGCAATTATACATTTAATACGCGATAGAAAACAAAATATAGCGCGCAAACTAGGATAA
ATTATCGCGCGCGGTGTCATCTATGTTACTAGATCGACGCTACTAGAATTCGAGCTCGGAGTG
ATCAAAAGTCCCACATCGATCAGGTGATATATAGCAGCTTAGTTTATATAATGATAGAGTCGA
CATAGCGATTGTTCACGGGATTGTTGCAGCGTTTTAGAGCTAGAAATAGCAAGTTAAAATAA
GGCTAGTCCGTTATCAACTTGAAAAAGTGGCACCGAGTCGGTGCTTTTTTTCTAGACCCAGCT
TTCTTGTACAAAGTTGGCATTACGCTTTACGAGGATGCACATGTGACCGAGGGACACGAAGT
GATCCGTTTAAACTATCAGTGTTTGACAGGATATATTGGCGGGTAAACCTAAGAGAAAAGAG
CGTTTATTAGAATAATCGGATATTTAAAAGGGCGTGAAAAGGTTTATCCGTTCGTCCATTTGT
ATGTGCCAGCCGTGCGGCTGCATGAAATCCTGGCCGGTTTGTCTGATGCCAAGCTGGCGGCCT
GGCCGGCCAGCTTGGCCGCTGAAGAAACCGAGCGCCGCCGTCTAAAAAGGTGATGT

c

CTTGTTTACTCTGACCAACTTGGGCGCGCCTGCAGCCTTCAAGTACTTCGACACCACCATAGA
CAGAAAGCGGTACACCTCTACAAAGGAGGTCCTGGACGCCACACTGATTCATCAGTCAATTA
CGGGGCTCTATGAAACAAGAATCGACCTCTCTCAGCTCGGTGGAGACAGCAGGGCTGACCCC
AAGAAGAAGAGGAAGGTGTGAGCTTGTCAAGCAGATCGTTCAAACATTTGGCAATAAAGTTT
CTTAAGATTGAATCCTGTTGCCGGTCTTGCGATGATTATCATATAATTTCTGTTGAATTACGTT
AAGCATGTAATAATTAACATGTAATGCATGACGTTATTTATGAGATGGGTTTTTATGATTAGA
GTCCCGCAATTATACATTTAATACGCGATAGAAAACAAAATATAGCGCGCAAACTAGGATAA
ATTATCGCGCGCGGTGTCATCTATGTTACTAGATCGACGCTACTAGAATTCGAGCTCGGAGTG
ATCAAAAGTCCCACATCGATCAGGTGATATATAGCAGCTTAGTTTATATAATGATAGAGTCGA
CATAGCGATTGATTACGGTGGTGGGAGTCAGTTTTAGAGCTAGAAATAGCAAGTTAAAATAA
GGCTAGTCCGTTATCAACTTGAAAAAGTGGCACCGAGTCGGTGCTTTTTTTCTAGACCCAGCT
TTCTTGTACAAAGTTGGCATTACGCTTTACGGAGTGATCAAAAGTCCCACATCGATCAGGTGA
TATATAGCAGCTTAGTTTATATAATGATAGAGTCGACATAGCGATTGTTCACGGGATTGTTGC
AGCGTTTTAGAGCTAGAAATAGCAAGTTAAAATAAGGCTAGTCCGTTATCAACTTGAAAAAG
TGGCACCGAGTCGGTGCTTTTTTTCTAGACCCAGCTTTCTT

(Figure legend on next page)

Supplementary figure 3.1 The sequencing results of completed CRISPR constructs for knocking out *Hakai*. (**a**) *Hakai*-CRISPR1M. (**b**) *Hakai*-CRISPR2P. (**c**) *Hakai*-CRISPR2cr. Nucleotides in purple represent part sequence of *Cas9*; those in blue represent *AtU6* promoter; those in red represent sgRNA target sites; those in yellow background represent overhangs in Golden Gate cloning.

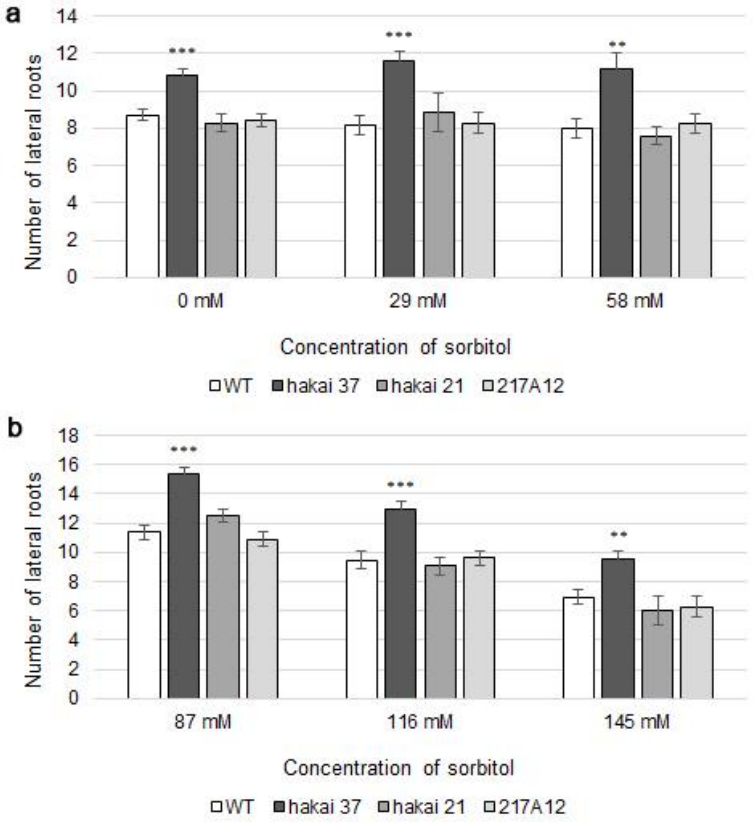

Supplementary figure 3.2 Root phenotypes of *hakai* mutants compared with WT vertically cultured on 1/2 MS plus different concentrations of sorbitol. (**a**) The number of lateral roots of 8-d old seedlings. (**b**) The number of lateral roots of 9-d old seedlings. Data represent mean ± SEM and statistically significant differences compared with WT via One-Way ANOVA are marked with asterisks (**, $p<0.01$; ***, $p<0.001$).

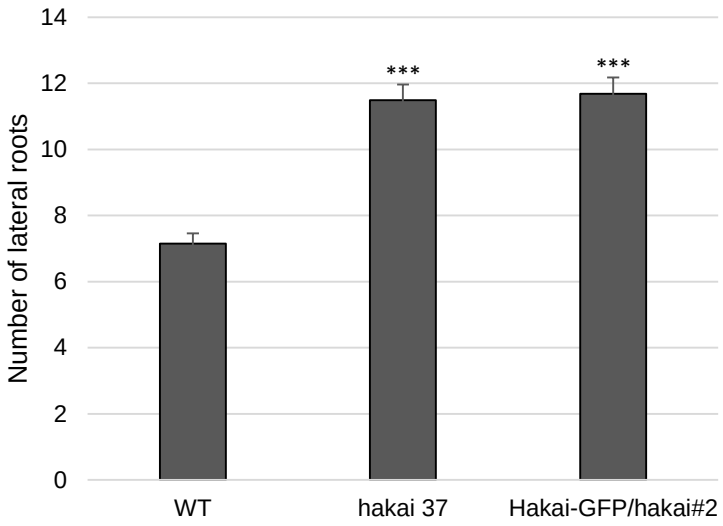

Supplementary figure 3.3 The number of lateral roots of 9-d old *hakai* 37 and its complementation line vertically cultured on 1/2 MS plus 3% sucrose. Data represent mean ± SEM and statistically significant differences compared with WT via One-Way ANOVA are marked with asterisks (***, $p<0.001$).

CHAPTER 4 STUDYING INTERACTIONS AMONG COMPONENTS OF THE MTASE COMPLEX

4.1 ABSTRACT

The methyltransferase (MTase) complex responsible for m^6A formation (m^6A writer complex) in *Arabidopsis* composes of MTA, MTB, FIP37, Virilizer and Hakai. However, how these proteins interact with each other remains unclear. Thus, the current study focused on elucidating their interactions based on generating and characterising double mutants for m^6A writer proteins and GFP-tagged m^6A writer proteins in *hakai*, *mta* or *fip37* mutant backgrounds, followed by *GFP* expression assays and proteomic analysis. Among all generated double mutants, *mta hakai*, *mta virilizer* double mutants showed more severe developmental defects than corresponding single mutants, suggesting MTA, Hakai and Virilizer function in concert to regulate the same developmental processes. Likewise, Hakai acts synergistically with FIP37 and Virilizer as *hakai fip37* and *hakai virilizer* seem to be lethal. In contrast, MTA functions as a suppressor of FIP37, supported by the fact that the knockdown of *MTA* partially rescued the severe developmental defects of *fip37* while the introduction of *MTA-GFP* transgene caused stronger defects of *fip37*. The pull-down analysis revealed that Hakai interacts with MTA, FIP37 and Virilizer while its interaction with MTB is much weaker. In addition, one heat shock protein (Hps70-15) and two zinc finger proteins (AT1G32360 and AT5G53440) were co-purified with both MTA and Hakai and the interaction between MTA and AT1G32360 disappeared upon the knockout of *Hakai*. Collectively, Hakai is an important

member of the MTase complex and acts synergistically with other members in regulating well-tuned m^6A modification and the growth and development in *Arabidopsis*. Additionally, zinc finger proteins might be novel members of the m^6A writer complex, but their function(s) in mRNA methylation needs further investigation.

4.2 AIMS AND OBJECTIVES OF THIS CHAPTER

Members of the plant m^6A MTase complex identified to date include MTA, MTB, FIP37, Virilizer and Hakai. However, how they interact with and affect each other remains largely unknown. The aim of the study in this chapter is to elucidate interactions between different members of the MTase complex based on crossing to generate double mutants and GFP-tagged m^6A writer proteins in *hakai*, *mta* or *fip37* mutant backgrounds. The generation and analysis of double mutants related to m^6A writer proteins may show us whether they act in a cooperative manner in regulating plant growth and development processes modulated by m^6A. The analysis of crossing progenies between transgenic lines containing GFP-tagged m^6A writers and m^6A mutants except for itself (e.g., Hakai-GFP/WT crossed with *fip37*) will aid the comparation of the interacting partners of one m^6A writer protein with or without the presence of another m^6A writer protein and this will further elucidate the interaction between these two m^6A writer proteins. By undertaking m^6A measurements, plant phenotyping, GFP localisation analysis, GFP-tagged protein expression assays and proteomic analysis using the above transgenic lines, it is hoped that a fuller understanding of the plant MTase complex will emerge.

4.3 PLANT MATERIALS AND METHODS

4.3.1 Plant Materials

Transgenic *Arabidopsis* lines used in this chapter include *hakai* mutants (*hakai* 37 and 217A12), ABI3A6 (SALK_074069 with T-DNA inserted in exon 4 of *MTA* genomic DNA and complemented with *MTA* coding sequence driven by *ABI3* promoter), *fip37* (SALK_018636 with T-DNA inserted in intron 7 of *FIP37* genomic DNA), *virilizer* (G to A mutation at the beginning of intron 5 of *Virilizer* genomic DNA, which disrupts its correct 5′ splicing), MTA-GFP (SALK_114710 with T-DNA inserted in exon 6 of *MTA* genomic DNA and complemented with *MTA* coding sequence under its own promoter, with GFP tag downstream), Hakai-GFP/*hakai*#2, Hakai-GFP/WT#1, MTA-GFP/WT (*MTA* coding sequence under its own promoter in WT background, with GFP tag downstream), MTB-GFP (*MTB* genomic DNA under its own promoter in *mtb* mutant background, with GFP tag downstream) and Virilizer-GFP (*Virilizer* genomic DNA under its own promoter, with GFP tag between them). Apart from *hakai* 37 and Hakai-GFP lines, other above lines were generated by previous researchers in our lab or by collaborators in other research institutes (detailed in Table 2.1).

4.3.2 Generation of FIP37-GFP Line

The *FIP37-GFP* construct was generated by Gateway cloning using ready-to-use Gateway entry vector *FIP37*p-gDNA-pDONR(Amp^{+}), which contains

FIP37 genomic DNA (without stop codon and 3' UTR) under its own promoter and has ampicillin resistance for growth in *E. coli* (generated by previous researchers in our group). It was confirmed by sequencing prior to use. *FIP37*p-gDNA-pDONR(Amp^+) was then reacted with Gateway destination vector pGKGWG in the presence of Gateway® LR Clonase™ II Enzyme Mix (Invitrogen). After transforming the reaction mixture to competent *E. coli* OneShot® TOP10 cells and analysing the transformants by PCR, plasmids were prepared from correct single colonies and transformed to *Agrobacterium* strain C58 together with pSoup plasmid.

After floral dip transformation to wild-type *Arabidopsis*, T_1 plants were screened by planting T_0 seeds on 1/2 MS medium plus 50 $mg \cdot L^{-1}$ Kan. Positive T_1 plants were transplanted to the compost and confirmed by PCR. In the T_2 generation, homozygous lines were screened by planting 40-50 seeds on 1/2 MS medium containing 50 $mg \cdot L^{-1}$ Kan. Afterwards, GFP signal was checked by confocal microscopy (Leica TCS SP5).

4.3.3 Crossing

To further study the role of Hakai in the MTase complex and facilitate the study of the interactions between different components of the MTase complex, crosses were made between different mutants and between mutants and GFP-tagged lines. Crosses to be carried out are listed in Table 4.1.

Table 4.1 Summary of crosses to be made

Female parent	Male parent	Aim of cross
217A12	ABI3A6	To obtain *mta hakai* double mutant
ABI3A6	*hakai* 37	To obtain *mta hakai* double mutant
ABI3A6	*fip37*	To obtain *mta fip37* double mutant
fip37	*hakai* 37	To obtain *hakai fip37* double mutant
hakai 37	*virilizer*	To obtain *hakai virilizer* double mutant
ABI3A6	*virilizer*	To obtain *mta virilizer* double mutant
hakai 37	MTA-GFP	To obtain MTA-GFP line in *hakai* mutant background
hakai 37	MTB-GFP	To obtain MTB-GFP line in *hakai* mutant background
hakai 37	FIP37-GFP/WT	To obtain FIP37-GFP line in *hakai* mutant background
hakai 37	Virilizer-GFP	To obtain Virilizer-GFP line in *hakai* mutant background
Hakai-GFP/WT#1	ABI3A6	To obtain Hakai-GFP line in *mta* mutant background
FIP37-GFP/WT	ABI3A6	To obtain FIP37-GFP line in *mta* mutant background
fip37	Hakai-GFP/WT#1	To obtain Hakai-GFP line in *fip37* mutant background
fip37	MTA-GFP/WT	To obtain MTA-GFP line in *fip37* mutant background

4.3.4 Screening Double Mutants

Because the low m^6A line, ABI3A6, demonstrates specific phenotypes – bushy and crinkled rosette leaves and shorter inflorescence internode lengths (Bodi et al., 2012), therefore, to easily screen progenies from crosses with ABI3A6, F_2 plants showing ABI3A6 phenotypes were selected and then further checked by PCR to confirm them as homozygotes for SALK_074069 T-DNA insertion and containing the *ABI3*::*MTA* construct. In the F_3 generation, screening homozygous mutant alleles for the other gene was carried out by the restriction enzyme site loss method (Voytas, 2013) and further sequencing for *hakai,* genotyping PCR for *fip37,* and sequencing for *virilizer*. For crosses between *hakai* 37 and *fip37*, F_2 plants which were very tiny (resembling *fip37* phenotypes)

were confirmed by genotyping PCR as homozygotes for SALK_018636 T-DNA insertion and the next generation was used for screening homozygous *hakai* mutant alleles. As *virlizer* showed very severe developmental defects and produced very few seeds under the conditions in our phytotron, screening of *hakai virilizer* double mutant started with selecting homozygous *hakai* lines which were heterozygous for *virlizer* in the F_2 generation, followed by screening for homozygous *virilizer* mutant alleles in the F_3 generation. Primers used in screening are listed in Appendix 1.

4.3.5 Screening Mutants Crossed with GFP-tagged Lines

In the F_1 generation, the presence of *GFP*-tagged transgene was confirmed by PCR using the forward primer on the transgene and the reverse one on *GFP* or by checking the GFP signal under the Stereo Fluorescence Microscope (Leica). The presence of mutant alleles was confirmed using methods as above in 4.3.4. In F_2 and the subsequent generations, homozygous mutant alleles were screened from GFP-positive lines. Finally, lines homozygous for both *GFP*-tagged transgenes and mutant alleles were used for the following analysis. Primers used in screening are listed in Appendix 1.

4.3.6 Protein Expression Assay in Progenies of *hakai* 37 Crossed with GFP-tagged Lines

GFP-fused protein levels in original GFP-tagged lines and crossing progenies with *hakai* 37 were analysed by western blotting according to the protocol

detailed in 2.16. The GFP antibody used is a mixture of two monoclonal antibodies from mouse IgG1κ (Sigma-Aldrich).

4.3.7 Proteomic Analysis

In this part, culturing of plant materials and crosslinking were carried out in the University of Nottingham and the following procedures prior to mass spectrometry analysis were carried out during a visit to Gordon G. Simpson's lab, the University of Dundee, following the protocol established by their group.

4.3.7.1 Chemicals

1% (v/v) formaldehyde: Dilute from 37% (v/v) formaldehyde (Sigma-Aldrich) using cold sterile water just before use.

2 M glycine: Dissolve 150.14 g glycine powder (MW = 75.07 $g \cdot mol^{-1}$) in 1 L of sterile water. Keep at 4°C after filter-sterilisation.

HONDA buffer (for nuclei isolation): 20 mM Hepes KOH pH 7.4, 10 mM $MgCl_2$, 440 mM sucrose, 1.25% (v/v) Ficoll, 2.5% (v/v) Dextran T40, 0.5% (v/v) Triton X-100, 5 mM DTT, 5 mM PMSF, 1% (v/v) Plant Protease Inhibitors (Sigma-Aldrich). Store at 4°C and add DTT, PMSF and Plant Protease Inhibitors just before use.

Nuclei lysis buffer: 50 mM Tris-HCl pH 8.0, 10 mM EDTA pH 8.0, 1% (w/v) SDS, 1 mM PMSF, 1% (v/v) Plant Protease Inhibitors. Store at 4°C and add PMSF and Plant Protease Inhibitors just before use.

IP dilution buffer: 16.7 mM Tris-HCl pH 8.0, 1.2 mM EDTA pH 8.0, 167 mM NaCl, 1.1% (v/v) Triton X-100, 1% (v/v) Plant Protease Inhibitors. Store at 4°C and add Plant Protease Inhibitors just before use.

Beads washing buffer: 20 mM Tris-HCl pH 8.0, 150 mM NaCl, 2 mM EDTA pH 8.0, 1% (v/v) Triton X-100, 0.1% (w/v) SDS, 1 mM PMSF. Store at 4°C and add PMSF just before use.

4.3.7.2 Crosslinking via formaldehyde

Two-week old seedlings were prepared on round petri dishes containing 1/2 MS and 1% (w/v) sucrose as described in 2.1. Freshly harvested seedlings were placed in a beaker and washed with cold sterile water for 4 times. Seedlings were then soaked in 1% (v/v) formaldehyde with the beaker inside a desiccator and the vacuum on for 15 min. Afterwards, the vacuum was removed gently and 2 M glycine solution (to a final concentration of 0.125 M) was evenly added onto the top of the formaldehyde solution and mixed well to quench the crosslinking reaction. The vacuum was turned on for another 5 min and then gently removed. Crosslinked seedlings were washed with cold sterile water for 4 times and then dried between several sheets of tissue paper. Finally, seedlings were divided into 50 ml Falcon tubes. After snap freezing in liquid nitrogen, frozen samples were kept at -80°C until use.

4.3.7.3 Nuclei isolation

Frozen samples were ground into powder and divided into 50 ml tubes with about 7.5 ml of powder in each. The nuclei isolation was performed as follows with all samples and solutions kept on ice all the time. (1) 6 tubes were dealt with in one preparation; thus, 6 new 50 ml tubes and a clean glass beaker were prepared on ice. Enough pieces of miracloth and a funnel were also prepared. (2) 3 tubes were placed on ice and 15 ml of HONDA buffer were added to each tube and mixed well. Afterwards, this step was repeated for the remaining 3 tubes. (3) A funnel was placed on top of a new 50 ml tube and 2 layers of miracloth were placed inside the funnel. (4) The extract from one tube was filtered through the miracloth and squeezed to extract as much nuclei as possible from the miracloth. (5) The miracloth was rinsed in a beaker with 10 ml of fresh HONDA buffer. (6) The rinsed miracloth was squeezed again to recover the remaining buffer with nuclei to the beaker. (7) The extract from the beaker was filtered through 2 new layers of miracloth to the same tube as that in step (3). (8) The filtrates were stored on ice. (9) Steps (3)-(8) were repeated for the remaining 5 tubes. (10) Tubes were equilibrated using HONDA buffer and centrifuged at 2,000 g for 17 min at 4°C. (11) The supernatant was carefully removed and each pellet was resuspened in 1 ml of HONDA buffer. (12) The mixture from each 50 ml tube was transferred to a 1.5 ml Protein LoBind tube (Eppendorf). (13) Tubes were centrifuged at 1,500 g for 15 min at 4°C. (14) The supernatant was discarded and the pellet was washed again using 1 ml of HONDA buffer. (15) After centrifuging at 1,500 g for 15 min at 4°C, supernatants were discarded and pellets were used for the subsequent nuclei lysis.

4.3.7.4 Nuclei lysis

Pellets from the last step were resuspended in 500 µl of Nuclei lysis buffer and then samples were sonicated using waterbath sonicator (Diagenode Bioruptor 200) on low power with 4 cycles of 30 s ON and 60 s OFF. Afterwards, tubes were centrifuged at 16,100 g for 15 min at 4°C. During this period, 12.15 ml of IP dilution buffer was prepared in a 15 ml falcon tube (2 tubes in total) for sample dilution. After centrifugation, three samples of the same genotype were pooled together by taking 450 µl of the supernatant to a 15 ml tube containing IP dilution buffer.

4.3.7.5 Immunoprecipitation

GFP-Trap agarose beads (ChromoTek) were prepared by pre-washing 17 µl of beads using IP dilution buffer for 3 times and resuspended in 210 µl of IP dilution buffer. Beads were equally divided into 2 tubes of diluted protein samples and incubated for 5 h at 4°C with rotation. Subsequently, tubes were centrifuged at 200 g for 3 min at 4°C. Most of the supernatant was removed carefully and leaving about 1 ml at the bottom of the tube. Beads were resuspended and transferred to a 1.5 ml Protein LoBind tube. Afterwards, beads were washed 3 times with Beads washing buffer. Between washes, tubes were centrifuged at 400 g for 2 min at 4°C. After the last wash, as much of the liquid as possible was removed using yellow or white tips and tubes containing beads were frozen in liquid nitrogen and stored at -80°C until use.

4.3.7.6 Mass spectrometry analysis

Mass spectrometry analysis was performed by staff in the Proteomics and Mass Spectrometry Facility "FingerPrints" at the School of Life Sciences, University of Dundee. In short, 6 tubes of beads after pull-down were pooled together in 80 µl of 1× LDS sample buffer (Invitrogen) as 1 biological replicate. Samples were incubated at 90°C for 30 min to reverse formaldehyde crosslinking. After running samples on SDS-PAGE gel, the gel for the same lane was cut into 5 slices. Protein samples were digested into peptides by trypsin and then analysed on LTQ Orbitrap Velos Pro mass spectrometer (Thermo Scientific).

4.3.7.7 Data analysis

Raw files corresponding to five slices from the same lane were merged together in MaxQuant software. Peptide analysis was performed via MaxQuant. *Arabidopsis* Uniprot protein database was used as a reference. The MaxQuant output files containing proteins that were identified in each sample were used for further analysis using Perseus software. The Student t-test was used in the statistical analysis for two samples (False discovery rate [FDR] = 0.1). Data were visualised on a volcano plot and proteins were plotted based on their enrichment versus that in the wild type using label free quantification (LFQ) and the significance was analysed based on the negative logarithm of the p-value derived from the t-test ($-\log_{10}^{\text{p-value}}$). Proteins that were significantly enriched were separated from other proteins by a hyperbolic curve.

4.4 RESULTS

4.4.1 Generation and Characterisation of Double Mutants

4.4.1.1 Homozygous mta hakai double mutant

To generate *mta hakai* double mutant, we firstly tried crossing *hakai* 37 into ABI3A6. The screening strategy for *mta hakai* double mutant was as follows. F_1 progenies should be heterozygous for *MTA* SALK_074069 T-DNA insertion and contain the *ABI3*::*MTA* construct. In the F_2 generation, some plants should show ABI3A6 phenotypes and be homozygous for *MTA* SALK_074069 T-DNA insertion. Genotyping PCR for F_2 progenies showing ABI3A6 phenotypes confirmed that some of them were homozygous for *MTA* SALK_074069 T-DNA insertion (Figure 4.1a) and heterozygous for *Hakai* CRISPR target site (Figure 4.1b). Homozygous *mta hakai* double mutants (termed *mta hakai*#1) were obtained in the F_3 generation and they demonstrated more severe developmental defects than ABI3A6 in terms of above-ground tissues (Figure 4.1c, 4.2). Another cross between 217A12 and ABI3A6 confirmed stronger above-ground phenotypes of homozygous *mta hakai* double mutant (termed *mta hakai*#2) (Figure 4.3). To analyse root phenotypes, *mta hakai*#1 and its parent lines were planted on vertical plates containing 1/2 MS plus 1% (w/v) sucrose. *mta hakai*#1 demonstrated significantly shorter primary roots and reduced lateral roots compared with its parents (Figure 4.4, 4.5).

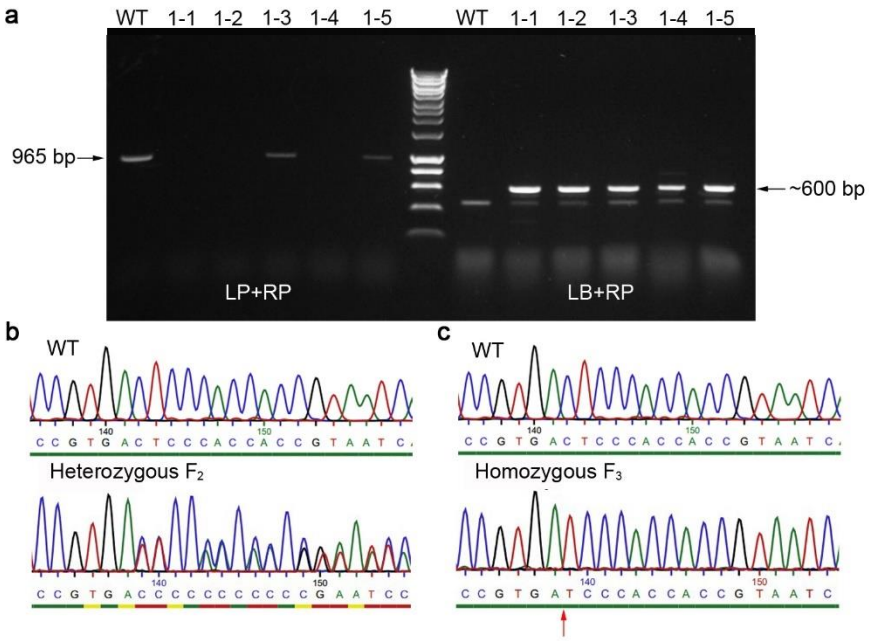

Figure 4.1 Screening F_2 and F_3 generations of ABI3A6 crossed with *hakai* 37. (**a**) Genotyping PCR to screen F_2 lines homozygous for *MTA* SALK_074069 T-DNA insertion. Lines 1-1, 1-2 and 1-4 were homozygotes. (**b**) Sequencing profile showing an F_2 line heterozygous for *Hakai* CRISPR target site. (**c**) Sequencing profile showing an F_3 line homozygous for *Hakai* CRISPR target site.

Figure 4.2 4-week old *mta hakai*#1 double mutant and its parents. Scale bar = 1 cm.

Figure 4.3 4-week old *mta hakai#*2 double mutant and its parents. Scale bar = 1 cm.

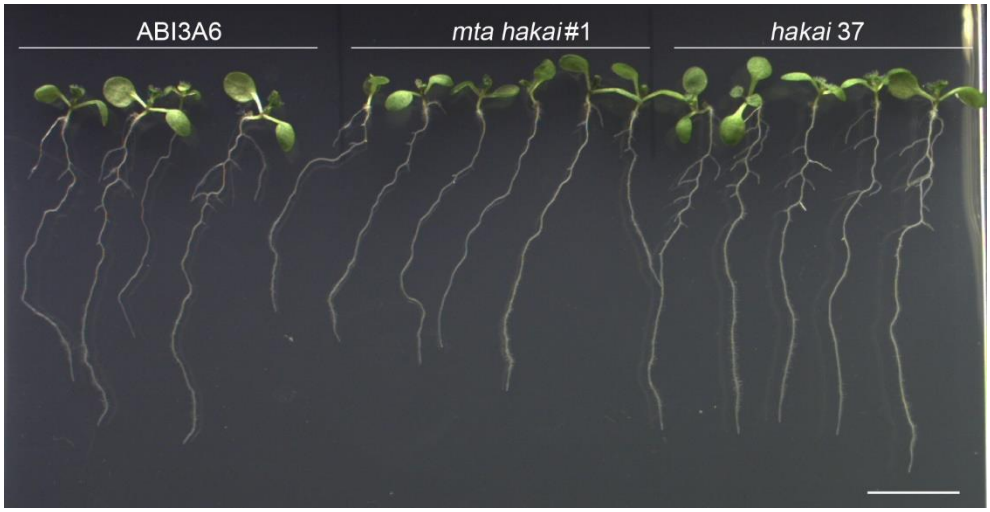

Figure 4.4 8-d old *mta hakai#*1 and its parents planted on vertical plates containing 1/2 MS plus 1% (w/v) sucrose. Scale bar = 1 cm.

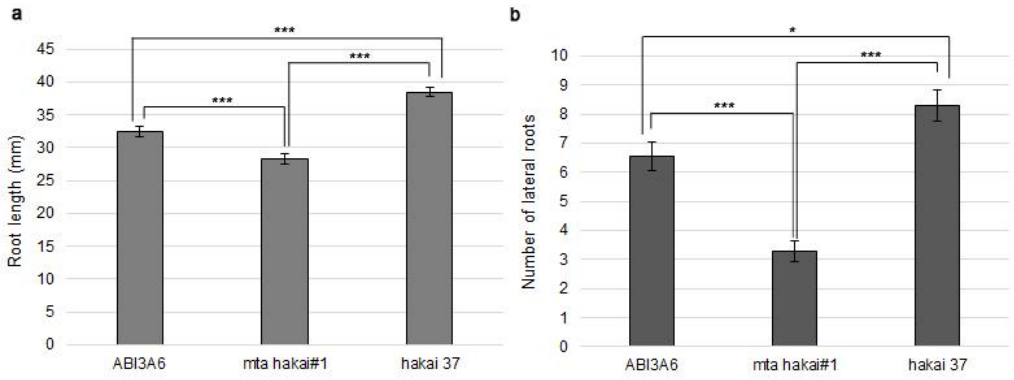

Figure 4.5 Root phenotypes of 8-d old *mta hakai#*1 and its parents planted on vertical plates containing 1/2 MS plus 1% (w/v) sucrose. (**a**) Root lengths. (**b**) The number of lateral roots. Data represent mean ± SEM and statistically significant differences were compared by One-Way ANOVA and marked with asterisks (*, $p<0.05$; ***, $p<0.001$).

4.4.1.2 Homozygous mta fip37 double mutant

To generate *mta fip37* double mutant, *fip37* was crossed into ABI3A6. The screening procedure was similar to that in 4.4.1.1. F_2 progenies showing ABI3A6 phenotypes were confirmed homozygous for *MTA* SALK_074069 T-DNA insertion and very surprisingly, some of these plants were also homozygous for *FIP37* SALK_018636 T-DNA insertion (Supplementary figure 4.1, 4.2). Phenotyping of the following generations confirmed that *mta fip37* double mutant (denominated as *mta fip37*) resembled ABI3A6, showing less severe developmental defects than *fip37* (Figure 4.6).

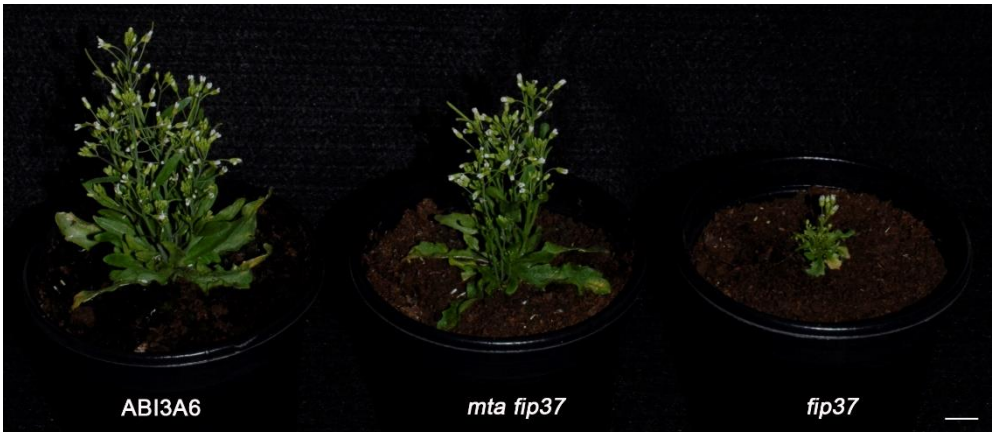

Figure 4.6 4-week old *mta fip37* double mutant and its parents. Scale bar = 1 cm.

4.4.1.3 Lethal hakai fip37 double mutant

hakai 37 was crossed into *fip37* to generate *hakai fip37* double mutant. F_2 progenies showing *fip37* phenotypes were checked to select those homozygous for *FIP37* SALK_018636 T-DNA insertion and heterozygous for *Hakai* CRISPR target site simultaneously (Figure 4.7, Supplementary figure 4.3). Because *fip37* phenotypes can be recognised from those planted on plates, F_2 seeds were planted on plates containing 1/2 MS plus 1% (w/v) sucrose and *Hakai* CRISPR target site was checked by the restriction enzyme site loss method (Figure 4.8). The screening results showed that 50 out of 73 (68.5%) seedlings were heterozygotes and the rest (31.5%) were WT (Supplementary table 4.1). No homozygous mutants at *Hakai* CRISPR target site were found in all checked F_3 progenies, including those germinated but dead ones and those very tiny ones (Figure 4.9, Supplementary table 4.1). Thus, homozygous *hakai fip37* double mutant appears to be lethal at a very early developmental stage.

Figure 4.7 4-week old F_2 progeny of *fip37* crossed with *hakai* 37. Scale bar = 1 cm.

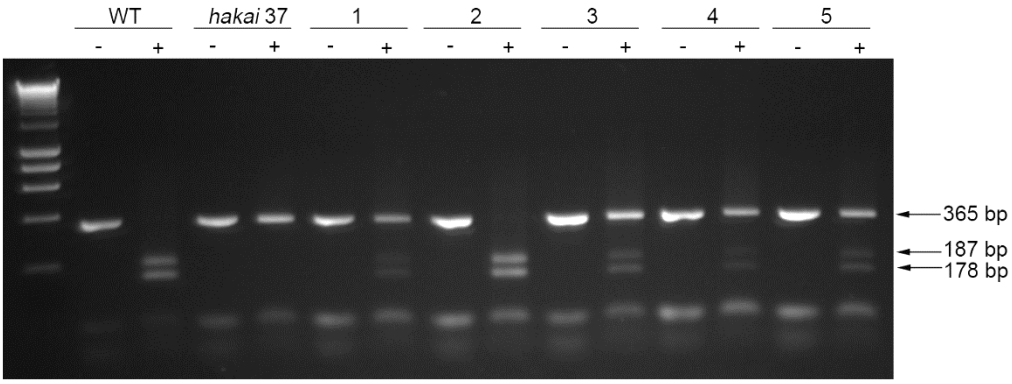

Figure 4.8 Screening the F_3 generation of *fip37* crossed with *hakai* 37 at *Hakai* CRISPR target site by the restriction enzyme site loss method. Samples were loaded on 1.5% (w/v) agarose gel. -, undigested PCR product using primers flanking the CRISPR target site; +, PCR product digested by *Sch*I (an isoschizomer of *Mly*I having the same recognition and cleavage specificity and working better than *Mly*I). Sample 1 to 5 were five individual F_3 plants of *fip37* crossed with *hakai* 37.

Figure 4.9 2-week old F_3 progenies of *fip37* crossed with *hakai* 37. Those germinated but dead ones and those very tiny ones (arrows) were heterozygous or WT for *Hakai* CRISPR target site (Refer to Supplementary table 4.1, samples fip×h m18 and fip×h m25). Scale bar = 1 cm.

4.4.1.4 Homozygous mta virilizer double mutant

To acquire *mta virilizer* double mutant, *virilizer* was crossed into ABI3A6. In the F_2 generation, some of them showed ABI3A6 phenotypes while some were very tiny, resembling *virilizer* (Supplementary figure 4.4). The genotyping PCR confirmed that some of those showing ABI3A6 phenotypes were homozygous for *MTA* SALK_074069 T-DNA insertion and contained the *ABI3*::*MTA* construct whereas those resembling *virilizer* were heterozygous for *MTA* SALK_074069 T-DNA insertion or WT (Figure 4.10a,b). Because those resembling *virilizer* were too sick to generate seeds, those homozygous for *MTA* SALK_074069 T-DNA insertion were used for checking *virilizer* mutagenesis status. Most of them were heterozygous for *virilizer* G to A mutation (Figure 4.10c).

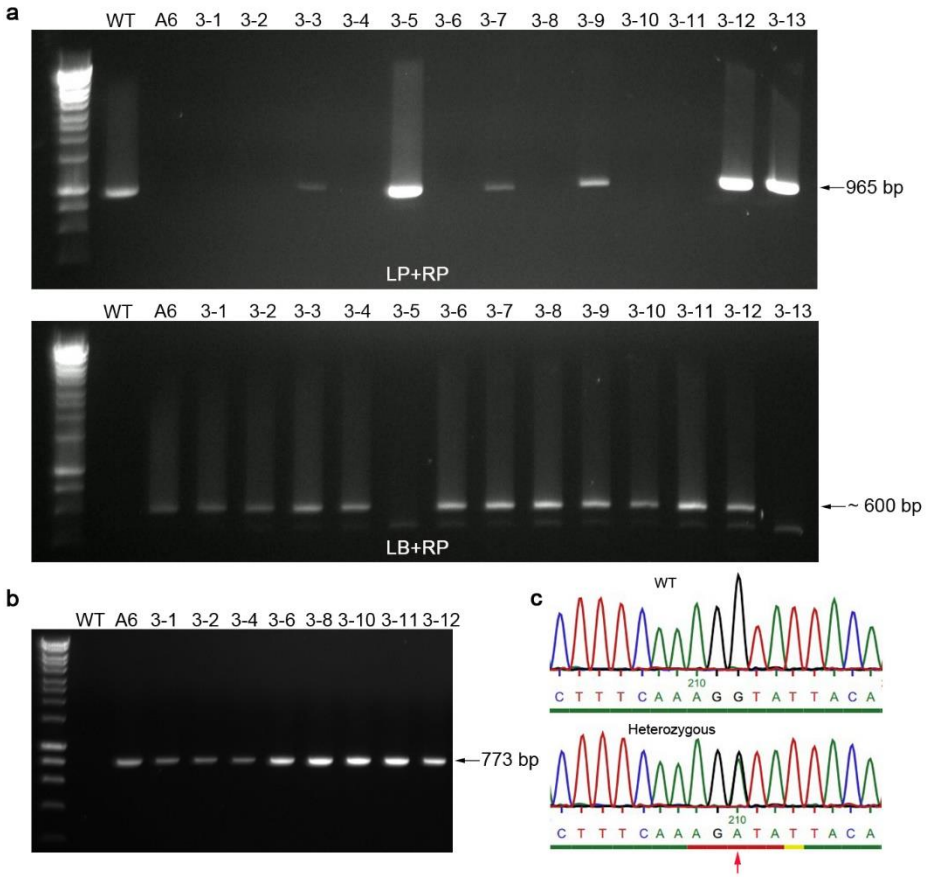

Figure 4.10 Screening F_2 progenies of ABI3A6 crossed with *virilizer*. (**a**) Genotyping PCR to check *MTA* SALK_074069 T-DNA insertion. A6 refers to ABI3A6. Samples 3-5, 3-12, 3-13 resembled *virilizer* but were not homozygous for *MTA* SALK_074069 T-DNA insertion. (**b**) Those homozygous for *MTA* SALK_074069 T-DNA insertion also contained the *ABI3*::*MTA* construct. (**c**) Those homozygous for *MTA* SALK_074069 T-DNA insertion were WT or heterozygous for *virilizer* G to A mutation (labelled with a red arrow).

F_2 progenies homozygous for *MTA* SALK_074069 T-DNA insertion, containing the *ABI3*::*MTA* construct and heterozygous for *virilizer* were further screened by planting about 130 seeds on the square plate together with *virilizer*. Among all geminated seedlings, only 4 were very tiny, even smaller than *virilizer* (Supplementary figure 4.5). Sequencing of these 4 tiny and 8 bigger seedlings showed that 3 of these 4 tiny ones were homozygous for *virilizer* mutation

whereas all bigger ones were WT or heterozygous for *virilizer* (Figure 4.11). Screening of approximately 520 more seeds on plates by phenotyping and sequencing of relatively smaller seedlings did not give more homozygotes for *virilizer* (Data not shown). Taken together, it suggests that homozygous *mta virilizer* double mutants account for a small amount among the segregating progenies and exhibit more severe developmental defects relative to both parents.

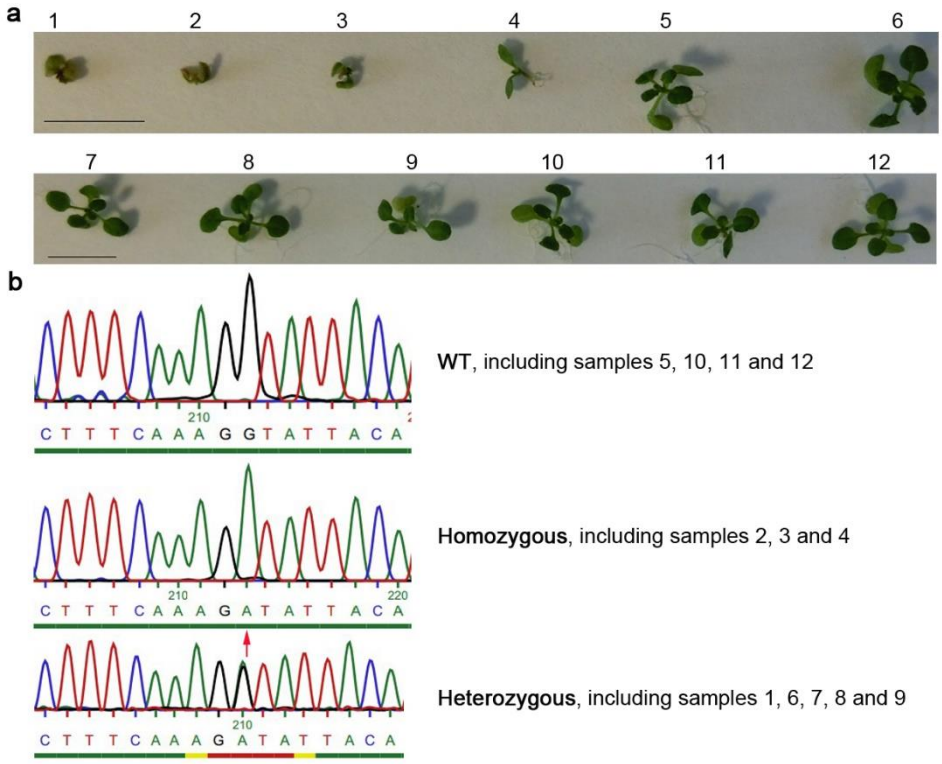

Figure 4.11 Screening F_3 progenies of ABI3A6 crossed with *virilizer*. (**a**) Representative 2-week old F_3 progenies of ABI3A6 crossed with *virilizer*. Scale bar = 1 cm. (**b**) Sequencing profiles of representative seedlings in (**a**). *virilizer* G to A mutation site is labelled with a red arrow.

4.4.1.5 Lethal hakai virilizer double mutant

Similar to generating and screening *mta virilizer* double mutant, *virilizer* was also crossed into *hakai* 37. Most of the F_2 progenies looked normal, resembling *hakai* 37, while several were tiny ones showing *virilizer* phenotypes. Though those resembling *virilizer* were homozygous for *virilizer* G to A mutation, they generated only a few seeds or no seeds, which made the further screening too difficult (Data not shown). Therefore, those homozygous for *Hakai* CRISPR target site and heterozygous for *virilizer* mutation were selected for further screening (Figure 4.12).

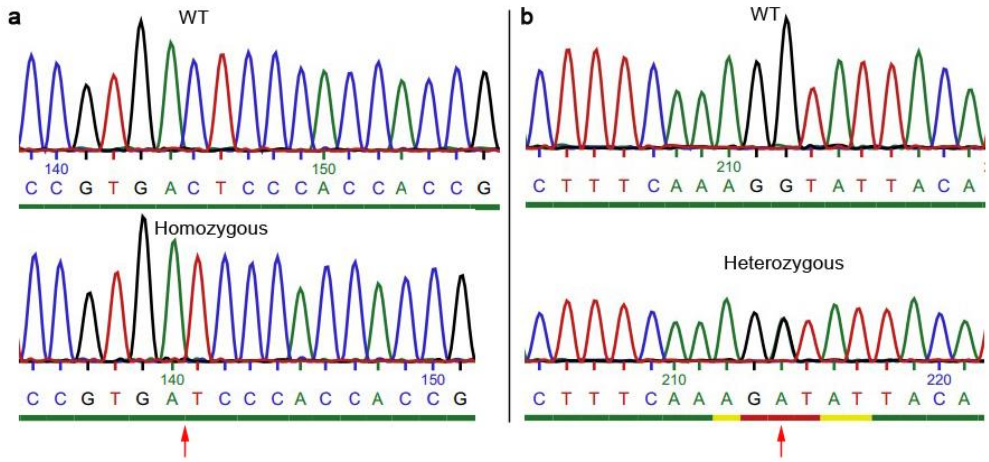

Figure 4.12 Sequencing profiles for F_2 progenies of *hakai* 37 crossed with *virilizer* that were homozygous for *Hakai* CRISPR target site (**a**) and heterozygous for *virilizer* G to A mutation (**b**). Mutation sites are labelled with red arrows.

The F_3 generation of those homozygous for *Hakai* CRISPR target site and heterozygous for *virilizer* mutation was screened in the same way as screening F_3 progenies of ABI3A6 crossed with *virilizer*. None of the geminated seeds (around 130) demonstrated *virilizer* phenotypes and sequencing of some relatively smaller seedlings and other bigger ones showed that none of them were

homozygous for *virilizer* mutation (Figure 4.13). Screening of more seedlings revealed that 22 out of 30 (73.3%) were heterozygous, WT accounted for 26.7% and no homozygous ones could be found (Supplementary table 4.2). This suggests that homozygous *hakai virilizer* double mutant may be lethal.

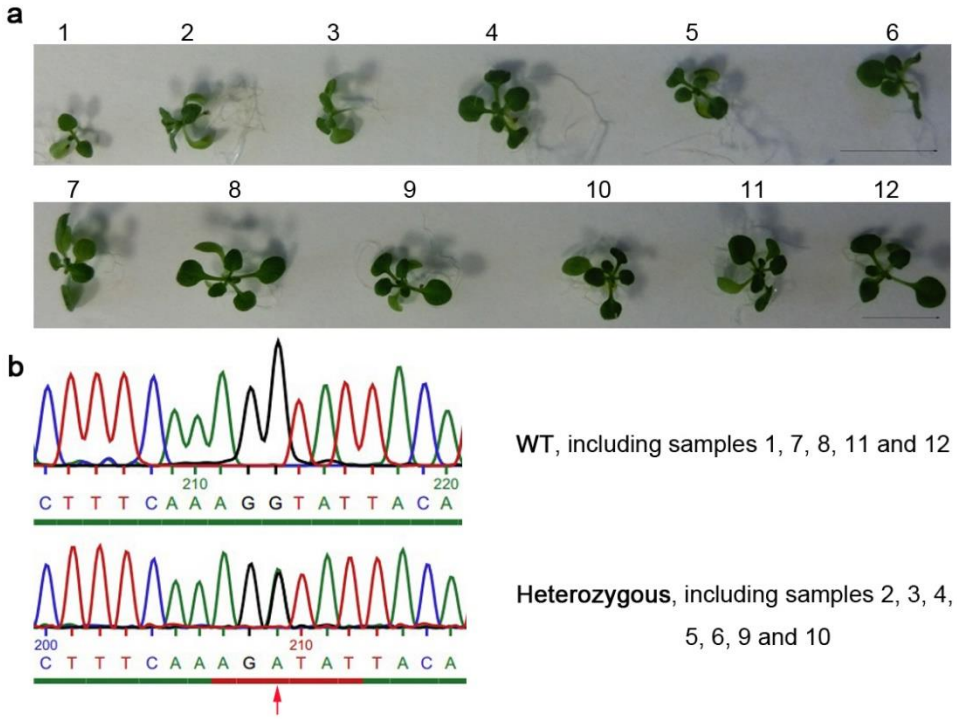

Figure 4.13 Screening F_3 progenies of *hakai* 37 crossed with *virilizer* at *virilizer* mutation site. (**a**) Representative 2-week old F_3 progenies of *hakai* 37 crossed with *virilizer*. Scale bar = 1 cm. (**b**) Sequencing profiles of representative seedlings in (**a**). *virilizer* G to A mutation site is labelled with a red arrow.

4.4.1.6 m^{6}A levels in homozygous double mutants

m^{6}A measurement via two-dimensional TLC analysis using leaves from 4-week old double mutants, their parent lines and WT planted on the compost revealed that the abundance of m^{6}A in *mta hakai#*1, *mta fip37* and ABI3A6 was 86-90% decreased relative to WT. Furthermore, there were no significant differences of m^{6}A levels between *mta hakai#*1 and ABI3A6. The m^{6}A level in *mta fip37* was

slightly higher than that in ABI3A6 but the difference was negligible (Figure 4.14).

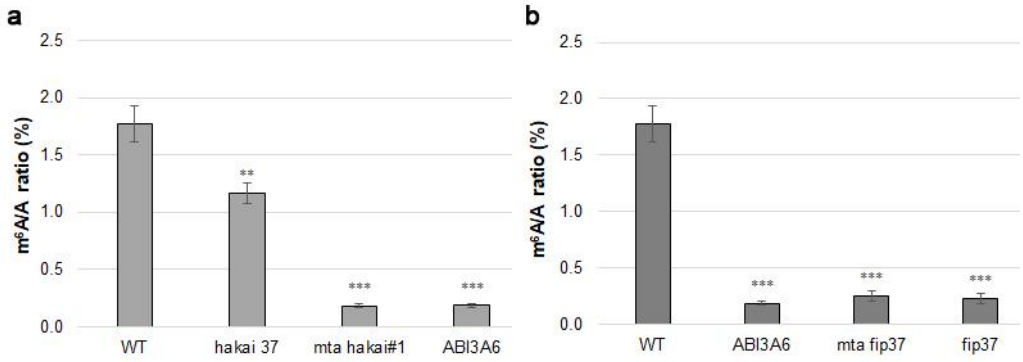

Figure 4.14 m^6A levels in double mutants and their parents checked by two-dimensional TLC analysis. Samples used were leaves from 4-week old plants planted on compost. Data represent mean ± SEM from three biological replicates and statistically significant differences relative to WT were analysed by One-Way ANOVA and marked with asterisks (**, $p<0.01$; ***, $p<0.001$).

4.4.2 Generation and Characterisation of GFP-tagged Lines in *hakai* Background

4.4.2.1 Generation of FIP37-GFP lines

To generate the FIP37-GFP recombinant construct, the available Gateway entry vector containing *FIP37* genomic DNA under its own promoter (*FIP37*p-gDNA-pDONR[Amp^+]) was confirmed by sequencing using a forward primer on exon 6 (018636LP, Appendix 1) and a reverse one on exon 1 (FIP37exon1rev, Appendix 1) of *FIP37* genomic DNA (Figure 4.15a,b). After Gateway LR reaction, the recombinant constructs were checked by PCR using primer pairs on *FIP37* genomic DNA (018636LP and 018636RP, Appendix 1) and sequenced

using a reverse primer on *GFP* (GFPrev) (Figure 4.15c,d). The correct recombinant construct was used for the subsequent transformation to WT *Arabidopsis*. Kan-resistant T_1 plants were further confirmed by PCR using a forward primer on *FIP37* and a reverse one on *GFP* (018636LP and GFPrev, Appendix 1) (Figure 4.15e). A homozygous line (termed FIP37-GFP/WT#1-2) was identified by screening F_2 seeds on MS medium plus 50 $mg \cdot L^{-1}$ Kan (Figure 4.16).

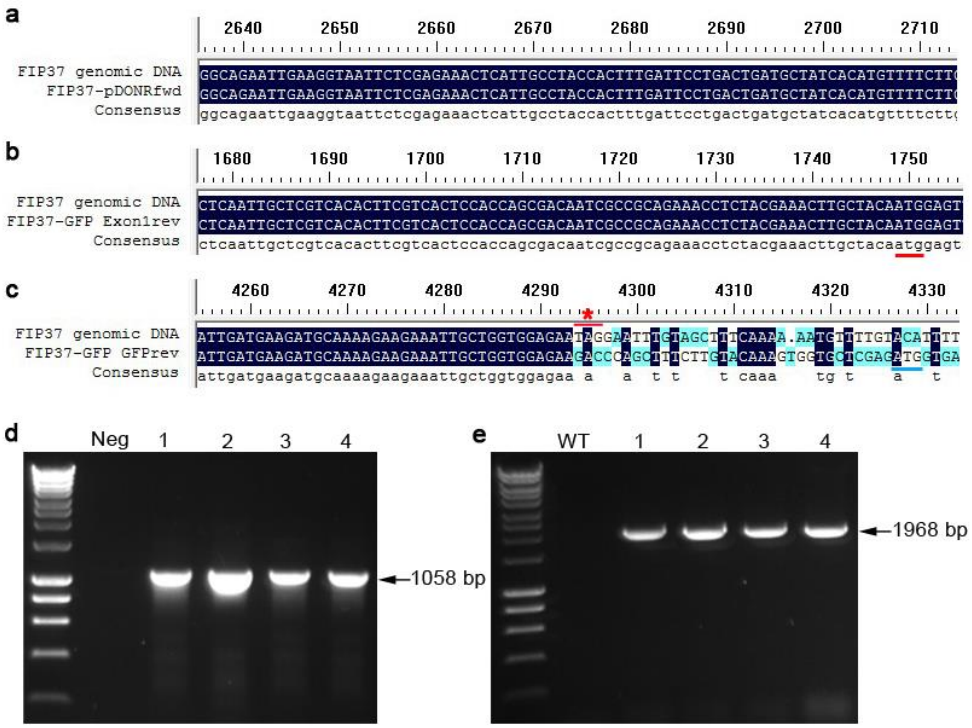

Figure 4.15 Generation of FIP37-GFP transgenic line. (**a and b**) Sequence alignments via DNAMAN showing the presence of *FIP37* genomic DNA (**a**) and its own promoter (**b**) on Gateway entry vector FIP37p-gDNA-pDONR(Amp^+). The start codon is underlined in red. (**c**) Sequence alignments via DNAMAN showing the presence of GFP tag and no stop codon for *FIP37* transgene. The start codon of *GFP* is underlined in blue and the stop codon site of *FIP37* is labelled with a red asterisk. (**d**) PCR to check *E. coli* single colonies (Sample 1 to 4) after Gateway LR reaction. Neg, negative control. (**e**) PCR to confirm positive T_1 plants selected by Kan. Sample 1 to 4 were from four individual T_1 plants.

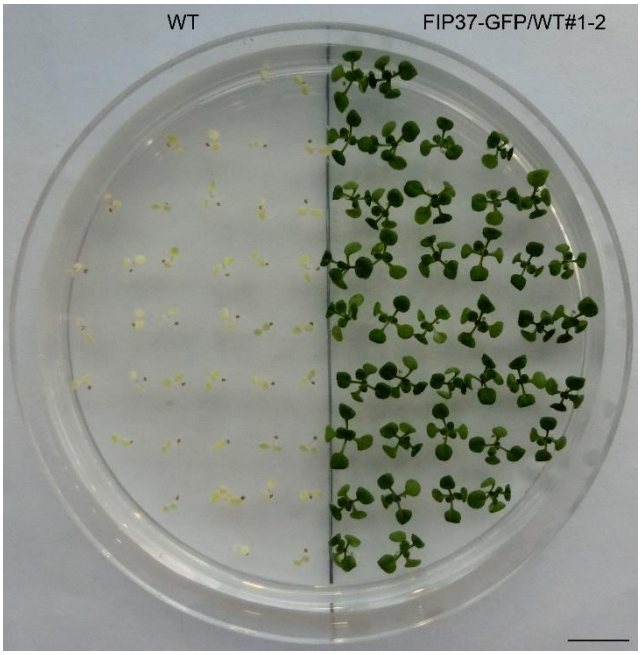

Figure 4.16 10-d old homozygous FIP37-GFP line planted on MS medium plus Kan. Scale bar = 1 cm.

4.4.2.2 Generation of MTA-GFP in hakai background

To generate MTA-GFP in *hakai* background, MTA-GFP was crossed into *hakai* 37. In the F_1 generation, MTA-GFP positive plants were selected via checking the GFP signal under the Stereo Fluorescence Microscope (Leica) and these plants were confirmed heterozygous for *Hakai* CRISPR target site (Figure 4.17a). In the F_2 generation, progenies homozygous for *Hakai* CRISPR target site were identified and used for further screening (Figure 4.17a). In the subsequent generation, progenies were checked to identify those homozygous for MTA-GFP and also homozygous for *MTA* SALK_114710 T-DNA insertion (Figure 4.17b). Together, transgenic lines that were simultaneously homozygous for *hakai* mutation, *MTA-GFP* transgene and *MTA* T-DNA insertion were obtained and these were denominated as *hakai* MTA-GFP.

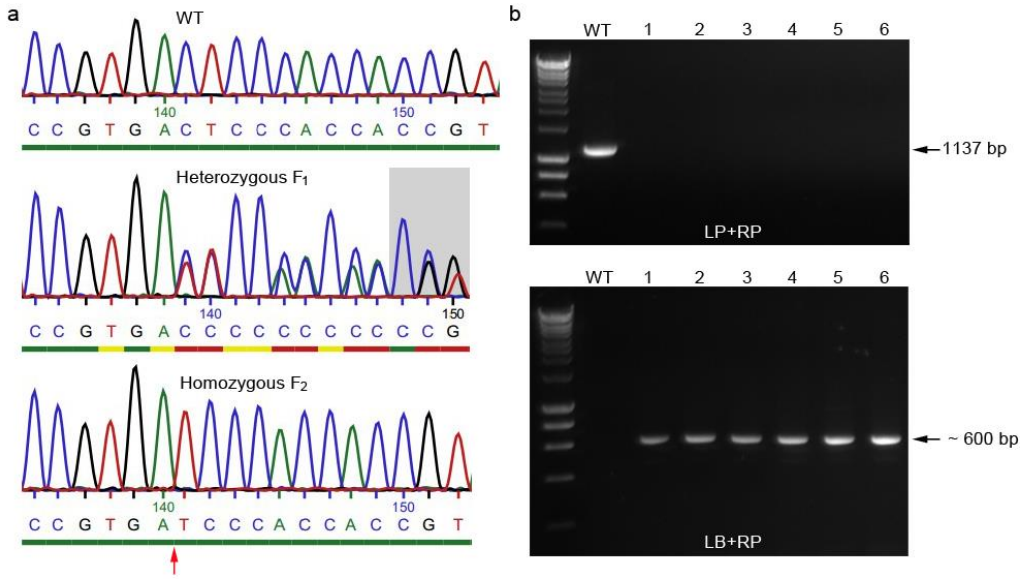

Figure 4.17 Screening progenies of *hakai* 37 crossed with MTA-GFP. (**a**) Sequencing profiles showing heterozygous F_1 progenies and homozygous F_2 progenies at *Hakai* CRISPR target site. (**b**) Genotyping PCR demonstrating F_3 progenies homozygous for *Hakai* CRISPR target site were also homozygous for *MTA* SALK_114710 T-DNA insertion.

4.4.2.3 Generation of other GFP-tagged lines in hakai background

Likewise, MTB-GFP, FIP37-GFP/WT and Virilizer-GFP were crossed into *hakai* 37 separately. The screening of the crossing progenies was the same as that for the cross between *hakai* 37 and MTA-GFP. Eventually, progenies that were homozygous for not only *hakai* mutation but also *GFP*-tagged transgenes were obtained, which were termed *hakai* MTB-GFP, *hakai* FIP37-GFP and *hakai* Virilizer-GFP. However, the status of *MTB* or *Virilizer* alleles could not be confirmed in *hakai* MTB-GFP or *hakai* Virilizer-GFP because the original GFP lines used for these two crosses were homozygous mutants complemented with their corresponding genomic DNAs, thus it is difficult to determine the mutation status in these crossing progenies.

4.4.2.4 Phenotyping of GFP-tagged lines in hakai background

Interestingly, *hakai* MTA-GFP and *hakai* MTB-GFP rather than *hakai* FIP37-GFP and *hakai* Virilizer-GFP demonstrated slower growth and shorter inflorescence stems compared with their parental GFP-tagged lines (Figure 4.18). Consistently, root phenotyping of 8-d old seedlings cultured on vertical plates containing 1/2 MS plus 1% (w/v) sucrose showed that *hakai* MTA-GFP and *hakai* MTB-GFP produced significantly shorter primary roots than either parent and emerging lateral roots in *hakai* MTA-GFP and *hakai* MTB-GFP were extremely reduced relative to either parental line (Figure 4.19, 4.20). In addition, the lateral root length of *hakai* MTA-GFP and *hakai* MTB-GFP was generally shorter than that of their parental lines (Figure 4.19).

Figure 4.18 4-week old *hakai* MTA-GFP and *hakai* MTB-GFP compared with their parental GFP-tagged lines. Scale bar = 1 cm.

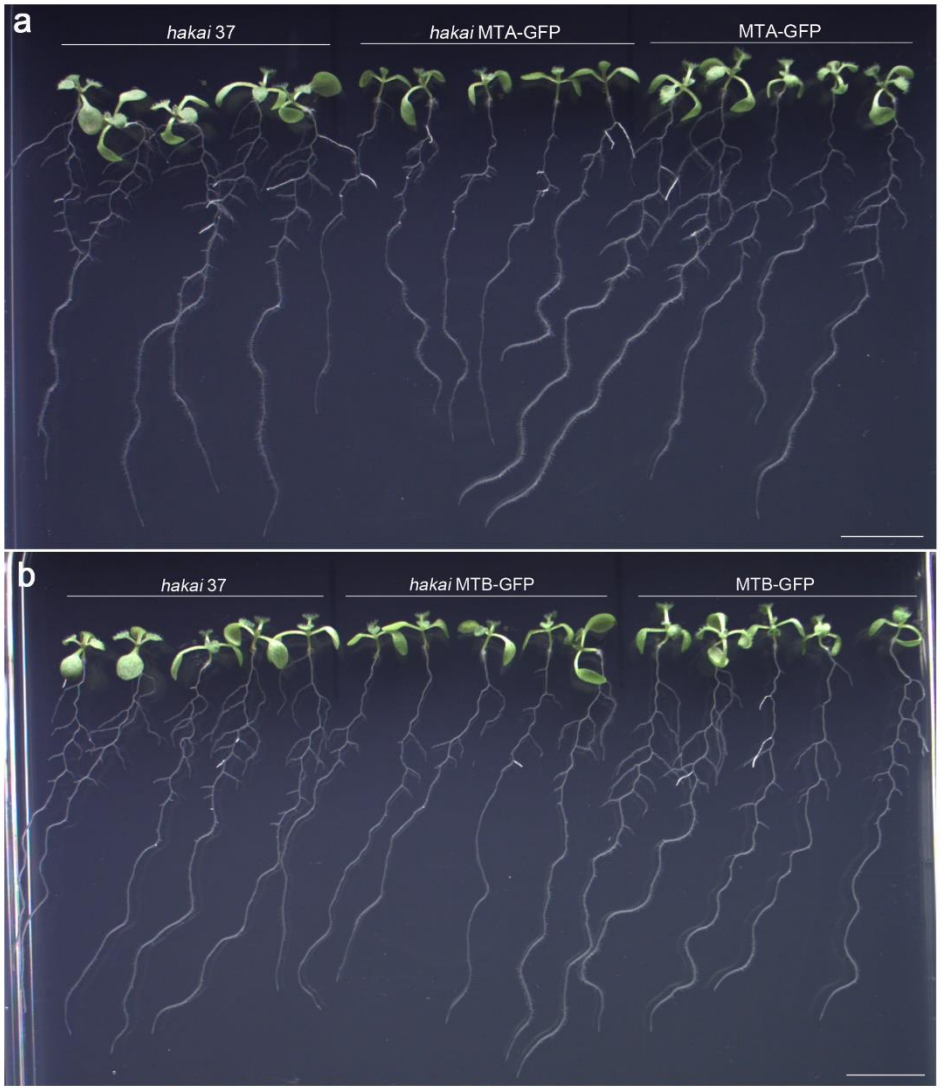

Figure 4.19 8-d old *hakai* MTA-GFP (**a**) and *hakai* MTB-GFP (**b**) compared with their parental lines on 1/2 MS plus 1% (w/v) sucrose. Scale bar = 1 cm.

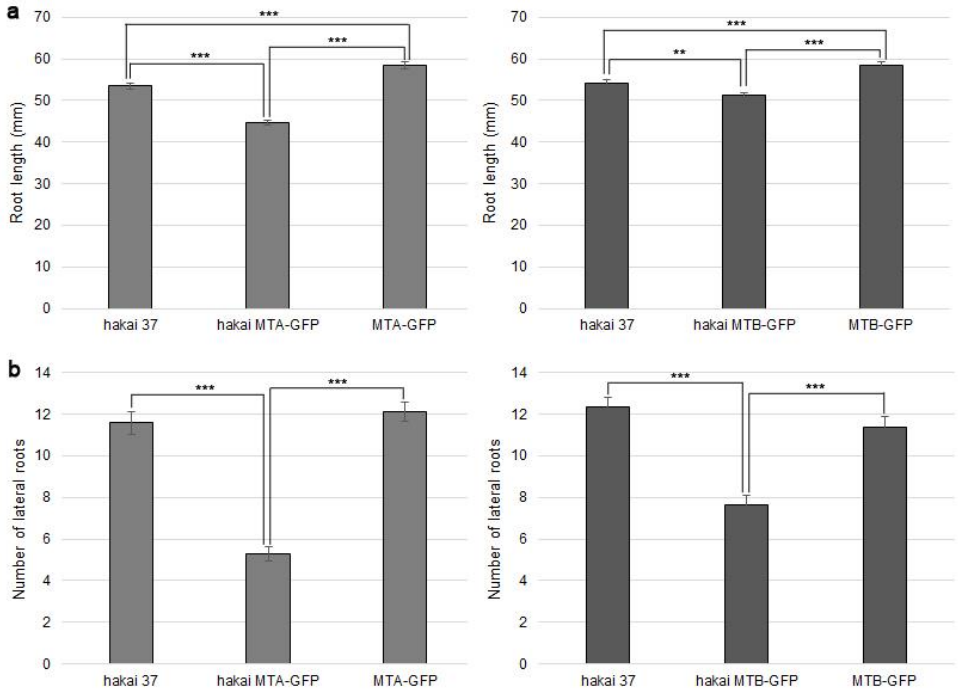

Figure 4.20 Root phenotypes of 8-d old *hakai* MTA-GFP and *hakai* MTB-GFP compared with their parental lines on 1/2 MS plus 1% (w/v) sucrose. (**a**) Root lengths. (**b**) The number of lateral roots. Data represent mean ± SEM and statistically significant differences were compared by One-Way ANOVA and marked with asterisks (**, $p<0.01$; ***, $p<0.001$).

4.4.2.5 Localisation of GFP-tagged proteins in hakai background

Analysis of 5-d old seedlings by confocal microscopy showed that *MTB-GFP*, *FIP37-GFP* and *Virilizer-GFP* were primarily expressed in the nuclei of cells in the primary root tip while the expression of *MTA-GFP* was the strongest, not only in the nuclei but also in the cytoplasm of cells (Figure 4.21, 4.22). Upon the knockout of *Hakai*, the localisation of these GFP-tagged proteins remained the same (Figure 4.21, 4.22).

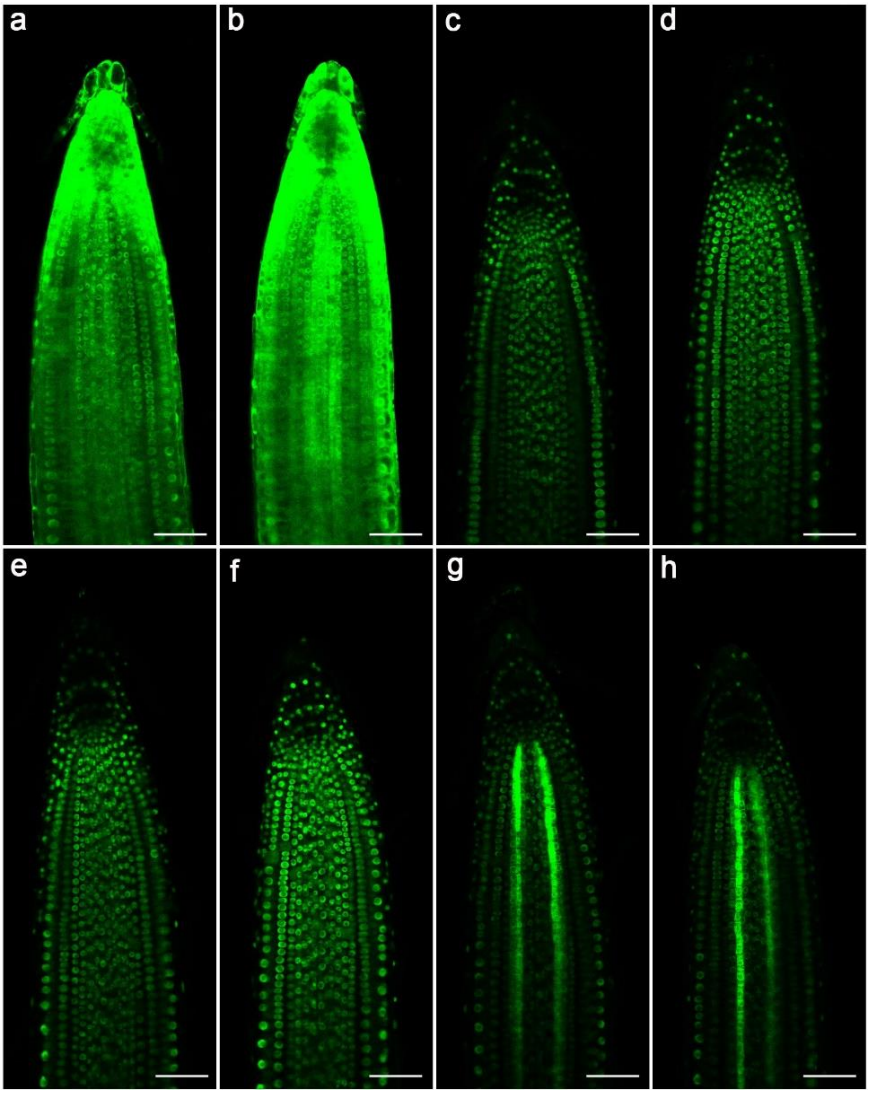

Figure 4.21 GFP localisations in primary root tips of m^6A-related transgenic lines tagged with GFP and in WT or *hakai* knockout background. (**a**) MTA-GFP. (**b**) *hakai* MTA-GFP. (**c**) MTB-GFP. (**d**) *hakai* MTB-GFP. (**e**) FIP37-GFP/WT. (**f**) *hakai* FIP37-GFP. (**g**) Virilizer-GFP. (**h**) *hakai* Virilizer-GFP. Samples were 5-d old seedlings. Scale bar = 50 μm.

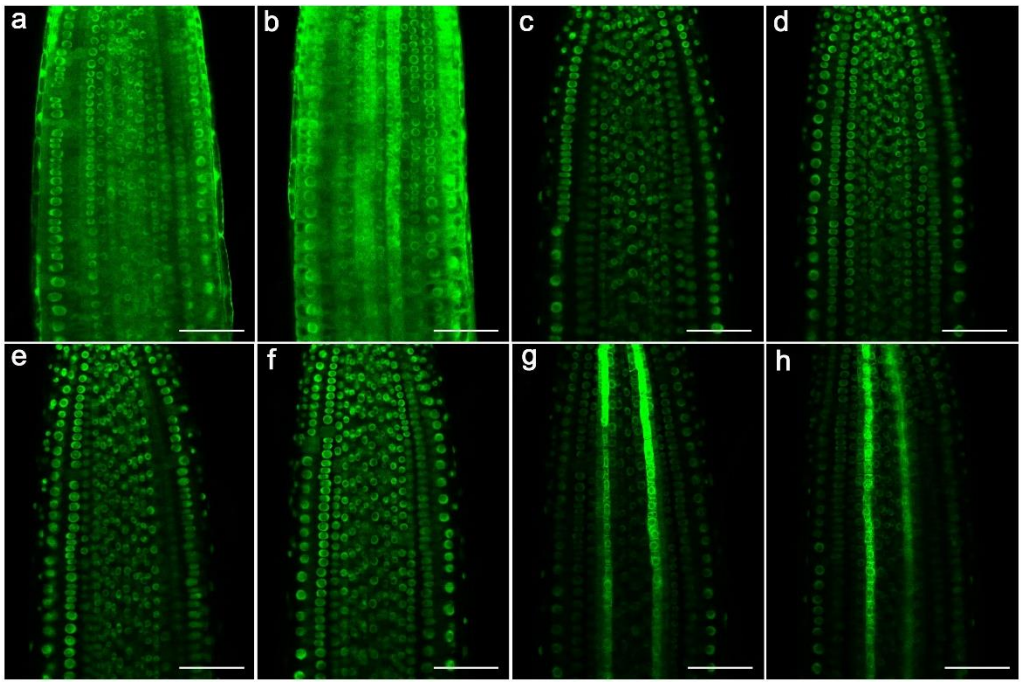

Figure 4.22 Enlarged confocal images showing GFP localisations in primary root tips of m^{6}A-related transgenic lines tagged with GFP and in WT or *hakai* knockout background. (**a**) MTA-GFP. (**b**) *hakai* MTA-GFP. (**c**) MTB-GFP. (**d**) *hakai* MTB-GFP. (**e**) FIP37-GFP/WT. (**f**) *hakai* FIP37-GFP. (**g**) Virilizer-GFP. (**h**) *hakai* Virilizer-GFP. Samples were 5-d old seedlings. Scale bar = 50 μm.

4.4.2.6 GFP-tagged protein levels in hakai background

Due to the unclear genetic background of *hakai* MTB-GFP and *hakai* Virilizer-GFP, *hakai* MTA-GFP, *hakai* FIP37-GFP and their parental GFP-tagged transgenic lines were used for protein expression assays. The western blotting confirmed that GFP-tagged proteins were expressed in all tested transgenic lines but no obvious change of protein levels was detected upon *Hakai* knockout (Figure 4.23).

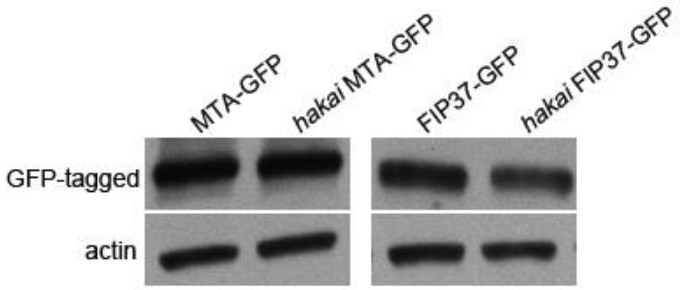

Figure 4.23 Checking GFP-tagged protein levels by western blotting.

4.4.3 Generation and Characterisation of GFP-tagged Lines in *mta* or *fip37* Mutant Backgrounds

4.4.3.1 Generation of Hakai-GFP or FIP37-GFP in mta background

To generate Hakai-GFP in *mta* background, Hakai-GFP/WT#1 was crossed into ABI3A6. Likewise, FIP37-GFP/WT#1-2 was crossed into ABI3A6. In the F_1 generation, progenies heterozygous for *MTA* SALK_074069 T-DNA insertion and with the presence of *ABI3*::*MTA* construct were identified in both of the above crosses (Figure 4.24, 4.25). These progenies harboured the *Hakai-GFP* or *FIP37-GFP* transgene as well (Figure 4.24c, 4.25c). Primer pairs used for PCRs were the same as mentioned earlier.

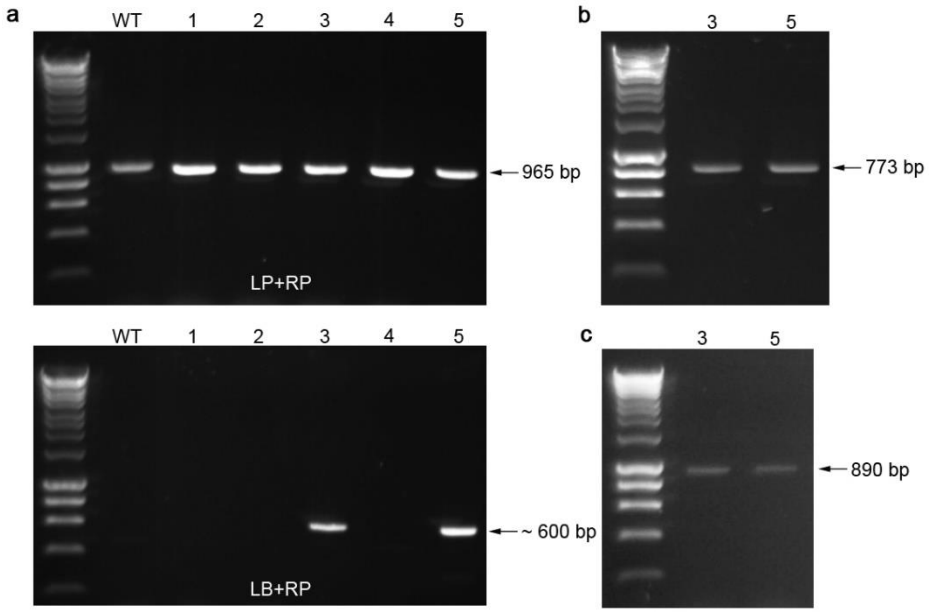

Figure 4.24 Screening F_1 progenies of Hakai-GFP/WT crossed with ABI3A6. (**a**) Genotyping PCR confirmed that plant 3 and 5 were heterozygous for *MTA* SALK_074069 T-DNA insertion. (**b**) PCR to check the presence of *ABI3*::*MTA* construct in plant 3 and 5. (**c**) PCR to check the presence of *Hakai-GFP* construct in plant 3 and 5.

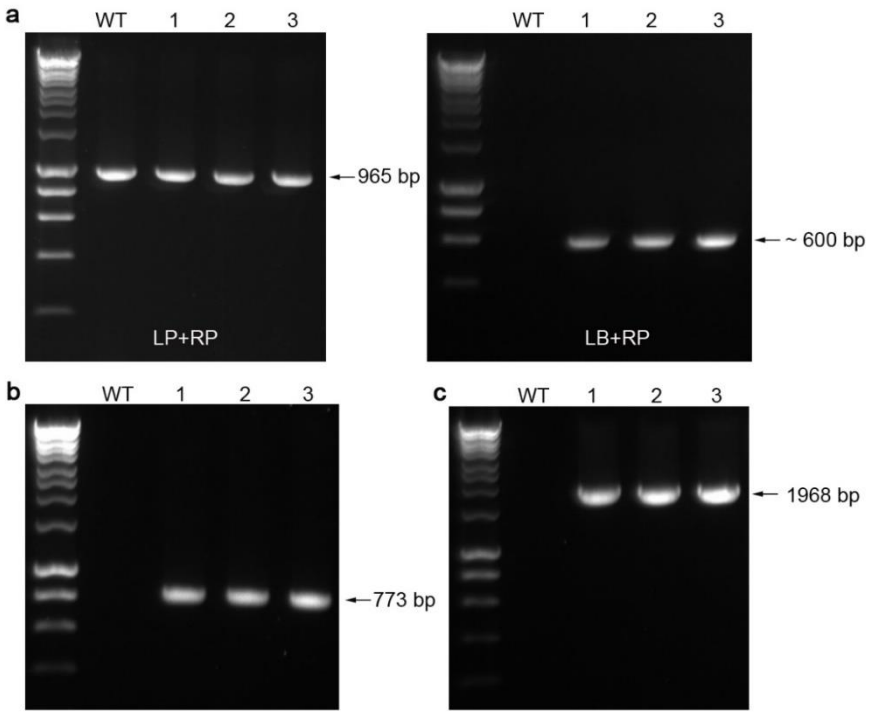

Figure 4.25 Screening F_1 progenies of FIP37-GFP/WT crossed with ABI3A6. (**a**) Genotyping PCR confirmed that all three checked F_1 plants were heterozygous for *MTA* SALK_074069 T-DNA insertion. (**b**) PCR to check the presence of *ABI3*::*MTA* construct in three checked F_1 plants. (**c**) PCR to check the presence of *FIP37-GFP* construct in three checked F_1 plants.

Among F_2 progenies, some demonstrating ABI3A6 phenotypes were confirmed homozygous for *MTA* SALK_074069 T-DNA insertion (Figure 4.26, 4.27). Of course, these plants also contained *ABI3*::*MTA* constructs (Supplementary figure 4.6, 4.7). The presence of *GFP*-tagged transgenes was checked in the F_3 generation under the Stereo Fluorescence Microscope (Leica). Except for line 2-1 for FIP37-GFP/WT crossed with ABI3A6, all the other checked lines for these two crosses were GFP-positive. In particular, line 5-1 for Hakai-GFP/WT crossed with ABI3A6 (termed *mta* Hakai-GFP) and line 1-3, 2-2, 2-4 for FIP37-GFP/WT crossed with ABI3A6 (termed *mta* FIP37-GFP#1-3, #2-2, #2-4, respectively) were homozygous for *GFP*-tagged transgenes.

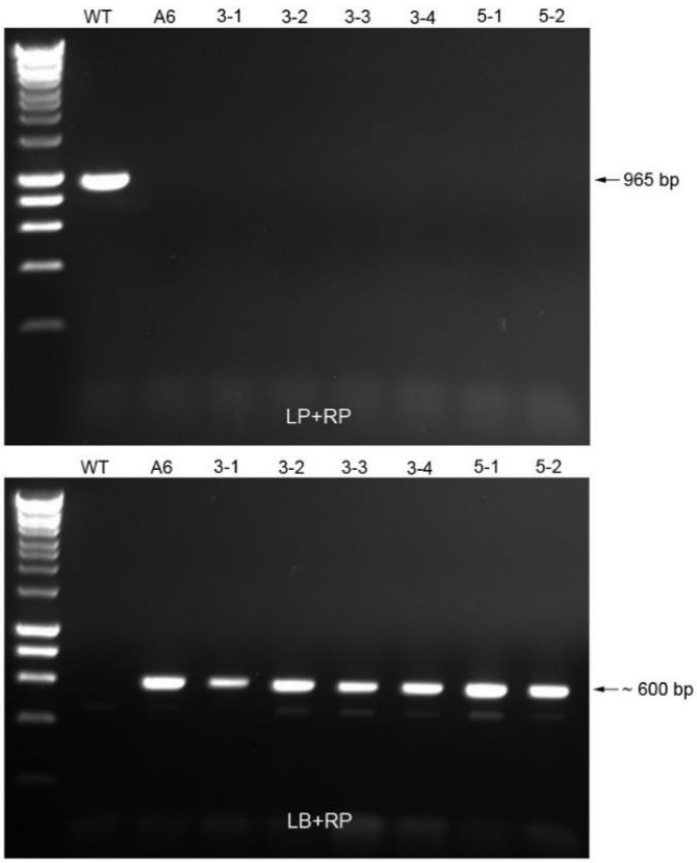

Figure 4.26 Genotyping PCR to confirm some F_2 progenies of Hakai-GFP/WT crossed with ABI3A6 were homozygous for *MTA* SALK_074069 T-DNA insertion. A6 refers to ABI3A6. Sample 3-1 to 3-4 represent four individual F_2 plants from F_1 plant 3 while sample 5-1 and 5-2 represent two individual F_2 plants from F_1 plant 5.

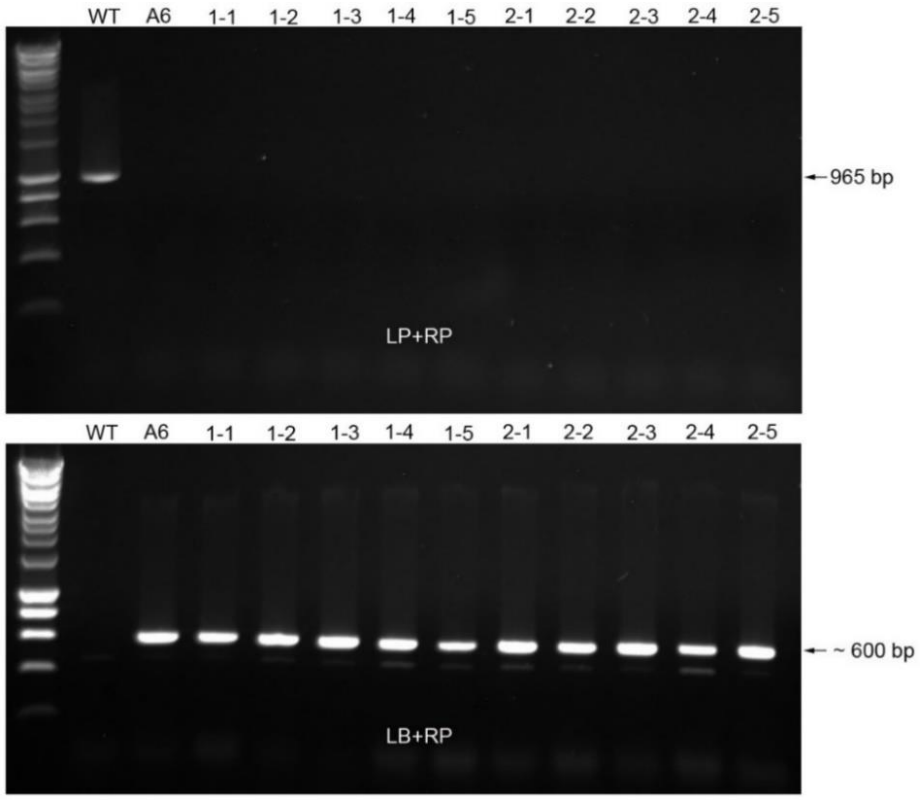

Figure 4.27 Genotyping PCR to confirm some F_2 progenies of FIP37-GFP/WT crossed with ABI3A6 were homozygous for *MTA* SALK_074069 T-DNA insertion. A6 refers to ABI3A6. Sample 1-1 to 1-5 represent five individual F_2 plants from F_1 line 1 while sample 2-1 to 2-5 represent five individual F_2 plants from F_1 line 2.

4.4.3.2 Generation of Hakai-GFP and MTA-GFP in fip37 background

To generate Hakai-GFP in *fip37* background, *fip37* was crossed into Hakai-GFP/WT#1. As a comparison, *fip37* was also crossed into MTA-GFP/WT. The screening of F_1 progenies started with checking *GFP*-tagged transgenes. PCR using forward primers on *Hakai* or *MTA* and the reverse one on *GFP* showed that all F_1 progenies except for line 3 of *fip37* crossed with Hakai-GFP/WT possessed *Hakai-GFP* transgene while one of two checked F_1 progenies of *fip37* crossed with MTA-GFP/WT contained the *MTA-GFP* construct (Figure 4.28a,b).

Genotyping PCRs confirmed that all these lines were heterozygous for *FIP37* SALK_018636 T-DNA insertion (Figure 4.28c).

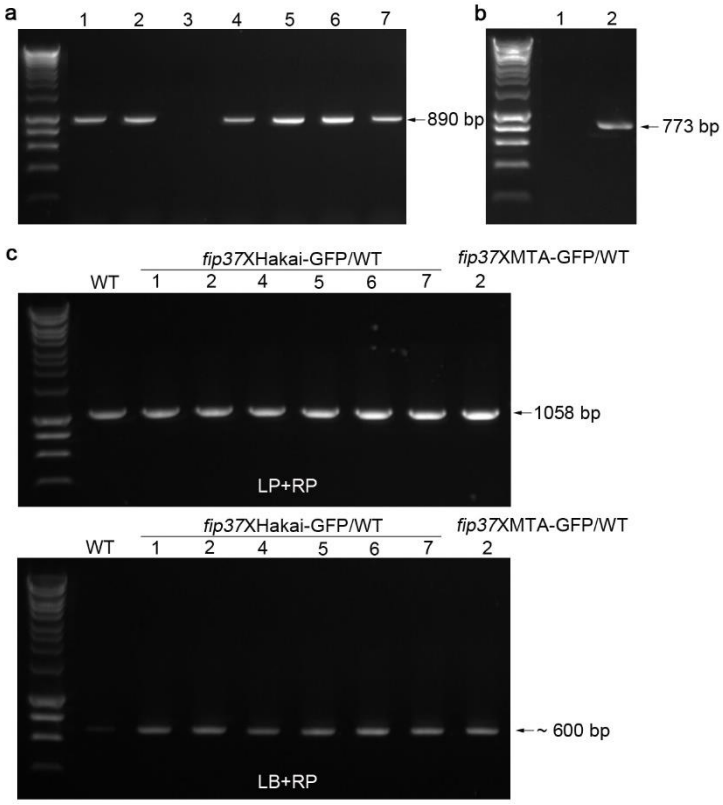

Figure 4.28 Screening F_1 progenies of *fip37* crossed with Hakai-GFP/WT or MTA-GFP/WT. (**a**) PCR to check the presence of *Hakai-GFP* construct in seven F_1 progenies of *fip37* crossed with Hakai-GFP/WT. (**b**) PCR to check the presence of *MTA-GFP* construct in two F_1 progenies of *fip37* crossed with MTA-GFP/WT. (**c**) Genotyping PCR confirmed that all GFP-positive plants were heterozygous for *FIP37* SALK_018636 T-DNA insertion.

Similar to that in GFP-tagged lines crossed with ABI3A6, some F_2 progenies of *fip37* crossed with Hakai-GFP/WT or MTA-GFP/WT showed *fip37* phenotypes. Firstly, *GFP*-tagged transgenes were checked by PCR in those showing *fip37* phenotypes. The results showed that about 60% of these plants contained *Hakai-GFP* or *MTA-GFP* transgenes (Figure 4.29, 4.30). Genotyping PCRs confirmed

that all these GFP-positive plants were homozygous for *FIP37* SALK_018636 T-DNA insertion (Figure 4.31, 4.32). In the F_3 generation, line 1-2 for *fip37* crossed with Hakai-GFP/WT (denominated as *fip37* Hakai-GFP) were homozygous for *Hakai-GFP* while other checked lines were heterozygous for *Hakai-GFP* or *MTA-GFP*. F_4 progenies of line 2-1 and 2-3 for *fip37* crossed with MTA-GFP/WT were used to screen homozygous lines for *MTA-GFP* transgene. Analysis of 24 seedlings from each line under the Stereo Fluorescence Microscope (Leica) confirmed that line 2-1-2 and 2-3-3 were homozygous for *MTA-GFP* transgene (termed *fip37* MTA-GFP#2-1-2 and #2-3-3, respectively).

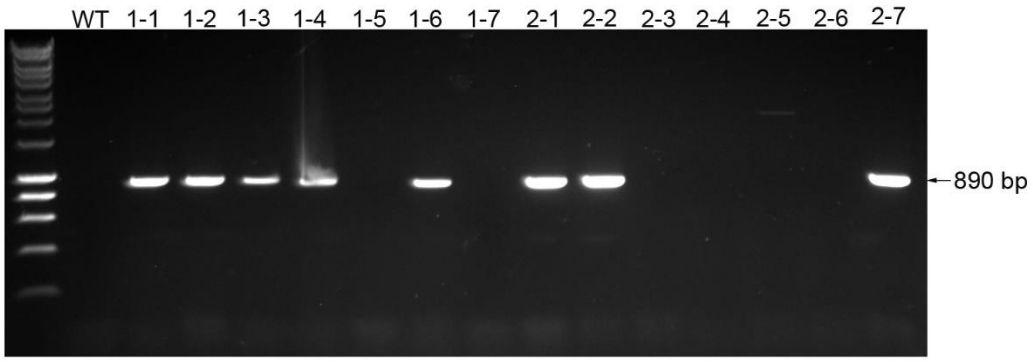

Figure 4.29 PCR to check the presence of *Hakai-GFP* transgene in F_2 progenies of *fip37* crossed with Hakai-GFP/WT. Sample 1-1 to 1-7 represent seven individual F_2 plants from F_1 line 1 while sample 2-1 to 2-7 represent seven individual F_2 plants from F_1 line 2.

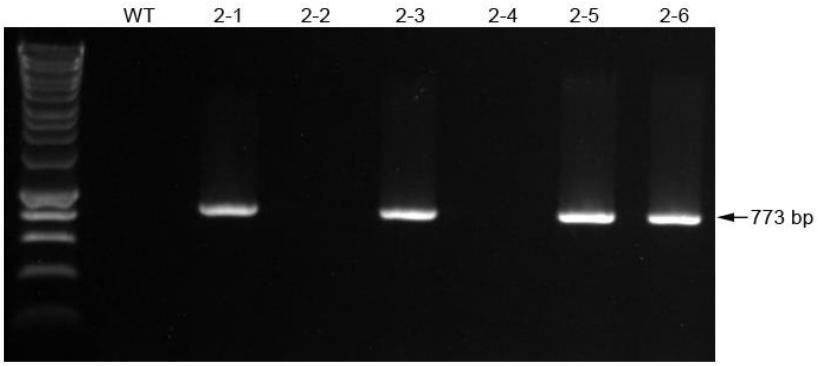

Figure 4.30 PCR to check the presence of *MTA-GFP* transgene in F_2 progenies of *fip37* crossed with MTA-GFP/WT. Sample 2-1 to 2-6 represent six individual F_2 plants from F_1 line 2.

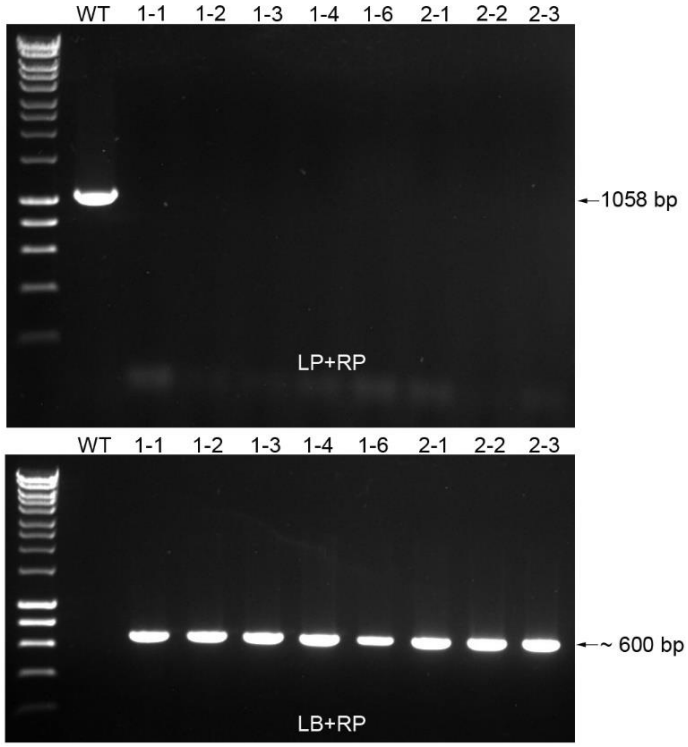

Figure 4.31 Genotyping PCR to check *FIP37* SALK_018636 T-DNA insertion in GFP-positive F_2 progenies of *fip37* crossed with Hakai-GFP/WT. Checked samples except for WT represent individual F_2 plants from F_1 line 1 and 2.

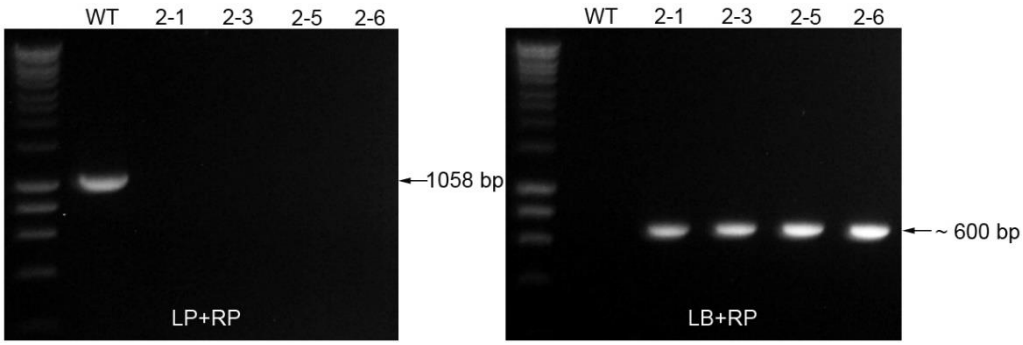

Figure 4.32 Genotyping PCR to check *FIP37* SALK_018636 T-DNA insertion in GFP-positive F_2 progenies of *fip37* crossed with MTA-GFP/WT. Checked samples except for WT represent individual F_2 plants from F_1 line 2.

In terms of phenotypes, progenies of *fip37* crossed with MTA-GFP/WT looked even smaller than *fip37* and produced fewer seeds relative to *fip37* even when they were not homozygous for *MTA-GFP* transgene (Figure 4.33), suggesting that the introduction of *MTA-GFP* transgene in *fip37* increases the developmental defects of *fip37*. This difference was confirmed by culturing seedlings on 1/2 MS plus 1% (w/v) sucrose. *fip37* MTA-GFP plants were sicker and much smaller than *fip37* (Supplementary figure 4.8).

Figure 4.33 5-week old *fip37* MTA-GFP (homozygous for both *FIP37* SALK_018636 T-DNA insertion and *MTA-GFP* transgene) compared with its parental lines. Scale bar = 1 cm.

4.4.3.3 Localisation of GFP-tagged proteins in mta or fip37 background

As shown in Figure 4.34, there were no recognisable differences of GFP localisation between Hakai-GFP/WT and *mta* Hakai-GFP. This was also the case for FIP37-GFP/WT and *mta* FIP37-GFP (Figure 4.34). In contrast, the localisation of Hakai-GFP or MTA-GFP was modified when *FIP37* was knocked down (Figure 4.35). The GFP signal in the nuclei of *fip37* Hakai-GFP was slightly less than that in Hakai-GFP/WT and the difference was more obvious in *fip37* MTA-GFP compared with MTA-GFP/WT, with *fip37* MTA-GFP demonstrating increased GFP localisation in the cytoplasm (Figure 4.35). In lateral roots, MTA-GFP in WT background was primarily localised to the nuclei whereas the GFP signal in *fip37* MTA-GFP was predominantly localised

in the cytoplasm, which was even stronger than that in MTA-GFP complementing *mta* knockout mutant (Figure 4.36, 4.37). This difference was not found between Hakai-GFP and *fip37* Hakai-GFP (Figure 4.38). Aside from primary and lateral root tips, strong GFP signal was also detected in other regions of the root of *fip37* MTA-GFP, for example, the elongation zone, whereas the GFP signal in this region of MTA-GFP/WT was negligible and that in MTA-GFP complementing *mta* knockout mutant was much less (Figure 4.36d,h, 4.37d).

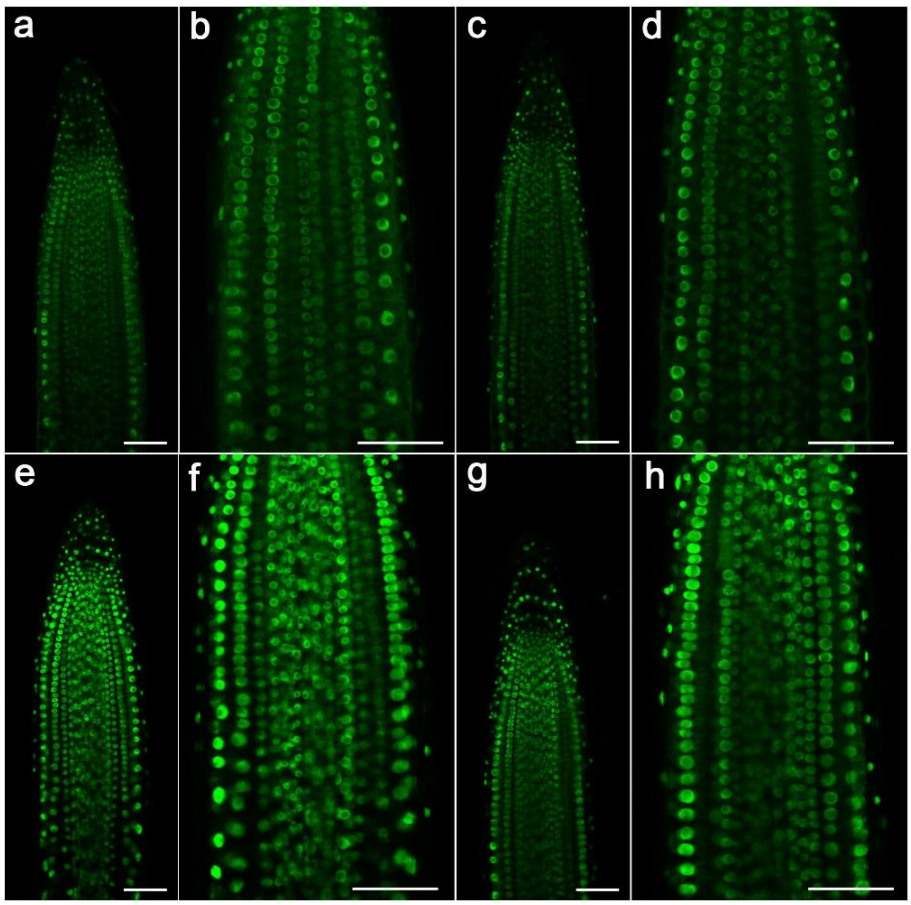

Figure 4.34 GFP localisations in primary root tips of m^6A-related transgenic lines tagged with GFP and in WT or *mta* knockdown background. (**a and b**) Hakai-GFP/WT. (**c and d**) *mta* Hakai-GFP. (**e and f**) FIP37-GFP/WT. (**g and h**) *mta* FIP37-GFP. Samples were 5-d old seedlings. Scale bar = 50 μm.

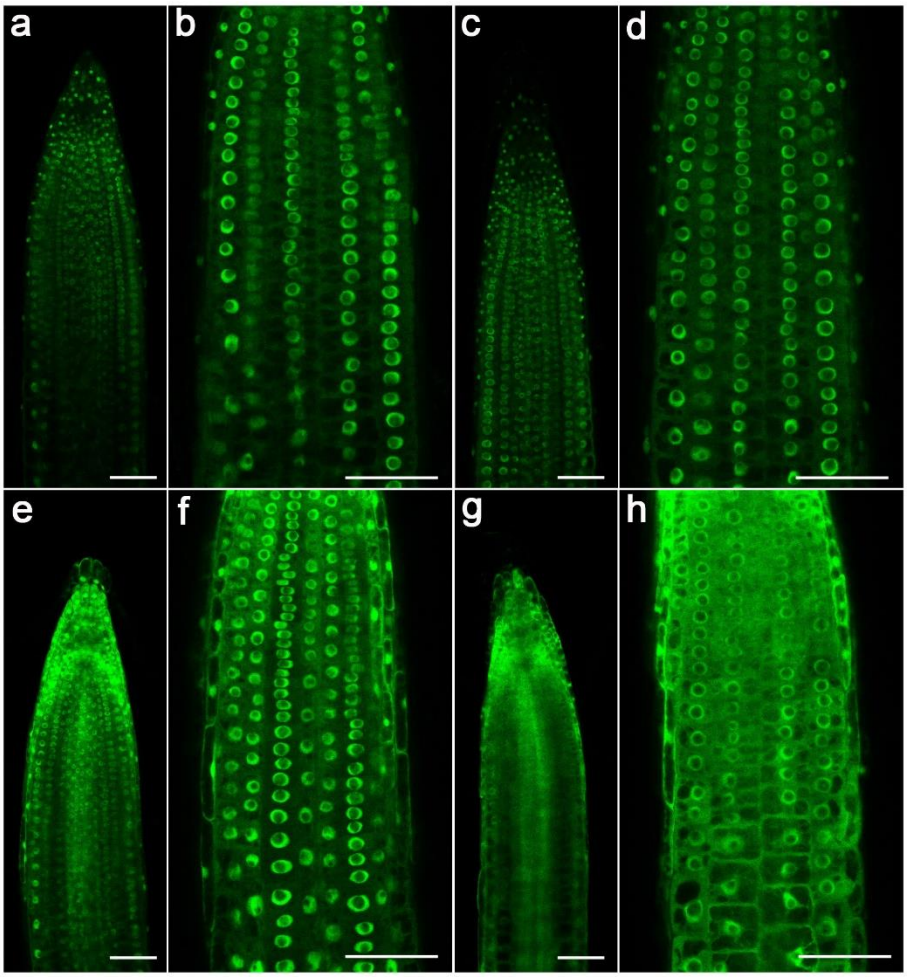

Figure 4.35 GFP localisations in primary root tips of m^{6}A-related transgenic lines tagged with GFP and in WT or *fip37* knockdown background. (**a and b**) Hakai-GFP/WT. (**c and d**) *fip37* Hakai-GFP. (**e and f**) MTA-GFP/WT. (**g and h**) *fip37* MTA-GFP. Samples were 5-d old seedlings. Scale bar = 50 μm.

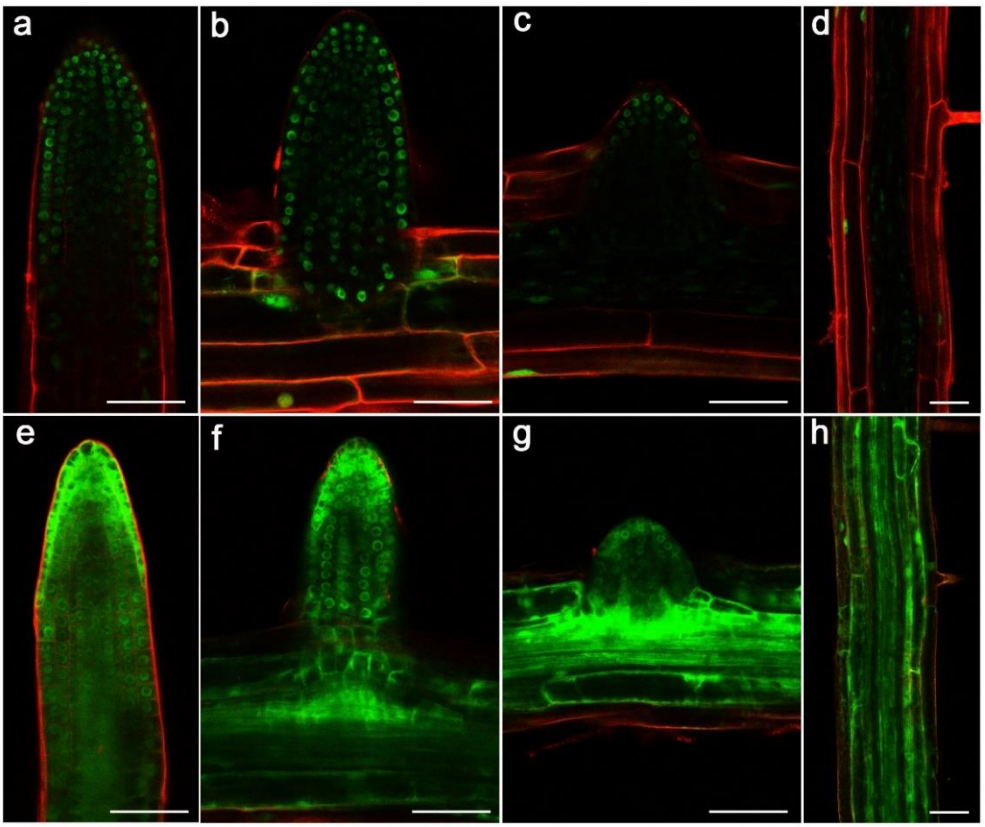

Figure 4.36 GFP localisations in roots of MTA-GFP in WT or *fip37* knockdown background. (**a-d**) MTA-GFP/WT. (**e-h**) *fip37* MTA-GFP. (**a and e**) Long lateral root tips. (**b and f**) Short lateral roots. (**c and g**) Just emerged lateral roots. (**d and h**) Elongation zones of primary roots. Samples were 9-d old seedlings. Scale bar = 50 μm.

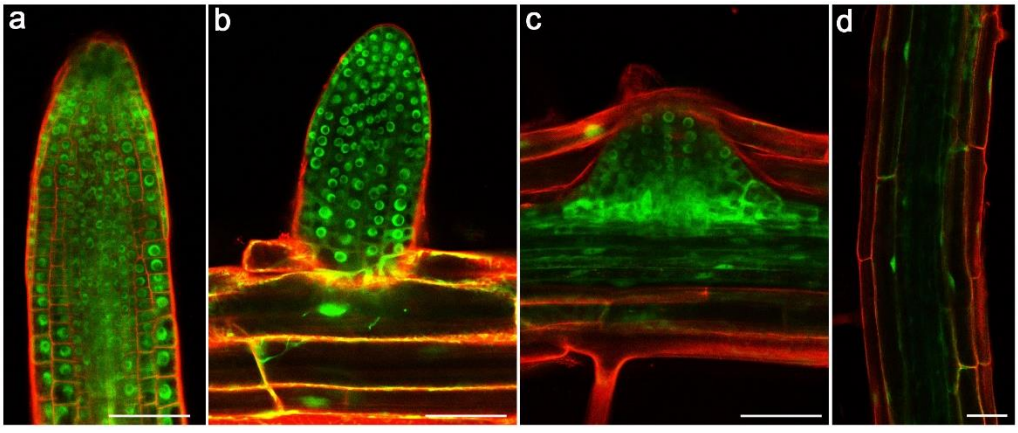

Figure 4.37 GFP localisations in roots of MTA-GFP complementing *mta* knockout mutant. (**a**) Long lateral root tip. (**b**) Short lateral root. (**c**) Emerging lateral root. (**d**) Elongation zone of the primary root. Samples were 9-d old seedlings. Scale bar = 50 μm.

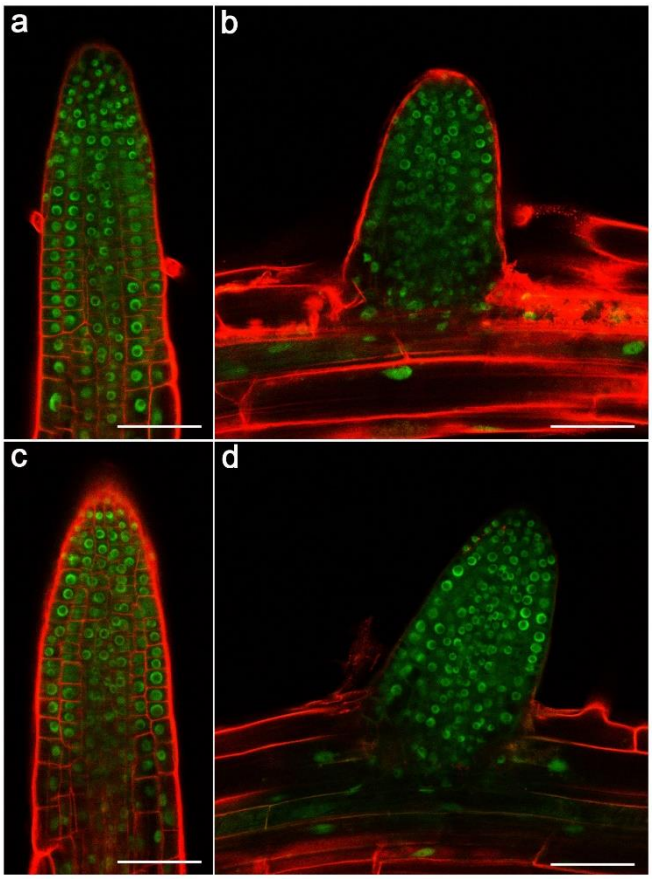

Figure 4.38 GFP localisations in roots of Hakai-GFP in WT or *fip37* knockdown background. (**a and b**) Hakai-GFP/WT. (**c and d**) *fip37* Hakai-GFP. (**a and c**) Long lateral root tips. (**b and d**) Short lateral roots. Samples were 9-d old seedlings. Scale bar = 50 μm.

4.4.4 Protein Interaction Analysis via Mass Spectrometry

To identify proteins that interact with Hakai, Hakai-GFP/*hakai*#2 was used for immunoprecipitation via GFP-trap agarose beads and the subsequent analysis by mass spectrometry, with WT as a control. Mass spectrometry data analysed via Maxquant and Perseus demonstrated that the major proteins interacting with Hakai include FIP37, Virilizer, MTA, two zinc finger proteins (AT1G32360 and AT5G53440) and a protein belonging to heat shock protein 70 family (Hps70-

15, protein ID: A0A178W9Z4) whereas MTB was not a significantly interacting protein with Hakai (Figure 4.39).

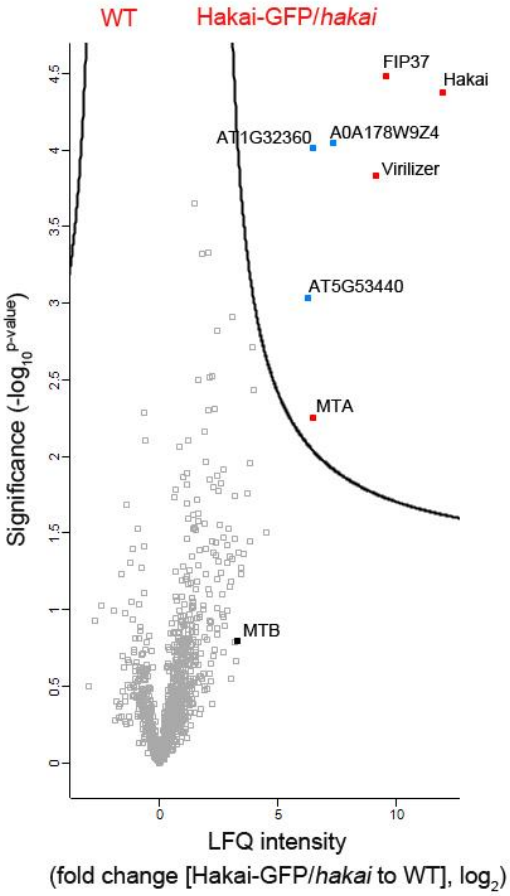

Figure 4.39 Volcano plot showing interacting proteins with Hakai (using Hakai-GFP as a bait). Hakai-GFP/*hakai* was plotted on the right and WT on the left. The enrichment of pulled-down proteins was caculated using label free quantification (LFQ) and the significance was analysed based on the negative logarithm of the p-value derived from the t-test ($-\log_{10}^{\text{p-value}}$). Proteins that were significantly enriched were separated from other proteins by a hyperbolic curve and marked with red or blue filled squares (red: known m^6A writer proteins; blue: new pulled-down proteins). MTB is indicated by a black filled square.

To check whether interacting proteins with MTA would change when *Hakai* was knocked out, pulled-down proteins from MTA-GFP were compared with those

from *hakai* MTA-GFP. Generally, fewer proteins were pulled down in *hakai* MTA-GFP relative to those in MTA-GFP (Figure 4.40). Important proteins that interact with MTA include all known m^6A writer proteins (Virilizer, FIP37, MTB and Hakai), AT1G32360, AT5G53440 and Hps70-15. However, the knockout of *Hakai* led to the disappearance of the interaction between MTA and AT1G32360 (Figure 4.40, 4.41).

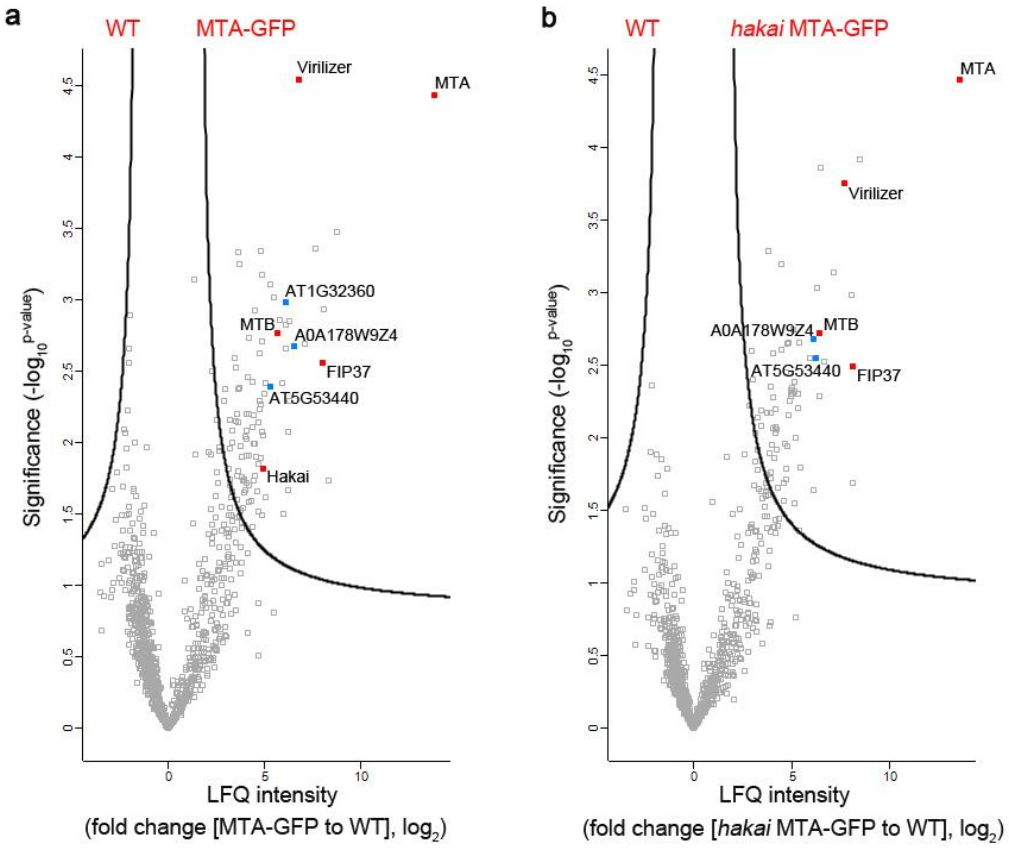

Figure 4.40 Volcano plot showing interacting proteins with MTA (using MTA-GFP as a bait). (**a**) MTA-GFP (right) versus WT (left). (**b**) *hakai* MTA-GFP (right) versus WT (left). The enrichment of pulled-down proteins was caculated using label free quantification (LFQ) and the significance was analysed based on the negative logarithm of the p-value derived from the t-test ($-\log_{10}^{\text{p-value}}$). Proteins that were significantly enriched were separated from other proteins by a hyperbolic curve and important ones are marked with red or blue filled squares (red: known m^6A writer proteins; blue: new pulled-down proteins).

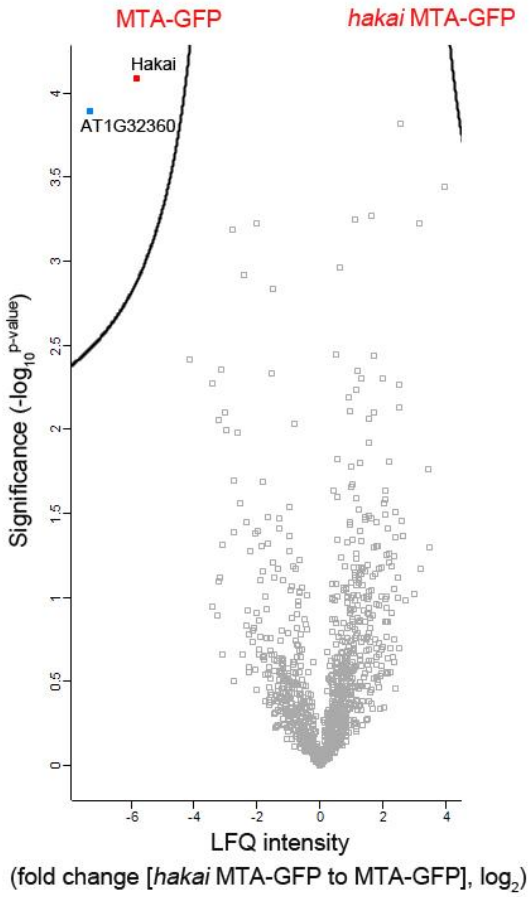

Figure 4.41 Volcano plot showing the comparison of pulled-down proteins between MTA-GFP (left) and *hakai* MTA-GFP (right) (using MTA-GFP as a bait). The enrichment of pulled-down proteins was caculated using label free quantification (LFQ) and the significance was analysed based on the negative logarithm of the p-value derived from the t-test ($-\log_{10}^{\text{p-value}}$). Proteins that were significantly enriched were separated from other proteins by a hyperbolic curve and marked with red or blue filled squares (red: known m^6A writer proteins; blue: new pulled-down proteins).

4.5 DISCUSSION

4.5.1 The Importance of Hakai in the MTase Complex

Work described in Chapter 3 demonstrates that Hakai is required for full m^6A methylation in plants. The function of Hakai was further analysed here. First of all, studying proteins interacting with Hakai via immunoprecipitation and the subsequent mass spectrometry analysis reveals that Hakai interacts with known proteins in the MTase complex, including MTA, FIP37 and Virilizer, verifying that Hakai is a bona fide member of the MTase complex. This is consistent with the identification of Hakai as an interacting protein with Virilizer in our previous tandem affinity purification (TAP) followed by mass spectrometry analysis (Růžička et al., 2017). In addition, homozygous *mta hakai* double mutant showed stronger developmental defects than *mta* single mutant and homozygous *hakai fip37*, *hakai virilizer* double mutants appeared to be lethal while all these single mutants were viable. Furthermore, when *Hakai* was knocked out, MTA-GFP and MTB-GFP could no longer fully complement the phenotypes of their corresponding mutants. Taken together, Hakai is a crucial member of the MTase complex, acting synergistically with other members not only in maintaining the correct m^6A deposition but also in ensuring proper growth and development in *Arabidopsis*.

To know about the transcripts influenced by Hakai in terms of mRNA methylation, MeRIP-seq has been performed to compare the methylome of WT and *hakai* knockout mutant. The quality of libraries constructed for MeRIP-seq

was good and decreased methylation peaks could be seen in some checked transcripts. Detailed bioinformatic analysis of *hakai* MeRIP-seq data compared with the methylome of WT and other m^6A writer mutants is ongoing and will give us a clearer understanding of transcripts and relevant biological pathways regulated by m^6A modification dependent on Hakai.

Human Hakai is an E3 ubiquitin ligase, catalysing the ubiquitination of E-cadherin in the epithelial cells, leading to the disruption of cell-cell connection (Fujita et al., 2002). However, no cadherins have been discovered in plants and it would not be expected as plant cells are joined via their cell walls rather than plasma membranes (Seymour et al., 2004; Hulpiau and Van Roy, 2009). Though the homology of *Arabidopsis* Hakai and human Hakai is rather low, they share the conserved RING domain and it remains worthwhile to investigate the ubiquitination specificity of *Arabidopsis* Hakai and its candidate targets, probably starting with proteins involved in the MTase complex, which have been confirmed as Hakai interacting partners by the mass spectrometry analysis in the current study.

4.5.2 Implications from Interaction Assay Among Members of the MTase Complex

Combining characterisation of double mutants and pull-down analysis in this study with yeast two hybrid (Y2H) and TAP analysis in our previous studies (Zhong et al., 2008; Růžička et al., 2017), the relationship between different components of the MTase complex is proposed as shown in Figure 4.42.

Generally, the interactions between MTA and FIP37, MTA and Virilizer, Hakai and FIP37, Hakai and Virilizer are relatively strong as FIP37 and Virilizer were the top two proteins pulled down with MTA and Hakai. Given that MTA and MTB are counterparts of mammalian METTL3 and METTL14, which function as a heterodimer (Wang et al., 2016), the interaction between MTA and MTB should also be strong and this is indeed supported by the mass spectrometry data here. Our mass spectrometry data also indicates that the interaction between MTA and Hakai is not as strong as the above interactions while that between Hakai and MTB is weak because MTB was only pulled down twice by GFP-tagged Hakai from three biological replicates, which is consistent with the Y2H result (Růžička et al., 2017). In addition, the interaction between Virilizer and MTB is also suggested to be weak, revealed by TAP analysis (Růžička et al., 2017).

Phenotyping of double mutants for m^6A writer proteins indicates that MTA, Hakai and Virilizer act synergistically in regulating plant growth and development. Hakai and FIP37 also function in concert to influence plant growth and development whereas MTA acts somewhat antagonistically towards FIP37, revealed by reduced developmental defects of *fip37* upon the knockdown of *MTA* and more severe defects of *fip37* due to the introduction of *MTA-GFP* transgene. The interaction between MTA and FIP37 was discovered early in 2008 (Zhong et al., 2008) and the current study further reveals that MTA acts as a suppressor of FIP37. Likewise, removal of one copy of *Drosophila* Ime4 can rescue female lethality of single amino acid substitution alleles *fl(2)d* (homologous to *Arabidopsis* FIP37) and *virilizer* (Haussmann et al., 2016). In

contrast, double knockdown of *METTL3* and *WTAP* in zebrafish leads to an increased apoptosis compared with that in either *METTL3* or *WTAP* knockdown mutant (Ping et al., 2014). To further elucidate the underlying molecular differences between *mta hakai* and *mta fip37* double mutants, transcriptome-wide m^{6}A modification and transcription analysis will give some clues. In addition, the knockdown of *FIP37* caused increased MTA-GFP in the cytoplasm, indicating that FIP37 might participate in regulating the distribution of MTA between the nuclei and the cytoplasm. This can be checked by western blotting following purification of nuclear and cytoplasmic fractions.

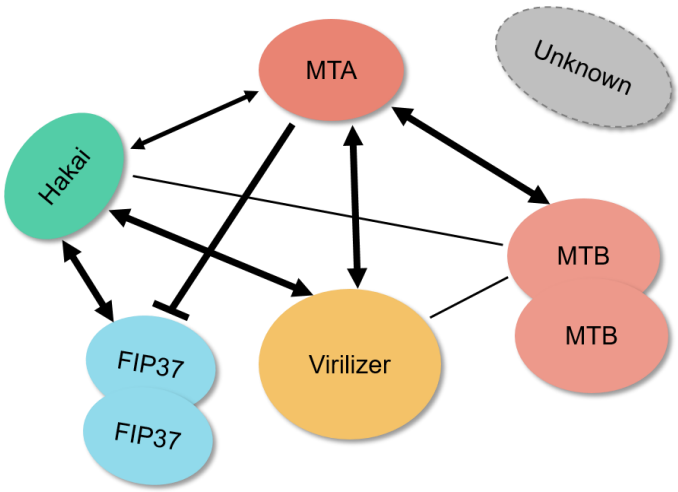

Figure 4.42 A proposal of interactions among components of m^{6}A writer complex based on previous studies (Zhong et al., 2008; Růžička et al., 2017) and results from this study. The thickness of black lines equals the strength of interactions; Arrows at the ends of lines refer to synergistical functions while line segments represents inhibition. Unchecked interactions were not labelled. FIP37 and MTB are suggested to be able to form homodimers (Růžička et al., 2017). Unknown proteins involved in catalysing m^{6}A formation await to be identified.

4.5.3 Novel Proteins That Might Be Involved in the MTase Complex

Mass spectrometry analysis in the current study demonstrated that aside from known m^6A writer proteins, some novel proteins were also pulled down by both MTA-GFP and Hakai-GFP, including Hps70-15 and two zinc finger proteins (AT1G32360 and AT5G53440). Strikingly, AT1G32360 is the only significantly enriched protein apart from Hakai among pulled-down proteins with MTA compared with those upon the knockout of *Hakai*.

In mammalian cells, *Hsp70* has been shown to be a target of m^6A in response to heat shock stress. m^6A in the 5' UTR of *Hsp70* promotes its cap-independent translation initiation upon heat shock (Meyer et al., 2015; Zhou et al., 2015). A tight interaction between m^6A writer proteins and Hps70 in the current study also indicates the potential involvement of m^6A in response to heat shock stress in plants, which is in accordance with a suggested role of m^6A in stress response in previous studies (detailed in 1.6.2.4). In turn, whether Hps70 is included in mediating m^6A formation remains to be investigated.

Zinc finger proteins belong to a large transcription factor family which is further classified into several subfamilies according to the number of conserved cysteine and histidine residues and the spacing between these conserved residues (Xu, 2014). Both AT1G32360 and AT5G53440 belong to CCCH-type zinc finger proteins, which contain one or more motifs with three cysteines and one histidine residues (Wang et al., 2008). There are around 60 or more CCCH zinc finger proteins in some eukaryotic species, such as human, mouse and plants (including

Arabidopsis, rice, tomato and citrus [Clementine mandarin]) (Wang et al., 2008; Liu et al., 2014; Xu, 2014; Fu and Blackshear, 2017). Functions of most of these zinc finger proteins remain obscure, but where they have been characterised, they often function as RNA binding proteins and emerging evidence suggests that some human CCCH zinc finger proteins are associated with immune responses and plant CCCH zinc finger proteins are involved in stress responses (Liu et al., 2014; Xu, 2014; Fu and Blackshear, 2017). While AT5G53440 has not been well characterised in *Arabidopsis*, AT1G32360 has been reported to be associated with plant response to phosphorus deficiency as the knockout of AT1G32360 leads to increased root hair density under scarce phosphorus (Stetter et al., 2015). In terms of the relationship between zinc finger proteins and m^6A modification, one reported study demonstrates a C_2H_2-type zinc finger protein – ZFP217 in mouse negatively regulates METTL3 to prevent the methylation of the core pluripotency and reprogramming factors and thus positively regulates the embryonic stem cell transcriptome (Aguilo et al., 2015). In *Arabidopsis*, our phenotyping to date of a transgenic line containing AT1G32360 genomic DNA driven by constitutive CaMV 35S promoter exhibits similar root phenotypes as the m^6A writer mutants described earlier (data unpublished). Collectively, these results indicate a negative role of zinc finger proteins in regulating m^6A formation and the relevant biological processes. It is very interesting that the knockout of *Hakai* caused the decreased interaction between MTA and AT1G32360, which implies a potential role of Hakai as a "bridge" connecting zinc finger proteins and other m^6A writer proteins to provide well-tuned m^6A modification in plants. However, whether AT1G32360

is also a ubiquitination target of Hakai's presumed E3 ligase activity remains to be tested.

4.6 CONCLUSIONS

In summary, the interactions among components of the m^6A MTase complex were analysed by generating and characterising double mutants for m^6A writer proteins and GFP-tagged m^6A writer proteins in *hakai*, *mta* or *fip37* mutant backgrounds. In terms of double mutants, *mta hakai* and *mta virilizer* double mutants demonstrated stronger developmental defects than parental single mutants while *hakai fip37* and *hakai virilizer* double mutants appear to be lethal, suggesting MTA, Hakai and Virilizer function synergistically in regulating the growth and development in *Arabidopsis*. This is also the case for the interaction between Hakai and FIP37. In contrast, *mta fip37* double mutant resembled *mta* single mutant, showing less severe developmental defects than *fip37* single mutant while *fip37* MTA-GFP exhibited even stronger phenotypes than *fip37*, indicating MTA acts as a suppressor upstream of FIP37. In turn, the knockdown of *FIP37* leads to increased localisation of MTA-GFP in the cytoplasm. In addition, the immunoprecipitation followed by mass spectrometry analysis confirmed that Hakai interacts with MTA, FIP37 and Virilizer *in vivo*. Moreover, three new proteins were pulled down with both MTA and Hakai, including two zinc finger proteins and Hakai is required for one of them to interact with MTA. Taken together, Hakai is a bona fide and important member of the MTase complex, acting in concert with other members in regulating m^6A formation and plant growth and development. Additionally, novel proteins might be involved

in the MTase complex to maintain well-tuned m^6A modification in plants, however, these await further characterisation.

4.7 REFERENCES

AGUILO, F., ZHANG, F., SANCHO, A., FIDALGO, M., DI CECILIA, S., VASHISHT, A., LEE, D.-F., CHEN, C.-H., RENGASAMY, M., ANDINO, B., et al. 2015. Coordination of m^6A mRNA methylation and gene transcription by ZFP217 regulates pluripotency and reprogramming. Cell Stem Cell, 17, 689-704.

BODI, Z., ZHONG, S., MEHRA, S., SONG, J., GRAHAM, N., LI, H., MAY, S. & FRAY, R. G. 2012. Adenosine methylation in *Arabidopsis* mRNA is associated with the 3′ end and reduced levels cause developmental defects. Frontiers in Plant Science, 3.

FU, M. & BLACKSHEAR, P. J. 2017. RNA-binding proteins in immune regulation: a focus on CCCH zinc finger proteins. Nature Reviews Immunology, 17, 130-143.

FUJITA, Y., KRAUSE, G., SCHEFFNER, M., ZECHNER, D., LEDDY, H. E. M., BEHRENS, J., SOMMER, T. & BIRCHMEIER, W. 2002. Hakai, a c-Cbl-like protein, ubiquitinates and induces endocytosis of the E-cadherin complex. Nature Cell Biology, 4, 222-231.

HAUSSMANN, I. U., BODI, Z., SANCHEZ-MORAN, E., MONGAN, N. P., ARCHER, N., FRAY, R. G. & SOLLER, M. 2016. m^6A potentiates Sxl alternative pre-mRNA splicing for robust *Drosophila* sex determination. Nature, 540, 301-304.

HULPIAU, P. & VAN ROY, F. 2009. Molecular evolution of the cadherin superfamily. The International Journal of Biochemistry & Cell Biology, 41, 349-369.

LIU, S., KHAN, M. R. G., LI, Y., ZHANG, J. & HU, C. 2014. Comprehensive analysis of CCCH-type zinc finger gene family in citrus (Clementine mandarin) by genome-wide characterization. Molecular Genetics and Genomics, 289, 855-872.

MEYER, K. D., PATIL, D. P., ZHOU, J., ZINOVIEV, A., SKABKIN, M. A., ELEMENTO, O., PESTOVA, T. V., QIAN, S.-B. & JAFFREY, S. R. 2015. 5' UTR m^6A promotes cap-independent translation. Cell, 163, 999-1010.

PING, X.-L., SUN, B.-F., WANG, L., XIAO, W., YANG, X., WANG, W.-J., ADHIKARI, S., SHI, Y., LV, Y., CHEN, Y.-S., et al. 2014. Mammalian WTAP is a regulatory subunit of the RNA N6-methyladenosine methyltransferase. Cell Research, 24, 177-189.

RŮŽIČKA, K., ZHANG, M., CAMPILHO, A., BODI, Z., KASHIF, M., SALEH, M., EECKHOUT, D., EL-SHOWK, S., LI, H., ZHONG, S., et al. 2017. Identification of factors required for m^6A mRNA methylation in *Arabidopsis* reveals a role for the conserved E3 ubiquitin ligase HAKAI. New Phytologist, 215, 157-172.

SEYMOUR, G. B., TUCKER, G. & LEACH, L. A. 2004. Cell adhesion molecules in plants and animals. Biotechnology and Genetic Engineering Reviews, 21, 123-132.

STETTER, M. G., SCHMID, K. & LUDEWIG, U. 2015. Uncovering genes and ploidy involved in the high diversity in root hair density, length and response to local scarce phosphate in *Arabidopsis thaliana*. PLoS One, 10, e0120604.

VOYTAS, D. F. 2013. Plant genome engineering with sequence-specific nucleases. The Annual Reviews of Plant Biology, 64, 327-350.

WANG, D., GUO, Y., WU, C., YANG, G., LI, Y. & ZHENG, C. 2008. Genome-wide analysis of CCCH zinc finger family in Arabidopsis and rice. BMC Genomics, 9, 44.

WANG, X., FENG, J., XUE, Y., GUAN, Z., ZHANG, D., LIU, Z., GONG, Z., WANG, Q., HUANG, J. & TANG, C. 2016. Structural basis of N6-adenosine methylation by the METTL3-METTL14 complex. Nature, 534, 575-578.

XU, R. 2014. Genome-wide analysis and identification of stress-responsive genes of the CCCH zinc finger family in *Solanum lycopersicum*. Molecular Genetics and Genomics, 289, 965-979.

ZHONG, S., LI, H., BODI, Z., BUTTON, J., VESPA, L., HERZOG, M. & FRAY, R. G. 2008. MTA is an *Arabidopsis* messenger RNA adenosine methylase and interacts with a homolog of a sex-specific splicing factor. The Plant Cell, 20, 1278-1288.

ZHOU, J., WAN, J., GAO, X., ZHANG, X. & QIAN, S.-B. 2015. Dynamic m^6A mRNA methylation directs translational control of heat shock response. Nature, 526, 591-594.

4.8 SUPPLEMENTARY DATA

4.8.1 Supplementary Figures

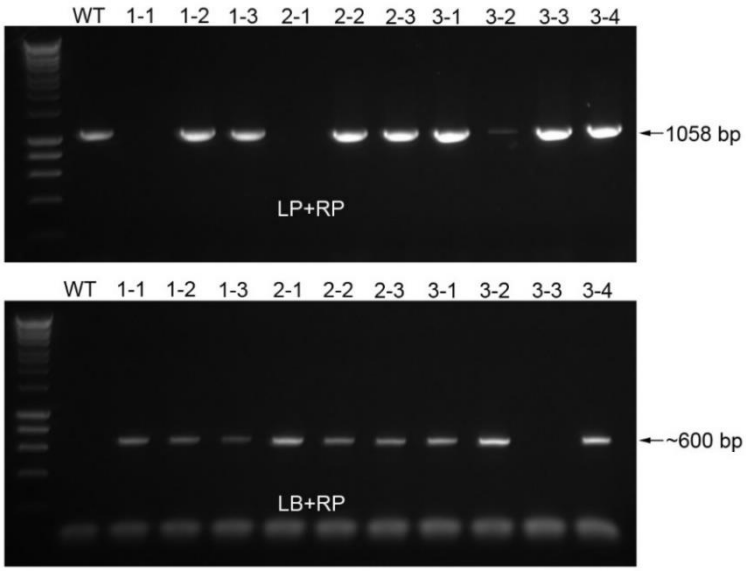

Supplementary figure 4.1 Genotyping PCR to check *FIP37* SALK_018636 T-DNA insertion in F_2 progenies of ABI3A6 crossed with *fip37*. Lines 1-1 and 2-1 were homozygous for SALK_018636 T-DNA insertion.

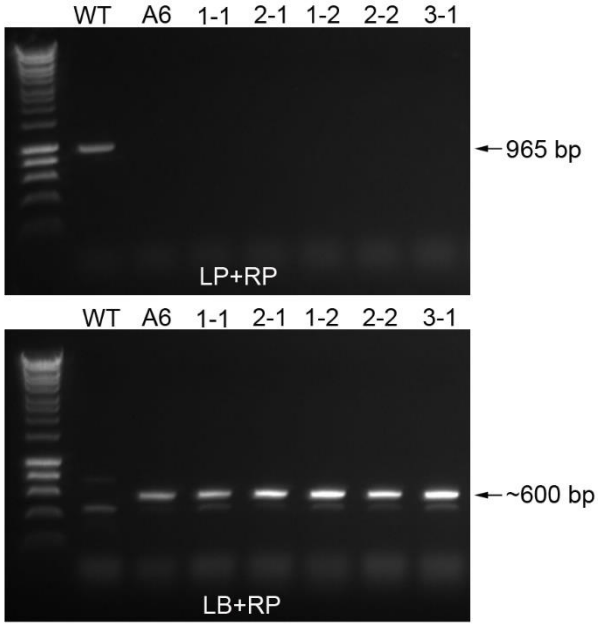

Supplementary figure 4.2 Genotyping PCR to check *MTA* SALK_074069 T-DNA insertion in F_2 progenies of ABI3A6 crossed with *fip37*. A6 represents ABI3A6. All checked samples were homozygotes.

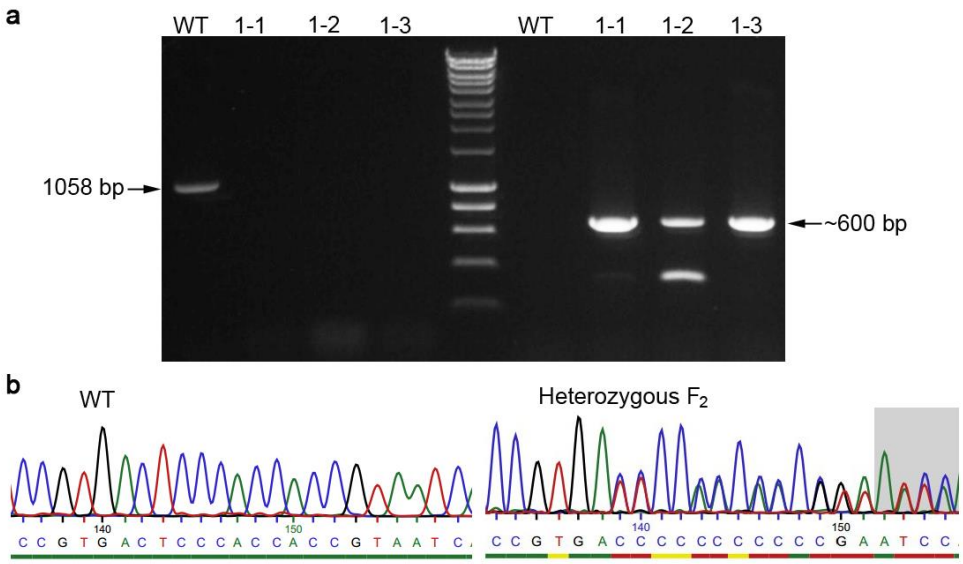

Supplementary figure 4.3 Screening the F_2 generation of *fip37* crossed with *hakai* 37. (**a**) Genotyping PCR to screen F_2 lines homozygous for *FIP37* SALK_018636 T-DNA insertion. All checked lines were homozygotes. (**b**) Sequencing profile showing F_2 progenies heterozygous for *Hakai* CRISPR target site.

Supplementary figure 4.4 5-week old *virilizer* compared with WT. Scale bar = 1 cm.

Supplementary figure 4.5 2-week old F_3 progenies of ABI3A6 crossed with *virilizer* planted on 1/2 MS plus 1% (w/v) sucrose. Tiny seedlings are labelled with red arrows. Scale bar = 1 cm.

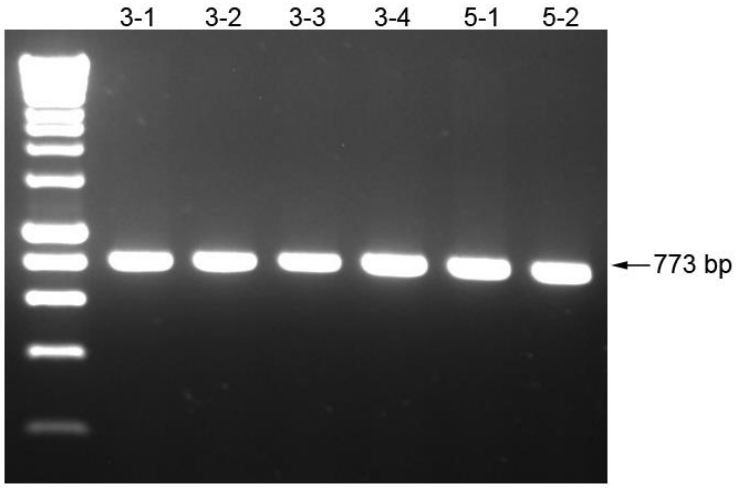

Supplementary figure 4.6 PCR showing the presence of *ABI3*::*MTA* construct in all checked F_2 progenies of Hakai-GFP/WT crossed with ABI3A6.

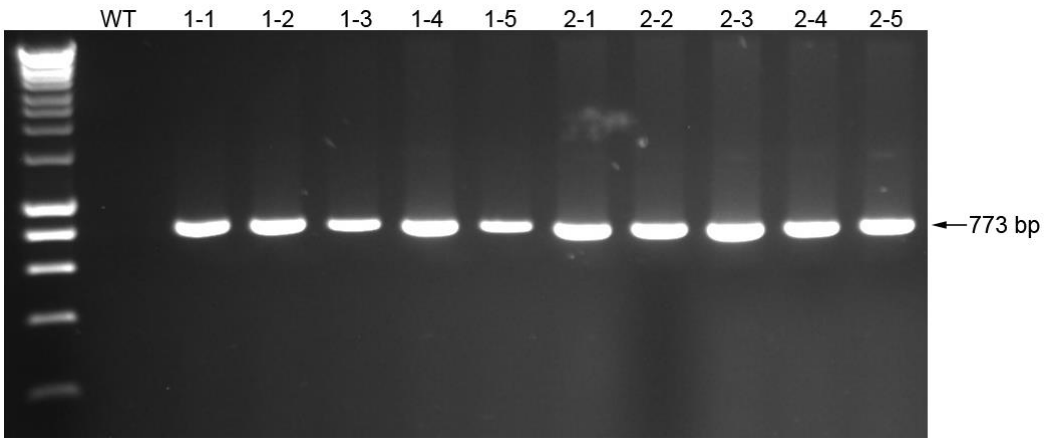

Supplementary figure 4.7 PCR showing the presence of *ABI3*::*MTA* construct in all checked F_2 progenies of FIP37-GFP/WT crossed with ABI3A6.

Supplementary figure 4.8 2-week old *fip37* and *fip37* MTA-GFP cultured on 1/2 MS plus 1% (w/v) sucrose. Scale bar = 1 cm.

4.8.2 Supplementary Tables

Supplementary table 4.1 Screening *Hakai* CRISPR target site in the F_3 generation of *fip37* crossed with *hakai* 37

Sample name	Separation status	Sample name	Separation status
fip×h M1	heterozygous	fip×h m18	heterozygous
fip×h M2	heterozygous	fip×h m19	WT
fip×h M3	heterozygous	fip×h m20	WT
fip×h M4	WT	fip×h m21	heterozygous
fip×h M5	heterozygous	fip×h m22	heterozygous
fip×h M6	heterozygous	fip×h m23	heterozygous
fip×h M7	heterozygous	fip×h m24	heterozygous
fip×h M8	heterozygous	fip×h m25	WT
fip×h M9	WT	fip×h m26	WT
fip×h M10	heterozygous	fip×h m27	heterozygous
fip×h M11	WT	fip×h m28	heterozygous
fip×h M12	heterozygous	fip×h m29	heterozygous
fip×h M13	WT	fip×h m30	WT
fip×h M14	heterozygous	fip×h m31	WT
fip×h M15	WT	fip×h m32	heterozygous
fip×h M16	heterozygous	fip×h m33	heterozygous
fip×h M17	WT	fip×h m34	WT
fip×h M18	WT	fip×h m35	heterozygous
fip×h M19	WT	fip×h m36	heterozygous
fip×h M20	heterozygous	fip×h m37	heterozygous
fip×h m1	heterozygous	fip×h m38	heterozygous
fip×h m2	WT	fip×h m39	heterozygous
fip×h m3	heterozygous	fip×h m40	heterozygous
fip×h m4	heterozygous	fip×h m41	heterozygous
fip×h m5	heterozygous	fip×h m42	heterozygous
fip×h m6	heterozygous	fip×h m43	heterozygous
fip×h m7	WT	fip×h m44	heterozygous
fip×h m8	heterozygous	fip×h m45	WT
fip×h m9	heterozygous	fip×h m46	heterozygous
fip×h m10	heterozygous	fip×h m47	heterozygous
fip×h m11	heterozygous	fip×h m48	heterozygous
fip×h m12	heterozygous	fip×h m49	heterozygous
fip×h m13	heterozygous	fip×h m50	heterozygous
fip×h m14	WT	fip×h m51	WT
fip×h m15	WT	fip×h m52	WT
fip×h m16	heterozygous	fip×h m53	heterozygous
fip×h m17	WT		

Supplementary table 4.2 Screening *virilizer* mutation site in the F_3 generation of *hakai* 37 crossed with *virilizer*

Sample name	Separation status	Sample name	Separation status
h×v 2-12-1	WT	h×v 2-12-17	heterozygous
h×v 2-12-2	heterozygous	h×v 2-12-19	heterozygous
h×v 2-12-3	heterozygous	h×v 2-12-20	heterozygous
h×v 2-12-4	heterozygous	h×v 2-12-21	heterozygous
h×v 2-12-5	heterozygous	h×v 2-12-23	WT
h×v 2-12-6	heterozygous	h×v 2-12-25	heterozygous
h×v 2-12-7	WT	h×v 2-12-26	heterozygous
h×v 2-12-8	WT	h×v 2-12-27	heterozygous
h×v 2-12-9	heterozygous	h×v 2-12-28	heterozygous
h×v 2-12-10	heterozygous	h×v 2-12-29	heterozygous
h×v 2-12-11	WT	h×v 2-12-30	heterozygous
h×v 2-12-12	WT	h×v 2-12-33	heterozygous
h×v 2-12-13	WT	h×v 2-12-34	heterozygous
h×v 2-12-14	WT	h×v 2-12-35	heterozygous
h×v 2-12-16	heterozygous	h×v 2-12-36	heterozygous

CHAPTER 5 STUDYING THE EFFECT OF m^{6}A ON ROOT DEVELOPMENT

5.1 ABSTRACT

Our previous studies, and work in this study, suggests a regulatory function of m^{6}A in root development. This question was further investigated here by analysing root phenotypes of m^{6}A writer mutants (including *hakai* 37, ABI3A6, *fip37* and *virilizer*) under normal conditions and upon auxin treatment by NPA and NAA to induce synchronous lateral roots (LRs). In addition, auxin transport, accumulation and response in m^{6}A writer mutants were analysed based on crosses with AUX1-YFP, DII-VENUS and *DR5*::*VENUS* reporter lines. m^{6}A writer mutants, especially *fip37* and *virilizer*, demonstrated significantly shorter primary roots and fewer LRs on 1/2 MS plus 1% (w/v) sucrose and LR developmental defects remained after treatments with NPA and NAA. Marked by *CycB1;1*::*GUS*, ABI3A6 demonstrated decreased LR primordia. Taken together, these results indicate that reduction in m^{6}A modification leads to decreased auxin response and affects proper LR formation, especially LR initiation. Contrarily, the expression of *VENUS* driven by *DR5* promoter was stronger in m^{6}A writer mutants, suggesting the involvement of post-transcriptional regulation. Strikingly, *fip37* and *virilizer* exhibited dramatically increased ARF7 protein levels but unchanged transcriptional levels. In contrast, there was no change for ARF8 protein levels in these two mutants. Given that ARF7 contains upstream open reading frames (uORFs) in its 5' UTR but this is not the case for ARF8, we speculate that m^{6}A might be involved in regulating

translation reinitiation by affecting the translation capacity of uORFs. To better understand the molecular machineries underlying the correlation among m^6A modification, auxin signalling pathway and translation reinitiation, further studies are necessary.

5.2 INTRODUCTION

As an important group of phytohormones, auxin has been implicated in regulating diverse aspects of plant growth and development, including embryogenesis, vascular formation, tropic responses, root and flower development (Teale et al., 2006; Swarup and Péret, 2012; Weijers and Wagner, 2016). Indole-3-acetic acid (IAA) is the predominant form of auxin in higher plants and other widely used synthetic auxin derivatives include 2,4-dichlorophenoxyacetic acid (2,4-D) and 1-naphthalene acetic acid (NAA) (Teale et al., 2006). The mechanism through which auxin is perceived and transported and how it mediates gene expression is described below.

5.2.1 Auxin Transport

Unlike other hormones in plants, auxin exhibits polar transport; it is primarily synthesized in the shoot apex and leaf primordia and then transported to distal target tissues (Swarup and Péret, 2012). The polar transport of auxin leads to auxin accumulation in certain cells, which triggers various developmental responses, such as lateral root (LR) development (Vieten et al., 2007). Polar auxin transport and the chemiosmotic polar diffusion hypothesis is supported by

early studies from the 1970s (Rubery and Sheldrake, 1974; Raven, 1975; Goldsmith, 1977) (Figure 5.1). IAA is a weak acid and the majority of IAA inside cells is in an anion form (IAA^-) rather than the undissociated form (IAAH) (Goldsmith, 1977). Upon mildly acidic apoplastic ambient (pH 5.0-5.5) and higher pH of the cytoplasm (pH 7.0-7.5), the active uptake of IAA into the cell would require a carrier and its export from the cell would also require efflux carriers (Vieten et al., 2007; Swarup and Péret, 2012). It is now well known that cellular movement of IAA is facilitated by auxin influx and efflux carriers (Vieten et al., 2007; Swarup and Péret, 2012). In *Arabidopsis,* AUXIN1/LIKE-AUX1 (AUX/LAX) family members (AUX1, LAX1, LAX2, LAX3) are major auxin influx carriers while PIN-FORMED (PIN) and P-GLYCOPROTEIN (PGP) family members are major auxin efflux carriers (Swarup and Péret, 2012). The direction of intercellular auxin movement is determined by asymmetric localisation of PIN proteins and AUX/LAX proteins. For example, AUX1 is located on the upper side of root protophloem cells whereas PIN1 is enriched on the basal rootward face of the same cells (Vieten et al., 2007; Swarup and Péret, 2012). *N*-1-naphthylphthalamic acid (NPA) is one of the most popular auxin transport inhibitors which has contributed to our understanding of the molecular mechanisms of polar auxin transport (Casimiro et al., 2001; Teale and Palme, 2017). Though NPA targets remain unclear, PIN1 is suggested as one protein candidate of NPA binding based on genetic data (Teale and Palme, 2017).

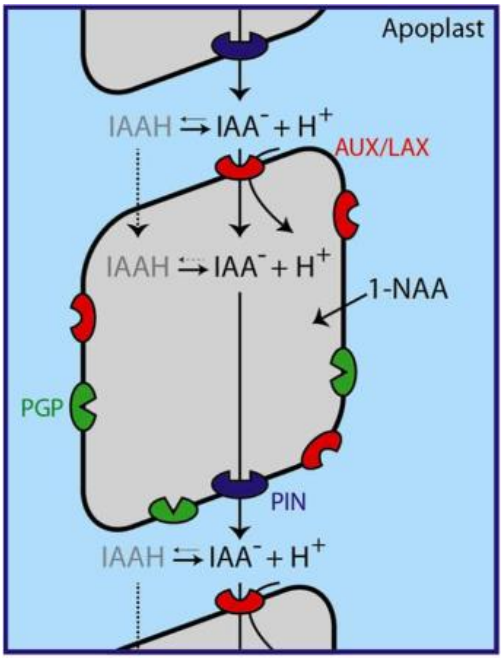

Figure 5.1 Chemiosmotic hypothesis of auxin transport (Swarup and Péret, 2012).

5.2.2 Auxin Signalling Pathway

In plants, auxin signalling is predominantly mediated through a $SCF^{TIR1/AFB}$-Aux/IAA-ARF signalling module, in which, auxin is perceived by a co-receptor complex composing of an F-box protein from TRANSPORT INHIBITOR RESPONSE 1/AUXIN SIGNALING F-BOX PROTEINS (TIR1/AFBs) family and a member of the Auxin/INDOLE ACETIC ACID (Aux/IAA) family (Figure 5.2) (Wang and Estelle, 2014; Weijers and Wagne, 2016). TIR1/AFBs reside in a SKP1-Cul1-F-box (SCF)-type E3 ubiquitin ligase complex (termed $SCF^{TIR1/AFB}$). AUXIN RESPONSE FACTORS (ARFs) are transcriptional factors that recognise auxin response elements (AuxREs) in promoters of auxin responsive genes (Wang and Estelle, 2014). When the auxin level is low, Aux/IAA proteins bind to ARFs and inhibit the transcriptional activity of ARFs. When the auxin level rises, the affinity between $SCF^{TIR1/AFB}$ and Aux/IAA increases and this promotes degradation of the latter. Consequently, ARFs are

released from inhibition and the transcriptional responses are activated (Figure 5.2) (Teale et al., 2006; Wang and Estelle, 2014; Liao et al., 2015).

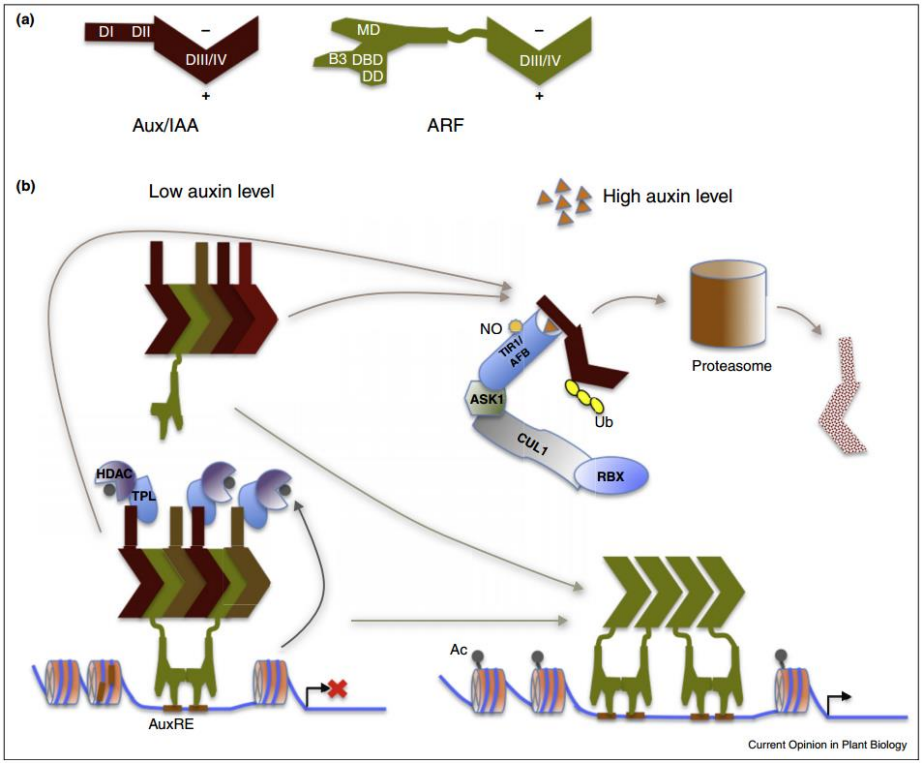

Figure 5.2 A model for the SCF$^{TIR1/AFB}$-Aux/IAA-ARF-mediated auxin signalling pathway (Wang and Estelle, 2014). (**a**) Schematic showing domains of Aux/IAAs and ARFs. Their DIII and DIV domains are homologues which ease their interactions. DBD: DNA binding domain; MD: middle domain. (**b**) A model demonstrating how the SCF$^{TIR1/AFB}$-Aux/IAA-ARF signalling pathway mediates auxin responsive genes under different auxin levels. TOPLESSs (TPLs) and histone deacetylases (HDACs) are included in co-repressor complexes of Aux/IAAs, facilitating transcriptional repression of target promoter through removing acetyls (Ac) from the local chromatin. ARABIDOPSIS SKP1 HOMOLOGUE (ASK1), CULLIN 1 (CUL1) and RING-BOX 1 (RBX1) are components of the SCF$^{TIR1/AFB}$ ubiquitin ligase complex.

In *Arabidopsis*, there are 6 members in the TIR/AFB family: TIR1 and AFB1-5. TIR1 was the first identified and is the major auxin receptor, whilst AFB1-3 are indicated to function in a partially redundant manner to TIR1 in mediating auxin responses (Teale et al., 2006; Wang and Estelle, 2014). Functions of AFB4 and AFB5 have diverged substantially from those of other members in the TIR/AFB family, with AFB4 negatively regulating auxin response and AFB5 possessing a high affinity for a synthetic auxin – picloram (Greenham et al., 2011; Calderón Villalobos et al., 2012). Other members of the $SCF^{TIR1/AFB}$ ubiquitin ligase complex, such as ARABIDOPSIS SKP1 HOMOLOGUE (ASK1), CULLIN 1 (CUL1) and RING-BOX 1 (RBX1) have also been shown to be involved in auxin sensing (Weijers and Wagne, 2016). Functional variations among TIR/AFBs may contribute to the diversity and specificity of auxin response (Wang and Estelle, 2014).

Currently, there are 29 identified Aux/IAA proteins in *Arabidopsis* and most of them have four conserved domains (I-IV) (Figure 5.2a) (Wang and Estelle, 2014). The *N*-terminal domain I (DI) is required for the recruitment of co-repressor proteins including TOPLESS (TPL) and the subsequent transcriptional repression. Domain II (DII) contains a 13-amino acid degron motif, which is responsible for the characteristic instability of Aux/IAA proteins. Domain III and IV (DIII/IV) are homologous to similar domains in ARFs and are involved in mediating the interaction between Aux/IAAs and ARFs (Teale et al., 2006; Calderón Villalobos et al., 2012; Wang and Estelle, 2014).

Arabidopsis possesses 23 ARF proteins and they also consist of conserved domains. In addition to DIII/IV that are homologous to those in Aux/IAAs, they also contain an amino-terminal DNA binding domain (DBD) and a middle domain (MD) (Guilfoyle and Hagen, 2007). DBD binds AuxREs in auxin-response genes and MD contains either an activation or a repression motif which determines a specific ARF as an activator or a repressor (Guilfoyle and Hagen, 2007; Wang and Estelle, 2014). Five *Arabidopsis* ARFs (ARF5, ARF6, ARF7, ARF8 and ARF19) have been characterised as transcriptional activators while others are classified as repressors (Guilfoyle and Hagen, 2007; Wang and Estelle, 2014).

To sensitively and quantitatively study auxin response, a set of fluorescent reporters have been developed (Liao et al., 2015). Among them, the synthetic *DR5* promoter (consisting of 7-9 TGTCTC AuxRE repeats) and fluorescent protein tagged auxin-dependent degradation DII of Aux/IAA proteins have been widely used (Ulmasov et al., 1997; Brunoud et al., 2012; Liao et al., 2015). For example, a fast maturing yellow fluorescent protein reporter VENUS driven by *DR5* promoter (*DR5*::*VENUS*) can be used to mark transcriptional auxin response sites (Liao et al., 2015). Another reporter line DII-VENUS, which is composed of a fragment of IAA28 containing DII fused with VENUS is rapidly degraded in response to auxin and can be used to check cellular auxin distribution and abundance (Brunoud et al., 2012).

5.2.3 Lateral Root Development

`

Arabidopsis primary root consists of root caps (columella root cap and lateral root cap), three external layers, namely the epidermis, the cortex and the endodermis, a single-layer pericycle and the inner vasculature (Figure 5.3a) (Marchant et al., 1999; Péret et al., 2009; Lavenus et al., 2013). Aside from root caps, the remainder of the primary root is divided into apical meristem, basal meristem, the elongation zone and the differentiation zone according to characteristics of cells in each region (Wilson et al., 2013). LR formation from the primary root consists of several stages, including LR initiation, emergence, patterning and elongation of the new LR. Auxin is a key regulator of LR development and is required for several stages of LR development (Casimiro et al., 2001, 2003).

LR development starts with the formation of LR founder cells, which is activated by auxin obtained via polar auxin transport (Reed et al., 1998; Casimiro et al., 2001; Dubrovsky et al., 2008). Within the *Arabidopsis* primary root, auxin transport has been reported to occur in two distinct polarities, acropetally in the central cylinder of the root (from the base of the root towards the root tip) and basipetally through the peripheral cells (from the tip towards the base) (Rashotte et al., 2000). It has been reported that both directions of auxin transports affect LR development (Reed et al., 1998; Casimiro et al., 2001).

Arabidopsis pericycle is composed of two different types of cells, with xylem pole pericycle cells showing strong competence to initiate cell division and

another group of cells, associated with the phloem, appearing to remain quiescent (Parizot et al., 2008). Auxin perception by xylem pole pericycle cells causes the priming (undergoing a cyclic pre-initiation event) of these cells to become pericycle founder cells (Figure 5.3b) (Péret et al., 2009; Lavenus et al., 2013). The triggering of xylem pole pericycle cells priming is suggested to take place in a zone several millimetres distal to the root apical meristem, which is termed the basal meristem (Figure 5.3) (Casimiro et al., 2001; De Smet et al., 2007); LRs are initiated when two adjacent pericycle founder cells undergo several rounds of anticlinal divisions to produce a single-layered primordium composed of up to ten small cells of similar lengths (termed Stage I; Figure 5.4). Afterwards, these cells divide periclinally and form a two-layered primordium (Stage II). Following subsequent rounds of anticlinal and periclinal divisions, a dome-shaped primordium is created (Stage III-VII) and finally emerges from the parent root (Stage VIII) (Figure5.4) (Casimiro et al., 2003; Péret et al., 2009; Lavenus et al., 2013). The spacing of LRs along the primary root is in a regular left-right alternating pattern which is correlated with gravity-induced waving dependent on AUX1 and controlled by the auxin response oscillation in the basal meristem (De Smet et al., 2007). This auxin response oscillates with peaks of expression at regular intervals of 15 hours and each peak in the auxin-reporter maximum correlates with the formation of a consecutive LR (De Smet et al., 2007).

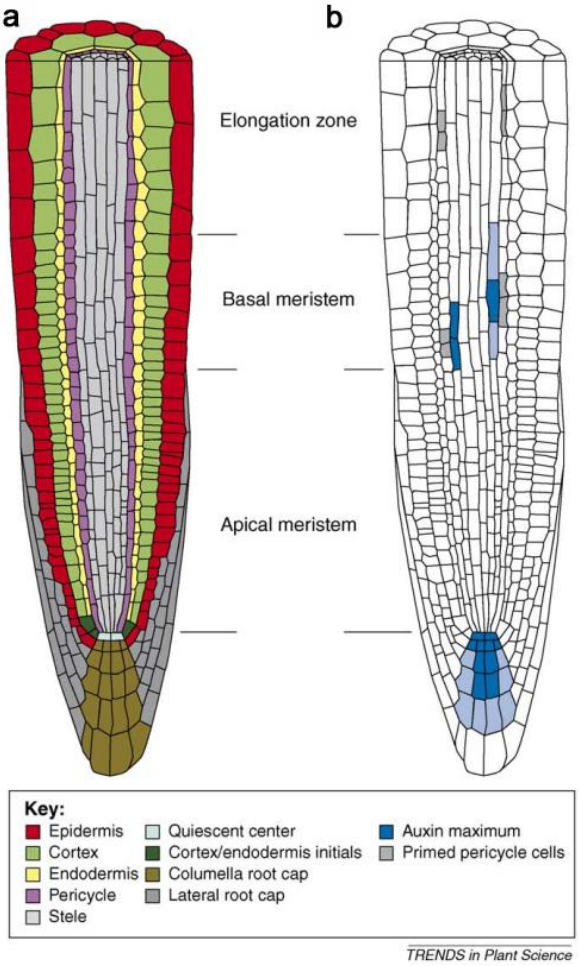

Figure 5.3 Schematic overview of different root tissues (**a**) and the auxin signalling maximum sites reported by the *DR5*::*GUS* marker line (**b**) (Péret et al., 2009).

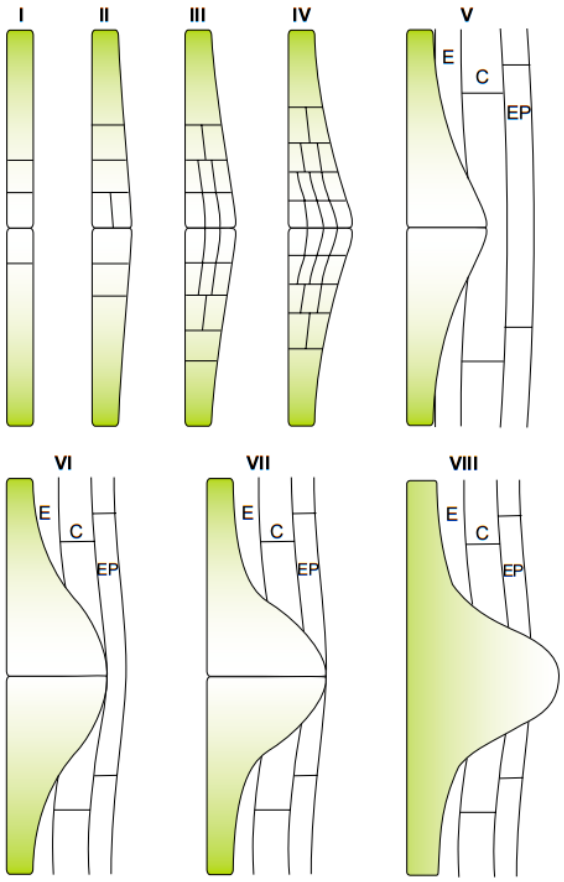

Figure 5.4 Developmental stages of lateral root formation in *Arabidopsis* (Casimiro et al., 2003).

As reviewed by Bellini et al. (2014), many factors influence LR development, including those involved in auxin transport and signalling pathways, proteins mediating other plant hormone metabolism pathways and environmental stimuli, with factors within the auxin network as the predominant ones. For example, auxin influx carriers – AUX1 and LAX3 have been implicated in regulating LR development (Marchant et al., 2002; Swarup et al., 2008). AUX1 is required for correct IAA distribution between source and sink tissues and facilitates IAA unloading in the primary root apex and the development of the LR primordium (Marchant et al., 2002). The expression of *LAX3* is strictly limited to the cortex and epidermis overlaying new lateral root primordia. LAX3 regulates the expression of several cell-wall-remodelling enzymes in adjacent cells and causes

their cell walls to separate, which facilitates LR emergence (Swarup et al., 2008). Throughout the whole LR development processes, ARF7 and ARF19 are crucial regulators (Lavenus et al., 2013). They positively regulate LR formation via direct activation of downstream *LATERAL ORGAN BOUNDARIES-DOMAIN*/*ASYMMETRIC LEAVES2-LIKE* (*LBD*/*ASL*) genes (Okushima et al., 2007; Goh et al., 2012). *arf7 arf 19* double knockout mutant normally forms no LRs (Wilmoth et al., 2005). The activity of ARF7 and ARF 19 are directly and negatively regulated by SOLITARY-ROOT (SLR)/IAA14, a member of the Aux/IAA family (Fukaki et al., 2002, 2005). Normally, SLR/IAA14 is degraded in an auxin-dependent way during LR initiation and its repression effect on ARF7 and ARF19 is relieved (Péret et al., 2009). A dominant *slr-1* mutant completely lacks LRs, and transgenic *Arabidopsis* plants expressing the stabilised mutant SLR/IAA14 (mIAA14) give rise to a similar phenotype as *slr-1*. mIAA14 is suggested to directly inactivate functions of ARF7 and ARF19 (Fukaki et al., 2002, 2005).

5.2.4 Aims and Objectives of This Chapter

Our previous studies demonstrate that the expression of *MTA*, which encodes the main plant m^6A methylase, is strongly associated with emerging LRs (Zhong et al., 2008), indicating the involvement of mRNA methylation in LR development. Therefore, the aim of this chapter is to further study the role of m^6A in LR formation. More specifically, root phenotypes of m^6A writer mutants under normal conditions and upon auxin treatment are analysed. Moreover, auxin transport, distribution and response in m^6A writer mutants are studied based on

crosses with AUX1-YFP, *DR5*::*VENUS* and DII-VENUS reporter lines and analysing transcriptional and translational levels of ARFs. These assays will shed new light on the correlation between m^6A and LR development and possibly elucidate how m^6A mediates LR formation.

5.3 PLANT MATERIALS AND METHODS

5.3.1 Plant Materials

Plant materials used in this chapter include m^6A writer mutants (ABI3A6, *hakai* 37, *fip37*, *virilizer* and double mutants [*mta hakai#*1, *mta fip37*]), MTA-GFP, *CycB1;1*::*GUS*, ABI3A6×*CycB1;1*::*GUS*, AUX1-YFP, *DR5*::VENUS and DII-VENUS. Among all the above lines, ABI3A6, ABI3A6×*CycB1;1*::*GUS* and MTA-GFP were generated by previous researchers in our group; *fip37* and *virilizer* were obtained from collaborators in other research institutes; other lines were from other research groups within the division of Plant and Crop Sciences in the University of Nottingham (detailed in Table 2.1).

5.3.2 Analysing Root Phenotypes of m^6A Writer Mutants

m^6A writer mutants were planted on vertical plates containing 1/2 MS with 1% (w/v) sucrose. Primary root lengths and the number of LRs were recorded on the 8th day of culturing in the tissue culture room.

5.3.3 Lateral Root Induction

Arabidopsis seedlings were first treated with auxin transport inhibitor NPA and then with NAA to induce synchronous LRs along the whole primary root (Himanen et al., 2002). After germinating on 1/2 MS for 5 days, *Arabidopsis* seedlings were transferred to vertical square plates containing 1/2 MS and 10 μM NPA. On the third day, they were transferred to 1/2 MS plus 10 μM NAA. For histochemical GUS assay, roots of *CycB1;1*::*GUS* (Casimiro et al., 2001) and ABI3A6× *CycB1;1*::*GUS* plants were sampled at 0 h, 6 h, 12 h, 1 d, 2 d, 3 d and 5 d after being transferred to NAA. MTA-GFP seedlings were sampled at 0 d, 1 d, 2 d, 3 d, 4 d and 5 d after being transferred to NAA for observing the GFP activity by confocal microscopy (Leica TCS SP5).

5.3.4 GUS Expression Assay

Harvested roots were immersed in GUS staining reagent mix (50 mM phosphate buffer, 10 mM EDTA, 20% [w/v] methanol, 0.1% [w/v] TritonX-100 and 1 $mg \cdot ml^{-1}$ X-Gluc) while shaking for 12 h. Afterwards, stained roots were soaked in 100% (v/v) ethanol for destaining. The blue precipitate represents the site where *GUS* expresses. Photos were taken under the Stereo Dissecting Microscope (Zeiss Stemi SV6).

5.3.5 Crossing and the Subsequent Analysis

To further study the possible involvement of m^6A modification in regulating auxin transport and auxin signalling pathway, m^6A writer mutants were crossed with fluorescent reporter lines related to auxin transport or response: AUX1-YFP (Swarup et al., 2004), *DR5*::*VENUS* and DII-VENUS (Band et al., 2012; Brunoud et al., 2012). Among the above lines, AUX1-YFP was used to monitor the auxin influx carrier – AUX1; *DR5*::*VENUS* was used to mark transcriptional auxin response sites and DII-VENUS was used to check the auxin accumulation (Liao et al., 2015).

After crossing, F_2 lines homozygous for the mutant and showing fluorescent signal were selected and subsequent generations were used for analysing the expression and localisation of fluorescent proteins by confocal microscopy (Leica TCS SP5).

5.3.6 Western Blotting and Northern Blotting for ARFs

ARFs are crucial transcriptional factors in regulating downstream auxin response genes. Transcriptional levels and protein levels of ARF7 and ARF8 were analysed via northern blotting and western blotting, respectively, following protocols described in 2.12 and 2.16. Primers used for preparing RNA probes in northern blotting are listed in Appendix 1. ARF7 and ARF8 antibodies were obtained from Ranjan Swarup's group, and are the same as those used by Rosado et al. (2012). A set of actin proteins were used as the internal control.

5.4 RESULTS

5.4.1 Root Phenotypes of m^{6}A Writer Mutants on Normal MS Medium

m^{6}A writer mutants (including *hakai* 37, *fip37*, *virilizer* and ABI3A6), especially *fip37* and *virilizer*, demonstrated significantly shorter primary roots and fewer LRs on 1/2 MS plus 1% (w/v) sucrose (Figure 5.5, 5.6).

Figure 5.5 8-d old seedlings planted on 1/2 MS plus 1% (w/v) sucrose. Scale bar = 1 cm.

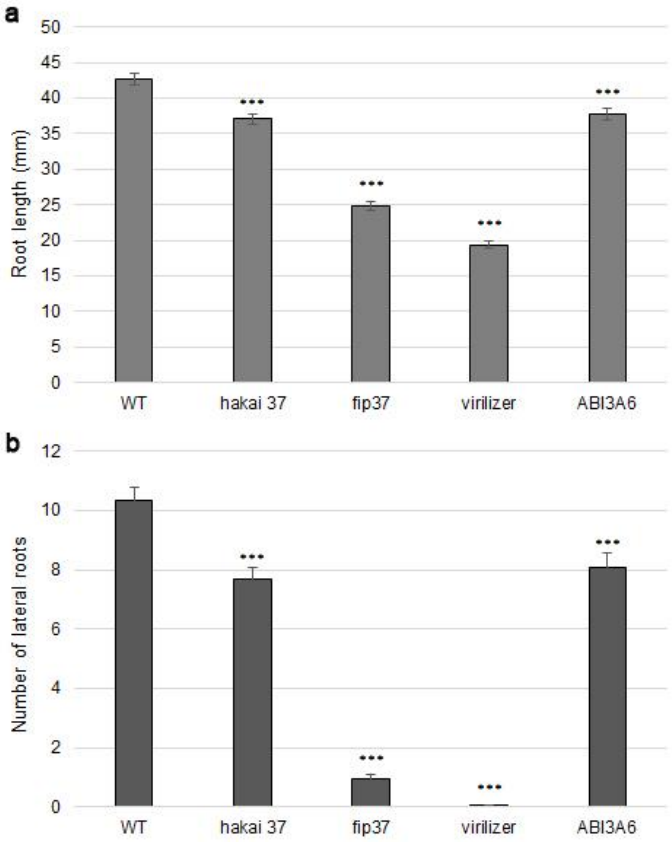

Figure 5.6 Root phenotypes of 8-d old seedlings planted on 1/2 MS plus 1% (w/v) sucrose. (**a**) Root lengths. (**b**) The number of lateral roots. Data represent mean ± SEM and statistically significant differences relative to WT were analysed by One-Way ANOVA and marked with asterisks (***, $p<0.001$).

5.4.2 Root Phenotypes of m^{6}A Writer Mutants after Auxin Treatment

After treatment with NPA and NAA, LRs were clearly seen along the whole primary root of WT on the 5th day of NAA treatment. Fewer induced LRs were seen in low m^{6}A mutants (including ABI3A6, *fip37*, *virilizer*, *mta hakai#*1 and *mta fip37*) and this reduction was the most severe in the case of *virilizer*. The number of induced LRs in *fip37* and *mta hakai#*1 was also strongly reduced relative to WT (Figure 5.7, 5.8). In addition, the phenotype of reduced induced

LRs in ABI3A6 was complemented in MTA-GFP, which showed abundant induced LRs, similar to WT (Figure 5.7, 5.8).

This phenotype was further confirmed by checking the *GUS* expression in *CycB1;1*::*GUS* and ABI3A6×*CycB1;1*::*GUS* undergoing the same treatment. The GUS staining assay showed that ABI3A6×*CycB1;1*::*GUS* demonstrated less *GUS* expression, which indicates less cell division (required for LR initiation and development) was taking place (Figure 5.9). In contrast, *GFP* expression analysis of MTA-GFP treated with NPA and NAA showed that MTA-GFP was strongly expressed during the whole LR induction process, primarily in root tips and LR initiation sites (Figure 5.10). In addition, time-course observation of MTA-GFP treated with NPA and NAA under the confocal microscope clearly showed the developmental status of induced LRs. After treatment with NAA for 1 d, the root tip of MTA-GFP started to expand (Figure 5.10c). In the following 1 d, LR primordia formed (Figure 5.10d) and then emerged from the root epidermis on the third day (Figure 5.10e,f). In the meanwhile, LR primordia formed along the whole root (Figure 5.10f). Afterwards, LRs elongated and became very clear on the 5th day of NAA treatment (Figure 5.10h,i).

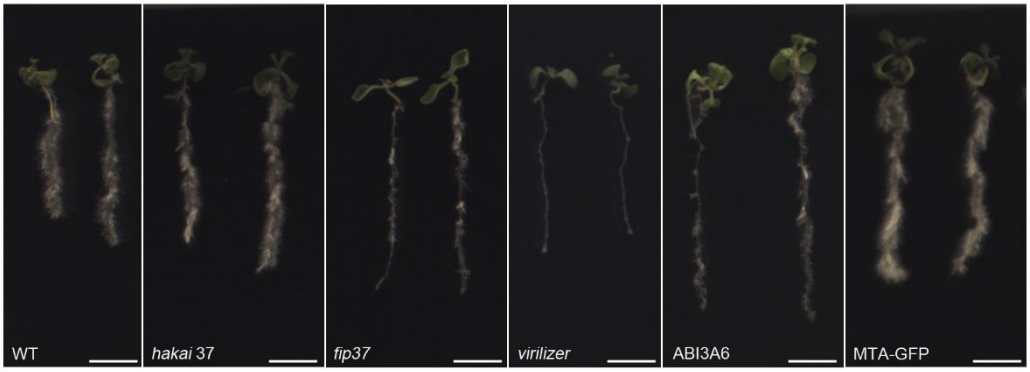

Figure 5.7 Roots after treatment with NPA and then transferred onto 1/2 MS with NAA for 5 days. Scale bar = 5 mm.

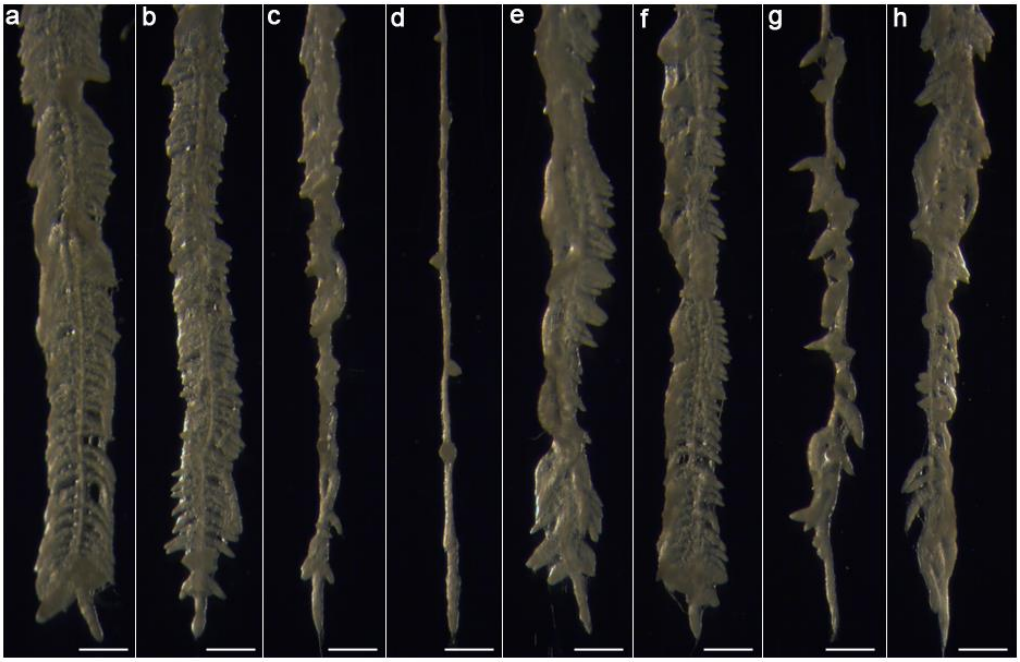

Figure 5.8 Roots under the Stereo Dissecting Microscope after treatment with NPA and then transferred onto 1/2 MS with NAA for 5 days. (**a**) WT. (**b**) *hakai* 37. (**c**) *fip37*. (**d**) *virilizer*. (**e**) ABI3A6. (**f**) MTA-GFP. (**g**) *mta hakai#*1. (**h**) *mta fip37*. Scale bar = 100 μm.

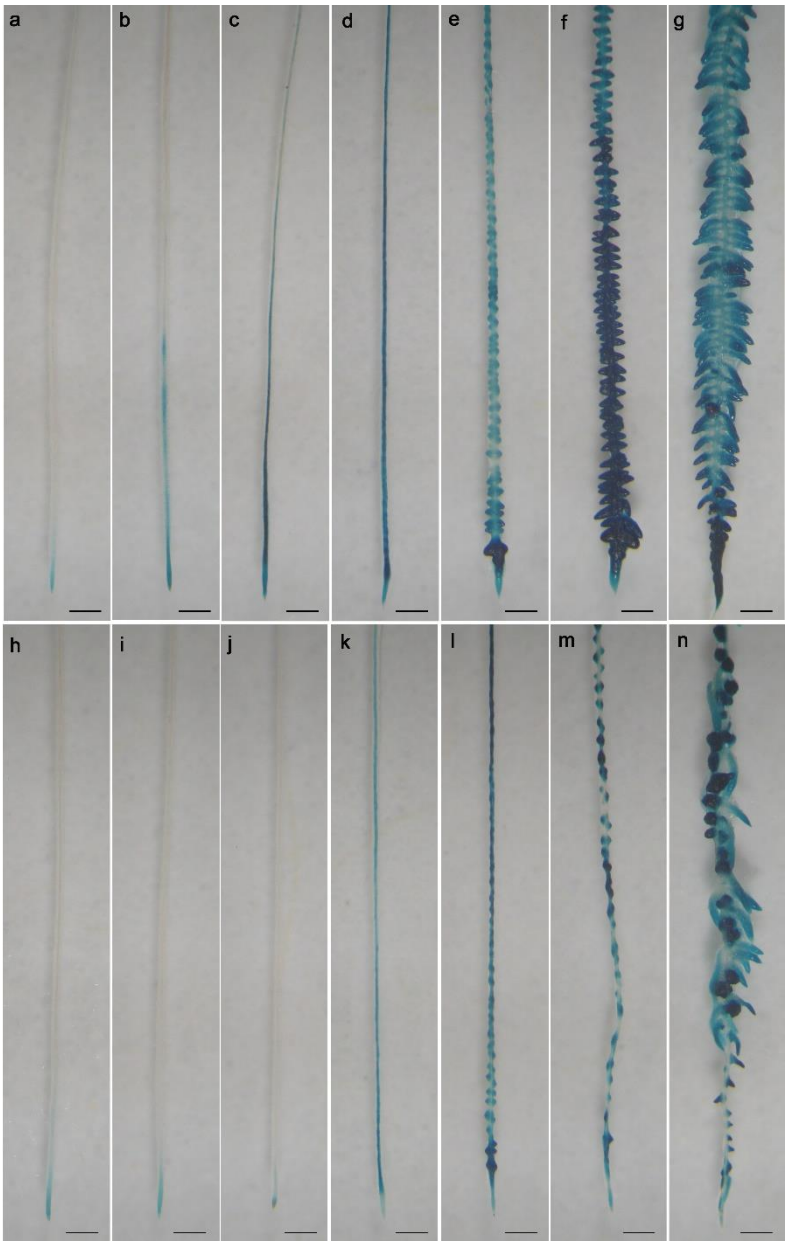

Figure 5.9 *GUS* expression in roots under the Stereo Dissecting Microscope after treatment with NPA and then transferred onto 1/2 MS with NAA. (**a-g**) *CycB1;1*::*GUS* roots induced by NAA for 0 h, 6 h, 12 h, 1 d, 2 d, 3 d and 5 d, respectively. (**h-n**) ABI3A6× *CycB1;1*::*GUS* roots induced by NAA for 0 h, 6 h, 12 h, 1 d, 2 d, 3 d and 5 d, respectively. Scale bar = 400 μm.

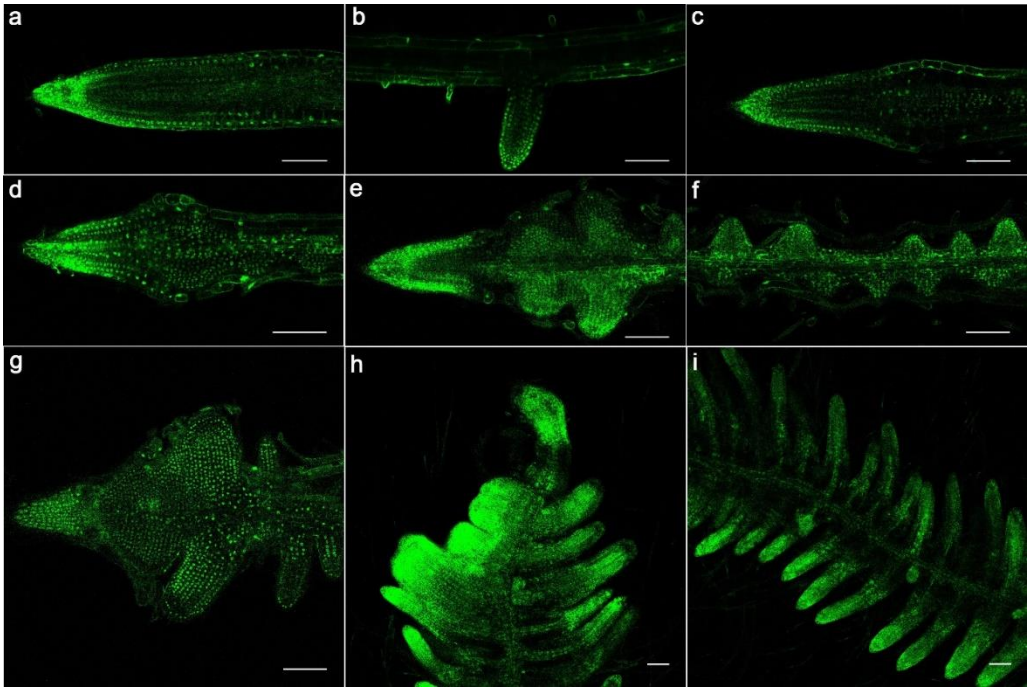

Figure 5.10 MTA-GFP roots under the confocal microscope after treatment with NPA and then transferred onto 1/2 MS with NAA. (**a**) The primary root tip without treatments. (**b**) The elongation zone of the primary root without treatments. (**c**) The primary root tip induced by NAA for 1 d. (**d**) The primary root tip induced by NAA for 2 d. (**e**) The primary root tip induced by NAA for 3 d. (**f**) The elongation zone of the primary root induced by NAA for 3 d. (**g**) The primary root tip induced by NAA for 4 d. (**h**) The primary root tip induced by NAA for 5 d. (**i**) The elongation zone of the primary root induced by NAA for 5 d. Scale bar = 100 μm.

5.4.3 m^{6}A Writer Mutants Crossed with AUX1-YFP

5.4.3.1 Screening m^{6}A writer mutants crossed with AUX1-YFP

To study whether m^{6}A modification is involved in regulating auxin transport, AUX1-YFP (*aux1* complemented with *AUX1* genomic DNA driven by its own promoter and tagged with YFP) was crossed into *hakai* 37 and ABI3A6

separately. The screening of the crossing progenies is similar to that in 4.4.2 and 4.4.3. The screening of F_1 progenies after the cross between *hakai* 37 and AUX1-YFP started with selecting YFP-positive plants, heterozygous mutations for *Hakai* CRISPR target site in these plants were then confirmed by sequencing (Figure 5.11). YFP-positive F_2 plants were further screened for the *Hakai* CRISPR target site by the restriction enzyme site loss method (Voytas, 2013) and sequencing (Supplementary figure 5.1, Figure 5.11). Those homozygous for *hakai* mutation were denominated as *hakai* AUX1-YFP and used in the following analysis.

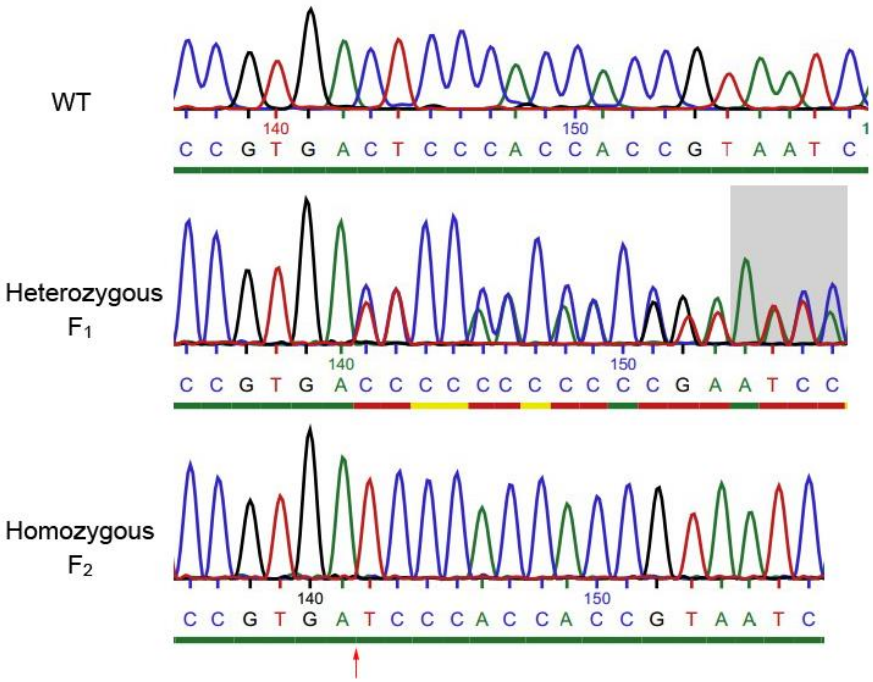

Figure 5.11 Sequencing profiles for *Hakai* CRISPR target site in progenies of *hakai* 37 crossed with AUX1-YFP. The mutation site is labelled with a red arrow.

As shown in Figure 5.12 and 5.13, F_1 progenies of ABI3A6 crossed with AUX1-YFP were heterozygous for *MTA* SALK_074069 T-DNA insertion and two of eight checked ones contained the *ABI3*::*MTA* construct. F_2 progenies of these two lines demonstrating ABI3A6 phenotypes were checked by genotyping PCR

and all of them were homozygous for *MTA* SALK_074069 T-DNA insertion (Figure 5.14). The subsequent generation was used to check YFP signal and those expressing *AUX1-YFP* were termed *mta* AUX1-YFP and used for the following analysis.

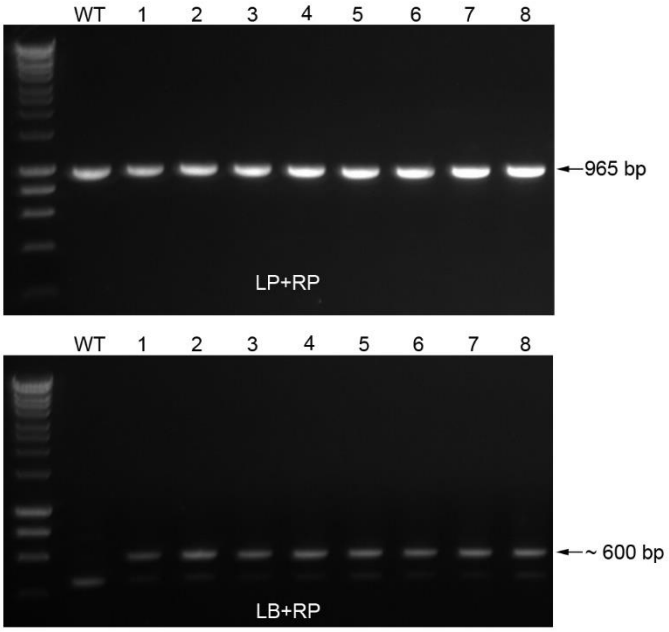

Figure 5.12 Genotyping PCR to check *MTA* SALK_074069 T-DNA insertion in F_1 progenies of ABI3A6 crossed with AUX1-YFP. Sample 1 to 8 represent eight individual F_1 plants.

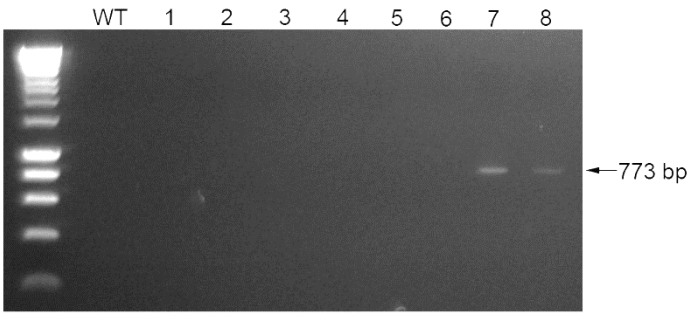

Figure 5.13 PCR to check the presence of *ABI3*::*MTA* construct in F_1 progenies of ABI3A6 crossed with AUX1-YFP. Sample 1 to 8 represent eight individual F_1 lines and line 7 and 8 contained the *ABI3*::*MTA* construct.

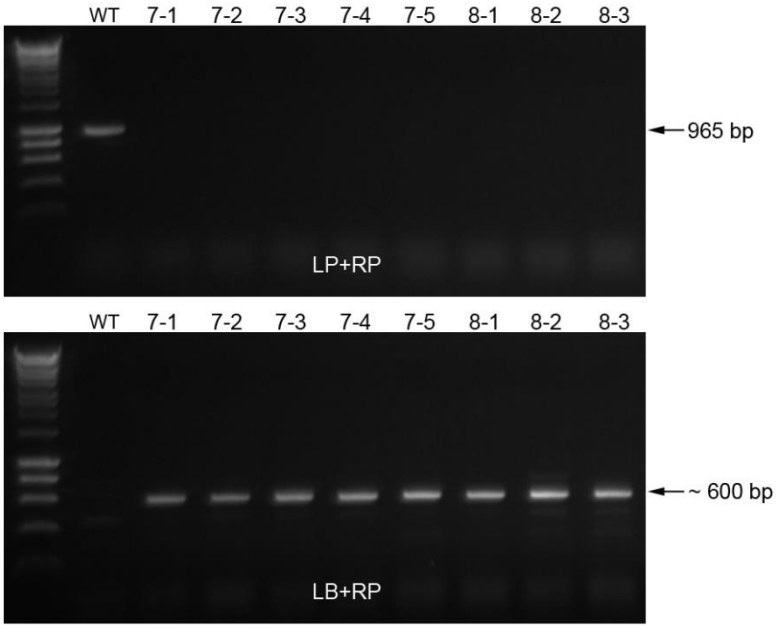

Figure 5.14 Genotyping PCR to check *MTA* SALK_074069 T-DNA insertion in F_2 progenies of ABI3A6 crossed with AUX1-YFP. Sample 7-1 to 7-5 represent five individual F_2 plants from F_1 line 7 while sample 8-1 to 8-3 represent three individual F_2 plants from F_1 line 8. All checked lines were homozygotes.

5.4.3.2 YFP localisation in m^{6}A writer mutants crossed with AUX1-YFP

As shown in Figure 5.15, the expression and distribution of YFP signal in *hakai* AUX1-YFP and *mta* AUX1-YFP exhibited no obvious differences from original AUX1-YFP, indicating that knocking down *MTA* or knocking out *Hakai* does not affect the levels or localisation of auxin influx carrier AUX1.

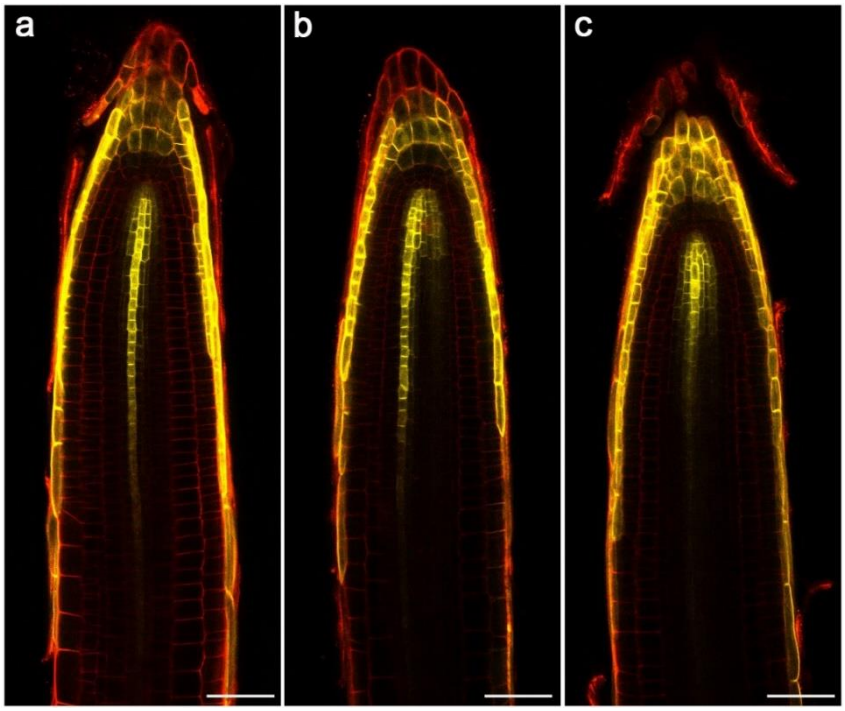

Figure 5.15 Confocal images showing AUX1-YFP localisation in primary root tips of 5-d old seedlings. (**a**) AUX1-YFP. (**b**) *hakai* AUX1-YFP. (**c**) *mta* AUX1-YFP. Scale bar = 50 μm.

5.4.4 m^{6}A Writer Mutants Crossed with Auxin Response Reporter Lines

5.4.4.1 Screening m^{6}A writer mutants crossed with auxin response reporter lines

m^{6}A writer mutants – *hakai* 37, ABI3A6 and *fip37* were crossed with *DR5*::*VENUS* and DII-VENUS separately. The screening procedures were similar to those in 5.4.3 and 4.4.3.2. In terms of the cross between *hakai* 37 and *DR5*::*VENUS* or DII-VENUS, crossing progenies that were homozygous for the mutation at *Hakai* CRISPR target site were obtained in F_3 progenies (Figure 5.16, 5.17). Among them, crossing progenies that were also homozygous for *VENUS* transgene were characterised via the Stereo Fluorescence Microscope (Leica)

and these lines were termed *hakai DR5*::*VENUS* and *hakai* DII-VENUS, respectively.

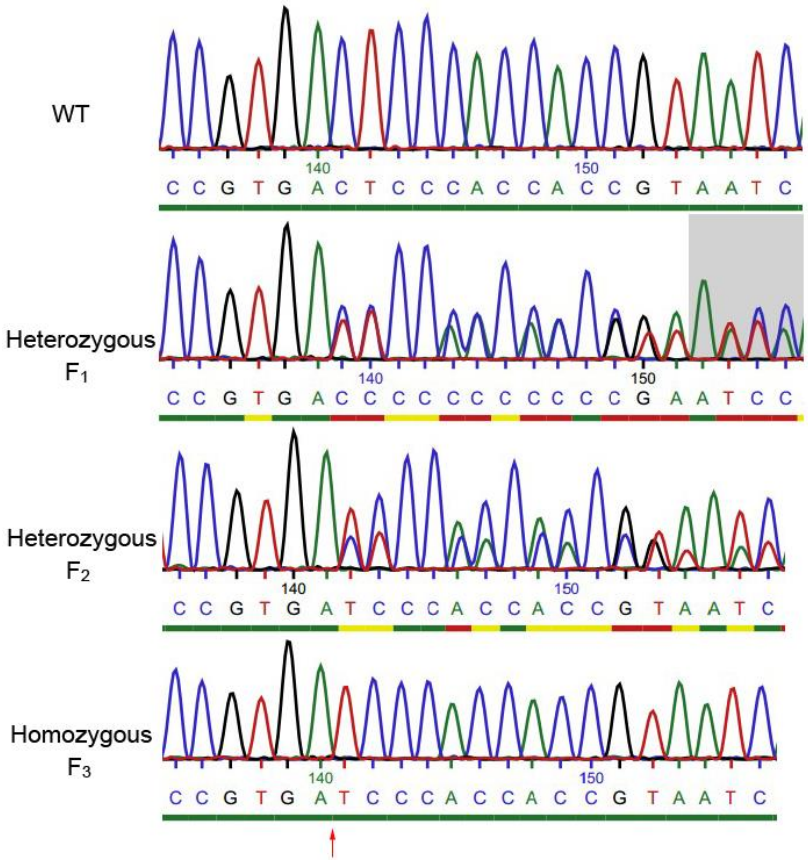

Figure 5.16 Sequencing profiles for *Hakai* CRISPR target site in progenies of *hakai* 37 crossed with *DR5*::*VENUS*. The mutation site is labelled with a red arrow.

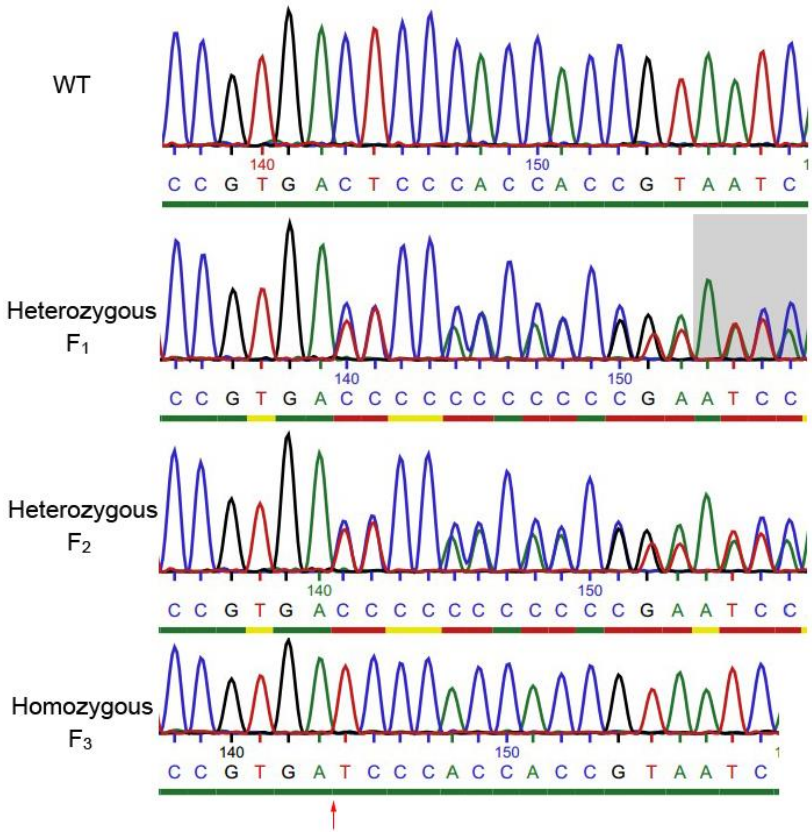

Figure 5.17 Sequencing profiles for *Hakai* CRISPR target site in progenies of *hakai* 37 crossed with DII-VENUS. The mutation site is labelled with a red arrow.

As to the screening of crosses between ABI3A6 and *DR5*::*VENUS* or DII-VENUS, F_1 progenies of both crosses that were heterozygous for *MTA* SALK_074069 T-DNA insertion and contained the *ABI3*::*MTA* construct were selected (Supplementary figure 5.2-5.5). In the subsequent generation, those demonstrating ABI3A6 phenotypes were further confirmed homozygous for *MTA* SALK_074069 T-DNA insertion with the presence of *ABI3*::*MTA* constructs (Figure 5.18-5.21). In the F_3 generation of above lines, those also homozygous for *DR5*::*VENUS* or DII-VENUS were acquired and denominated as *mta DR5*::*VENUS* or *mta* DII-VENUS.

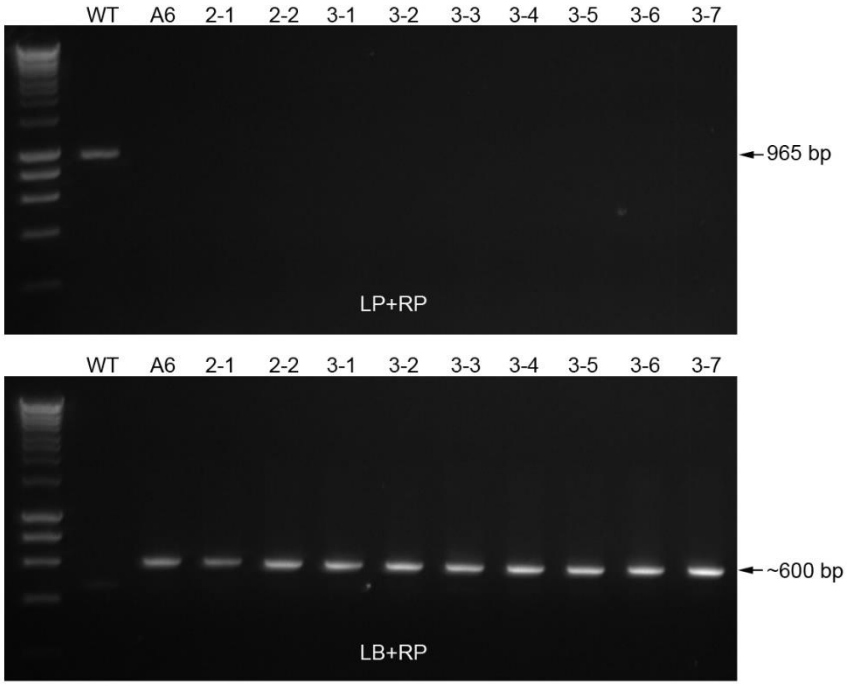

Figure 5.18 Genotyping PCR to check *MTA* SALK_074069 T-DNA insertion in F_2 progenies of ABI3A6 crossed with *DR5*::*VENUS*. A6 represents ABI3A6. Sample 2-1 and sample 2-2 represent two individual F_2 plants from F_1 line 2 while sample 3-1 to 3-7 represent seven individual F_2 plants from F_1 line 3.

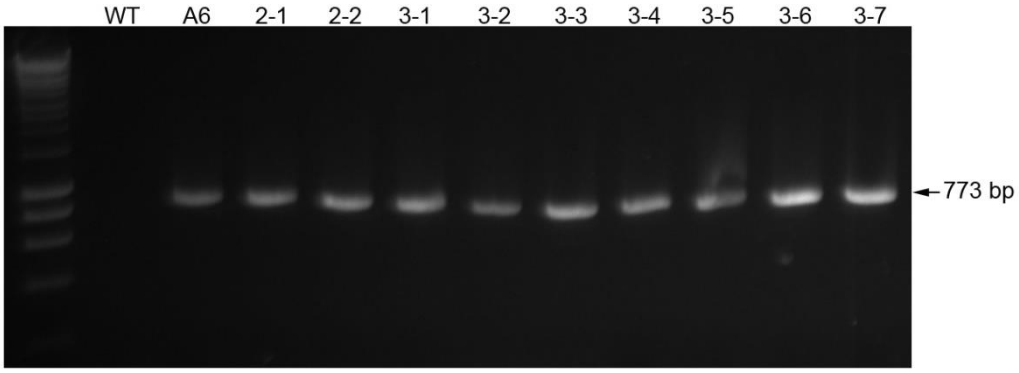

Figure 5.19 PCR to check the presence of *ABI3*::*MTA* construct in F_2 progenies of ABI3A6 crossed with *DR5*::*VENUS*. A6 represents ABI3A6. Sample 2-1 and sample 2-2 represent two individual F_2 plants from F_1 line 2 while sample 3-1 to 3-7 represent seven individual F_2 plants from F_1 line 3.

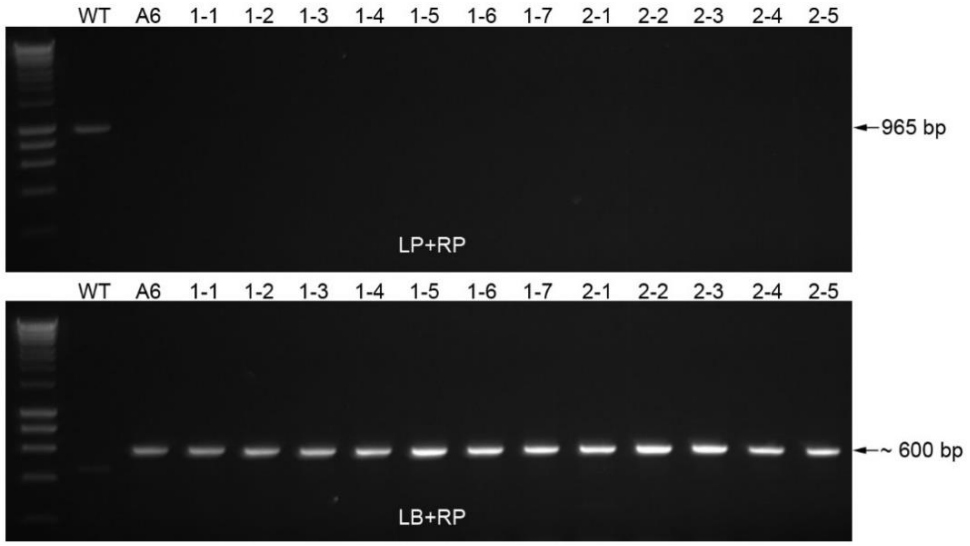

Figure 5.20 Genotyping PCR to check *MTA* SALK_074069 T-DNA insertion in F_2 progenies of ABI3A6 crossed with DII-VENUS. A6 represents ABI3A6. Sample 1-1 to 1-7 represent seven individual F_2 plants from F_1 line 1 while sample 2-1 to 2-5 represent five individual F_2 plants from F_1 line 2.

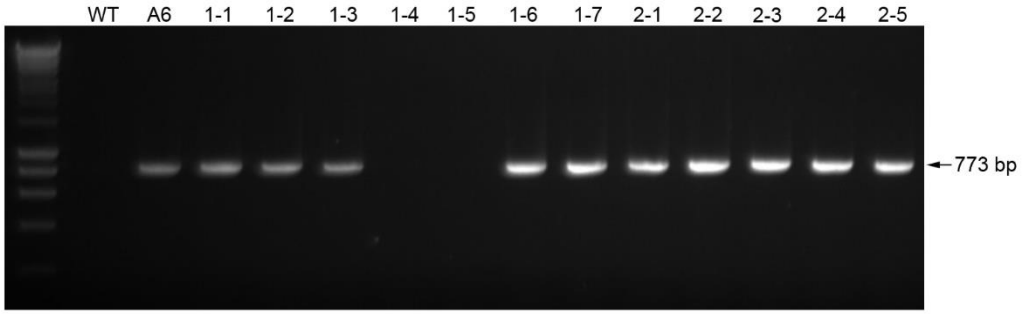

Figure 5.21 PCR to check the presence of *ABI3*::*MTA* construct in F_2 progenies of ABI3A6 crossed with DII-VENUS. A6 represents ABI3A6. Sample 1-1 to 1-7 represent seven individual F_2 plants from F_1 line 1 while sample 2-1 to 2-5 represent five individual F_2 plants from F_1 line 2.

Likewise, genotyping PCR of F_1 progenies of *fip37* crossed with *DR5*::*VENUS* or DII-VENUS confirmed that all checked progenies were heterozygous for *fip37* (Figure 5.22). In the F_2 generation, progenies showing *fip37* phenotypes were double checked by genotyping PCRs and lines homozygous for *fip37* were obtained (Figure 5.23, 5.24). In the subsequent generation, lines homozygous for transgenes containing *VENUS* were characterised via the Stereo Fluorescence Microscope (Leica) and termed *fip37 DR5*::*VENUS* and *fip37* DII-VENUS.

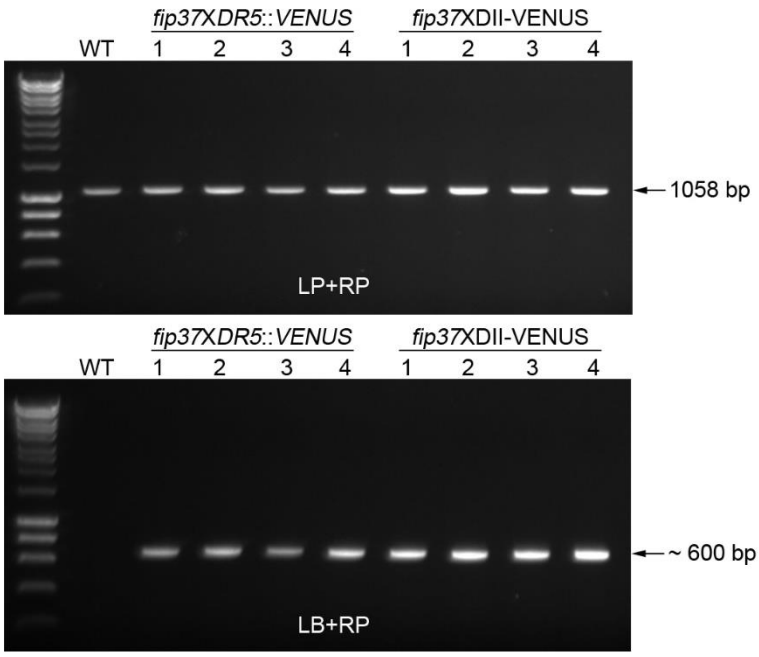

Figure 5.22 Genotyping PCR to check *FIP37* SALK_018636 T-DNA insertion in F_1 progenies of *fip37* crossed with *DR5*::*VENUS* or DII-VENUS. Sample 1 to 4 in both crosses represent four individual F_1 lines.

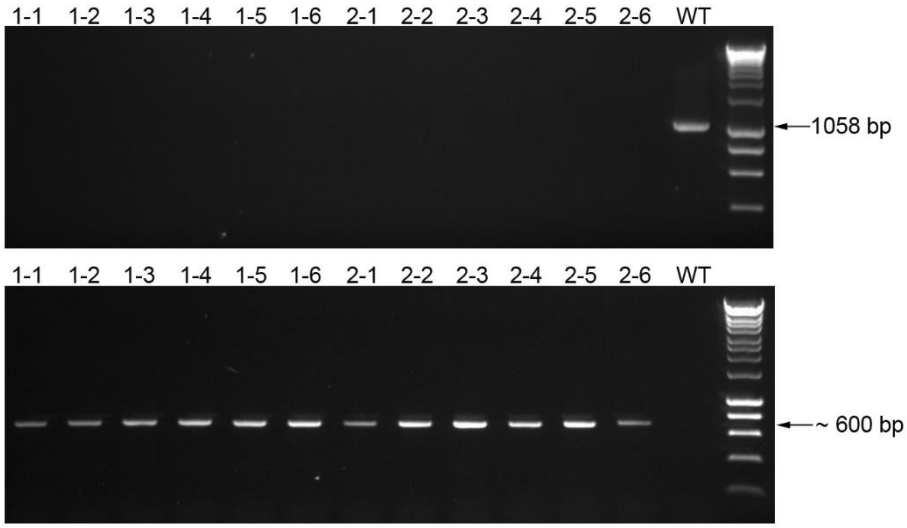

Figure 5.23 Genotyping PCR to check *FIP37* SALK_018636 T-DNA insertion in F_2 progenies of *fip37* crossed with *DR5*::*VENUS*. Sample 1-1 to 1-6 represent six individual F_2 plants from F_1 line 1 while sample 2-1 to 2-6 represent six individual F_2 plants from F_1 line 2.

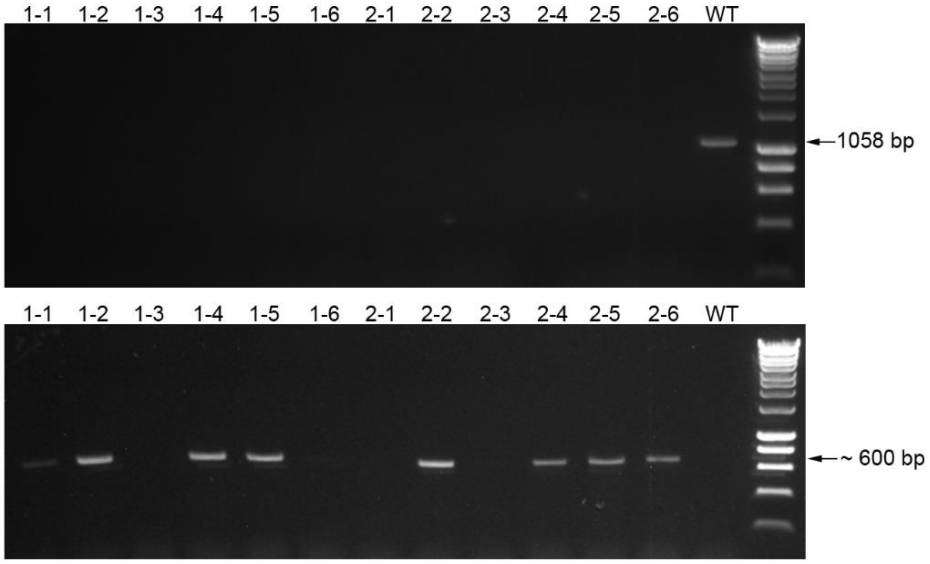

Figure 5.24 Genotyping PCR to check *FIP37* SALK_018636 T-DNA insertion in F_2 progenies of *fip37* crossed with DII-VENUS. Sample 1-1 to 1-6 represent six individual F_2 plants from F_1 line 1 while sample 2-1 to 2-6 represent six individual F_2 plants from F_1 line 2.

5.4.4.2 VENUS expression in progenies of m^6A writer mutants crossed with auxin response reporter lines

The expression of *DR5*::*VENUS* and *DII-VENUS* in *hakai*, *mta* and *fip37* background were analysed by confocal microscopy using homozygous crossing progenies obtained above. Though the expression of *VENUS* in original *DR5*::*VENUS* and DII-VENUS reporter lines were not stable (Supplementary figure 5.6, 5.7), generally the expression of *VENUS* driven by *DR5* promoter in all crossing lines, including *hakai DR5*::*VENUS*, *mta DR5*::*VENUS* and *fip37 DR5*::*VENUS*, were stronger than that in the original *DR5*::*VENUS* (Figure 5.25a-d). The expression of *DII-VENUS* in *hakai*, *mta* and *fip37* background were not consistent with each other, with that in *hakai* DII-VENUS was similar to that in original DII-VENUS, that in *mta* DII-VENUS much less compared with original DII-VENUS and *fip37* DII-VENUS exhibiting a somewhat stronger DII-VENUS signal (Figure 5.25e-h, Supplementary figure 5.7).

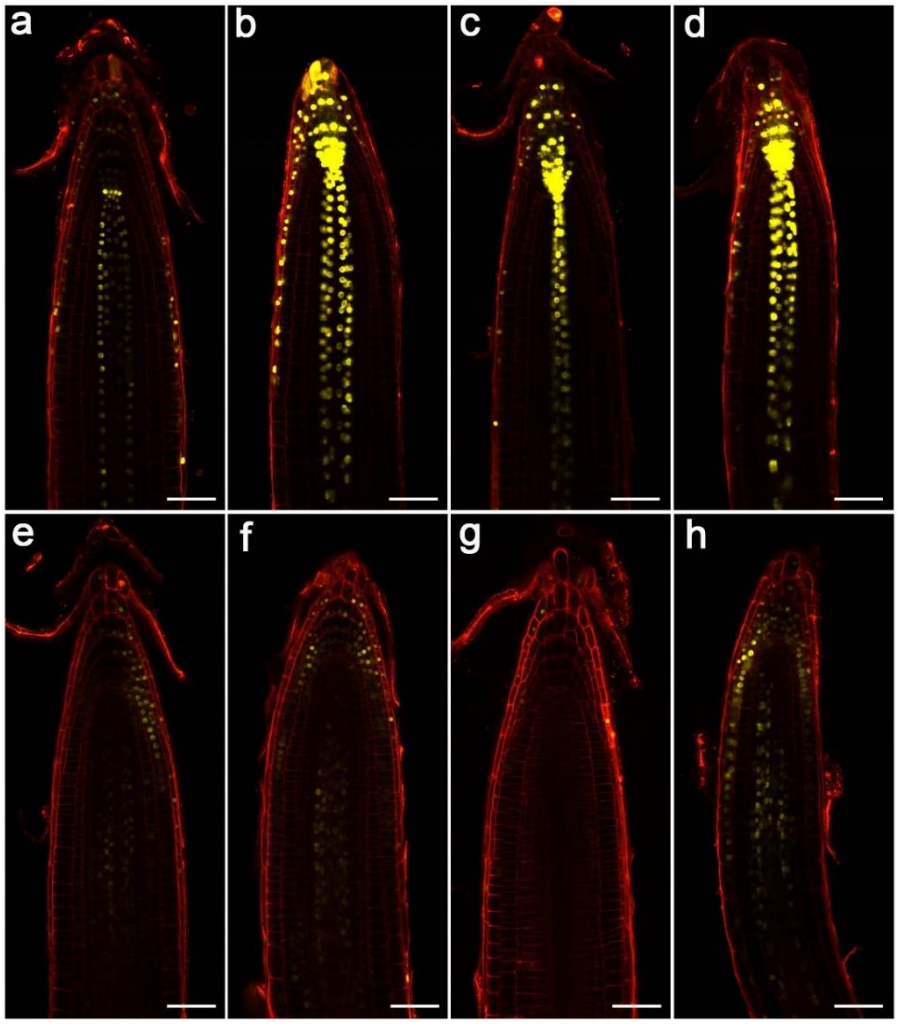

Figure 5.25 Confocal images showing VENUS localisation in primary root tips of 5-d old seedlings. (**a**) *DR5*::*VENUS*. (**b**) *hakai DR5*::*VENUS*. (**c**) *mta DR5*::*VENUS*. (**d**) *fip37 DR5*::*VENUS*. (**e**) DII-VENUS. (**f**) *hakai* DII-VENUS. (**g**) *mta* DII-VENUS. (**h**) *fip37* DII-VENUS. The expression level of *VENUS* shown in the selected images represented the medium expression level of each line. Scale bar = 50 μm.

5.4.5 The Transcriptional and Translational Expression of ARFs

To further study the potential of m^6A in affecting the outcome of the auxin signalling pathway, protein levels of ARF7 and ARF8 were checked by western blotting. As shown in Figure 5.26, ARF7 protein levels in *fip37* and *virilizer* were much higher than that in WT whereas there was no significant change of

ARF8 protein levels in these two mutants relative to WT (Figure 5.26a). The protein levels of ARF7 and ARF8 in *hakai* 37 were slightly higher than that in WT (Figure 5.26a). Interestingly, the increased ARF7 protein levels in *fip37* and *virilizer* were not due to more transcripts because the northern blotting showed that the expression of *ARF7* in these two mutants was not stronger compared with that in WT (Figure 5.26b).

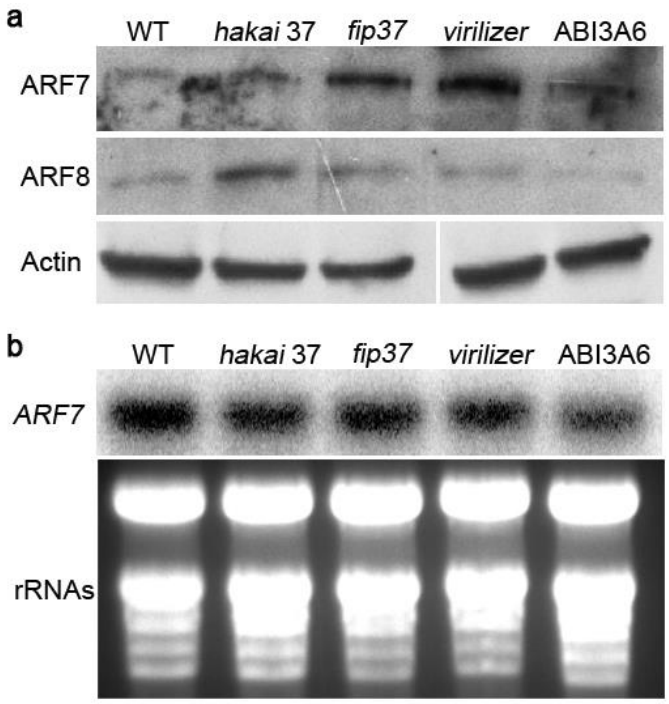

Figure 5.26 The translational and transcriptional levels of ARFs checked by western blotting (**a**) and northern blotting (**b**).

5.5 DISCUSSION

It is very clear that m^6A writer mutants, particularly *virilizer*, *fip37* and *mta hakai* double mutant demonstrated retarded primary root growth and decreased (or inhibited) LR formation. *Arabidopsis* primary root elongation is accompanied by two linked processes: cell division and expansion (Beemster and Baskin, 1998). Cell division and expansion mainly occur in the meristem zone and

ongoing cell division and expansion result in a flux of cells away from the root tip (Beemster et al., 2002, 2003). Cytokinin and auxin are two key phytohormones in mediating these processes and their interactions determine the eventual primary root growth rate (Sabatini et al., 1999; Swarup et al., 2002; Dello Ioio et al., 2008). In *Arabidopsis* primary root, a distal auxin maximum is crucial for correct pattern formation and the orientation and extent of cell division (Blilou et al., 2005). Five PIN genes are shown to collectively regulate cell division and expansion in the primary root by stabilising the auxin maximum at the distal root tip and negatively interacting with *PLETHORA* (*PLT*) genes, major determinants for root stem cell specification (Blilou et al., 2005). Another study also shows that the cross-talk between cytokinin and auxin signal is through interactions between PIN, PIN auxin efflux facilitators, SHY2/IAA3 (SHY2, a repressor of auxin signalling) and ARR1 (a primary cytokinin-response transcription factor) (Dello Ioio et al., 2008). ARR1 activates SHY2, which negatively regulate PIN auxin efflux facilitators and cause auxin redistribution and cell differentiation. In turn, auxin mediates degradation of the SHY2 protein, sustaining PIN activities and cell divisions (Dello Ioio et al., 2008). Though polar auxin transport is involved in regulating primary root elongation, our current study showed significantly shorter primary roots in m^6A writer mutants but no change regarding the localisation and expression of YFP-tagged AUX1. The function of PIN in m^6A writer mutants might be worthwhile investigating.

LR formation is a highly regulated progress, with many factors influencing LR developmental stages (Casimiro et al., 2003; Péret et al., 2009; Lavenus et al.,

2013; Bellini et al., 2014). Reduced LR formation in m^6A writer mutants even after the synchronous LR induction by NPA and NAA treatment indicates that the auxin response in m^6A writer mutants, especially *virilizer*, *fip37* and *mta hakai* double mutant was dramatically decreased. The *GUS* expression assay demonstrated that fewer LR primordia were generated in ABI3A6 relative to WT. Conversely, m^6A writer proteins are primarily expressed at LR initiation sites in *Arabidopsis* roots (Data in Chapter 4; Zhong et al., 2008). Taken together, m^6A modification may participate in regulating LR initiation based on mediating auxin signalling. However, our attempt to unveil the underlying mechanisms using *DR5*::*VENUS* and DII-VENUS reporter lines gave us divergent outcomes. Firstly, the expression of *VENUS* driven by *DR5* promoter were stronger in all three checked m^6A writer mutants, including *hakai* 37, ABI3A6 and *fip37*, suggesting strong auxin response transcriptionally, which is contrary to the phenotypic auxin response observed when knocking down/out m^6A writer genes. This indicates that post-transcriptional regulation may be involved. Secondly, the expression of *DII-VENUS* in *hakai* 37, ABI3A6 and *fip37* was distinct from each other, with that in *hakai* 37 exhibiting negligible differences from the original DII-VENUS, that in ABI3A6 decreased dramatically and that in *fip37* stronger relative to the VENUS signal in DII-VENUS. This suggests that auxin is distributed everywhere in the root when knocking down *MTA* while knocking down *FIP37* decreases the auxin accumulation in the root, partially explaining stronger root developmental defects in *fip37* and is consistent with less severe developmental defects in *mta fip37* double mutant compared with *fip37* single mutant in terms of the above-ground tissues (Data in Chapter 4).

Interestingly, ARF7 protein levels in *fip37* and *virilizer* were significantly increased while ARF8 protein levels were unchanged in these two mutant lines. Though both ARF7 and ARF8 belong to the ARF family and act as activators in regulating auxin response, their sequence differences lie in 5' UTRs, with ARF7 containing upstream open reading frames (uORFs) whereas there are no uORFs in ARF8 (Rosado et al., 2012). uORFs refer to a single or multiple protein-coding elements often found in long 5' UTRs (>100 nt) that can repress the translation of the main ORF (mORF) and translation reinitiation is required for proper translation of mORF (Rosado et al., 2012). It has been shown that non-core subunit h of eukaryotic initiation factor 3 (eiF3h), ribosomal proteins, the target of rapamycin (TOR) signalling pathway (a pathway connecting growth with environmental signal perception) and auxin are involved in modulating translation reinitiation (Zhou et al., 2010; Rosado et al., 2012; Schepetilnikov et al., 2013; Schepetilnikov and Ryabova, 2017). In plants, ARFs are particularly enriched with uORFs whereas other proteins involved in the auxin network have few or no uORFs (von Arnim et al., 2014). Rosada et al. (2012) showed that ARF7 protein levels are reduced in ribosomal mutants – *rpl4d* and *rpl5a* while ARF8 protein levels remain the same. In these plants, *ARF7* expression shows no change in the transcriptional level, indicating translational regulation of ARF7 by ribosomal proteins (Rosada et al., 2012). The findings in the current study showed a similar trend but with increased ARF7 protein levels in *fip37* and *virilizer*. Another study in mammals suggests that uORFs typically reduce protein expression by 30-80%, with a modest impact on mRNA levels (Calvo et al., 2009). Given that m^6A modification is predominantly located in 3' UTRs, we speculate that m^6A modification in 3' UTRs might have a regulatory function on

translation reinitiation factors to control the translation of uORF-containing transcripts, such as ARF7. However, this cannot explain phenotypes related to reduced auxin response in m^6A writer mutants. Therefore, more investigations are needed to address this contradiction.

5.6 CONCLUSIONS

In summary, m^6A writer mutants, particularly *fip37* and *virilizer*, demonstrated significantly shorter primary roots and reduced LRs compared with WT on 1/2 MS plus 1% (w/v) sucrose. Reduced LR formation could not be rescued upon synchronous LR induction using NPA and NAA. In addition, under NPA and NAA treatments, fewer LR primordia were produced in ABI3A6 marked by *CycB1;1*::*GUS* whereas MTA-GFP formed WT-level induced LRs with strong expression in LR initiation sites, suggesting m^6A modification might be involved in regulating LR initiation dependent on mediating the auxin signalling network. However, auxin response in roots of m^6A writer mutants (including *hakai* 37, ABI3A6 and *fip37*) were very strong at the transcriptional level checked via the *DR5*::*VENUS* reporter regardless of the auxin level in these mutants (analysed via the DII-VENUS reporter), indicating post-transcriptional regulation of actual auxin response exists. In addition, obviously increased ARF7 protein levels but unchanged *ARF7* transcripts and ARF8 protein levels in *fip37* and *virilizer* indicate that m^6A modification might be involved in regulating translation reinitiation in uORF-containing transcripts dependent on FIP37 or Virilizer. Experiments addressing this are currently underway. Given that the auxin regulatory network is complicated, more investigations are required to address

how m^6A might regulate auxin signalling pathway and functions of proteins involved.

5.7 REFERENCES

BAND, L. R., WELLS, D. M., LARRIEU, A., SUN, J., MIDDLETON, A. M., FRENCH, A. P., BRUNOUD, G., SATO, E. M., WILSON, M. H., PÉRET, B., et al. 2012. Root gravitropism is regulated by a transient lateral auxin gradient controlled by a tipping-point mechanism. Proceedings of the National Academy of Sciences, 109, 4668-4673.

BEEMSTER, G. T. & BASKIN, T. I. 1998. Analysis of cell division and elongation underlying the developmental acceleration of root growth in *Arabidopsis thaliana*. Plant Physiology, 116, 1515-1526.

BEEMSTER, G. T., DE VUSSER, K., DE TAVERNIER, E., DE BOCK, K. & INZÉ, D. 2002. Variation in growth rate between Arabidopsis ecotypes is correlated with cell division and A-type cyclin-dependent kinase activity. Plant Physiology, 129, 854-864.

BEEMSTER, G. T., FIORANI, F. & INZE, D. 2003. Cell cycle: the key to plant growth control? Trends in Plant Science, 8, 154-158.

BELLINI, C., PACURAR, D. I. & PERRONE, I. 2014. Adventitious roots and lateral roots: similarities and differences. Annual Review of Plant Biology, 65, 639-666.

BLILOU, I., XU, J., WILDWATER, M., WILLEMSEN, V., PAPONOV, I., FRIML, J., HEIDSTRA, R., AIDA, M., PALME, K. & SCHERES, B. 2005. The

PIN auxin efflux facilitator network controls growth and patterning in *Arabidopsis* roots. Nature, 433, 39-44.

BRUNOUD, G., WELLS, D. M., OLIVA, M., LARRIEU, A., MIRABET, V., BURROW, A. H., BEECKMAN, T., KEPINSKI, S., TRAAS, J., BENNETT, M. J. & VERNOUX T. 2012. A novel sensor to map auxin response and distribution at high spatio-temporal resolution. Nature, 482, 103-106.

CALDERÓN VILLALOBOS, L. I. A., LEE, S., DE OLIVEIRA, C., IVETAC, A., BRANDT, W., ARMITAGE, L., SHEARD, L. B., TAN, X., PARRY, G., MAO, H., et al. 2012. A combinatorial TIR1/AFB-Aux/IAA co-receptor system for differential sensing of auxin. Nature Chemical Biology, 8, 477-485.

CALVO, S. E., PAGLIARINI, D. J. & MOOTHA, V. K. 2009. Upstream open reading frames cause widespread reduction of protein expression and are polymorphic among humans. Proceedings of the National Academy of Sciences, 106, 7507-7512.

CASIMIRO, I., BEECKMAN, T., GRAHAM, N., BHALERAO, R., ZHANG, H., CASERO, P., SANDBERG, G. & BENNETT, M. J. 2003. Dissecting *Arabidopsis* lateral root development. Trends in Plant Science, 8, 165-171.

CASIMIRO, I., MARCHANT, A., BHALERAO, R. P., BEECKMAN, T., DHOOGE, S., SWARUP, R., GRAHAM, N., INZÉ, D., SANDBERG, G., CASERO, P. J. & BENNETT, M. 2001. Auxin transport promotes Arabidopsis lateral root initiation. The Plant Cell, 13, 843-852.

DE SMET, I., TETSUMURA, T., DE RYBEL, B., DIT FREY, N. F., LAPLAZE, L., CASIMIRO, I., SWARUP, R., NAUDTS, M., VANNESTE, S., AUDENAERT, D., et al. 2007. Auxin-dependent regulation of lateral root positioning in the basal meristem of *Arabidopsis*. Development, 134, 681-690.

DELLO IOIO, R. D., NAKAMURA, K., MOUBAYIDIN, L., PERILLI, S., TANIGUCHI, M., MORITA, M. T., AOYAMA, T., COSTANTINO, P. & SABATINI, S. 2008. A genetic framework for the control of cell division and differentiation in the root meristem. Science, 322, 1380-1384.

DUBROVSKY, J. G., SAUER, M., NAPSUCIALY-MENDIVIL, S., IVANCHENKO, M. G., FRIML, J., SHISHKOVA, S., CELENZA, J. & BENKOVÁ, E. 2008. Auxin acts as a local morphogenetic trigger to specify lateral root founder cells. Proceedings of the National Academy of Sciences, 105, 8790-8794.

FUKAKI, H., NAKAO, Y., OKUSHIMA, Y., THEOLOGIS, A. & TASAKA, M. 2005. Tissue-specific expression of stabilized SOLITARY-ROOT/IAA14 alters lateral root development in Arabidopsis. The Plant Journal, 44, 382-395.

FUKAKI, H., TAMEDA, S., MASUDA, H. & TASAKA, M. 2002. Lateral root formation is blocked by a gain-of-function mutation in the *SOLITARY-ROOT*/*IAA14* gene of *Arabidopsis*. The Plant Journal, 29, 153-168.

GOH, T., JOI, S., MIMURA, T. & FUKAKI, H. 2012. The establishment of asymmetry in *Arabidopsis* lateral root founder cells is regulated by LBD16/ASL18 and related LBD/ASL proteins. Development, 139, 883-893.

GOLDSMITH, M. 1977. The polar transport of auxin. Annual Review of Plant Physiology, 28, 439-478.

GREENHAM, K., SANTNER, A., CASTILLEJO, C., MOONEY, S., SAIRANEN, I., LJUNG, K. & ESTELLE, M. 2011. The AFB4 auxin receptor is a negative regulator of auxin signaling in seedlings. Current Biology, 21, 520-525.

GUILFOYLE, T. J. & HAGEN, G. 2007. Auxin response factors. Current Opinion in Plant Biology, 10, 453-460.

HIMANEN, K., BOUCHERON, E., VANNESTE, S., DE ALMEIDA ENGLER, J., INZÉ, D. & BEECKMAN, T. 2002. Auxin-mediated cell cycle activation during early lateral root initiation. The Plant Cell, 14, 2339-2351.

LAVENUS, J., GOH, T., ROBERTS, I., GUYOMARC'H, S., LUCAS, M., DE SMET, I., FUKAKI, H., BEECKMAN, T., BENNETT, M. & LAPLAZE, L. 2013. Lateral root development in *Arabidopsis*: fifty shades of auxin. Trends in Plant Science, 18, 450-458.

LIAO, C.-Y., SMET, W., BRUNOUD, G., YOSHIDA, S., VERNOUX, T. & WEIJERS, D. 2015. Reporters for sensitive and quantitative measurement of auxin response. Nature Methods, 12, 207-210.

MARCHANT, A., BHALERAO, R., CASIMIRO, I., EKLÖF, J., CASERO, P. J., BENNETT, M. & SANDBERG, G. 2002. AUX1 promotes lateral root formation by facilitating indole-3-acetic acid distribution between sink and source tissues in the Arabidopsis seedling. The Plant Cell, 14, 589-597.

MARCHANT, A., KARGUL, J., MAY, S. T., MULLER, P., DELBARRE, A., PERROT-RECHENMANN, C. & BENNETT, M. J. 1999. AUX1 regulates root gravitropism in *Arabidopsis* by facilitating auxin uptake within root apical tissues. The EMBO Journal, 18, 2066-2073.

OKUSHIMA, Y., FUKAKI, H., ONODA, M., THEOLOGIS, A. & TASAKA, M. 2007. ARF7 and ARF19 regulate lateral root formation via direct activation of *LBD*/*ASL* genes in *Arabidopsis*. The Plant Cell, 19, 118-130.

PARIZOT, B., LAPLAZE, L., RICAUD, L., BOUCHERON-DUBUISSON, E., BAYLE, V., BONKE, M., DE SMET, I., POETHIG, S. R., HELARIUTTA, Y.,

PÉRET, B., DE RYBEL, B., CASIMIRO, I., BENKOVÁ, E., SWARUP, R., LAPLAZE, L., BEECKMAN, T. & BENNETT, M. J. 2009. *Arabidopsis* lateral root development: an emerging story. Trends in Plant Science, 14, 399-408.

RASHOTTE, A. M., BRADY, S. R., REED, R. C., ANTE, S. J. & MUDAY, G. K. 2000. Basipetal auxin transport is required for gravitropism in roots of Arabidopsis. Plant Physiology, 122, 481-490.

RAVEN, J. 1975. Transport of indoleacetic acid in plant cells in relation to pH and electrical potential gradients, and its significance for polar IAA transport. New Phytologist, 74, 163-172.

REED, R. C., BRADY, S. R. & MUDAY, G. K. 1998. Inhibition of auxin movement from the shoot into the root inhibits lateral root development in Arabidopsis. Plant Physiology, 118, 1369-1378.

ROSADO, A., LI, R., VAN DE VEN, W., HSU, E. & RAIKHEL, N. V. 2012. *Arabidopsis* ribosomal proteins control developmental programs through translational regulation of auxin response factors. Proceedings of the National Academy of Sciences, 109, 19537-19544.

RUBERY, P. & SHELDRAKE, A. 1974. Carrier-mediated auxin transport. Planta, 118, 101-121.

SABATINI, S., BEIS, D., WOLKENFELT, H., MURFETT, J., GUILFOYLE, T., MALAMY, J., BENFEY, P., LEYSER, O., BECHTOLD, N., WEISBEEK, P. & SCHERES B. 1999. An auxin-dependent distal organizer of pattern and polarity in the *Arabidopsis* root. Cell, 99, 463-472.

SCHEPETILNIKOV, M., DIMITROVA, M., MANCERA-MARTÍNEZ, E., GELDREICH, A., KELLER, M. & RYABOVA, L. A. 2013. TOR and S6K1

promote translation reinitiation of uORF-containing mRNAs via phosphorylation of eIF3h. The EMBO Journal, 32, 1087-1102.

SCHEPETILNIKOV, M. & RYABOVA, L. A. 2017. Auxin signaling in regulation of plant translation reinitiation. Frontiers in Plant Science, 8, 1014.

SWARUP, K., BENKOVÁ, E., SWARUP, R., CASIMIRO, I., PÉRET, B., YANG, Y., PARRY, G., NIELSEN, E., DE SMET, I., VANNESTE, S., et al. 2008. The auxin influx carrier LAX3 promotes lateral root emergence. Nature Cell Biology, 10, 946-954.

SWARUP, R., KARGUL, J., MARCHANT, A., ZADIK, D., RAHMAN, A., MILLS, R., YEMM, A., MAY, S., WILLIAMS, L., MILLNER, P., et al. 2004. Structure-function analysis of the presumptive Arabidopsis auxin permease AUX1. The Plant Cell, 16, 3069-3083.

SWARUP, R., PARRY, G., GRAHAM, N., ALLEN, T. & BENNETT, M. 2002. Auxin cross-talk: integration of signalling pathways to control plant development. In: PERROT-RECHENMANN and HAGEN (Eds.) Auxin Molecular Biology, pp. 411-426. Springer.

SWARUP, R. & PÉRET, B. 2012. AUX/LAX family of auxin influx carriers – an overview. Frontiers in Plant Science, 3, 225.

TEALE, W. & PALME, K. 2017. Naphthylphthalamic acid and the mechanism of polar auxin transport. Journal of Experimental Botany, exr323.

TEALE, W. D., PAPONOV, I. A. & PALME, K. 2006. Auxin in action: signalling, transport and the control of plant growth and development. Nature Reviews. Molecular Cell Biology, 7, 847-859.

ULMASOV, T., MURFETT, J., HAGEN, G. & GUILFOYLE, T. J. 1997. Aux/IAA proteins repress expression of reporter genes containing natural and highly active synthetic auxin response elements. The Plant Cell, 9, 1963-1971.

VIETEN, A., SAUER, M., BREWER, P. B. & FRIML, J. 2007. Molecular and cellular aspects of auxin-transport-mediated development. Trends in Plant Science, 12, 160-168.

VON ARNIM, A. G., JIA, Q. & VAUGHN, J. N. 2014. Regulation of plant translation by upstream open reading frames. Plant Science, 214, 1-12.

VOYTAS, D. F. 2013. Plant genome engineering with sequence-specific nucleases. The Annual Reviews of Plant Biology, 64, 327-350.

WANG, R. & ESTELLE, M. 2014. Diversity and specificity: auxin perception and signaling through the TIR1/AFB pathway. Current Opinion in Plant Biology, 21, 51-58.

WEIJERS, D. & WAGNER, D. 2016. Transcriptional responses to the auxin hormone. Annual Review of Plant Biology, 67, 539-574.

WILMOTH, J. C., WANG, S., TIWARI, S. B., JOSHI, A. D., HAGEN, G., GUILFOYLE, T. J., ALONSO, J. M., ECKER, J. R. & REED, J. W. 2005. NPH4/ARF7 and ARF19 promote leaf expansion and auxin-induced lateral root formation. The Plant Journal, 43, 118-130.

WILSON, M., GOH, T., VOß, U., BISHOPP, A., PÉRET, B. & BENNETT, M. 2013. SnapShot: root development. Cell, 155, 1190-1190. e1.

ZHONG, S., LI, H., BODI, Z., BUTTON, J., VESPA, L., HERZOG, M. & FRAY, R. G. 2008. MTA is an *Arabidopsis* messenger RNA adenosine methylase and interacts with a homolog of a sex-specific splicing factor. The Plant Cell, 20, 1278-1288.

ZHOU, F., ROY, B. & VON ARNIM, A. G. 2010. Translation reinitiation and development are compromised in similar ways by mutations in translation initiation factor eIF3h and the ribosomal protein RPL24. BMC Plant Biology, 10, 193.

5.8 SUPPLEMENTARY FIGURES

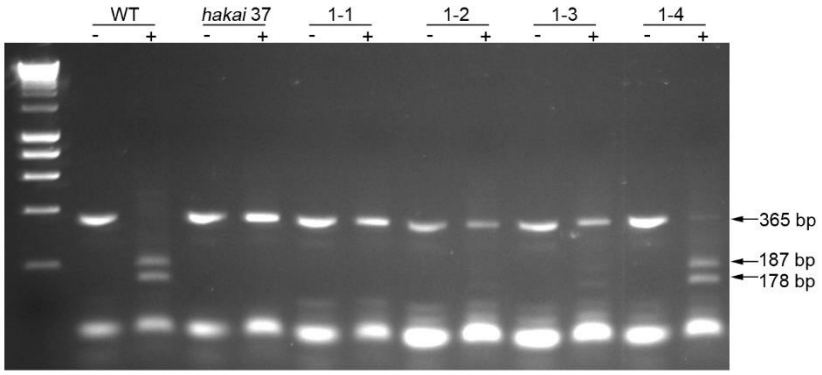

Supplementary figure 5.1 Screening F_2 generation of *hakai* 37 crossed with AUX1-YFP at *Hakai* CRISPR target site by the restriction enzyme site loss method. Sample 1-1 to 1-4 represent four individual F_2 plants from F_1 line 1. Samples were loaded on 1.5% (w/v) agarose gel. -, undigested PCR product using primers flanking the CRISPR target site; +, PCR product digested by *Sch*I (an isoschizomer of *Mly*I having the same recognition and cleavage specificity and working better than *Mly*I). Sample 1-1 was uncut, resembling *hakai* 37.

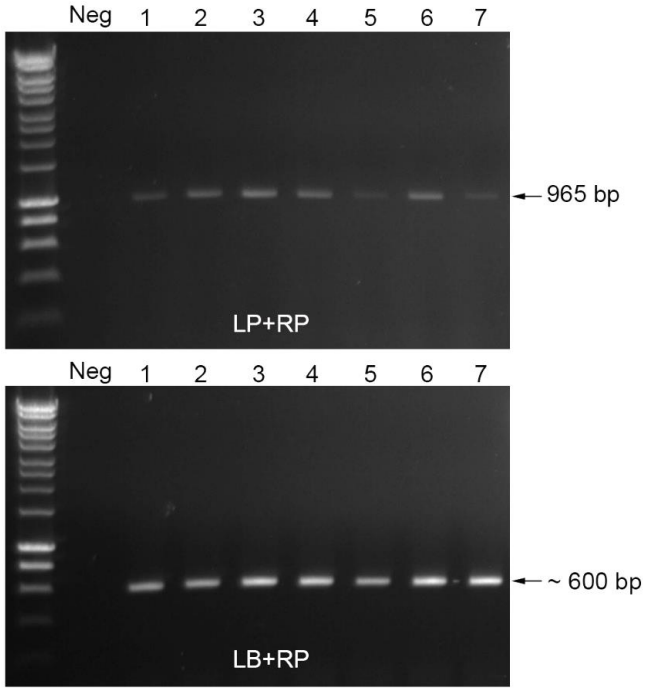

Supplementary figure 5.2 Genotyping PCR to check *MTA* SALK_074069 T-DNA insertion in F_1 progenies of ABI3A6 crossed with *DR5*::*VENUS*. Neg represents negative controls. Sample 1 to 7 represent seven individual F_1 lines.

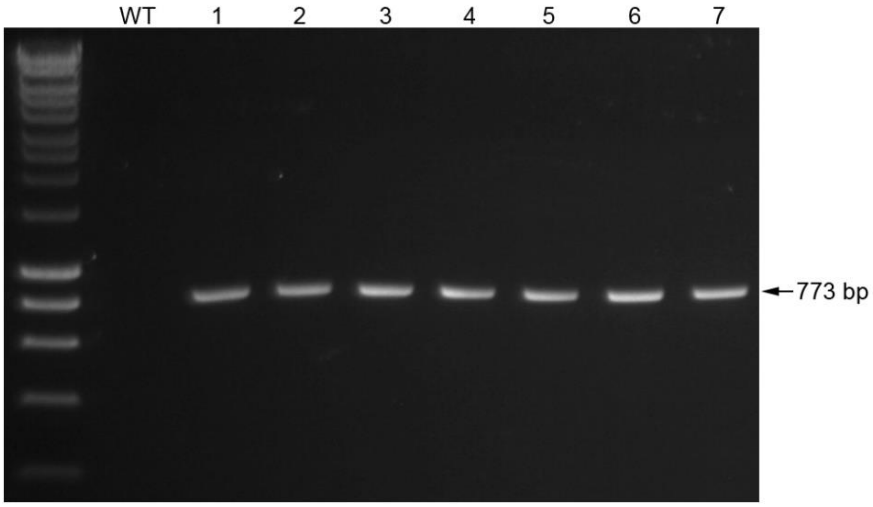

Supplementary figure 5.3 PCR to check the presence of *ABI3*::*MTA* construct in F_1 progenies of ABI3A6 crossed with *DR5*::*VENUS*. Sample 1 to 7 represent seven individual F_1 lines.

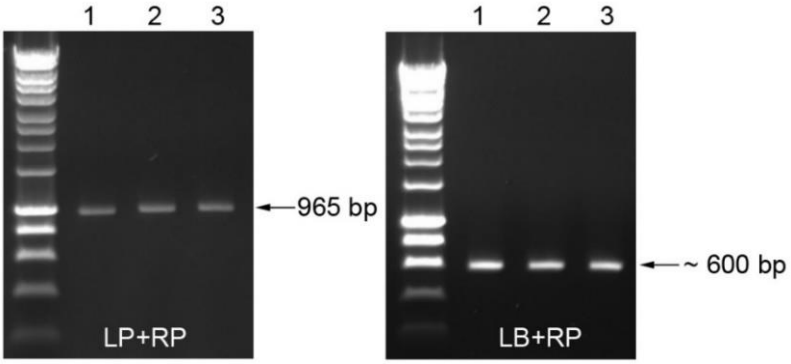

Supplementary figure 5.4 Genotyping PCR to check *MTA* SALK_074069 T-DNA insertion in F_1 progenies of ABI3A6 crossed with DII-VENUS. Sample 1 to 3 represent three individual F_1 lines.

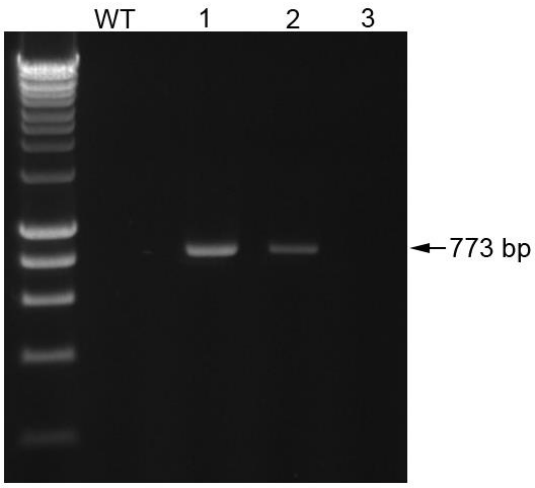

Supplementary figure 5.5 PCR to check the presence of *ABI3*::*MTA* construct in F_1 progenies of ABI3A6 crossed with DII-VENUS. Sample 1 to 3 represent three individual F_1 lines.

Supplementary figure 5.6 Confocal images showing different expression levels of *VENUS* in primary root tips of 5-d old *DR5*::*VENUS*. Only 16 out of 95 checked ones showing strong VENUS signal. Scale bar = 50 μm.

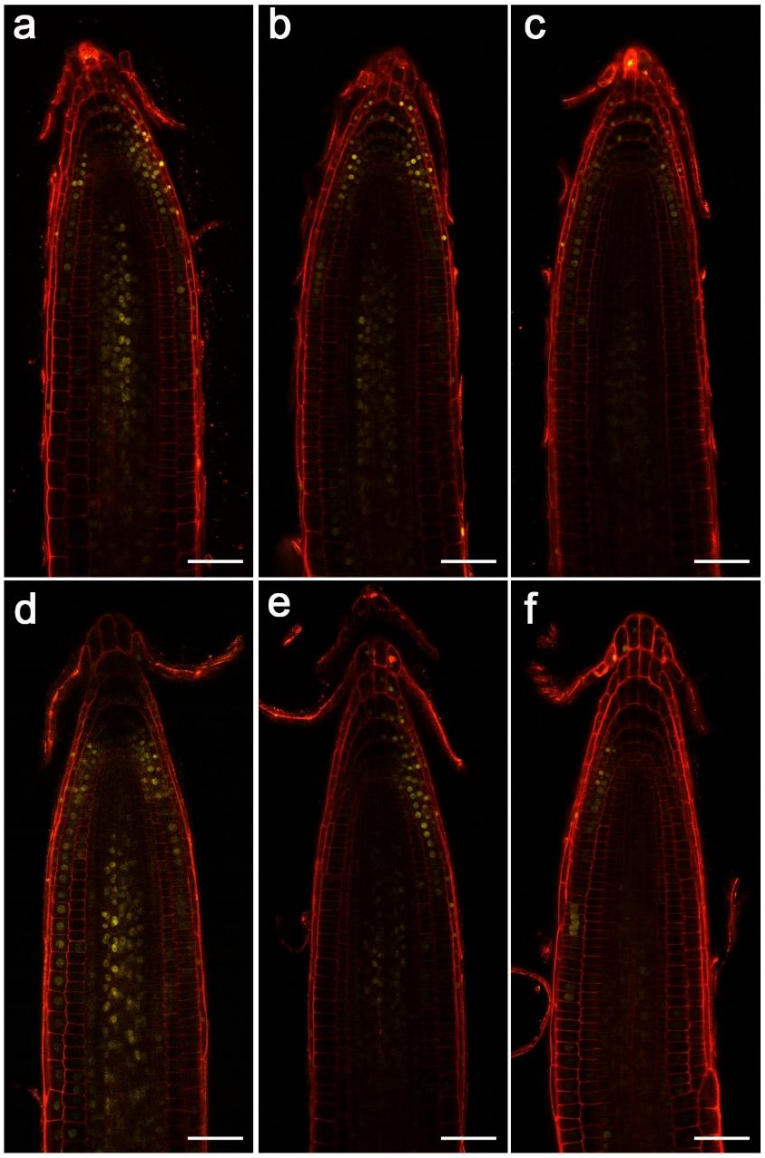

Supplementary figure 5.7 Confocal images showing different expression levels of *VENUS* in primary root tips of 5-d old *hakai* DII-VENUS (**a-c**) and DII-VENUS (**d-f**). Scale bar = 50 μm.

CHAPTER 6 GENERAL DISCUSSION

6.1 BIOLOGICAL FUNCTIONS OF m^6A IN REGULATING PLANT GROWTH AND DEVELOPMENT

Studies about m^6A mRNA modification have become increasingly numerous in the past decade. Diverse biological functions of m^6A have been reported in several eukaryotes, particularly in mammals. Our previous studies for the first time showed that m^6A is required for the embryonic development and other growth and development processes at the mature stage in *Arabidopsis* (Zhong et al., 2008; Bodi et al., 2012). The analysis of single mutants, double mutants and other transgenic lines related to m^6A writer proteins in the current study reveals that m^6A modification is necessary for almost all developmental stages throughout the whole life of *Arabidopsis*.

m^6A is essential for the embryonic progression during *Arabidopsis* seed development. Null mutations in all identified m^6A writer proteins except for Hakai are embryonic lethal (Vespa et al., 2004; Zhong et al., 2008; Bodi et al., 2012; Růžička et al., 2017). Although complete knockout of *Hakai* is viable, homozygous *hakai fip37*, *hakai virilizer* double mutants are lethal, which probably occurs at a very early developmental stage. In contrast, homozygous *mta hakai* can survive but demonstrates more severe developmental defects than *mta* single mutant (ABI3A6). The *mta* hypomorph is homozygous for the *MTA* T-DNA insertion but is complemented by *MTA* cDNA driven by the *ABI3* promoter, this produces plants with very low levels of MTA post germination

but which have high levels of MTA during embryo growth. This expression of *MTA* driven by *ABI3* promoter during the embryonic development may explain why it is possible to obtain the double mutant with *hakai*. Together, these data suggest that Hakai is also important for embryogenesis, by influencing the regulatory functions of other m^6A writers during this process.

Though ABI3A6 and hypomorphic mutants for *FIP37* and *Virilizer* (*fip37* and *virilizer*) are viable, they all demonstrate similar developmental defects during post-embryonic organogenesis. The formation of post-embryonic organs initiates from the shoot and root apical meristems (Perianez-Rodriguez et al., 2014). All three above mutant lines and two double mutants (*mta hakai* and *mta fip37*) show retarded growth of aerial organs relative to WT. Using the same *fip37* mutant line, Shen et al. (2016) showed that lacking *FIP37* leads to a massive over-proliferation of shoot meristems, which is consistent with *fip37* phenotypes in the current study. It is suggested that FIP37-dependent m^6A mRNA modification negatively correlates with mRNA stability of shoot meristem genes to prevent shoot meristem over-proliferation and maintain the shoot meristem as a renewable source for the continuous production of all aerial organs in plants (Shen et al., 2016). Phenotypes of all m^6A writer mutants except for *hakai* in the current study support this proposal, indicating that in general the reduction of m^6A mRNA modification in *Arabidopsis* affects the proper development of the shoot meristem and consequently influences the formation of all aerial organs. This is in accordance with an important role of m^6A modification in maintaining well-tuned stem cell development in mammals, though contrary conclusions exist (Batista et al., 2014; Wang et al., 2014; Geula

et al., 2015). In addition to the retarded growth, low m^{6}A mutants (including ABI3A6, *fip37*, *virilizer*, *mta hakai* and *mta fip37*) also demonstrated other developmental defects, for example, crinkled rosette leaves, shorter inflorescence stems, abnormal flower architectures, shorter siliques and dead seeds, with *fip37*, *virilizer* and *mta hakai* exhibiting the most severe defects. This suggests that m^{6}A mRNA modification is also involved in regulating the development of leaves, flowers and seeds.

In terms of root development, all characterised low m^{6}A mutants showed auxin-insensitive phenotypes: significantly shorter primary roots and reduced lateral roots. Even after the synchronous lateral root induction by NPA and NAA, the root developmental defects in these mutants could not be rescued. Consistent with this, *GUS* driven by *MTA* promoter is predominantly expressed in lateral root initiation sites (Zhong et al., 2008). Though efforts have been made to uncover the molecular mechanism underlying this, it remains unclear which factors within the auxin network are being influenced by m^{6}A modification. In addition, among all m^{6}A writer mutants, only *hakai* showed varied root phenotypes depending on the concentration of sucrose, generally increased lateral roots in seedlings cultured on higher concentration of sucrose (>3% [w/v]), indicating that Hakai might also interact with other regulatory pathways and associate them with m^{6}A modification. However, this hypothesis needs further investigations.

6.2 EMERGING REGULATORY ROLES OF m^6A

Since its discovery, m^6A mRNA modification has been shown to be involved in regulating the fate of transcripts in multiple ways, including mediating mRNA stability, splicing, nuclear export and translation (detailed in 1.6.1). The involvement of m^6A modification in promoting translation has been revealed in mammals through four different mechanisms. One is via the interaction between m^6A reader YTHDF1 and translation initiation factor eiF3 complex (Wang et al., 2015). A second mechanism is that m^6A located in 5' UTRs can directly binds eiF3 and promotes translation independently of 5' cap-binding proteins (Meyer et al., 2015; Zhou et al., 2015). A very recent study shows that m^6A and m^5C in the 3' UTR of p21, a factor associated with stress-induced cellular senescence, cooperatively enhance its expression at the translational level, though the underlying mechanism is unclear (Li et al., 2017). Another study demonstrates a different translational control pathway wherein cytoplasmic METTL3 enhances translation independently of its methyltransferase activity and m^6A readers (Lin et al., 2016).

In the current study, the knockdown of *FIP37* or *Virilizer* led to enhanced translation of ARF7 while its mRNA level remained unchanged. In addition, the localisation of MTA in the cytoplasm increased upon the knockdown of *FIP37*. According to the findings in mammals (Lin et al., 2016), one possible regulatory way may be that increased MTA in the cytoplasm upon the knockdown of *FIP37* facilitates the translation of some transcripts, including *ARF7*. Given that ARF7 contains uORFs in its 5' UTR but this is not the case for ARF8, another

reasonable hypothesis is that m^6A located in 3' UTRs interacts with some translation reinitiation factors (e.g., eiF3h and ribosomal proteins) to regulate the translation of uORF-containing transcripts, like *ARF7*. This is in accordance with a previous study in which the protein level of ARF7 decreases whilst that of ARF8 remains unchanged in ribosomal mutants (Rosado et al., 2012). Further investigations on how AFR7 is regulated translationally upon reducing the mRNA methylation will shed new light on the translational control mechanisms associated with m^6A modification.

Overall, diverse functions of m^6A mRNA modification have been uncovered and more new functions are emerging. However, the underlying regulatory mechanisms remain far from well understood, particularly in plants. To date, only two m^6A demethylases and no m^6A reader proteins have been characterised in plants. Moreover, whether the fate of certain plant transcripts is influenced by differential m^6A modifications at different developmental stages or in response to environment is still not clear. Further studies are needed to clarify these issues. Nevertheless, outcomes from the present study will aid our understanding of how the plant MTase complex works and the biological processes regulated by m^6A modification in plants. The current study will also shed new light on how gene expression is regulated post-transcriptionally in plants.

6.3 REFERENCES

BATISTA, P. J., MOLINIE, B., WANG, J., QU, K., ZHANG, J., LI, L., BOULEY, D. M., LUJAN, E., HADDAD, B., DANESHVAR, K., et al. 2014. m^6A RNA modification controls cell fate transition in mammalian embryonic stem cells. Cell Stem Cell, 15, 707-719.

BODI, Z., ZHONG, S., MEHRA, S., SONG, J., GRAHAM, N., LI, H., MAY, S. & FRAY, R. G. 2012. Adenosine methylation in *Arabidopsis* mRNA is associated with the 3′ end and reduced levels cause developmental defects. Frontiers in Plant Science, 3.

GEULA, S., MOSHITCH-MOSHKOVITZ, S., DOMINISSINI, D., MANSOUR, A. A., KOL, N., SALMON-DIVON, M., HERSHKOVITZ, V., PEER, E., MOR, N., MANOR, Y. S., et al. 2015. m^6A mRNA methylation facilitates resolution of naïve pluripotency toward differentiation. Science, 347, 1002-1006.

LI, Q., LI, X., TANG, H., JIANG, B., DOU, Y., GOROSPE, M. & WANG, W. 2017. NSUN2-mediated m5C methylation and METTL3/METTL14-mediated m6A methylation cooperatively enhance p21 translation. Journal of Cellular Biochemistry, 9999.

LIN, S., CHOE, J., DU, P., TRIBOULET, R. & GREGORY, R. I. 2016. The m^6A methyltransferase METTL3 promotes translation in human cancer cells. Molecular Cell, 62, 335-345.

MEYER, K. D., PATIL, D. P., ZHOU, J., ZINOVIEV, A., SKABKIN, M. A., ELEMENTO, O., PESTOVA, T. V., QIAN, S.-B. & JAFFREY, S. R. 2015. 5' UTR m^6A promotes cap-independent translation. Cell, 163, 999-1010.

PERIANEZ-RODRIGUEZ J., MANZANO C. & MORENO-RISUENO M. A. 2014. Post-embryonic organogenesis and plant regeneration from tissues: two sides of the same coin? Frontiers in Plant Science, 5, 219.

ROSADO, A., LI, R., VAN DE VEN, W., HSU, E. & RAIKHEL, N. V. 2012. *Arabidopsis* ribosomal proteins control developmental programs through translational regulation of auxin response factors. Proceedings of the National Academy of Sciences, 109, 19537-19544.

RŮŽIČKA, K., ZHANG, M., CAMPILHO, A., BODI, Z., KASHIF, M., SALEH, M., EECKHOUT, D., EL-SHOWK, S., LI, H., ZHONG, S., et al. 2017. Identification of factors required for m^6A mRNA methylation in *Arabidopsis* reveals a role for the conserved E3 ubiquitin ligase HAKAI. New Phytologist, 215, 157-172.

SHEN, L., LIANG, Z., GU, X., CHEN, Y., TEO, Z. W. N., HOU, X., CAI, W. M., DEDON, P. C., LIU, L. & YU, H. 2016. N^6-methyladenosine RNA modification regulates shoot stem cell fate in *Arabidopsis*. Developmental Cell, 38, 186-200.

VESPA, L., VACHON, G., BERGER, F., PERAZZA, D., FAURE, J.-D. & HERZOG, M. 2004. The immunophilin-interacting protein AtFIP37 from Arabidopsis is essential for plant development and is involved in trichome endoreduplication. Plant Physiology, 134, 1283-1292.

WANG, X., ZHAO, B. S., ROUNDTREE, I. A., LU, Z., HAN, D., MA, H., WENG, X., CHEN, K., SHI, H. & HE, C. 2015. N^6-methyladenosine modulates messenger RNA translation efficiency. Cell, 161, 1388-1399.

WANG, Y., LI, Y., TOTH, J. I., PETROSKI, M. D., ZHANG, Z. & ZHAO, J. C. 2014. N^6-methyladenosine modification destabilizes developmental regulators in embryonic stem cells. Nature Cell Biology, 16, 191-198.

ZHONG, S., LI, H., BODI, Z., BUTTON, J., VESPA, L., HERZOG, M. & FRAY, R. G. 2008. MTA is an *Arabidopsis* messenger RNA adenosine methylase and interacts with a homolog of a sex-specific splicing factor. The Plant Cell, 20, 1278-1288.

ZHOU, J., WAN, J., GAO, X., ZHANG, X. & QIAN, S.-B. 2015. Dynamic m^6A mRNA methylation directs translational control of heat shock response. Nature, 526, 591-594.

CHAPTER 7 CONCLUSIONS AND FUTURE WORK

7.1 CONCLUSIONS

The current study aimed to decipher the function of a novel member of m^6A methyltransferase (MTase) complex – Hakai, interactions between different components of the MTase complex and the role of m^6A in root development. Major results obtained are summarised as follows.

(1) The m^6A level in *hakai* knockout mutants was decreased by approximately 40% compared with that in WT and the m^6A abundance could be restored to the WT level in the complementation line (Hakai-GFP/*hakai*).

(2) A set of double mutants for m^6A writer proteins were generated and characterised. Among them, *mta hakai* and *mta virilizer* double mutants demonstrated stronger developmental defects than the corresponding single mutants while *hakai fip37* and *hakai virilizer* double mutants appear to be lethal at a very early developmental stage. In contrast, *mta fip37* double mutant resembled *mta* single mutant, demonstrating less severe developmental defects than *fip37* single mutant.

(3) MTA-GFP in *fip37* background (*fip37* MTA-GFP) exhibited stronger developmental defects and increased MTA-GFP localised to the cytoplasm relative to that in WT background.

(4) The immunoprecipitation followed by mass spectrometry analysis reveals that MTA, FIP37 and Virilizer are interacting partners of Hakai while MTA interacts with all other known m^6A writer proteins in *Arabidopsis*. In addition,

two zinc finger proteins (AT1G32360 and AT5G53440) and a heat shock protein (Hps70-15) were co-purified with both MTA and Hakai and the interaction between MTA and AT1G32360 disappeared upon the knockout of *Hakai*.

(5) Low m^6A mutants, especially *fip37*, *virilizer* and *mta hakai* double mutant demonstrated auxin-insensitive phenotypes: significantly shorter primary roots and reduced LRs compared with WT. Moreover, these root developmental defects could not be rescued upon synchronous LR induction using NPA and NAA. However, the auxin response analysis using *DR5*::*VENUS* reporter line showed strong auxin response transcriptionally in m^6A writer mutants. In addition, the protein level of uORF-containing ARF7 dramatically increased in *fip37* and *virilizer* whereas the mRNA level of *ARF7* remained unchanged. By contrast, ARF8 protein level was unchanged upon the knockdown of *FIP37* or *Virilizer*.

In conclusion, Hakai is a bona fide component of the MTase complex and is required for full m^6A mRNA methylation. Moreover, Hakai acts synergistically with other m^6A writer proteins in maintaining well-tuned mRNA methylation and regulating normal plant growth and development. In contrast to the interactions between other members of the MTase complex, MTA appears to function as a suppressor of FIP37 and in turn FIP37 influences the localisation of MTA between the nuclei and the cytoplasm. In addition, novel proteins might be involved in catalysing m^6A formation, with zinc finger proteins as promising candidates. m^6A modification is suggested to be involved in regulating lateral root development but the underlying machineries remain unclear. ARF7 protein levels increased in *fip37* and *virilizer* but this was not the case for ARF8. This

may indicate that m^6A modification might participate in translational regulation via a novel mechanism – potentially translation reinitiation associated with uORFs. The data obtained in the current study will provide a good foundation for further study to decipher the m^6A writer complex and functions of m^6A in plants and other organisms.

7.2 FUTURE WORK

Based on the results obtained in the current study, the following work can be carried out in the future to better understand diverse functions of m^6A in plants and other eukaryotic species.

(1) To analyse the MeRIP-seq data for *hakai* and compare the methylome of *hakai* with that of WT and other m^6A writer mutants with much higher m^6A reduction.

(2) To carry out proteomic analysis using GFP-tagged lines in m^6A writer mutant backgrounds (other than *hakai* MTA-GFP) to further understand the interactions between different components of the MTase complex.

(3) To analyse the ubiquitin specificity of Hakai and its targets by western blotting and Lys-ϵ-Gly-Gly (diGly) proteomics using transgenic lines generated in this study.

(4) To characterise novel candidate proteins of the MTase complex (such as zinc finger proteins), starting with m^6A measurement and protein interaction assays with known m^6A writer proteins.

(5) To study the potential of m^6A modification in mediating translation and to elucidate the underlying mechanisms by a comprehensive analysis combining polysome profiling, western blotting, high-throughput sequencing, etc. based on generation and characterisation of double mutants between m^6A writer mutants and mutants for proteins responsible for translation reinitiation.

APPENDICES

Appendix 1 Primers used in this study

Primer name	Sequence (5′-3′)	Function
148797LP	TCACAAGGAATCTGCAAAACC	Left primer flanking SALK_148797 T-DNA insertion site
148797RP	GACATCCTCTGCTTTGAGCAC	Right primer flanking SALK_148797 T-DNA insertion site
109428LP	TAGATTGCAATCGGAAAATCG	Left primer flanking SALK_109428 T-DNA insertion site
109428RP	GACATCCTCTGCTTTGAGCAC	Right primer flanking SALK_109428 T-DNA insertion site
259E01LP	GTCACGCAGACGATCTAGAGG	Left primer flanking GK_259E01 T-DNA insertion site
259E01RP	CGAACGCAGAAGTGAACTCTC	Right primer flanking GK_259E01 T-DNA insertion site
217A12LP	TAAATGCAGGCAAAAACTTGC	Left primer flanking GK_217A12 T-DNA insertion site
217A12RP	GAGCTGCACAGATGAAGATCC	Right primer flanking GK_217A12 T-DNA insertion site
LBb1	GCGTGGACCGCTTGCTGCAACT	Left board primer on the T-DNA of SALK lines
LBb1.3	ATTTTGCCGATTTCGGAAC	Another left board primer on the T-DNA of SALK lines
GabiTDNA	ATAATAACGCTGCGGACATCTACATTTT	Left board primer on the T-DNA of GABI lines
Oligo(dT)	TTTTTTTTTTTTTTTTT	Oligos for first-strand cDNA synthesis
AtActin2fwd	GATGCTCCCAGGGCTGTTTT	Forward primer for checking the expression of *AtActin2*
AtActin2rev	AAGTGCTGTGATTTCTTTGCT	Reverse primer for checking the expression of *AtActin2*
exHAKAIfwd	TTCCATCTGCTATCTATGTGATGAG	Forward primer across intron 2 for checking the expression of *Hakai*
exHAKAIrev	CGAAGGAAAACCAAACTGCTGT	Reverse primer for checking the expression of *Hakai* together with exHAKAIfwd
exHAKAIfwde1	TTCACTTCTGCGTTCGTTGC	Forward primer on exon 1 for checking the expression of *Hakai*
exHAKAIreve1	GAGTTATCGCTATCTGGAGGGT	Reverse primer for checking the expression of *Hakai* together with exHAKAIfwde1
HAKICrisp1M	tgtggtctcaATTGATTACGGTGGTGGGAGTCAGTTTTAGAGCTAGAAATAGCAAG	Forward primer for amplifying sgRNA 1 targeting *Hakai*
HAKICrisp2P	tgtggtctcaATTGTTCACGGGATTGTTGCAGCGTTTTAGAGCTAGAAATAGCAAG	Forward primer for amplifying sgRNA 2 targeting *Hakai*
sgRNArev	tgtggtctcaAGCGTAATGCCAACTTTGTAC	Reverse primer for amplifying sgRNA for CRISPR

Primer name	Sequence (5′-3′)	Function
CRISPR_seq_fwd	GCACAGGGATAAGCCCATCA	Forward primer for checking assembled CRISPR constructs by sequencing
CRISPR_seq_rev	CGGCTGGCACATACAAATGG	Reverse primer for checking assembled CRISPR constructs by sequencing
TTACU6Pro	TTTGAAGACAATTACGGAGTGATCAAAAGTCCCAC	Forward primer for amplifying AtU6p::sgRNA
GGGAU6rev	TGTGAAGACAATCCCTAATGCCAACTTTGTACAAG	Reverse primer for amplifying AtU6p::sgRNA
HAKICrisp1Mdf	CGTTCATGTAACTTTTACAGCG	Forward primer for checking mutagenesis at CRISPR target site 1
HAKICrisp1Mdr	CATATAGAAGAAGAGCCCCC	Reverse primer for checking mutagenesis at CRISPR target site 1
HAKICrisp2Pdf	AAGCCTATTACAAGCCGATGC	Forward primer for checking mutagenesis at CRISPR target site 2
HAKICrisp2Pdr	TTACTCCTGCCCAAAGCCATC	Reverse primer for checking mutagenesis at CRISPR target site 2
HAKICrisp2crdf	CTTCTATTCTCCTCCGTTGCC	Forward primer for checking mutations between two CRISPR target sites
HAKICrisp2crdr	GATTCATAGGCTGGGGGTAGT	Reverse primer for checking mutations between two CRISPR target sites
Cas9fwd	GGATGAACTCGTCAAAGTAATGG	Forward primer for checking the presence of Cas9
Cas9rev	GGCTTATCCCTGTGCTTATTGT	Reverse primer for checking the presence of Cas9
Hakai-allf	CACCTAGTGAGAATGAACTCTAAGTCGAT	Forward primer for amplifying *Hakai* genomic DNA under its own promoter
Hakai-allr	CTCCTGCCCAAAGCCATCACGGTTC	Reverse primer for amplifying *Hakai* genomic DNA under its own promoter
GFPrev	GAAGTCGTGCTGCTTCATGTGG	Reverse primer on GFP to check constructs with GFP tag
HAKAIprobefwd	GAAGCCTATTACAAGCCGATGC	Forward primer for preparing *Hakai* RNA probe template and checking Hakai-GFP lines
T7HAKAIrev	TAATACGACTCACTATAGGCCACCCAAAACTTTGACCGT	Reverse primer for preparing *Hakai* RNA probe template with T7 promoter
074069LP	TCGAAACGATTTGGAAAAATG	Left primer flanking the T-DNA of SALK_074069
074069RP	AGGATTGGTTTGCATGTCAAG	Right primer flanking the T-DNA of SALK_074069
018636LP	ATCGCAAAGAGAAAAGAAGCG	Left primer flanking the T-DNA of SALK_018636 and forward primer for checking *FIP37-GFP* transgene
018636RP	GTTCTGCACTTTGCCATAAGC	Right primer flanking the T-DNA of SALK_018636

Primer name	Sequence (5′-3′)	Function
virFwdExon5	CTGGCTGCTGTAGATTTGCC	Forward primer upstream of *virilizer* mutant site
virRevExon6	CAACTGAATGGCGTGTAGCC	Reverse primer downstream of *virilizer* mutant site
vir-seq-fwd	TTGTTCGGCTGTGACCAGTT	Forward primer for sequencing *virilizer* mutant site
MTAGFPfwd	ACGGTTTGATTTTCCTCTGGG	Forward primer on *MTA* cDNA to check *ABI3*::*MTA* construct or *MTA-GFP* transgene
FIP37exon1rev	GAAGCCCTGGTGGCATTAGC	Sequencing primer to confirm the presence of *FIP37* promoter on *FIP37*p-gDNA-pDONR(Amp+)
114710LP	GCTGAGAAATCTGTGCTGACC	Left primer flanking the T-DNA of SALK_114710
114710RP	TATGGAACTAGGCCGTGAATG	Right primer flanking the T-DNA of SALK_114710
ARF7probefwd	GCAGTGTCATCACGCCTCCG	Forward primer for preparing *ARF7* RNA probe template
T7ARF7Rev	TAATACGACTCACTATAGGCCGTAAGAAGTTCCAGAGGC	Reverse primer for preparing *ARF7* RNA probe template with T7 promoter

Note: Target sequences of sgRNAs for knocking out *Hakai* via CRISPR-Cas9 are in red. Restriction enzyme sites are underlined. The sequence of T7 promoter is in blue colour.

PUBLICATIONS ARISING FROM WORK IN THIS THESIS

RŮŽIČKA, K., **ZHANG, M.**, CAMPILHO, A., BODI, Z., KASHIF, M., SALEH, M., EECKHOUT, D., EL-SHOWK, S., LI, H., ZHONG, S., et al. 2017. Identification of factors required for m^6A mRNA methylation in *Arabidopsis* reveals a role for the conserved E3 ubiquitin ligase HAKAI. New Phytologist, 215, 157-172.